Activated hybrid cementitious system using Portland cement and high volume Colombian fly ash with sodium sulfate

Diego Felipe Velandia Manchego

Thesis submitted for the degree of Doctor of Philosophy

Department of Civil and Structural Engineering
University of Sheffield

May 2015

Abstract

Activated hybrid cementitious systems, including high volume fly ash with high loss on ignition (LOI) content and sodium sulfate as activator, are studied to explore more sustainable alternatives to Portland cement (PC) for reducing CO_2 emissions in the concrete industry. Most of the background of this project is on mortars with low LOI fly ashes. Performance and deterioration initiation periods have never been studied before for concretes with these materials. None of the following factors have been considered previously in one study: fly ash replacement level, nature of fly ashes obtained from Colombian sources (of high LOI), and the type and amount of activator. In addition, no specific study had encompassed all the parameters necessary for the development of systems viable for the Colombian concrete industry, on performance, environmental and economic grounds. Therefore, this study aims to address this.

This research covers characterization of raw materials before and after treatment, mortar evaluation, fresh and hardened state concrete evaluation of both laboratory samples and large size concrete elements cured outdoors, durability characterization, prediction of corrosion initiation period, CO_2 emissions and cost calculations. The characterization includes the evaluation of four different fly ashes (Termopaipa, Fabricato, Termoguajira, Tampa) before and after sieving and the evaluation of different activators; sodium sulfate, lime and quicklime at different dosages. The mortar and concrete studies were carried out for a period of up to one year. The concrete study evaluates the performance of a 50/50 Termopaipa fly ash/PC system with 1% sodium sulfate by weight of cementitious material. Beside compressive strength and maturity, the performance evaluation includes water permeability, sorptivity, chloride penetration, chloride diffusion, carbonation, sulfate attack and alkali silica reaction. Prediction models for corrosion initiation time are developed by correlating results from laboratory cured samples to those cured outdoors. Efficiency curves were developed to correlate CO_2 emissions and costs to compressive strength for the different cementitious systems.

Modifying the particle size distribution of the fly ash, through sieving, affected the compressive strength due to changes in the amorphous content. The benefits of sodium sulfate in terms of compressive strength are highlighted, with 1% found to be the optimum dosage for use in concrete. The higher ettringite formation, portlandite consumption and early compressive strengths are some of the characteristics of mixes incorporating sodium sulfate. In terms of concrete performance, it is found that the chloride diffusion coefficient is reduced significantly with time for the activated system compared to control samples (100% PC and 80% PC - 20% fly ash) of the same water to cementitious material ratio (W/CM). This behaviour is exhibited by samples cured under controlled laboratory conditions (100% RH and 23°C). On the other hand, outdoor curing increases concrete permeability for all concretes. Long term carbonation is also explored, and samples under outdoor curing have a significant carbonation depth. Alkali silica reaction and sulfate attack problems are mitigated with this activated hybrid system. The prediction equations developed take into account chloride and carbonation diffusion and the influence of other parameters such as the W/CM, fly ash replacement level and compressive strength. From knowledge of the 28-day compressive strength of concrete, the time for critical levels of chloride or carbonation to reach the steel can be predicted considering the cover depth and the level of cement replacement with or without activator. Reduction of CO_2 emissions and costs and the observed technical characteristics, demonstrate the viability of this green alternative in the short term.

Acknowledgements

I would like to express my deepest gratitude to Dr. Cyril Lynsdale for his expertise, supervision and thoughtful guidance; I would also like to thank Professor John Provis for sharing his experience and knowledge with me during all of this process. Their advice and support allowed me to conclude this important stage of my life.

I want to thank my company Argos for sponsoring my project. Thanks to Sika for its support with materials and technical information.

My wife and daughter played the most important role during my project; their love, understanding, patience and continuous support allowed me to pursuit my dream. This thesis is dedicated to you.

God has blessed me again with this experience.

List of Contents

List of Tables

List of Figures

1 Introduction

1.1 Introduction

CO_2 emissions have become the main environmental issue in the world in recent years. In 2012, a report from the PBL Netherlands Environmental Assessment Agency stated that 34 billion tonnes of CO_2 were produced worldwide in 2011, with a 3% annual increment (Olivier, *et al.*, 2012). The 2014 report published that CO_2 emissions were 35.3 billion tonnes in 2013 (Olivier, *et al.*, 2014). These numbers are leading different industries to focus on decreasing CO_2 emissions based on new technologies or innovations. The cement and concrete industry has been working hard in order to guarantee a carbon foot-print reduction; researchers and industrialists world-wide are working together in order to find ways or methods to decrease CO_2 emissions in the production of cement and concrete.

In the case of the concrete industry, it has an important role in this global issue considering that a product with less cement could decrease the carbon foot-print significantly. The impact of global cement producers is about 8% of the total anthropogenic CO_2 emissions (Olivier, *et al.*, 2012). In spite of this, there are many alternatives to reduce CO_2 emissions, but one of the most notable ways to do this is by using supplementary cementitious materials (SCMs) in the mix, yielding products which range from high volume fly ash concretes up to geopolymers depending on the replacement level (Yang, *et al.*, 2013). SCMs are available all around the world and for this industry it has been a challenge to include it in higher percentages.

Fly ash is a SCM which is a waste from the thermoelectric industry. Although pozzolans were used in ancient Rome, thermoelectric fly ash started to be used as cement replacement just after 1930 (ACI 232.2, 2003). In 1937, a document was published including a study about fly ash in hydraulic cement concrete (Davis, *et al.*, 1937). This document included some initial guidelines for the use of fly ash in concrete. Since that time, many efforts have been made in order to increase its proportion in a concrete mix, and replacement levels from 40% to 60% are now used in some applications (Malhotra, 2002).

Although there is an environmental pressure to increase the percentage of fly ash in concrete mixes, it is important to study some technical concerns such as durability in order to increase the cementitious material replacement degree from 60% to 80% (Shi, *et al.*, 2011); some of the main issues to study are related to strength, setting, durability and extra costs (i.e. high curing temperature, high superplasticizer dosages) in ready mixed concrete production (Hermida and Velandia, 2012).

The technical development in this area is growing rapidly in Colombia and different companies are starting to research how to use high volumes of fly ash; in spite of this interest, there are many technical barriers such as those mentioned above which hinder forward steps in this topic. It is necessary to research different ways to reach those high replacement percentages, such as the possibility of including a chemical activator and different mix adjustments (Velandia, *et al.*, 2013); consideration of these options will be the key to the evaluation of an activated hybrid cementitious system using Portland cement and high volume Colombian fly ash, with sodium sulfate as a chemical activator.

1.2   Background to the research

Fly ash concrete researchers have focused on two main topics in the past years: the use of high volume fly ash (40-60%) concrete using superplasticizers, and geopolymer concrete using 100% fly ash and a chemical activator. When a high volume fly ash concrete is designed, it is necessary to consider a reduction in the water to cementitious material ratio; as it is reduced, superplasticizer is increased to keep the same slump (Malhotra, 2002). Although it is a green alternative, it is not an optimum one due to the fact of increasing the amount of an expensive superplasticizer (polycarboxylate). Beside this, setting time and early strength are affected, becoming at some point critical issues to be controlled. Researchers have also studied the possibility of using binders based on 100% fly ash including an activator (Palomo, *et al.*, 1999); many of these studies relate the necessity of including high curing temperatures in order to reach the target strength for a lot of fly ashes, which makes this path less viable for real concrete production (Criado, *et al.,* 2010). Furthermore, it is necessary to develop different studies related to its durability and life cycle.

Intermediate mixes, where the fly ash percentages are between 50% and 100%, have not often presented successful behaviour (Hannesson, *et al.*, 2012), in terms of setting time, rheology, early strength evolution, 28 day strength accomplishment and costs. Further research is needed on durability issues (Shi, *et al.*, 2006; 2011); establishing the required fly ash reactive silica and alumina contents and activator dosage are the first steps towards achieving good performance.

1.3   Aims and Objectives

The main objective of this study is to investigate the performance in terms of durability, initiation periods and CO_2 emissions of an activated hybrid cementitious concrete, which considers inclusion of a high volume Colombian type F fly ash (of high LOI) and sodium sulfate. It is necessary to determine the main parameters which affect concrete performance, varying fly ash fineness, activator dosage, silica and amorphous content. Different engineering and durability properties are evaluated in order to draw conclusions regarding its viability as a real product for ready mix concrete production. The following is a list of the project objectives:

- To activate different Colombian fly ashes with high loss on ignition content using mixes with Portland cement and different activators. Chemical and physical parameters of the fly ashes are considered before the activation process.

- To perform laboratory and in situ durability tests covering mortar, concrete, and concrete elements (beams).

- To find the optimum amounts of activators, keeping constant the technical parameters of mixes (fresh concrete, engineering and durability properties).

- To evaluate the initiation period for corrosion of steel embedded in concrete using the correlations obtained from the durability evaluation. The initiation period is determined for attack by chloride and CO_2 diffusion. For chloride diffusion LIFE 365 is the reference and some of the main equations are modified depending on lab and outdoor results. For CO_2 diffusion, one simple model to propose in this study considers compressive strength, water to cementitious material ratio, fly ash percentage and sodium sulfate as activator; this applies for local environment conditions in Bogotá.

- To calculate CO_2 foot-print and costs from the evaluated mixes, evaluating any environmental and economic advantages.

1.4 Scope

The main scope of this thesis is to evaluate the effectiveness of an activated hybrid cementitious system using Portland cement and high volume Colombian fly ash (of high LOI) with sodium sulfate advantages, focusing on the fresh, hardened and durability properties of concrete. According to the literature review a high volume concrete considers 50% as the minimum fly ash content. This study considers this minimum percentage due to the presence of high LOI in the fly ash. Additionally, in order to understand the influence of the sodium sulfate, it is important to start with this level regarding that as the fly ash content is increased retardation in setting time and a reduction in early compressive strength occur.

Initially for this study, one source of Portland cement, three sources of Colombian fly ashes (Termopaipa FA, Fabricato FA and Termoguajira FA) and one North American fly ash (Tampa FA) are used. Full mineralogical, physical, and chemical characterization of the Portland cement and fly ashes are performed. The three local sources of fly ash consist of by-products from relatively young coal burning power plants in Colombia with little history of utilization in construction. The chemical activators considered for this study are Na_2SO_4, hydrated lime and quicklime.

The performance of different combinations of materials are assessed based on laboratory testing of mortars and concrete, including workability, flow, setting characteristics, strength gain, and durability. Parallel to the laboratory testing programme, concrete elements are evaluated outdoors. The testing of the elements is performed on cores, evaluating strength gain with time and durability. The initiation period calculation is based on the durability parameters evaluated initially. Environmental parameters such as the carbon foot-print and savings in CO_2 emissions are calculated. Table 1 presents the scope.

1.5   Research methodology

This research follows a methodology consisting of 6 main phases for its development. Table 1 shows all the tasks per activity and phase.

Phase 0

At the beginning of this project, a complete literature review is done, considering the main objectives of this research.

Phase 1

After collecting all the previous studies, certain tasks are developed in order to characterise all of the supplementary cementitious materials (SCMs).

a) The chemical composition is obtained from X-ray fluorescence (XRF). A complete comparison between the SCMs composition and the requirements of the ASTM C 618 are performed.

b) Mineralogy of these materials is analysed using X-ray diffraction (XRD). This evaluation is focused on the amount of not only the crystalline phases but also the amorphous one.

c) The fineness of each material is affected by a sieving process. Three different granulometries is obtained including the initial curve. As the fineness is increased, laser diffraction is the best option to measure their granulometry.

Phase 2

Mortar and pastes are evaluated using different activators, dosages and fly ash fineness.

a) Heat release from mortars during hydration is measured using a semiadiabatic calorimeter. This test allows understanding of the chemical effect of the fly ashes and activators.

b) Paste samples are used to evaluate the mineralogy using XRD

c) Thermogravimetry is used in order to find the calcium hydroxide consumption for each matrix.

d) Compressive strength is the main mechanical parameter to measure.

e) After this initial mortar and paste evaluation, the optimum activator and dosage is found.

Phase 3

Concrete samples with different water to cementitious material ratios, percentages of the original size Termopaipa FA and the optimum activator are studied in this phase. Air and mist curing are considered in order to simulate real field scenarios.

a) Slump, slump loss, setting time and air content tests are performed to evaluate fresh concrete state.

b) Compressive strength is evaluated at different ages.

c) The following are the different durability tests performed at this phase: drying shrinkage, water permeability, sorptivity, chloride permeability, diffusion coefficient, carbonation, sulfate attack, and alkali silica reaction.

Phase 4

Concrete elements (*Beams:* $0.3 \times 0.4 \times 1m$) are tested using original size Termopaipa FA and an activator with its optimum dosage.

a) The same fresh concrete, engineering and durability properties evaluated in phase three are considered for these concretes.

b) The durability data measured in the lab are compared with the data available from field samples. Cores are taken from the elements to measure carbonation, water permeability, chloride permeability and diffusion coefficient. ASR is measured directly in the beams following the procedure mentioned in section 6.2.7.

Phase 5

All the data are compiled and analysed in order to define the technical performance of the activated hybrid cementitious system. This is based on the main parameters which affect the behaviour of a hybrid activated system and their correlations presented at the end of the project.

a) Initiation periods are evaluated for CO_2 and chlorides

b) CO_2 emissions and costs are compared between the different samples.

c) Conclusions and recommendations related to activated hybrid cementitious system is developed.

Table 1 Phase activities and scope

Activated Hybrid Cementitious System	

	Activity	Phase 0
Literature review	Activity	Phase 0

			Activity	Phase 1
SCMs charaterization. Sieving treatment			Activity	Phase 1
Termopaipa FA, Fabricato FA, Termoguajira FA, Tampa FA			SCMs	Phase 1
Mineralogy	**Physical charateristics**	**Chemical characteristics**	Evaluation	Phase 1

					Activity	Phase 2
Mortars evaluation		**Pastes evaluation**			Activity	Phase 2
SCM: 50%					Constants	Phase 2
SCMs: Termopaipa FA, Fabricato FA, Termoguajira FA, Tampa FA **SCMs particle size:** Original size, <75μm, <45μm **Activator 1 SIKA (0%, 0.5%, 1%, 1.5%, 3,5%):** Na$_2$SO$_4$ **Activator 2 (0%, 1%, 3%, 5%):** Hydrated lime **Activator 3 (0%, 1%, 3%, 5%):** Quicklime **Activator 4 (0%, 1%, 3%, 5%):** Na$_2$SO$_4$					Variables	Phase 2
Compressive strength	**Heat of hydration**	**Mineralogy**	**SEM**	**Thermogravimetry**	Evaluation	Phase 2

18

Concrete evaluation	Activity
OS Termopaipa FA, optimum activator, plasticiser and superplasticiser	Constants
W/CM: 0.557, 0.483, 0.426 **Fly ash content:** Control (0%, 20% and 50%), 50% + Act 1 **Curing:** Laboratory curing, outdoor curing	Variables
Slump, Setting Time, Air Content	Fresh Properties
Compressive Strength (1, 3, 7, 28, 56, 90, 360 days)	Engineering Properties
Drying shrinkage (4, 7, 14, 28, 56, 112, 224, 448 days) **Water permeability** (90, 180, 270, 360 days) **Chloride permeability** (28, 90, 180, 270, 360 days) **Carbonation** (28, 90, 270, 260 days) **Sorptivity** (28, 90, 360 days) **Diffussion Coefficient** (90, 180, 270, 360 days) **ASR, Sulphate attack**	Durability

Phase 3

Elements testing	Activity
OS Termopaipa FA and activator	Constants
W/CM: 0.557, 0.483, 0.426 **Fly ash content:**50%	Variables
Compressive Strength (90, 360 days), **Maturity**	Engineering Properties
Drying shrinkage (4, 7, 14, 28, 56, 112, 224, 448 days) **Water permeability** (90, 360 days) **Chloride permeability** (90, 360 days) **Carbonation** (90, 360 days) **Sulphate attack** **Sorptivity** (90, 360 days) **Diffussion coefficient** (90, 360 days) **ASR, Sulphate attack, Water -Soluble Chloride**	Durability

Phase 4

Phase 5	Activity	Analysis of Results / Prediction Models /CO_2 emissions/Conclusions and Recommendations

2 Literature Review

2.1 Introduction

The literature review presented in this chapter highlights relevant information from different researchers related to high volume fly ash concrete, geopolymer concrete and high volume fly ash concrete using activators; the main fresh and hardened mortar or concrete properties are discussed. The main goal of this section is to understand the work which has been published related to high volume fly ash concrete, chemical activation, mechanical activation, transport mechanisms and concrete service life. Based on this information, the activated hybrid cementitious system will be evaluated in order to determine its viability in real-world ready mixed concrete production, accomplishing desirable fresh concrete and engineering properties including durability parameters. It is important to mention that most of the information related to activated hybrid cementitious systems is based on laboratory test work and has not yet been related to real field work.

2.2 Maximization of low calcium fly ash reactivity

There are four main methods used to maximize the reactivity of low calcium fly ash: water to cementitious material reduction (in high volume fly ash concrete), chemical activation, mechanical activation, and heat treatment.

2.2.1 High Volume Fly Ash Concrete

In order to consider a "high volume fly ash (HVFA) concrete" it is necessary to take into account that the minimum recommended fly ash content is 50% (Malhotra and Mehta, 2002):

2.2.1.1 Fresh concrete properties

Although in most of the literature HVFA concrete mixes are characterized for their effective behaviour in the fresh state, it is necessary to study how HVFA mix design really affects each of fresh concrete properties. In general some of its properties are improved just because the level of water is reduced due to the fly ash particle size distribution, morphology and surface characteristics; for instance, it is possible to reduce the amount of water for a given consistency using a small size and glassy

textured fly ash (Mehta, 1999). Nevertheless, unburned carbon present in the fly ash could affect this general behaviour significantly. An increment in the fly ash loss on ignition (LOI) increases the water requirement for a given consistency (Mehta and Monteiro, 1999). The same carbon cellular particles which affect the water content also affect the air content, making it necessary to increase the air entraining admixture significantly to achieve the desired air content (Freeman, *et al*., 1997). Figure 1 shows the air entraining admixture on carbon solid.
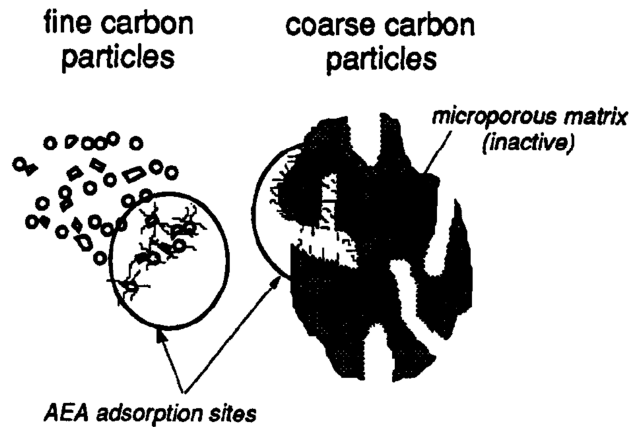
Figure 1 Air entraining admixture on carbon solid (Freeman, *et al.*, 1997)

Parameters such as flowability, pumpability, compactability and finishability can present outstanding behaviour in HVFA. Considering concretes with an inefficient aggregate fines content, HVFA binders can improve their cohesiveness, making easier the long distance pumping and finishability of these materials (Felekoglu, 2006).

Slump loss measurement allows understanding of the capacity of the mix to keep its consistency with time. HVFA concrete behaviour is improved when compared to a 100% Portland cement sample, and the two hour slump loss is reduced by increasing fly ash content (Herrera, *et al.,* 2011).

The heat release (as measured by calorimetry) is reduced by increasing the fly ash content of the mix (Atiş, 2002). HVFA concrete can be used for dams or high volume concrete structures, considering that the adiabatic temperature rise can be decreased considerably. However, the effect on heat evolution could also affect the setting time. Special treatment for HVFA concrete mixes must be considered, especially if these types of mixes are used in regular ready mixed concrete production.

As seen in Figure 2 setting time increases with increasing fly ash content and decreases with reducing water to cementitious materials ratio; Series A have the lowest W/CM while C the highest (Herrera, *et al.,* 2011).
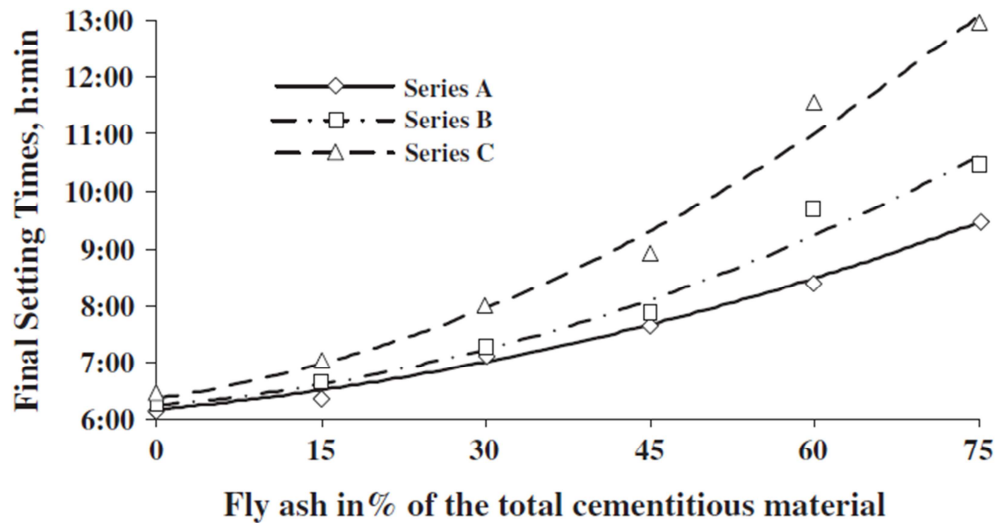
Figure 2 Final setting vs fly ash % (Herrera, et al., 2011)

2.2.1.2 Engineering properties

There are notable changes in the engineering properties of the HVFA materials compared to plain Portland cement; one of the main changes is in the strength development. As a pozzolanic material, fly ash begins to react only after cement reacts with water; after portlandite is formed by cement hydration, fly ash then starts to react, causing an initial delay in concrete strengths. There is a general decrease in the compressive, flexural, splitting tensile strength, modulus of elasticity and abrasion resistance at 28 days (Siddique, 2004). Special considerations must be implemented in order to achieve high strength, which at some point becomes a problem for a regular ready mixed concrete production; standards, committees and different project specifications require a material to accomplish its design strength at an age of 28 days.

Strength could be improved by reducing water to cementitious material ratio; in spite of this possible solution, it is necessary to keep the same slump by increasing the admixture content or the total paste content (Herrera, *et al.,* 2011). For instance, the strength of concretes using 40%, 45% and 50% of fly ash was still suitable for reinforced concrete construction according to the study developed by Siddique (2004).

23

Drying shrinkage is reduced with high volume addition of fly ash due to the reduction in the cement and water contents (Chindaprasirt, *et al.,* 2004). Measuring shrinkage after 365 days proves that a sample with 100% cement has a higher shrinkage than a comparable HVFA (Sahmaran, *et al.*, 2009).

2.2.1.3 Durability

The main advantage of using a HVFA concrete is related to durability improvements increasing the concrete service life cycle. For instance, water absorption of concrete decreases with an increase in fly ash dosage; it is correlated to permeable voids, which are diminished at later age when fly ash is included in higher proportions (Dinakar, *et al.*, 2008). Figure 3 shows how the permeable voids increase as fly ash content increases. There is a linear correlation between the volume of penetrable pores when using the absorption test and the sorptivity test (Sahmaran, *et al.*, 2009); according to Sahmaran, the measured transport properties determined by absorption and sorptivity tests do not show significant changes after 90 days. It is important to mention that the compressive strength evolution at later ages is more evident (90, 180 and 360 days).
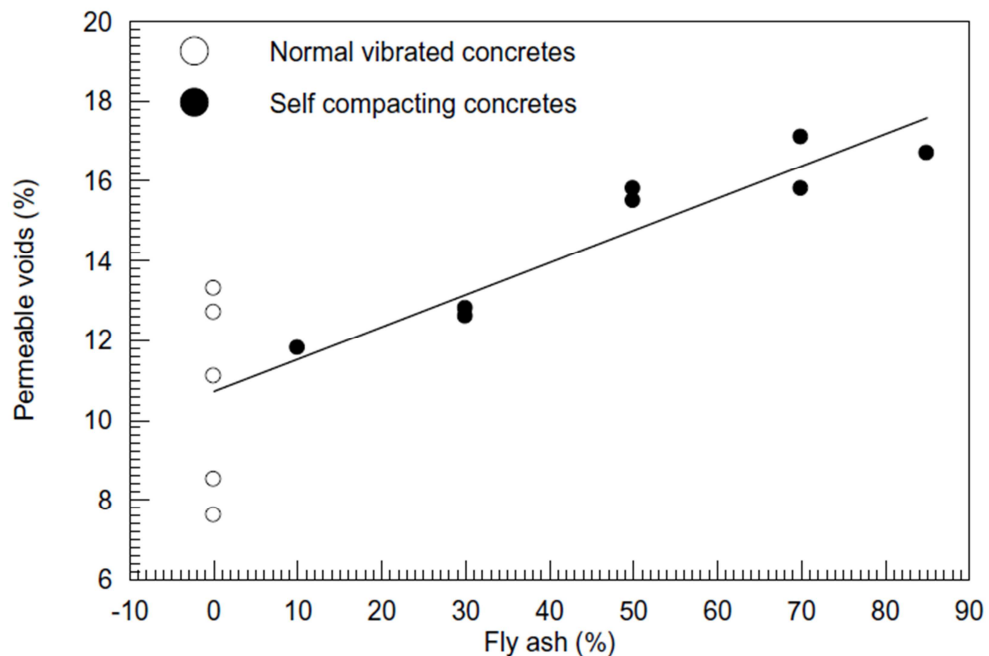
Figure 3 Permeable voids vs fly ash % (Dinakar, *et al.*, 2008)

Chloride permeability using the rapid chloride permeability test is reduced at an age of 56 days by increasing fly ash content (Velandia and Echeverri, 2010); for a

HVFA concrete, following the minimum mix design requirements proposed by Malhotra, the chloride permeability values usually lie in the "very low" band according to ASTM C 1202 (Dinakar, *et al.*, 2008).

When HVFA mortar bars are submerged in sodium sulfate solution, their expansions are lower than that of Portland cement due to the low total C_3A available and low permeability. When fly ash fineness is increased, the mortar structure becomes denser and stronger, reducing expansion significantly (Chindaprasirt, *et al.,* 2004).

Carbonation is a phenomenon mitigated by the presence of calcium hydroxide in a hydrated cement, which buffers the pH level around 12. When fly ash reacts with calcium hydroxide, the ability of this phase to react with in-coming CO_2 decreases, making it easier for carbonation to take place. In spite of this situation, HVFA concretes are characterized by having low permeabilities due to the inclusion of fly ash, a low water to cementitious ratio and a suitable curing process; this helps to reduce carbonation depth and increase the service life of a structure. When low water to cementitious material ratio samples are water cured, they become more resistant to carbonation due to their low porosity; this is seen in Figure 4 (Younsi, *et al.*, 2011).
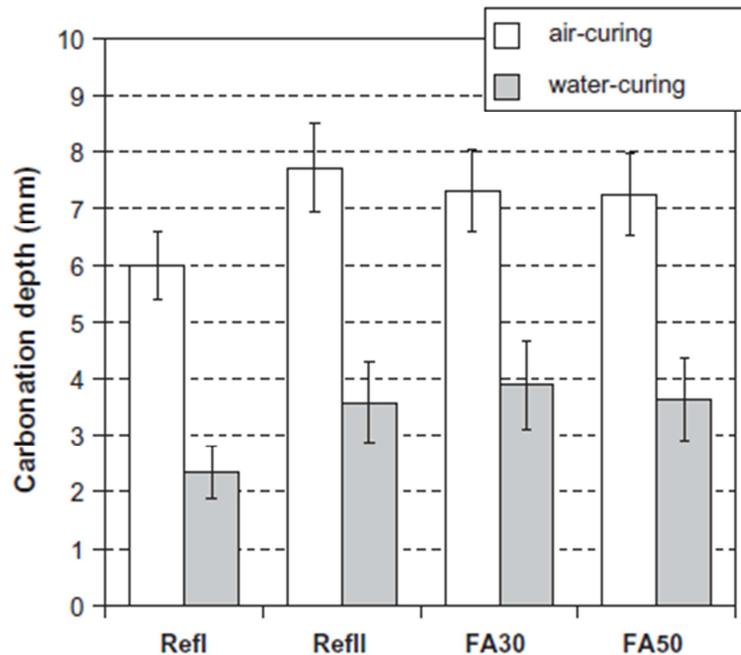
Figure 4 Carbonation depths after 1 year. Temp: 20°C, RH: 50-70%
(Younsi, *et al.*, 2011)

Alkali silica reaction can also be mitigated using HVFA. According to Shon (2002), the expansion resulting from the alkali-silica reaction decreases by using 58% fly ash in a PC blend; this occurs because the total cement alkali content is reduced by increasing fly ash content, and also because aluminium is known to protect against alkali silica reaction. ASTM C1260 was the standard used to evaluate this HVFA concrete. Additional studies have been developed by different authors showing how fly ash increase in concrete reduces alkali-silica reaction (Detwiler, 2002; Kosmatka, 2003; Velandia and Echeverri, 2010).

2.2.2   Chemical activation

The first patent on alkali activation was presented by Whiting (1895). In 1908, Kuhl also presented a patent (RILEM 224-AAM, 2014). Following a general chronological order of the main advances in alkali activation (Shi, *et al.,* 2006), Kuhl used potash solutions to activate ground slag focusing on setting in 1930. Seven years later Chassevent used the same mix to measure reactivity (Shi, *et al.,* 2006). Caustic soda and slag was the mix studied by Purdon in 1940 (Purdon, 1940); the main importance of this research was the fact of using a clinkerless cement. Glukhovsky developed a soil cement in 1957, which consisted of hydrous and anhydrous aluminosilicates and alkalis (Me_2O-MeO-Me_2O_3-SiO_2-H_2O) (Glukhovsky, 1959). In the 1970s and 1980s, Davidovits named various products such as geopolymers, Pyrament, Geopolycem and Geopolymites, which were the names of different products based on alkalis with kaolinite (calcined or uncalcined), lime-stone and dolomite mixes, sometimes containing Portland cement clinker as well (Davidovits, 1981).

According to Shi, *et al.* (2006), alkaline activation involves the mixing of a very high alkaline concentration liquid and a silicoaluminous solid material, resulting in a hardened structure. Al and Si dissolve in the medium forming poly-hydroxy-silicoaluminate complexes; the final geopolymer is an alkaline aluminosilicate hydrate ($Na_2O \cdot Al_2O_3 \cdot (2\text{-}6)SiO_2 \cdot nH_2O$, N-A-S-H gel).

The following is a summary of the process (Shi, *et al.*, 2011) which was first outlined by Glukhovsky:

1. *Destruction*: separation of Me-O, Si-O-Si, Al-O-Al and Al-O-Si bonds.

2. *Coagulation:* polycondensation appears based on accumulation of disaggregated products.

3. *Crystallization:* solid phase particles and condensation of microparticles lead to the product precipitation. Precipitated products depend on the mineralogical composition of the initial phase, the nature of the alkaline component and hardening conditions.

Poon, *et al.,* considered two main methods to develop the chemical activation of a high volume fly ash concrete including low cement content and activators: alkaline and sulfate activation (Poon, *et al.,* 2001). These activation methods work on breaking down the fly ash glassy phases, by providing an environment which accelerates the reaction due to the high alkaline content. The main alkaline reagents include $Ca(OH)_2$, NaOH and KOH. These chemicals break the Si-O, Al-O bonds in the vitreous ash particles, which accelerates the dissolution of Si and Al (Bao-min and Li-Jiu, 2003). The final product developed by using sulfates ($CaSO_4$ and Na_2SO_4) also involves a reaction with aluminium oxide from the solid precursor, forming ettringite.

It is important to differentiate between all the possible gels formed from all the cementitious systems (Garcia-Lodeiro, *et al.*, 2011; Duxson, *et al.*, 2007):

- C-S-H (calcium silicate hydrate): cement and water
- N-A-S-H (sodium aluminosilicate hydrate): low calcium fly ash, activators and water
- C-(A)-S-H (aluminate-substituted calcium silicate hydrate): high calcium fly ash, activators and water

2.2.2.1 Activation of fly ash as the sole binder

Alkali solutions react with silicon and aluminium from fly ash; the final product from this process is often called a geopolymer (Davidovits, 1994). A general formula is proposed to describe the alkali activation products:

$$M_n[-(Si-O_2)_z-Al-O]_n \cdot wH_2O \qquad (1)$$
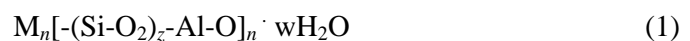
where M is the alkaline element, the symbol - indicates the presence of a bond, z is usually between 1 and 3, and n is the degree of polycondensation or polymerization.

Although theoretically almost any aluminosilicate can be activated, it is practically necessary to have a high availability of reactive silica and alumina (Panagiotopoulou, *et al.*, 2007).

There are some recommendations about fly ash characteristics for an activated system made by Fernandez-Jimenez and Palomo (2003):

- LOI percentage < 5%
- Fe_2O_3 and CaO ≤ 10%
- Reactive SiO_2 > 40%
- Particles < 45 μm: 80%-90%
- Glassy phase > 50%

Although the previous reference recommends low CaO contents, there are some ashes with higher values that could work even better than those with low CaO content.

A high concentration of OH^- is the main defining characteristic of alkali solutions (NaOH, KOH, water glass); the final product of the interaction of these materials with fly ash is an amorphous aluminosilicate gel (Palomo, *et al.* 1999).

Fernández-Jimenez and Palomo confirmed that the final product of this reaction is a low ordered crystalline structure composed of an alkali silicoaluminate gel which gives the final strength (Fernández-Jiménez and Palomo, 2005). Some zeolites could be as a secondary product; at some point this final product has been considered as *zeolite precursor*. The effect of high curing temperature on alkali-activated concrete is often positive, helping to increase the strength significantly, as it accelerates the dissolution process of the cementitious material (Mikuni, *et al.*, 2007). However, increasing time and temperature at some point increases zeolite formation and reduces gel content.

The effects of the concentration of sodium hydroxide and the activator to binder ratio were evaluated by Ravikumar, *et al.* (2010). It was found that alkali-activated ground granulated blast furnace slag (GGBFS) pastes were less porous compared to those based on fly ash; the latter contained a higher amount of pores of 10 μm in size. Curing at high temperatures (75°C) for mixes with fly ash was crucial

compared to slag mixes. Higher strength could be achieved by increasing the activator concentration and decreasing the activator to binder ratio. There was a shell around fly ash particles which stopped the activation process; it was found that due to the low reactivity of crystalline phases in the fly ash, the gel formation came from glassy phases only.

Alkali-activated concretes made with high calcium SCMs (Type C fly ash, slag) and water glass can have problems related to slump loss (Collins and Sanjayan, 1999); in the same way, setting time is decreased when water glass is included. Although strengths with water glass activators are similar to PC concretes, there are problems with shrinkage (Collins and Sanjayan, 1999).

Admixtures play an important role in geopolymer concretes. There are some opposite effects when activators are used; for instance, naphthalenes with water glass affect strength and workability while polycarboxylates do not produce any negative effect (Bakharev, *et al.*, 2000; Puertas, *et al.*, 2003), but also do not appear to function very effectively as superplasticizers. Water glass with air entraining admixtures causes low strengths and workability improvements. These activated mixes could change the effect of an admixture due to the pH; melamines are affected by a pH higher than 13. Admixtures with polypropylene glycol perform better than those mentioned before (Palacios and Puertas, 2004). Accelerating admixtures including Ca presents an accelerating effect. On the other hand, Mg does not present a significant effect (Lee and van Deventer, 2002). In the RILEM report (RILEM 224-AAM, 2014), it is concluded that the admixtures used for Portland cement concretes present a negative effect or do not work properly in alkali-activated binder systems.

When a test of alkali silica reaction is conducted for a PC and a geopolymer mortar, the latter expands less following ASTM C1260 standards (García-Lodeiro, *et al.*, 2007). Although alkali activated fly ash mortar expands less than PC, at some point after 30 days, it passes the maximum allowed expansion according to the test criteria. PC mixes present higher expansions than binary mixes, as the total calcium content affects significantly the expansion of mortars.

There are still some challenges which need to be solved before starting a real ready mixed concrete production. The following list of the main issues are based on Roy's research (Roy, 1999) and the recent RILEM report (RILEM 224-AAM, 2014):

1. Sourcing raw materials
2. Leaching of alkalis
3. Shrinkage
4. Carbonation
5. Long term performance
6. Alkali aggregate reaction
7. Air-entrainment agents
8. Standard admixtures for alkali activated concretes
9. Quality control
10. Standardisation
11. Database: costs, manufacture, and durability
12. Acceptance from the customers

Carbonation problem is not only related to steel depassivation but can also hinder strength gain. This phenomenon decreases pH levels, affecting fly ash activation resulting in low strength (Criado, *et al.*, 2005). Some of the solutions to this problem are thermal curing and sealed curing. It is important to consider additional alternatives such as varying the water to cementitious materials and improving the mix design in terms of permeability.

There are different opinions related to durability of concretes using high alkali contents. Pacheco-Torgal, *et al.* studied why there were different positions related to this topic; they were concerned about how for some researchers alkali activated binders performed better than PC and for some others it was still an unproven topic (Pacheco-Torgal, *et al.,* 2012). They concluded that in spite of the good observed chemical and ASR resistance, alkali activated concretes needed more research about carbonation effects; their resistance was lower compared to PC. In the same way, they considered that it was important to investigate efflorescence issues due to the fact that the possible solutions considered calcium aluminate admixtures or hydrothermal curing (Najafi Kani, *et al.*, 2012; Pacheco-Torgal, *et al.,* 2012). Figure 5 shows the

effect of admixtures. Pacheco, *et al.* concluded about the importance of finding different activators options due to their effect and costs.
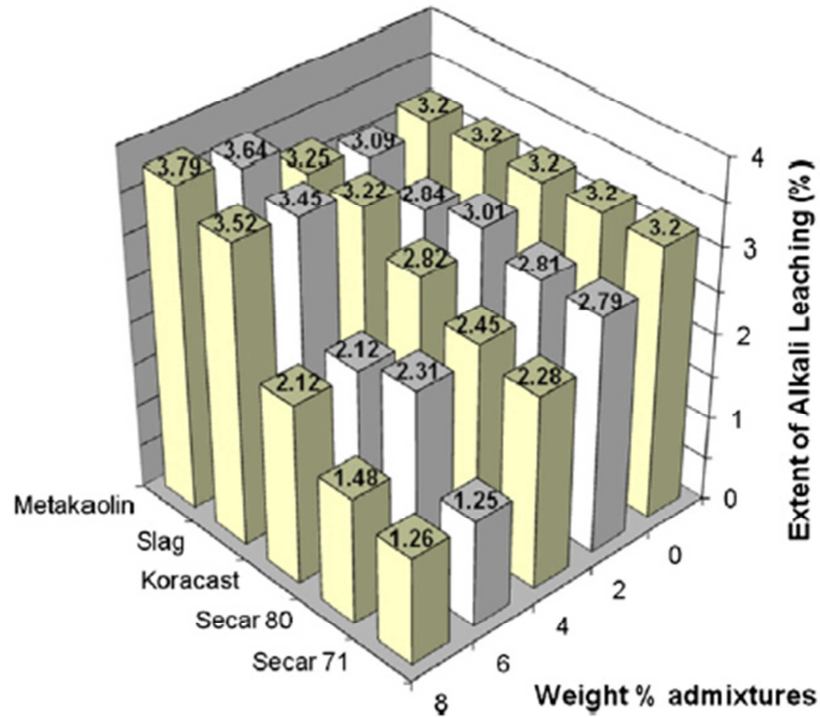
Figure 5 Alkali leaching for mixes with admixtures (Pacheco-Torgal, *et al.*, 2012)

The RILEM report (RILEM 224-AAM, 2014) recommends more work on comparing laboratory results with elements exposed to sulfates. In the case of alkali silica reaction, longer-term testing is needed. In terms of carbonation, the RILEM report mentions that samples older than 20 years presented a good resistance to carbonation in service, but as mentioned before, accelerated tests need to be compared to long term evaluations (RILEM 224-AAM, 2014). Although shrinkage could be higher for these concretes compared to PC concretes, curing and mix design could help to reduce it. On the other hand, creep is one of the topics which needs more lab work and model evaluation (RILEM 224-AAM, 2014).

2.2.2.2 Activation of high volume fly ash concrete

The experience of using high volume fly ash with both Portland cement and activators is not extensive; however, there are some studies which have focused on the strength evolution of mortar and concrete. The present main challenges are related to curing temperature, setting time delay, low early strength evolution and durability.

31

Calcium sulfate anhydrite ($CaSO_4$) and an amount of 55% of fly ash as cement replacement were studied using different curing methods (Poon, *et al.,* 2001); curing at 65°C per 6 hours before a normal curing allowed an increase in the strength by 70% compared to a control mix after 3 days (Poon, *et al.,* 2001). Large amounts of ettringite were found at early age. Gypsum was also used in this study; although gypsum was more effective than anhydrite for later age strength, anhydrite increased early age strengths. There was not a technical answer about this performance and it was recommended to conduct some further research. It was also mentioned the necessity of researching the durability of these concretes.

Portland fly ash and lime fly ash cements using Na_2SO_4 as activator increased in strength considering that the activation effect occurred at early ages (Qian, *et al.,* 2001). Na_2SO_4 had a better effect when using a higher fly ash percentage.

The following is a summary of the process using Na_2SO_4 (Qian, *et al.,* 2001):
1. Na_2SO_4 reacts with $Ca(OH)_2$

$$Na_2SO_4 + Ca(OH)_2 + 2H_2O \rightarrow CaSO_4 \cdot 2H_2O \downarrow + 2NaOH \qquad (2)$$

2. Reaction increases pH, accelerates the dissolution and pozzolanic reaction.
3. Ettringite formation due to the increase SO_4^{2-} concentration.
4. AFt (ettringite) increases the solid volume (164%), densifying the matrix and increasing early strength.

A mix with 30% Portland cement, 70% fly ash, and NaOH with water glass could achieve similar strengths compare to a control mix with 70% Portland cement and 30% fly ash (Palomo, *et al.*, 2007). This effect does not occur when using NaOH only. Although water glass allows the material to obtain the target strength, this activator increases the slump loss (Collins and Sanjayan, 1999). Donatello, *et al.*, (2014) evaluated pastes with high volumes of bottom ash (>70%) and sodium sulfate as activator. In this study, three gel phases were identified: C-S-H, N-A-S-H and C-A-S-H (Donatello, *et al.*, 2014).

When a type C fly ash (high calcium content) is activated, C-A-S-H is the main gel presented in the system, while on the other hand N-A-S-H is the gel produced

when a type F (low calcium content) fly ash is used with an activator. When Portland cement, type F fly ash and a sodium activator are used together, N-A-S-H and C-A-S-H are the final gels. Garcia-Lodeira, *et al.* studied a possible relation between these gels; N-A-S-H was stable at a low pH level (<12), while C-A-S-H was the predominant gel in the mix at a pH level higher than 12 (Garcia-Lodeiro, *et al.*, 2011).

One of the most effective alkaline activators is sodium silicate. At some point this activator has been used as an accelerator for shotcrete application. It is widely used in different applications such as adhesives, well cements, acid resistant concrete, and others (Shi, *et al.*, 2006).

K_2SO_4, Na_2SO_4, and triethanolamine were also studied in order to improve early strength behaviour (Lee, *et al.,* 2003). Figure 6 shows portlandite content for mixes with different activators at different ages. This study demonstrated a decrease in calcium hydroxide and an increment of ettringite when using 40% fly ash content. The latter effect helped to reduce the pore size. Strengths were mostly similar to the sample without activators; however, K_2SO_4 had the best effect, increasing the strength significantly. Lee, *et al.* summarized the sulfate activation mechanism in the following way:

1. It accelerates the reduction of $Ca(OH)_2$.
2. Glass phases are broken down due to a high alkaline environment. A high amount of ettringite is produced at early ages.
3. Pore size and porosity are reduced.
4. Early age strength is increased but there is not any improvement in later age strength.

Lee, *et al.* advised that more research is needed about the microstructure, and the effect of the activator dosage on strength evolution.
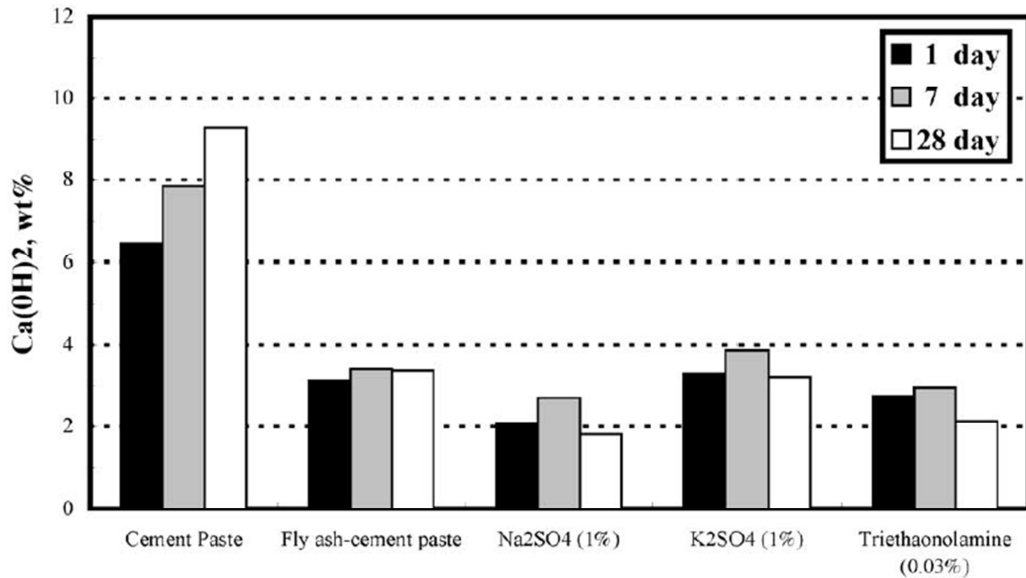
Figure 6 Amount of Ca(OH)₂ of cement paste, fly ash - cement paste, and chemicall (Lee, *et al.,* 2003)

Chemical activators such as sodium sulfate, calcium sulfate and sodium hydroxide have been used in cements with 50% fly ash replacement (Owens, *et al.,* 2010). Under different curing methods (first 24 hours at 60°C and the remaining 6 days at 20°C, against 7 days of curing at 20°C) each activator behaved in a different way. Calcium sulfate performed better for the first curing method, and sodium sulfate for the second curing method. After 1 and 7 days, it was possible to identify some unreacted anhydrite and gypsum. Sodium sulfate and calcium sulfate formed ettringite and C-S-H gel.

Donatello, *et al.* (2013) evaluated high volume fly ash pastes (80% fly ash and 20% PC clinker) using sodium sulfate as activator. According to this study, the reduction of the setting time and the increase of the compressive strength are due to the presence of SO_4^{2-} helping the alite dissolution (Donatello, *et al.,* 2013). In this study, a pH indicator is the level of ettringite formation; as alkalinity increases the formation of ettringite is inhibited. Ettringite is evident in the XRD presented in Figure 7. The same authors evaluated mortars with 80% fly ash, 20 % PC clinker and anhydrous sodium sulfate; in this case, this mortar presented an adequate resistance to sea water and sodium sulfate compared to mortars with a sulfate resistant cement. This was not the case when they were immersed in acid, being strongly degraded (Donatello, *et al.,* 2013).
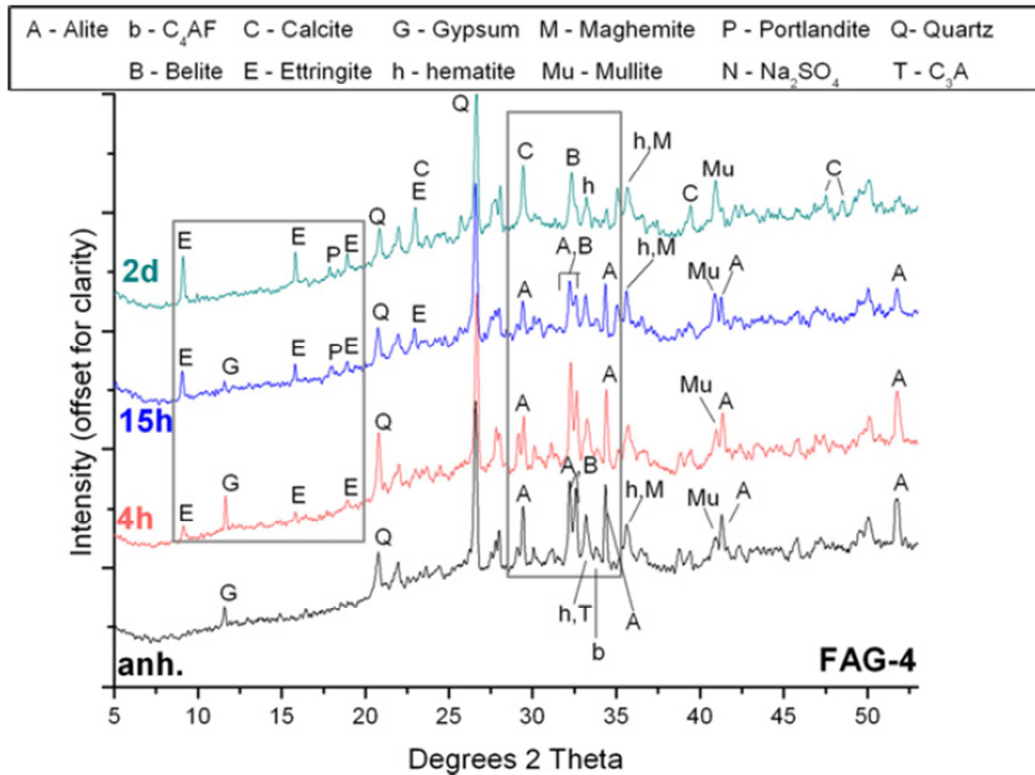
Figure 7 XRD for a mix with 78% FA and 4% Na$_2$SO$_4$ (Donatello, *et al.,* 2013)

High volume fly ash with sodium sulfate concretes need to be studied in terms of durability due to the lack of information. As mentioned by Lee *et al* and Shi and recent RILEM report (RILEM 224-AAM, 2014) mixes including activators needed more research in terms of shrinkage, carbonation, long term performance and alkali aggregate reaction

2.2.3 Mechanical activation

Paya, *et al.,* studied the effect of fineness on fly ash activity; they noticed some effect in mineralogical composition when changing the fly ash particle size, as the free calcium oxide present reacted with carbon dioxide to produce calcium carbonate. An increase in specific gravity was observed after the ash was crushed (Paya, *et al.,* 1995). The grinding process could be optimized depending on the time this process takes; for a specific fly ash, there was not a significant size change after 30 minutes of grinding.

As shape and morphology are affected by grinding and the spherical shape is lost, the ground fly ash material could not work as a water reducer after this process,

resulting in an increment of the water requirement for a given slump. Although specific gravity increased, bulk specific gravity decreased (Paya, *et al.,* 1996). Strength was directly affected by the particle size of the fly ash; as the size increased, strength decreased (Paya, *et al.,* 1997).

A higher specific surface area positively affects the pozzolanic activity of fly ash as seen in Figure 8. Grinding not only affects the specific surface area but also introduces imperfections to the original structure of the material; these defects are active centres which are in a higher energy state (Shi and Shao, 2002). For instance, in the quartz grinding process different physical and chemical characteristics change; some of these changes include particle breakage, surface area increase and surface amorphization (Mohammadnejad, *et al.,* 2013).
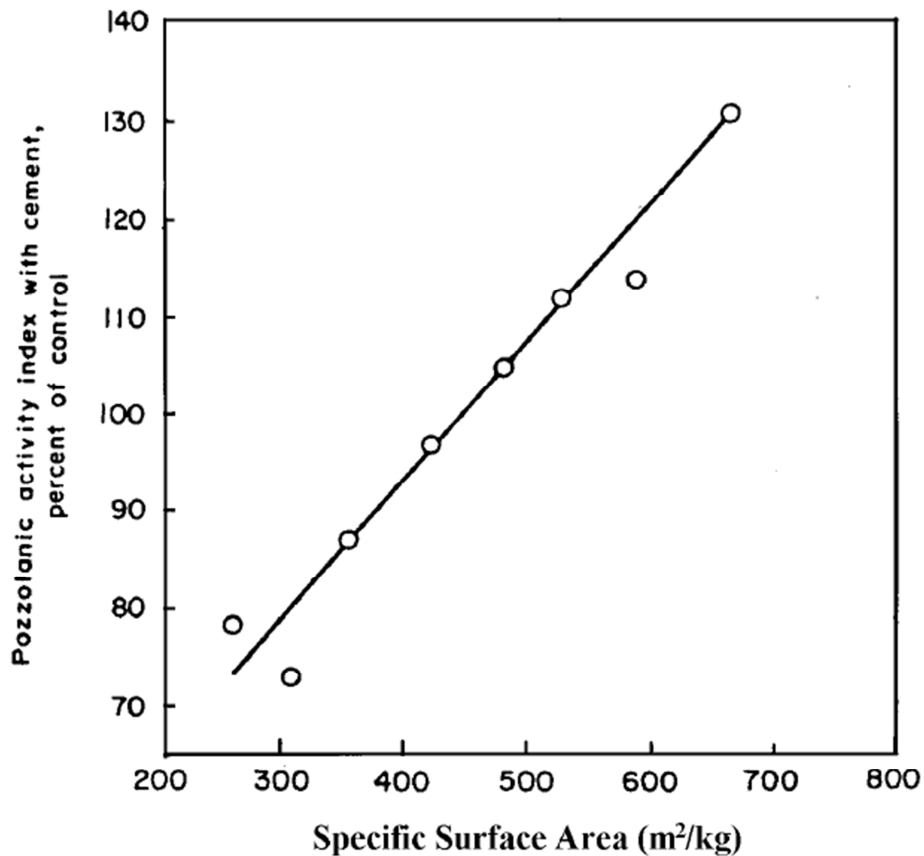
Figure 8 Pozzolanic activity index vs specific surface area (Shi and Shao, 2002)

Although increasing fly ash fineness by grinding could increase water requirement, this is not the case when an increased fineness is obtained by sieving the

material. In this case, the original shape of fly ash is kept the same, the glass content is increased, and the water requirement is reduced (Chindaprasirt, *et al*., 2001; 2004). The increase in the reacted calcium hydroxide using the fine fly ash compared to the coarse fly ash shows the significant effect of particle size on the pozzolanic reaction (Lee, *et al.*, 1999).

Strength is positively affected by sieving of ash, as is sulfate attack resistance (Erdogdu and Tucker, 1998; Chindaprasirt, *et al*., 2004); PC plus coarse fly ash mortar mixes are damaged by sulfates when they are exposed to this environment. Expansions are lower for mortars with fine fly ash. Shrinkage is also affected positively considering that a fine fly ash requires less water than a coarse fly ash. The pore volume of pastes is reduced by the inclusion of fine fly ash, helping to reduce the ingress of chemical solutions (de Belie, *et al.*, 1996; Chareerat, 2002).

A blended cement with 50% to 60% mechanically treated fly ash has the same compressive strength as a cement including 15% to 25% of fly ash without treatment (Kumar, *et al.,* 2007). In terms of geopolymers using fly ash with mechanical treatment, it allows designers to obtain different favourable characteristics of the products; for instance, a high strength geopolymer cement with 120 MPa (Kumar, *et al.,* 2007). In the same way for geopolymers, when fly ash is mechanically activated, a significant increment in compressive strength can be accomplished at ambient temperatures; there is an inverse correlation between the fly ash median size and compressive strength (Kumar and Kumar, 2011).

Mechanical treatment is an alternative to improve the performance of concrete with hybrid cementitious systems or geopolymers. Fly ash after a sieving process reduces both water and the pore volume size. On the other hand, although crushing the material increases water demand, this process creates defects that become active centres, increasing the reactivity. Costs are important to be defined for this highly energy demanding process; although mechanical treatment of fly ash helps to improve the performance of concrete, it is important to evaluate cost impact considering all the possible scenarios.

2.3 Deterioration of concrete

The deterioration of a concrete structure depends on its permeability; gases, ions and liquids penetrate the structure, reacting with concrete constituents and affecting the element. In this way, matrix deterioration is due to physical causes and chemical reactions (Mehta and Gerwick, 1982; Long, *et al.*, 2001; Basheer, *et al.*, 2001). Van Deventer, *et al.*, also illustrate how permeability is the main parameter to consider in terms of concrete durability (Van Deventer, *et al.*, 2012). Pores present in the matrix (aggregates, cement paste–aggregate interface and cement paste) affect different concrete mechanical properties such as strength and modulus of elasticity (Basheer, *et al.*, 2001).

2.3.1 Transport mechanisms

Penetration of different liquids, gases and ions in concrete and their movement inside the matrix are basically due to absorption, permeability and diffusion (Long, *et al.*, 2001); these processes depend on physicochemical gradients: pressure, concentration, temperature, voltage and humidity.

2.3.1.1 Absorption

Absorption occurs due to capillary forces in a non-saturated concrete (Bentz, *et al.*, 1999); water at the surface enters the structure and fills available pores depending on the concrete moisture content. The absorption tends to follow a linear pattern with respect to the square root of time in a specific range of time, and the correlation of this linear behaviour is known as sorptivity. There are often non-linear regions before and after the linear region. For instance, following the process proposed in ASTM C 1585, the absorption has a linear behaviour in the first day of being measured and in the following 7 days the rate of absorption decreases with a lower slope in the absorption increment from day 1 to 8.

The following equation was introduced (Hall, 1981):

$$i = st^{-0.5} \tag{3}$$

Where i is known as absorption, s is sorptivity and t is time. Then this equation was modified including a rapid initial absorption A (Hall and Tse, 1986):

$$i = st^{-0.5} + A \tag{4}$$

Absorption is a parameter which correlates effectively with other durability parameters; Basheer studied the effect on absorption of different water to cementitious material ratios (Basheer, *et al.*, 2001), and found that water absorption inter-relates with carbonation depth and chloride concentration. In the same way, open porosity measured by using absorption increases when the water to cementitious material ratio increases and the duration of the curing process is reduced (Rabehi, 2013).

Concretes with 50% of a high quality fly ash (19% retained on a 45μm sieve) and a water to cementitious material of 0.4 have a lower capillary water sorption, compared to a mix with 100% PC at 28 and 91 days (Van den Heede, *et al.,* 2010). From this study, a linear correlation was obtained between the permeable porosity (%) and capillary water (kg/m^2). On the other hand, an increase in water absorption, porosity, and initial and secondary sorptivity were found for high volume fly ash mixes (higher than 50%) probably due to the low fineness of fly ash and the curing conditions (23°C, RH 95% for 7 days, then air curing at 23°C, RH 50% from 8 to 28 days). By including FA with metakaolin (MK) and PC, the performance in terms of water absorption, porosity and sorptivity is improved (Özbay, *et al.,* 2010). In this study, the Blaine fineness of MK was higher, helping to increase the pozzolanic activity and reduce pores in the structure.

High volume fly ash concretes with low and high volume of paste were studied by Dinakar. It was found that absorption increased by increasing the paste content, considering an increase in pores (Dinakar, *et al.,* 2008). By increasing fly ash content in terms of weight, paste volume and capillary pores increase.

Another study evaluated concretes with alkali activated blends of slag and metakaolin; from this evaluation concretes with 10% of metakaolin presented the lowest absorption; on the other hand, 100% slag concrete had the highest water penetration (Bernal, *et al.,* 2012). Bernal also studied the effect of carbonation on absorption, finding an increase in the porosity of mixes exposed to CO_2 after 340h. Although there was a high absorption for mixes at 340 h, after this time this parameter was not affected significantly, possibly due to the space filling effect of the carbonation products (Bernal, *et al.,* 2010).

When fly ash content is increased in a combination of slag/fly ash geopolymer mortars (100/0, 70/30, 50/50, 30/70, 0/100), the absorption increases (Chi and Huang, 2013). As seen in Figure 9 absorption is higher for mixes with slag and fly ash than mixes with 100% cement (Ismail, *et al.,* 2013). The same authors mentioned that the microstructure of a C-A-S-H gel is higher in density than alkali aluminosilicate gels. The pre-drying process for absorption evaluations produces desiccation and chemical changes in C-A-S-H gels (Ismail, *et al.,* 2013). From a research work using X-ray microtomography, microstructures and pore networks of activated slag/fly ash pastes were analyzed (Provis, *et al.,* 2012). From this study, it was evident that an increment in curing time for mixes with 50% or higher slag content reduced the total porosity and increased the pore network tortuosity. Space filling C-(A)-S-H gel was the main binder in mixes from 25% to 50% of slag while for lower percentages was N-A-S-(H), which had a lower pore network obstruction due to the fact that this gel do not chemically bind water (Provis, *et al.,* 2012). Another study showed an increment in the percentage of permeable volume by including fly ash in mixes with slag (Aydin, 2013). On the other hand, the use of fibres helps to reduce water absorption for mixes with alkali activated slag (Bernal, *et al.*, 2010; Rashad, 2013). Increasing the fibre volume reduces absorption (Bernal, *et al.*, 2010). The effect of fibres seems to be the same as for plain PC, reducing the water transport due to the crack control effect.
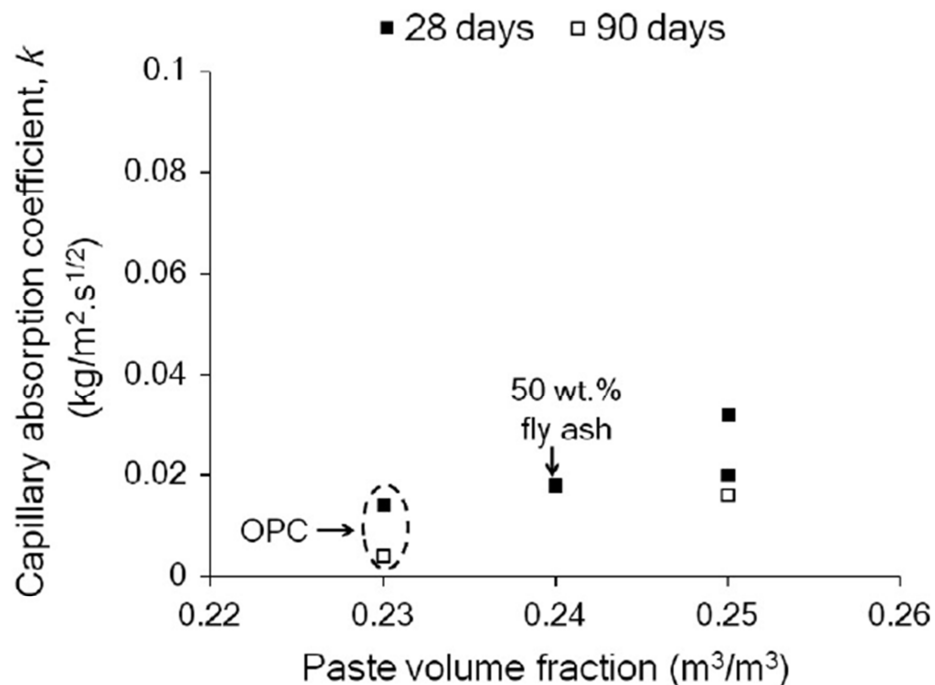
Figure 9 Absorption coefficients vs paste volume fraction (Ismail, et al., 2013)

2.3.1.2 Permeability

Permeability is related to how easily a fluid passes through a matrix due to a pressure gradient. This parameter in concrete is evaluated by applying a pressure of water or air on a specimen and measuring the passage of the fluid through the matrix. One way to characterize concrete permeability for laminar flow is by calculating the coefficient of water permeability based on Darcy's law:

$$Q = \frac{KA\Delta h}{l} \tag{5}$$

Where:

Q = flow rate [m^3/s]

K = water permeability [m/s]

A = cross section area [m^3]

Δh = water pressure differential across the specimen [m]

l = length of the specimen [m]

The following is the intrinsic permeability based on Darcy's law:

$$Ki = \frac{Q\eta l}{A\Delta P} \tag{6}$$

Where:

Ki = intrinsic permeability [m^2]

η = viscosity of the fluid [N.s/ m^2]

ΔP = fluid pressure head across the sample [N/m^2]

l = length of the sample [m]

Based on Equations (5) and (6), the intrinsic water permeability can be defined:

$$Ki = K\frac{\eta}{\rho g} \tag{7}$$

It is important to mention that the previous equation applies only for saturated samples and where water is present both up-stream and down-stream. In the case where water does not penetrate the complete sample, Valenta proposed an equation for the water permeability coefficient calculation based on the depth of water penetration (Valenta, 1970):

$$K = \frac{d_p^2\delta}{2ht} \tag{8}$$

Where:

d_p = depth of water penetration [m]

δ = sample porosity [%]. This parameter is calculated from the weights before and after the test is performed and using the penetration depths.

t = time to reach d_p [s]

h = head of water [m]

Claisse mentioned that 10^{-12} m/s would be the order of magnitude of concrete permeability and 10^{-19} m^2 for the intrinsic permeability (Claisse, 2005). The Colombian standards NTC 4483 classifies the water permeability coefficient and the penetration depth as "Low" (10^{-12} m/s, <30mm), "Medium" (10^{-12} - 10^{-10} m/s, 30 - 60 mm) and "High" (10^{-10} m/s, >60 mm); this test considers a constant pressure of 0.5 MPa during a test duration of 4 days.

Considering the effects of different variables affecting water permeability of concrete, this parameter can be correlated to compressive strength. In general, when strength increases, the water permeability decreases (Armaghani, *et al.*, 1992; Khatri, *et al.*, 1997), as both are related to the microstructural development of the material.

Water permeability was evaluated for mixes including PC, fly ash and calcium carbide residue; From Figure 10 it is seen how water permeability values became closer between all the mixes (PC, calcium carbide residue + PC, and fly ash + PC) as the compressive strength increased (Amnadnua, *et al.,* 2013). There was an effect of the curing process, where water permeability decreased by increasing the time of curing. By increasing the Portland cement content (from 10% to 20%), water permeability decreased; this research proposed a correlation between compressive strength evolution and water permeability. Another study shows how an increment of the water to cementitious material ratio increases the permeability coefficient of geopolymers (Olivia, *et al.*, 2008). Although there was a trend in this case, these values were in the low to medium water permeability range, and the permeability of geopolymer concrete was affected by the water to cementitious material ratio and the aggregate grading. These parameters had the same effect as in the PC concretes.
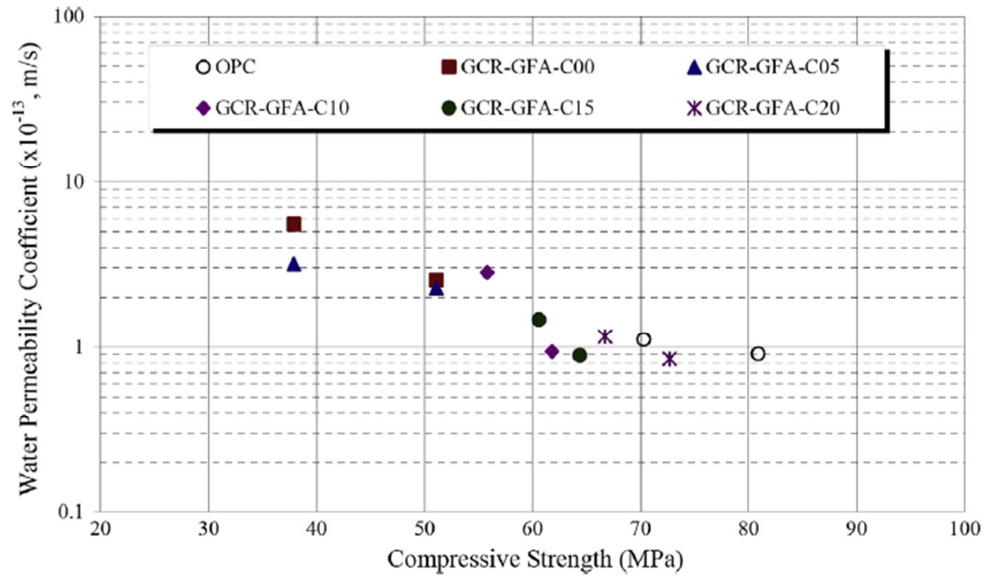
Figure 10 Water permeability coefficient and compressive strength relationship (Amnadnua, et al., 2013)

Water permeability of inorganic polymer concretes (rice husk, bark ash and fly ash) with sodium hydroxide and sodium silicate solutions is highly controlled by the SiO_2/Al_2O_3 (S/A) ratio (Wongpa, *et al.,* 2010): it not only controls water permeability but also compressive strength and modulus of elasticity. High S/A ratios led to low water permeability while low S/A ratios led to high water permeability. In the case of compressive strength, it increases 30% at 28 days when S/A≥1.9. The modulus of elasticity increases for S/A≥1.65 at 28 days (Duxson, *et al.*, 2007).

As mentioned before, when water permeability or absorption is evaluated for alkali activated mixes with fly ash and slag, the pre-treatment of the samples could have a negative effect (Ismail, *et al.,* 2013). The Colombian standard NTC 4483 does not require pre-treatment for the specimen and the evaluation starts just after 28 days of curing (ASTM C 192). The procedure of this test is mentioned in Chapter 6.

2.3.1.3 Diffusion

Diffusion is a transport mechanism which occurs due to a chemical potential or a concentration gradient (Claisse, 2005); some of the influencing parameters are the capillary pores size, concentration gradient, composition of the solution and cementitious material composition. Depending on the elements mentioned before, ions will move from areas of high to low concentration (Martys, 2005), and Fick's first law describes this movement for steady-state diffusion. In Fick's first law and in the

43

steady-state diffusion case in general, pressure and velocity are considered to be constant at any time (Crank, 1975):

$$J = -D \frac{\partial C}{\partial x} \qquad (9)$$

Where:

J = diffusive flux

D = diffusion coefficient

$\frac{\partial C}{\partial x}$ = concentration gradient

Fick's second law is considered for non-steady diffusion; the evolution of concentration with time at a specific depth can be described with equation 10:

$$\frac{\partial C}{\partial t} = -D \frac{\partial^2 C}{\partial x^2} \qquad (10)$$

Crank's solution is used for this previous differential equation:

$$C(x,t) = C_0 \left(1 - erf \left(\frac{x}{2\sqrt{D_c t}} \right) \right) \qquad (11)$$

Where:

$C_{(x,t)}$ = chloride concentration at a defined depth x and time t

C_0 = chloride concentration on the surface

D_c = diffusion coefficient (m^2/s)

erf = error function

Chloride diffusion

It is important to consider that the diffusion coefficient varies with time and that concrete is not homogeneous, as is assumed in the equations presented above. In this way, it is important to find this apparent coefficient through concrete evaluation tracking all the internal and external variables (Garboczi, 1990; Basheer, *et al*. 2001).

Supplementary cementitious materials used as a partial cement replacement often reduce chloride penetration; for instance, some results at 90 days and after show the advantage of including this pozzolanic material (Aït-Mokhtar, *et al.*, 2013; Deby, *et al.*, 2009). The reduction of chloride diffusion coefficient is not only achieved with the blending with fly ash, but also slag and metakaolin (Mejía, *et al.*, 2003; Thomas and Bamforth, 1999; Boddy, *et al.*, 2001). However, it is necessary to explore more how mixes with these materials mitigate corrosion in these environments due to the high variability (Shi, *et al*., 2012). The variability affecting the characterization of

chloride penetration is observed because there are different parameters affecting it, such as the type of the supplementary cementitious material, water to cementitious material ratio, cement type, curing, exposure condition and other factors. For instance, for concretes with 55% and 70% fly ash, an inadequate curing regime plus a low fineness of the fly ash could increase the concrete chloride penetration (Özbay, *et al.*, 2012).

In other case, normal strength concrete with silica fume has almost the same performance compared to a high performance concrete in terms of chloride diffusion (Baroghel-Bouny, *et al.*, 2011). The performance is improved with age and water curing, especially for fly ash concretes. It is important to consider that a high volume fly ash concrete (30%, 40% and 50%) could have poor performance compared to an PC concrete at 28 days, whereas after 90 days or a year this performance is improved as seen in Figure 11 (Burden, 2003). Comparing performance between HVFA (50%, 70% 85% fly ash) normally vibrated concretes and HVFA self compacting concretes, there is a reduction of the diffusion coefficient for the latter case, by 2 to 8 times (Dinakar, 2008), probably due to the differences in mix design and components.
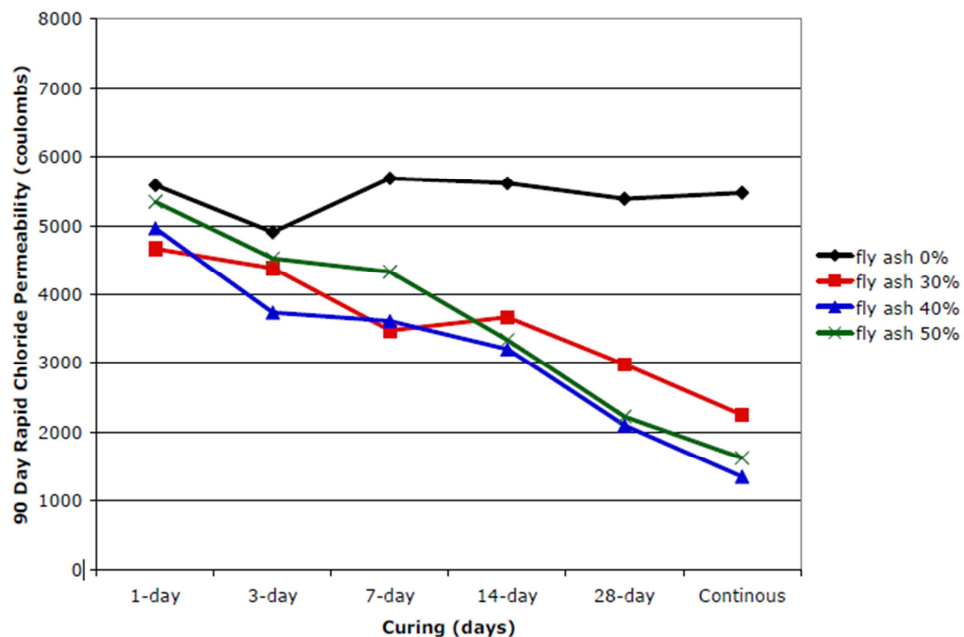
Figure 11 90 day RCP vs curing time (Burden, 2003)

The diffusion coefficient for specimens with pozzolans has been observed to be higher for samples exposed in a splash zone than in a tidal zone, while the opposite

behaviour occurs for mixes without pozzolans (Valipour, *et al.,* 2013). This is because this natural pozzolan (zeolite) requires a longer curing process and the tidal zone offers a constant curing, improving its properties with time. In that study, the amount of chloride concentration at 20 mm varied in concentration in the following order: splash>tidal>soil>atmosphere zone. This is due to the process in the splash zone, where the sprayed sea water evaporates, leaving the chloride ions crystallized and accumulated on the surface. In this way capillary absorption and diffusion mechanisms are present, influenced by moisture and oxygen. On the other hand, the chloride concentration on the surface followed the inverse order, which could be related to the presence of water which washes chlorides from the surface.

Ionic diffusivity depends strongly on water content and at some point there is a saturation level where the connection of the pores allows ions transport to increase (Zhang and Zhang, 2014). In this way the degree of saturation takes a significant role in chloride ion diffusion (Guimaraes and Helene, 2005). It is important to mention that parallel to diffusion, ion transport also includes convection (absorption and hydraulic pressure) and electrical potential, and the combination of these three mechanisms is considered in the Nernst – Planck equation to describe ion transport (Zhang and Lounis, 2009).

In terms of chloride ingress, well cured and good quality concretes with alkali activation can perform better than PC concretes (Roy, *et al*. 2000; Rashad, 2013; Ismail, *et al.,* 2013); this is presented in Figure 12. This is due to the microstructural reaction which reduces chloride penetration. Comparing different alkali activated binders, mixes with slag have a better performance than those with fly ash; there is an increase of chloride sorption with fly ash content (Ismail, *et al.,* 2013). Under steady state chloride diffusion, activated and non-activated mixes with 0% to 100% slag as PC substitution have a tendency of reducing the diffusion rate with slag increase. Roy *et al*. found that the steady state diffusion coefficient of PC-containing alkali-activated binders using slag (60% slag – 40% PC) and NaOH could be reduced to half of the values obtained with 100% PC concretes, using the test proposed by Hansson and Berke (1989)
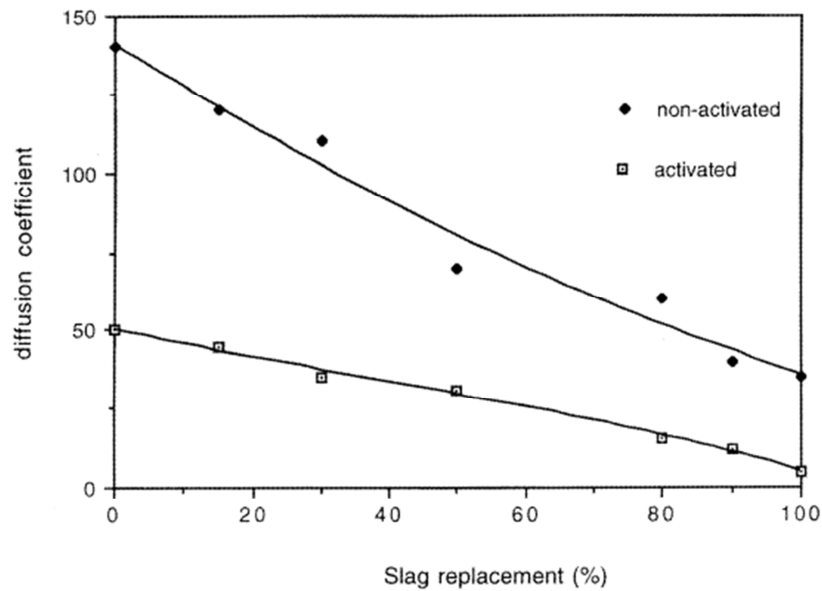
Figure 12 diffusion coefficient (10^{-15} m^2 s^{-1}) vs slag % (Roy, *et al*. 2000).

Ravikumar and Neithalath evaluated slag concretes using as activator alkali silicate powder and obtaining low chloride penetration with the rapid chloride permeability test (RCP), compared to water glass activated concretes and PC concretes. Relating the non-steady state migration, these values were similar for both the activated and PC concretes (Ravikumar and Neithalath, 2013). In this study, the correlations were similar between the critical pore sizes and SiO_2 to Na_2O ratio, and the RCP or non-steady state migration and SiO_2 to Na_2O ratio.

Concretes with activated slag including high activator (Na_2O) concentrations have higher chloride permeability using ASTM C 1202; this is probably due to the pore solution alkalinity (Bernal, *et al*., 2012; Puertas, *et al.,* 2004); in Bernal's study, chloride diffusion coefficients were coherent with sorptivity coefficients at 28 days. The addition of metakaolin to the mix reduced the diffusion coefficient, probably due to pore structure refinement.

Carbon dioxide diffusion and carbonation

Carbonation involves CO_2 diffusion through the pores and reactions with calcium silicate hydrates and calcium hydroxide; the consequence of the previous processes is a reduction in the pH levels (<9) (Pourbaix, 1974). Fick's first law is sometimes used to model CO_2 diffusion. Tutti's model uses the diffusion law to calculate the carbonation depth (Tutti, 1980):

47

$$x = K\sqrt{t} \qquad\qquad (12)$$

Where:

x = Carbonation depth (mm)

K = Carbonation coefficient (mm/year$^{1/2}$)

t = Time (year)

Different variables affect the carbonation coefficient, such as relative humidity, dry and wet cycles and CO_2 concentration (Castellote, *et al.*, 2009; Parrot, 1987). Based on all of these influencing parameters, there are different models referenced in different technical papers (Nagataki, *et al.*, 1986; Sisomphon and Franke, *et al.*, 2007; Ribeiro, *et al.*, 2003; Parrot, 1994; Papadakis, *et al.*, 1989).

One of the main parameters affecting the carbon dioxide diffusion is the water saturation degree (Thiery, *et al.*, 2007). When the cement is air cured, the carbonation coefficient increases, by as much as a factor of 10^4 compared to water curing (Younsi, *et al.*, 2011). A reduction in the water to cementitious material ratio and an increment in the curing time reduce the carbonation depth due to pore reduction (Claisse, 2005; Helene and Castro-Borges, 2009; Rabehi, *et al.*, 2013); water evaporation from concretes with higher water to cementitious materials ratios leaves pores, increasing the opportunity for carbon dioxide diffusion. In this study, there was a correlation between carbonation depths at 180 days and compressive strengths at 28 days. The carbonation depths for concretes with clinker and slag in external elements could be reduced with 150-175 kg/m^3 of these materials compared to conventional concrete (Proske, *et al.*, 2013).

For high volume fly ash concretes this effect is more relevant. Comparing mixes with 30% and 50% FA, the air curing increased the carbonation depth for HVFA concretes but when they were cured in water the carbonation depth was similar. A relative humidity between 50% and 70% increases carbonation compared to other relative humidity levels (Wierig, 1984; Saeki, *et al.*, 1991). Capillary pores are dry when a low relative humidity is present while they are saturated when relative humidity is high reducing the carbonation process (Thiery, *et al.*, 2007). Another factor influencing the difference of carbonation between 100% cement and HVFA concrete is the low portlandite content of the latter (Younsi, *et al.*, 2011); depending on the amount of portlandite, the carbonation process could be delayed considering that CO_2

reacts with portlandite (Papadakis, *et al.*, 1989). This study described how porosity could not be directly correlated to carbonation parameters; although 100% cement and HVFA concretes had similar porosities following different curing procedures, the latter had a higher carbonation depth. Figure 13 shows how concretes with 30% to 50% of fly ash at 28 days and 1 year without a curing treatment have a higher carbonation depth compared with 100% PC concretes (Burden, 2006).
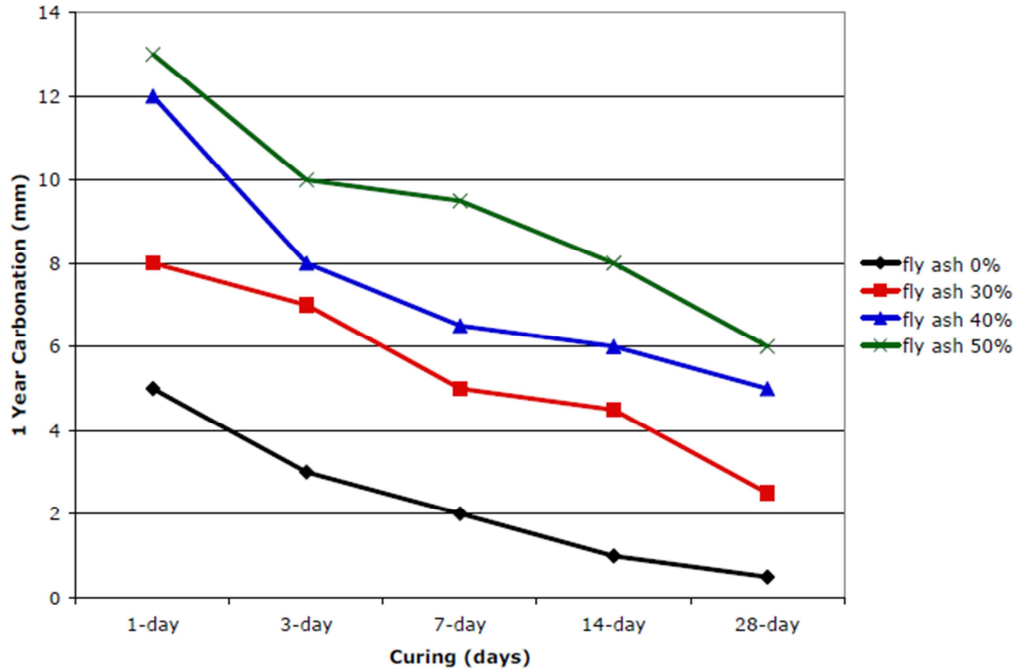
Figure 13 1 year outdoor carbonation vs Curing (Burden, 2006)

Samples including metakaolin in alkali activated slag mixes have an increment in carbonation depth when the replacement of slag by metakaolin is increased (Bernal, *et al.*, 2010). In this work, activated mixes with slag increased their carbonation depth when a low SiO_2/Na_2O ratio was used; the effect was reversed with metakaolin addition. Rashad compiled literature about alkali activated systems and found that different authors agree with the previous conclusion about the increment of the carbonation depth with the metakaolin increment in slag mixes (Rashad, 2013). Although there can still be different disadvantages with alkali activated slag mixes such as shrinkage, efflorescence, and carbonation, depending on the activator and mix design these problems can be mitigated.

In alkali activated mixes, the combination of slag and fly ash reduces carbonation compared to 100% fly ash geopolymer, lowering porosity due to the gaps filling with additional C-S-H gel formation (Nasvi, 2013). As seen in the X-ray microtomography the pore network tortuosity increases with the increase of slag in slag/fly ash pastes (Provis, *et al.*, 2012). This is presented in Figure 14. C-(A)-S-H is present as the slag percentage increases (25-50%), increasing the pore network tortuosity while for low slag contents (<25%) N-A-S-(H) gel predominates reducing the pore network obstruction. A high CO_2 concentration reduces compressive strength, and increases permeability in alkali activated mixes (Bernal, *et al.*, 2012). From this study, it was concluded that carbonation is not only controlled by CO_2 diffusion due to the fact of a nonlinear relationship between porosity and carbonation depth, and that tests performed during long periods would help to evidence what the other parameters controlling carbonation are.
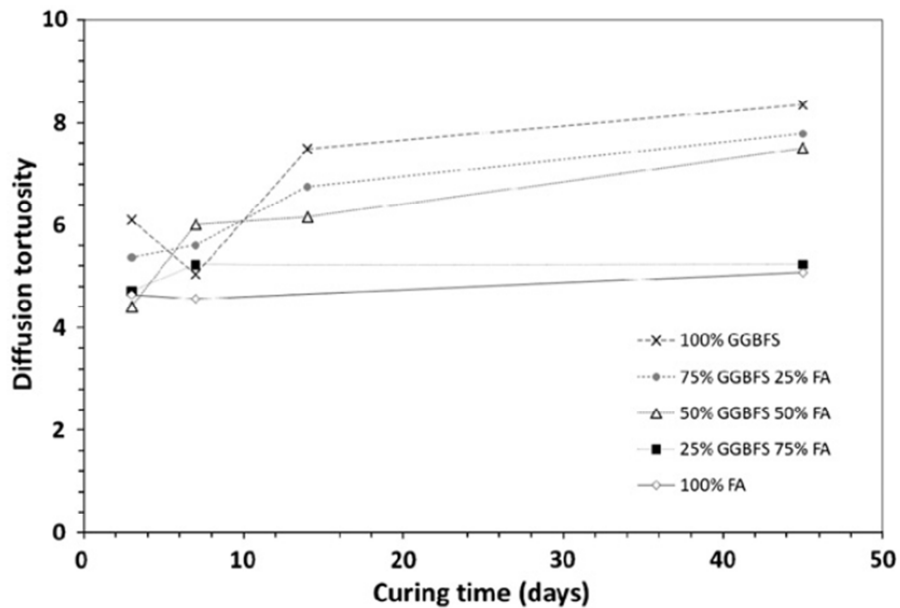
Figure 14 Diffusion tortuosity vs curing time (Provis, *et al.*, 2012)

2.3.2   Service life

Service life is defined as the period of time where a concrete element maintains acceptable performance (Pommersheim and Clifton, 1985). The American Concrete Institute specifically defines service life as "the period of time after installation during which all the properties exceed the minimum acceptable values when routinely

maintained" (ACI 365.1, 2000). The ACI standards references Tutti's model to divide the service life into two periods: initiation and propagation (Tutti, 1982). The model is presented in Figure 15. The period of initiation is the time which is taken for chlorides or carbon dioxide to pass through the concrete cover and reach a concentration where steel reinforcement starts to corrode (Conciatori, 2005; Conciatori, *et al*., 2008). The propagation period is the time between when corrosion starts, and when the element actually fails.
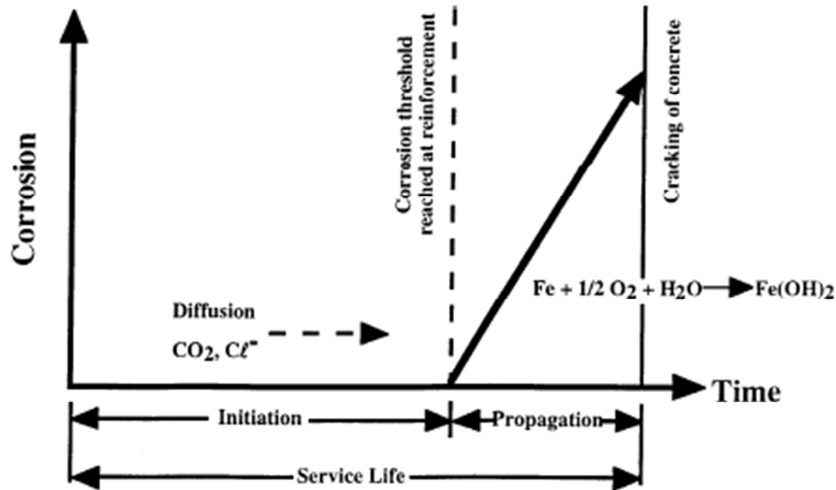
Figure 15 Service life model for steel corrosion (Tutti, 1982; ACI 365.1, 2000)

2.3.2.1   Carbonation

As mentioned before and referencing Tutti's model, in the carbonation process, the initiation period begins when the structure life starts until the concrete pH is reduced due to carbonation at levels that affects the steel passive layer. According to this model, when the carbonation depth is equal to the concrete cover depth, corrosion can occur. After ending the initiation period, the propagation period starts, being influenced by oxygen or presence of water, causing volume changes in the steel bar and cracks in the element. This period ends with a cracked or collapsed element. Although in a practical sense the service life is the sum of the initiation and propagation period, in most cases the initiation period is considered as the total service life. This is due to the difficulty in calculating the propagation period, and by not considering it, thus providing a safety factor (Monteiro, *et al.*, 2012).

Considering carbonation as a steady-state process, the carbonation depth can be described in the following equation (He and Jia, 2011):

51

$$L = \sqrt{\frac{2D_eC_s}{w_o}}\sqrt{t} \qquad (13)$$

Where,

L = Carbonation depth [m]

D_e = Effective diffusion coefficient [m^2/s]

C_s = Carbon dioxide coefficient at the surface [%]

w_o = Carbon dioxide absorbed per unit volume of concrete [kg/m^3]

t = Carbonation time [s]

As seen in equation 13, although carbonation depth increases as the diffusion coefficient increases, the carbonation coefficient is reduced as the absorbed carbon dioxide is increased. This effect is due to permeability reduction in the concrete matrix.

An additional analytical expression for fly ash blended Portland cement which includes the relative fractions of CH and C-S-H was also proposed (Wang and Lee, 2009).

$$x_c = \sqrt{\frac{2D_e[CO_2]_0 t}{[CH]+3[CSH]}} \qquad (14)$$

$$D_e = A\left(\frac{\varepsilon_c}{\frac{C}{\rho c}+\frac{P}{\rho P}+\frac{W}{\rho w}}\right)^a \left(1 - \frac{RH}{100}\right)^b \qquad (15)$$

Where,

x_c = Carbonation depth [m]

D_e = Effective diffusion coefficient [m^2/s]

$[CO_2]_0$ = CO$_2$ in the ambient air [%]

ε_c = Porosity [%]

ρc = Cement density [kg/ m^3]

ρP = Fly ash density [kg/ m^3]

ρw = Water density [kg/ m^3]

C = Cement content [kg]

P = Fly ash content [kg]

W = Water content [kg]

A, a, b = Parameters based on experimental results

As mentioned before, portlandite helps to delay carbonation. In the previous equation, portlandite content is included and directly reduces the carbonation coefficient. Porosity, presented as ε_c also has an influence increasing the carbonation

diffusion coefficient. According to equation 15, as the paste volume is increased the carbonation diffusion is reduced. The efficiency of the carbonation diffusion equation must be evaluated due to the fact that in the proposed scenario fly ash has the same effect as cement. From the previous equation, it is also needed to evaluate how the increment of the relative humidity reduces carbonation diffusion because as mentioned by Tutti, there is a certain relative humidity range where concrete carbonation rate reaches the maximum level and after this period it decreases significantly (Tutti 1980).

According to Morandeau, *et al.*, (2014), CH carbonation is reduced with time while C-S-H keeps carbonating. Porosity is reduced with carbonation due to the effect on the microstructure (Morandeau, *et al.*, 2014).

As mentioned before, Tutti's model is based on Equation 12. Different parameters have been included to this equation by researchers and standards, depending on environmental conditions, mix designs, etc. The Spanish standard *La Instrucción Española del Hormigón Estructural EHE*, includes different parameters affecting the carbonation coefficient (*EHE*, 2008). As seen in Equation 16, this coefficient is affected by the environmental conditions, air content, cementitious material and compressive strength.

$$K = c_{env}c_{air}af_{cm}^b \tag{16}$$

$$f_{cm} = f_{ck} + 8 \tag{17}$$

Where

c_{env} = Environmental coefficient

c_{air} = Air content coefficient

a, b = Cementitious material coefficients

f_{cm} = Mean compressive strength [N/mm^2]

f_{ck} = Characteristic compressive strength [N/mm^2]

The inclusion of compressive strength in the standards allows easy correlation between the main parameters of a concrete and the carbonation coefficient. This helps concrete specifiers and designers to have an approximate value related to carbonation depth. Although probably the accuracy is not as the one obtained with the equations including the effect of CH and C-S-H, it is a practical and simple way to have an approximation.

The Comité Européen du Béton CEB applies a carbonation model considering the compressive strength, environmental conditions and curing type in empirical equations (CEB, 1997; Marques, *et al.*, 2013).

$$x = K_{CO_2} \left(\frac{t_o}{t}\right) \sqrt{t} \tag{18}$$

$$K_{CO_2} = \sqrt{\frac{2D_{CO_2} C_s K_1 K_2}{a}} \tag{19}$$

$$D_{CO_2} = 10^{-\left(7+0,025\frac{f_{ck}}{10}\right)} \tag{20}$$

$$a = C \frac{\%CaO}{100} \frac{\left(50\frac{w}{c}+40\right)}{100} 0,8 \tag{21}$$

Where

x = Carbonation depth [m]

K_{CO_2} = Carbonation coefficient [m/s$^{1/2}$]

K_1, K_2 = Curing and environment conditions

t = Time [s]

t_0 = Reference time [s]

D_{CO_2} = CO$_2$ diffusion coefficient [m^2/s]

C_s = Air CO$_2$ concentration

a = CaO content in 1 m^3 [kg/m^3]

$\%CaO$ = CaO cement content [%]

$\frac{w}{c}$ = Water to cement ratio

Along with compressive strength, water to cementitious material ratio is a parameter referenced by standards to correlate concrete mix design inputs with carbonation. Environment conditions can also be changed as these equations allow it. In spite of being in the standards, it is important to perform some additional trials to check the calculated values from referenced equations.

The Portuguese National Laboratory of Civil Engineering (LNEC – 465) establishes a way to evaluate the performance of concrete exposed to CO$_2$ (Monteiro, *et al.,* 2012; Marques, *et al.*, 2013):

$$x = \sqrt{\left(\frac{(2Ct)}{R_{c65}}\right) \left[\sqrt{k_0 k_1 k_2} \left(\frac{1}{t}\right)^n\right]} \tag{22}$$

Where,

$$R_{c65} = \frac{2C_{accel}t_1}{x_1^2} \tag{23}$$

$$R_{c65} = 0{,}0016 f_{cm}^{3.106} \text{ for CEM I; CEM II/A} \tag{24}$$

$$R_{c65} = 0{,}0018 f_{cm}^{2.862} \text{ for CEM II/B; CEM III; CEM IV; CEM V} \tag{25}$$

x = Carbonation depth (m)

C = Environmental carbon dioxide concentration (kg/m^3)

t = Exposure period (years)

R_{c65} = Carbonation resistance coefficient (kg year/m$^{0.5}$ – from accelerated test)

k_0 = Test condition factor

k_1 = Exposure level factor

k_2 = Curing exposure level factor

f_{cm} = Mean compressive strength [MPa]

C_{accel} = Carbon dioxide concentration in the accelerated test [%]

Additional variations are proposed by different authors to the way to calculate the carbonation coefficient. For instance, some authors mentioned that the time of the drying process (t_i) must not be considered due to the blocking effect of the pore water to CO$_2$ ingress (Daimon, *et al.*, 1971). This variation is presented in the following equation:

$$x = \begin{cases} 0 & \text{for } 0 \leq t \leq t_i \\ K(t - t_i)^{\frac{1}{2}} & \text{for } t \geq t_i \end{cases} \tag{26}$$

Different authors agree that the calculation of the carbonation coefficient is difficult due to the fact that in most of the cases it does not include all the variables affecting this process (Bakker, 1988). Additional to the previous consideration, the variation in the production of cement, fly ash and materials composition could have a significant effect on this parameter.

Yu proposed another model where theoretical analysis and performance tests were developed (Yu and Lixue, 1998; Xiang, *et al.*, 2012). The proposed model considers the following calculation:

$$X(t) = k_{RH} k_{CO_2} k_T k_S 839(1 - RH)^{1.1} \sqrt{\frac{\frac{W}{C\gamma_c} - 0.34}{\gamma_{HD}\gamma_c C}} C_{CO_2} \sqrt{t} \tag{27}$$

Where,

k_{RH} = Relative humidity coefficient

k_{CO_2} = Carbon dioxide coefficient

k_T = Temperature coefficient

k_S = Stress state coefficient

γ_{HD} = Cement hydration degree coefficient

γ_c = Cement type correction factor

C_{CO_2} = CO_2 concentration [%]

C = Cement content [kg/m^3]

t = Carbonation time [d]

As seen in the previous equation, when the level of cement hydration is increased, the carbonation coefficient is reduced. By including cement hydration level, the porosity of concrete matrix is also considered.

The following equation is a model where curing conditions and compressive strength are considered (Haiyan, *et al.*, 2006)

$$X(t) = k_{nw} \left(\frac{T}{10}\right)^{0.713} (RH^2 - 1.98RH + 1.896) \sqrt{\frac{C_0}{0.03}} \left(\frac{15.806}{f_{cuk}} + 0.215\right) t^{0.42}$$

(28)

Where,

k_{nw} = Indoor or outdoor coefficient

RH = Relative humidity [%]

T = Environment temperature [°C]

C_0 = CO_2 concentration [%]

f_{cuk} = Compressive strength

In the previous case, environment conditions are considered instead of the mix design inputs (W/CM, cement and fly ash content). Beside relative humidity, environment temperature and CO_2 concentration, curing conditions are also included. In this scenario, special care must be taken in order to have a clear consideration depending on the cementitious material type.

The model presented in the following equation considers concrete carbonation randomness. It also includes compressive strength as an influencing parameter and its evolution compared to a reference (Ditao, 2003). This model specially considers concrete geometry and where in the element the analysis is going to be performed; for instance, carbonation depth is higher at the corner of an element. Not only geometry influences this model by including the corner correction coefficient, but also the surface of the element where the casting surface coefficient is used to influence the prediction in this equation.

$$X(t) = 2.56K_{mc}k_jk_{CO_2}k_pk_s\sqrt[4]{T}(1-RH)RH\left(\frac{57.94}{f_{cu}}m_c - 0.76\right)\sqrt{t} \qquad (29)$$

Where,

K_{mc} = Uncertainty random variable

k_j = Corner correction coefficient

k_{CO_2} = Carbon dioxide concentration coefficient

k_p = Casting surface coefficient

k_s = Work stress coefficient

T = Temperature (°C)

f_{cu} = Compressive strength of the concrete cube (MPa)

m_c = Mean compressive strength to design compressive strength ratio

The previous model was modified by including a water cement ratio coefficient $k_{w/c}$ (Xiang, *et al.*, 2012). This can be seen in the following equation (Xiang, *et al.*, 2012):

$$X(t) = 2.56K_{mc}k_jk_{CO_2}k_pk_sk_{w/c}\sqrt[4]{T}(1-RH)RH\left(\frac{57.94}{f_{cu}}m_c - 0.76\right)\sqrt{t} \quad (30)$$

Where,

$$k_{w/c} = 12.1\frac{w}{c} - 3.2 \qquad (31)$$

The inclusion of compressive strength and water to cementitious material ratio in the previous model could increase the accuracy. Anyway, there are many variables in this model including element geometry which need to be checked for applicability to local conditions. Probably, the accuracy of the previous model is higher, but its application becomes complex and that is the difference compared with models included in concrete standards.

In order to predict service life, accelerated tests are performed. In this way, when accelerated carbonation is measured, it is important to consider that an initial degree of carbonation could exist (Moreno, 2013). The following equation considers this initial carbonation depth:

$$k_{accel} = \sqrt{\frac{(x^2 - x_0^2)}{t}} \tag{32}$$

Where

k_{accel} = Carbonation coefficient at higher CO_2 concentration

t = Time of accelerated exposure [s]

x = Carbonation depth at time t [m]

x_0 = Initial carbonation depth [m]

Based on an accelerated carbonation test, the environmental carbonation coefficient can be calculated from the following procedure (Moreno, 2013):

$$k = \sqrt{\frac{2Dc}{M}} \tag{33}$$

$$t_1 = x_c^2 \frac{M}{2Dc_1} \tag{34}$$

$$t_2 = x_c^2 \frac{M}{2Dc_2} \tag{35}$$

$$x_c^2 = \frac{t_1 2Dc_1}{M} = \frac{t_2 2Dc_2}{M} \tag{36}$$

$$t_1 = t_2 \frac{c_2}{c_1} \tag{37}$$

$$x_c^2 = t_1 k_1^2 = t_2 k_2^2 \tag{38}$$

$$t_2 \frac{c_2}{c_1} k_1^2 = t_2 k_2^2 \tag{39}$$

$$k_1 = k_2 \sqrt{\frac{c_1}{c_2}} \tag{40}$$

$$k_{atm} = k_{accel} \sqrt{\frac{c_{atm}}{c_{accel}}} \tag{41}$$

Where

D = Diffusion coefficient

c = CO_2 concentration

M = Concentration of hydrated calcium compounds

k_{atm} = Atmospheric carbonation coefficient

The models presented by the standards are characterized by the inclusion of constants, meaning that it is simpler for engineers to apply to model structures. Most of these constants or coefficients correlate environment conditions (CO_2 concentration, temperature, relative humidity, curing conditions), cementitious material characteristics (cement type, supplementary cementitious material) and mix design inputs (water to cementitious materials ratio, cement content). Probably due to the number of correlations in the equations and simplicity of the models, the accuracy is not as high as the models proposed by different authors; models include variables such as cement hydration degree, CH and C-S-H content. Most of the models have in common the inclusion of water to cementitious material ratio and compressive strength.

2.3.2.2 Chloride diffusion

Different models have been developed with different criteria for the service life analysis in terms of chloride diffusion. In the same way, computational programs include algorithms with different service life models. There are various different computational models available, such as Life 365, ClinConc and STADIUM, between which the inputs and criteria in the analysis vary (Green, *et al.*, 2012).

Life 365 is a software which is based on Fick's second law (Thomas and Bentz, 2008; Garcia, 2004; Green, *et al.*, 2012). This software considers that the material is homogeneous, the surface concentration is constant and the element properties are constant at any time. In this case, diffusion is the mechanism for chloride movement inside concrete matrix.

$$\frac{\partial C}{\partial t} = D \frac{\partial^2 C}{\partial x^2} \tag{42}$$

Where:

$C =$ Chloride content [%]

$D =$ Apparent diffusion coefficient [m^2/s]

$x =$ Penetration depth [m]

$t =$ Time [s]

Life 365 considers the reduction of the diffusion coefficient with time based on a reference age (Figure 16):

$$D(t) = D_{ref} \left(\frac{t_{ref}}{t}\right)^m \tag{43}$$

Where:

$D(t)$ = Diffusion coefficient at time t [m²/s]

D_{ref} = Reference diffusion coefficient at a defined age (28 days) [m²/s]

t_{ref} = Reference age (28 days) [s]

m = Constant that depends on fly ash and slag replacement levels as seen in the following equation:

$$m = 0.2 + 0.4 \left(\frac{\%FA}{50} + \frac{\%S}{70}\right) \tag{44}$$
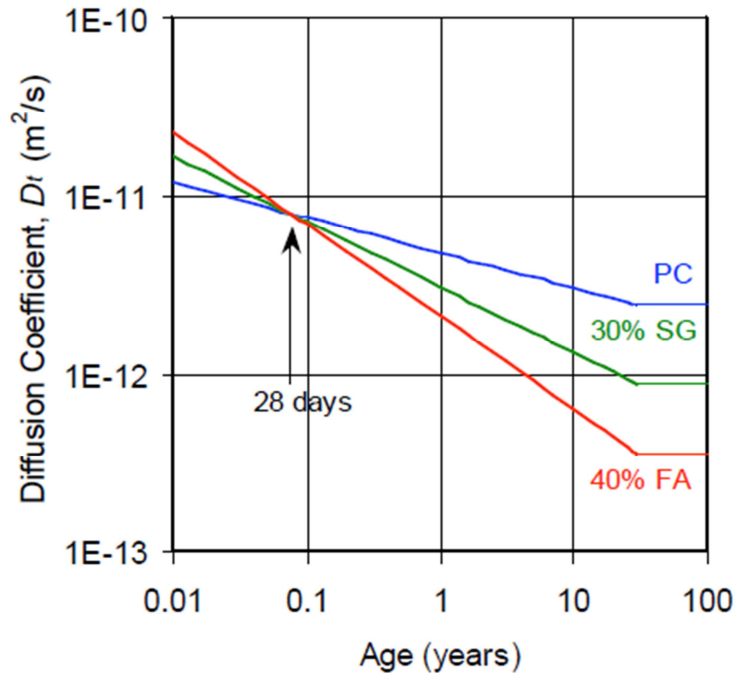
Figure 16 Effect of fly ash and slag on D$_t$, (Thomas and Bentz, 2008)

According to Life 365 and as seen in Figure 16, slag and fly ash do not have an effect on 28 day diffusion coefficient. The effect is shown after 28 days. The rate of the reduction is considered with the m factor. This factor is valid only for maximum fly ash levels of 50%. Table 2 presents different m and diffusion values for a W/CM of 0.4.

Table 2 Diffusion coefficients for slag and fly ash

	m (<=0.60)	D_{28} (x 10⁻¹³ m²/s)	D_{10y} (x 10⁻¹³ m²/s)	D_{25y} (x 10⁻¹³ m²/s)
PC	0.20	79	30	25
30% SG	0.37	79	13	9.3
40% FA	0.52	79	6.3	3.9

In the calculation of the reference diffusion at 28 days for the base case concrete mix, there is an influence of the W/CM as seen in the following equation and Figure 17:

$$D_{28} = 1 \times 10^{-12.06 + 2.4\frac{w}{cm}} \tag{45}$$
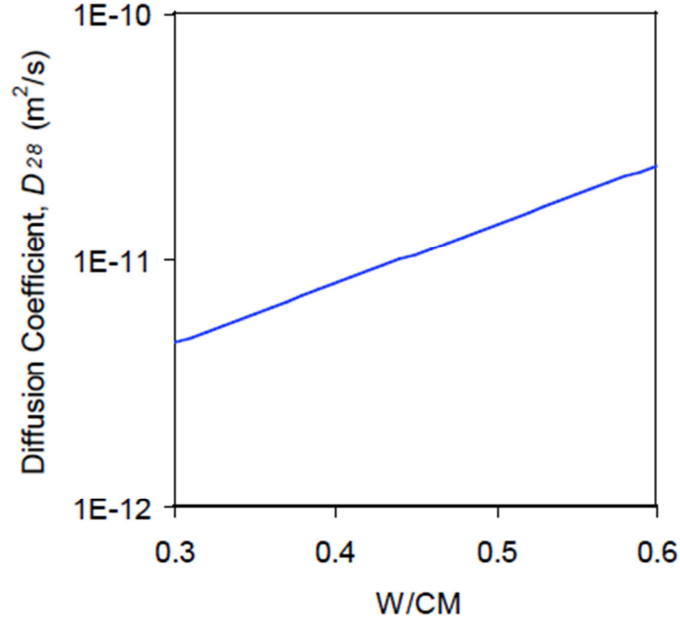
Figure 17 D_{28} vs W/CM (Thomas and Bentz, 2008)

The previous relationship applies for concretes with aggregates of normal density and may not be used for lightweight concretes.

As presented in the following equation, the calculated diffusion coefficient is corrected by temperature changes.

$$D(T) = D_{ref} exp\left[\frac{U}{R}\left(\frac{1}{T_{ref}} - \frac{1}{T}\right)\right] \tag{46}$$

Where:

$D(T)$ = Diffusion coefficient at time t and temperature T [m^2/s]

D_{ref} = Diffusion coefficient at a reference time t_{ref} and temperature T_{ref} [m^2/s]

U = Activation energy – 35000 J/mol

R = Gas constant – 8.31 J/mol·K

T = Temperature – [K]

The model considers a t_{ref} of 28 days and T_{ref} of 293K (20°C). Life 365 includes a temperature database for USA. There is also a database for chloride concentration at the surface depending on the element and geographic location.

When silica fume is used in a concrete matrix, the following equation is used:

$$D_{SF} = D_{PC}e^{-0.165SF} \tag{47}$$

Where:

D_{PC}= Portland cement diffusion coefficient [m²/s]

SF = Silica fume percentage level [%]

Another model is the one called Clinconc. In this case, additionally to the transport by diffusion, chemical interactions are considered. In this model, the free chloride concentration is predicted with the flux equation from Fick's second law (Green, *et al.*, 2012; Tang, *et al.*, 2012). It is important to consider that the total chloride concentration includes bound and free chlorides, where the latter are available to travel to the steel (Tang, 1996). The following is the equation used in this model:

$$\frac{c-c_i}{c_s-c_i} = 1 - erf\left[\frac{x}{2\sqrt{\frac{\xi_D D_{RCM6m}}{1-n}\left(\frac{t_{6m}}{t}\right)^{n'}\left[\left(1+\frac{t_{ex}}{t}\right)-\left(\frac{t_{ex}}{t}\right)^{1-n'}\right]t}}\right] \tag{48}$$

Where:

c = Free chlorides at depth x [%]

c_s = Chlorides at the surface [%]

c_i = Initial chlorides in concrete matrix [%]

n = Age factor

D_{RCM6m} = Concrete diffusion measured in the laboratory at 6 months [m²/s]

ξ_D = Bridging factor (From laboratory measurements to environment

conditions). It considers chemical interaction between chlorides and concrete:

hydroxide content, gel content, water accessible porosity.

One well-known model, popular due to the number of parameters considered in the analysis, is STADIUM®. In addition to diffusion and chemical reactions, this model also considers electrical coupling of ions. The following is the equation considered by this model (Green, *et al.*, 2012):

$$\underbrace{\frac{\partial(w_s c_i^s)}{\partial t}}_{\text{Ions diffusion}} + \underbrace{\frac{\partial(wc_i)}{\partial t}}_{\text{Electrical coupling}} - \frac{\partial}{\partial x}\left(wD_i\frac{\partial c_i}{\partial x} + w\underbrace{\frac{D_i z_i F}{RT}c_i\frac{\partial \psi}{\partial x} + wD_i c_i\frac{\partial \ln \gamma_i}{\partial x}}_{\text{Electrical process}} - c_i V_x\right) + \underbrace{wr_i}_{\text{Advection transport mechanism}} = 0 \tag{49}$$

Where:

w_s = Volumetric solid content [m^3/m^3]

c_i^s = Concentration (solid phase) [mol/m^3]

c_i = Concentration in the solution [mmol/L]

D_i = Diffusion coefficient [m^2/s]

z_i = Valence number

F = Faraday constant

R = Ideal gas constant

T = Temperature of the material [K]

ψ = Electrical potential [V]

γ_i = Chemical activity coefficient

V_x = Fluid average velocity when capillary suction takes place [m/s]

r_i = Term considering the creation of the ion i

In the complete study developed by Green, Nanukuttan and Basheer, where the previous models were analyzed, it was concluded that for the Life 365 the most influencing parameter was the W/CM, for Clinconc W/CM and aggregate content, and for STADIUM® the porosity level. Based on the number of parameters used in STADIUM® and the fact of using not only diffusion but also chemical reactions and electrical coupling, this model is more accurate when comparing it with results obtained from real structures.

The initiation period evaluated in this project does not include chemical interactions and ions electrical coupling; it considers diffusion variation depending on the effect of the compressive strength and the different fly ash percentages and sodium sulfate as activator. As mentioned, LIFE 365 considers diffusion only and W/CM is the most influencing parameter.

2.4 Summary

The following are the main general conclusions from the literature review:

- High volume fly ash concrete is a sustainable alternative construction material; it is characterized by the low water to cementitious material ratio, low water content and high superplasticizer dosages. Durability of structures is positively affected by this type of concrete. It can be used for mass

concrete such as dams. It is important to consider the effect of the high volume fly ash on setting time and initial compressive strengths which can be negatively affected. Although this is a green alternative, it could be an expensive option due to the high polycarboxylate contents.

- The use of 100% fly ash with an activator is another sustainable alternative but with different challenges. There are some recommendations to obtain an activated system with fly ash considering LOI, Fe_2O_3 and CaO content, reactive SiO_2 and glassy phase. It is important to consider high curing temperatures in the process. Although an activator such as water glass increases compressive strength, it reduces concrete workability. For its technical viability, it is important to obtain more data related to durability; one of the main concerns is the effect in terms of carbonation.

- Activation of mortars with Portland cement and high volume fly ash has been explored with different activators including sodium sulfate. The process of the reactions with sodium sulfate has been studied, with ettringite being the component which increases the matrix density. It is important to perform different durability studies due to the lack of information related to this specific area.

- There is not information about concretes using sodium sulfate with 50% pc and 50% Colombian fly ash. As mentioned before, what is present in the literature considers mortars with low LOI fly ash. Colombian fly ash which is used in this study has high LOI contents.

- It is important to identify the factors influencing early compressive strengths of concretes using high volumes of fly ash and sodium sulfate as activator. As mentioned before, some studies present an influence of ettringite on this parameter. Although most of the effect in terms of compressive strength is at early ages, it is important to evaluate at later ages. In the same way, evaluations of the setting time must be considered due to the presence of sodium sulfate. Significant work on concrete durability evaluations must be performed due to strong gaps evident in the literature; questions related to the performance of this system in terms of sorptivity, permeability, chloride penetration, and carbonation must be answered, due to the additional effect of the alkali activator.

- Concrete deterioration depends on its permeability; three main transport mechanisms must be considered: absorption, permeability and diffusion. Although an increment in fly ash addition could increase the absorption of the element, in general these three main parameters are affected positively. Curing has an important influence on increasing pore network obstruction. Some initial design inputs such as the water to cementitious material ratio and fly ash content reduce absorption, permeability and diffusion.

- There are some specifications including initiation period models; in general, they include coefficients considering water to cementitious material ratio, cementitious material type, environment and curing conditions. There are not models published including any type of activator for hybrid cementitious systems.

- Additionally to performance, CO_2 emission with this system considering Colombian fly ash is also a gap in knowledge. In this special case is important to consider CO_2 emissions in terms of compressive strength.

- There is not information in the literature related to the activated hybrid cementitious system using Portland cement and high volume Colombian fly ash in terms of fresh and hardened state, durability properties, service life, CO_2 emissions and cost evaluations.

3 Materials

3.1 Introduction

This chapter includes description of the sources of the supplementary cementitious materials used for this research. Chemical, mineralogical and physical characteristics were determined for each of the raw materials. Cement and the alkali activator is described at this part of the project.

3.2 Supplementary cementitious materials

According to ASTM C618, the fly ashes for this research are classified as class F. The following is the list of the supplementary cementitious materials used in this research:

- Termopaipa Fly Ash
- Termoguajira Fly Ash
- Fabricato Fly Ash
- Tampa Fly Ash

3.2.1 Fly ash sources

Most of these materials come from inside Colombia. Tampa fly ash, which comes from outside the country, is included in this research due to its high quality according to ASTM C618. Figure 18 includes a map where each of the locations is shown.
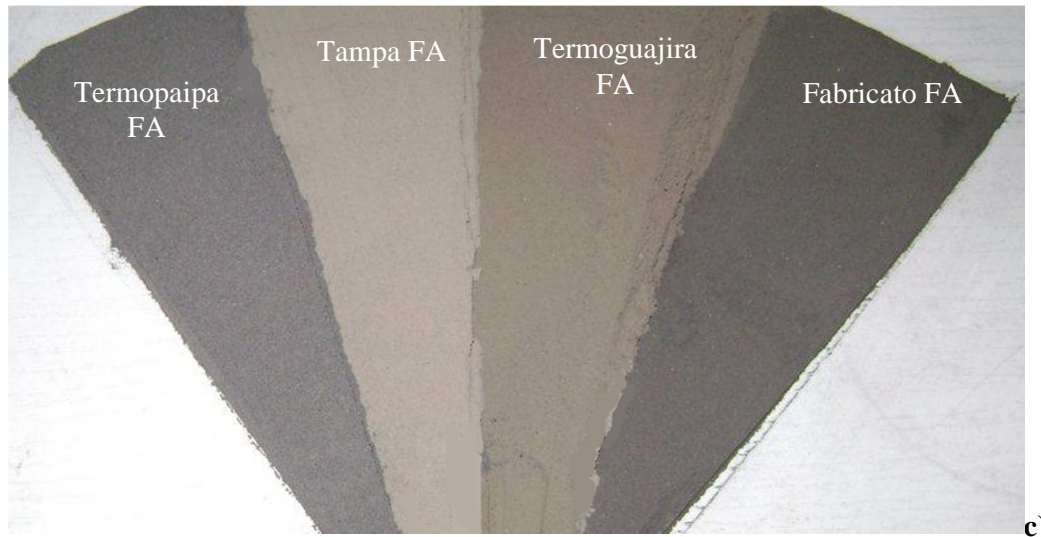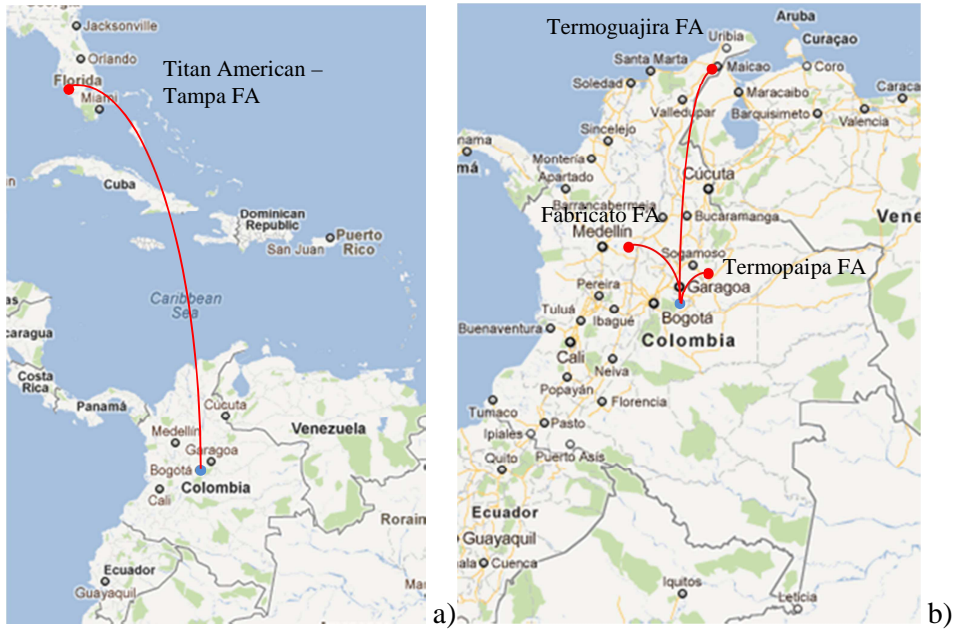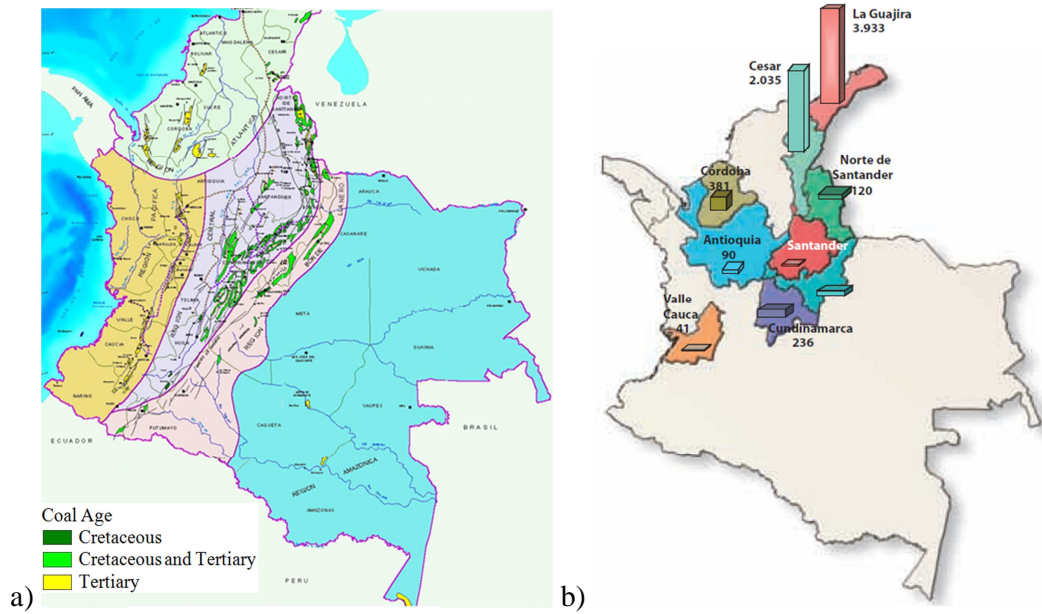
Figure 18 a) International SCMs, b) National SCMs, c) Termopaipa FA, Tampa FA, Termoguajira FA, Fabricato FA

One fly ash comes from Tampa FL, USA. Termoguajira fly ash comes from the North part of Colombia. In the North West, there is another source of fly ash which is Fabricato fly ash. Termopaipa fly ash source is located close to Bogotá, the capital city.

a)

b)

Figure 19 a) Coal distribution along the country of Colombia (From www.ingeominas.gov.co), b) Coal reserves (Mt) (From www.upme.gov.co)

3.2.2   Colombian coal

As seen in Figure 19 and Figure 20, the high amounts of coal in this country position coal as one of the main energy sources.
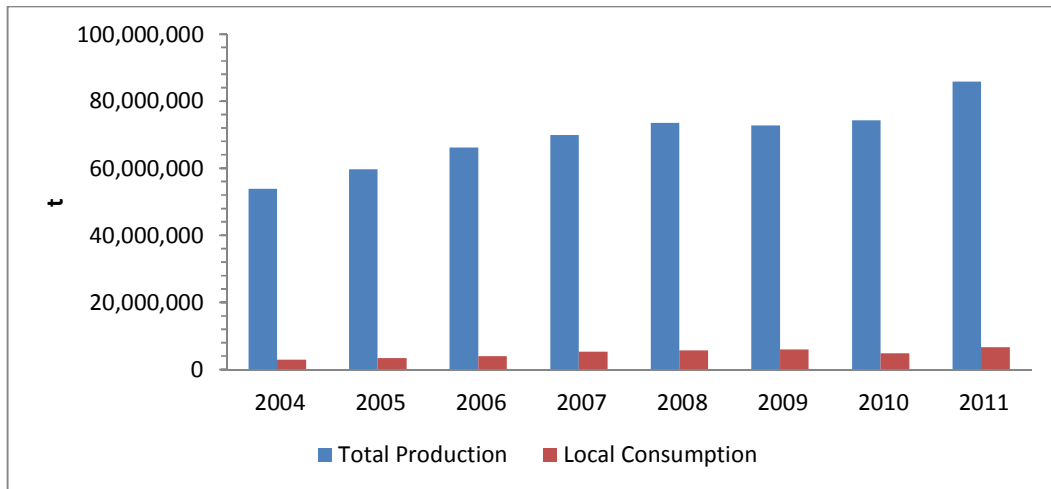

Figure 20 Colombian Coal production (From www.upme.gov.co)

From considering the total and local consumption presented in Figure 20 and the coal consumption distribution shown in Figure 21, the total fly ash production can be obtained. Figure 21 shows local consumption distribution
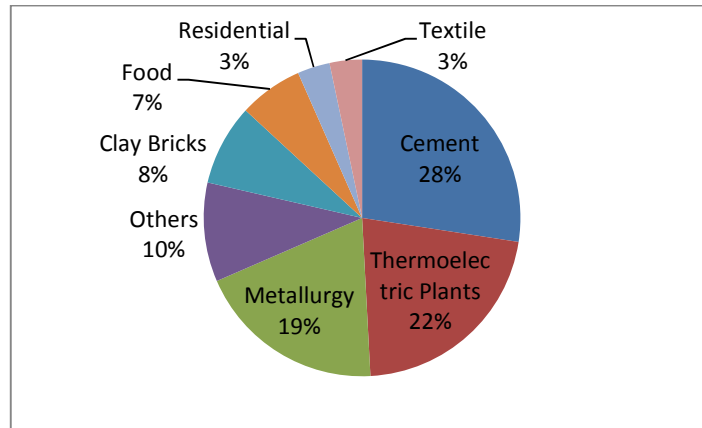
Figure 21 Coal distribution for different industries (From www.upme.gov.co)

The total amount of fly ash generated from Colombian coal in 2011 was 5'693.547 t; although the local fly ash seems as a low amount compared to the total one, 408.068 t per year could supply this country concrete production by using 50% - 80% as cementitious material (Figure 22).

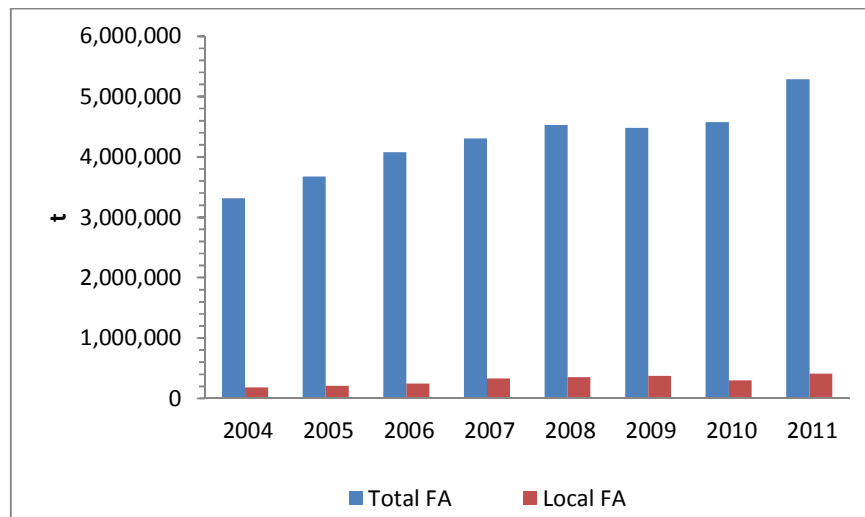**Figure 22 Fly ash generation from Colombian coal**

3.2.3 Supplementary cementitious material preliminary treatment

In order to improve their characteristics, fly ashes were subjected to a mechanical treatment. All the fly ashes were sieved using 75 µm and 45 µm sieves; the objective of this treatment was to obtain different sizes without crushing the material and keeping the original particle shape.

3.2.4 Chemical, mineralogical and physical characteristics of fly ashes

3.2.4.1 Chemical Composition

Table 3 presents the chemical compositions of the fly ashes. This characterization was obtained using a PANalytical Axios sequential wavelength dispersive XRF (WDXRF) spectrometer. From this characterization, it is concluded that Tampa FA has the highest silica content amongst the fly ashes studied. Although all of the fly ashes accomplish the required ASTM (SiO_2), (Al_2O_3) and (Fe_2O_3) sum for Class F classification, Tampa FA has the highest value and Fabricato FA the lowest. As they are classified as type F fly ashes, the calcium content is low; Fabricato FA has the highest value amongst them. ASTM C 618 allows a type F fly ash to have up to 12% of LOI; Fabricato FA has this value and the others are between 8% and 10%. Tampa FA is the only one that receives treatment, and has the lowest LOI percentage compared to the other ashes.

Colombian fly ashes are characterized by their high LOI content. Although they have a higher LOI than UK fly ashes, they also have a higher SiO_2 which is the most important component reacting with portlandite to form C-S-H (UK Quality Ash Association, 2011). The Al_2O_3 of UK fly ashes is higher than Colombian fly ashes. The CaO, MgO, K_2O, Na_2O and SO_3 levels are similar for both Colombian and UK fly ashes.

Table 3 Chemical Composition. LOI is loss on ignition at 750°C

Materials	Composition (%)									
	SiO_2	Al_2O_3	Fe_2O_3	$(SiO_2)+(Al_2O_3)+$ (Fe_2O_3)	SO_3	LOI	Na_2O	CaO	K_2O	MgO
Termopaipa FA	56.67	20.65	4.92	82.24	0.06	10.74	0.07	3.27	1.59	0.62
Fabricato FA	43.83	28.11	4.39	76.33	0.09	12.00	0.89	5.99	1.28	1.74
Termoguajira FA	55.14	17.63	9.77	82.54	0.11	8.74	0.56	3.64	1.78	1.38
Tampa FA	58.58	19.96	10.21	88.75	0.50	1.53	0.76	3.17	2.29	1.50

3.2.4.2 Mineralogy

The mineralogy of the SCMs was evaluated with a PANalytical XRD with an X 'PERT-PRO MPD system. Each sample was examined with a Bragg-Brentano optical configuration including an X'celerator data collector, which is a high speed

solid state detector. The Rietveld method was used to quantify the crystalline and amorphous structure.

It is important to mention that the vitreous phase is found in high proportions compared to the crystalline phase in the fly ashes considered in this study; the amorphous content is the halo presented between $2\theta=20°$ and $2\theta=35°$ in the diffractogram x axis. The regular crystalline main components are quartz, mullite, magnetite, hematite, CaO and TiO_2.

According to the results obtained from the mineralogical characterization, the highest amorphous content is exhibited by the Tampa FA. For almost all of the SCMs, quartz is the highest crystalline phase presented. This can be seen from Figures 23 to 26.

3.2.4.2.1 Termopaipa FA

For this fly ash, the amorphous content is 64.5%. Termopaipa FA has the lowest amorphous content compared with the other fly ashes. The highest amount between the crystalline phases of the fly ash comes from quartz; this amount was 18%. Calcite was particularly found in Termopaipa FA (Figure 23); this phase is not present in the other fly ashes.
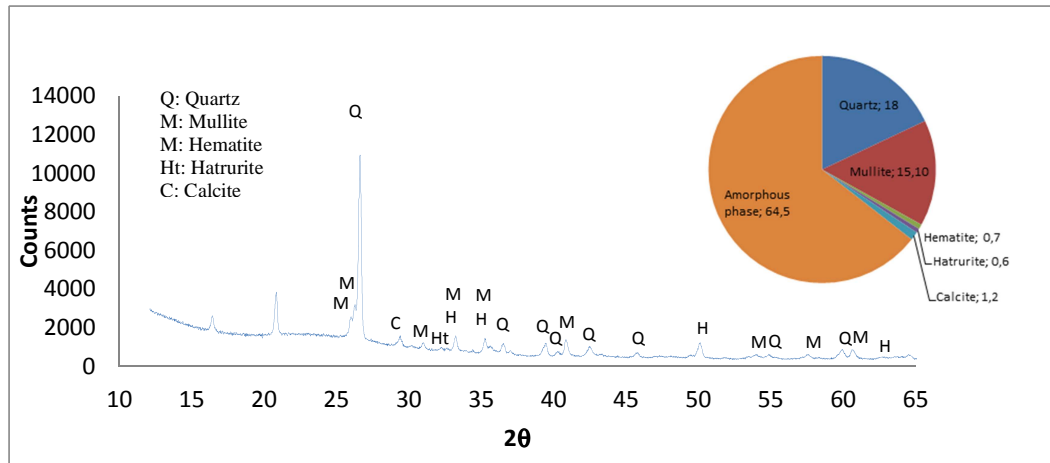

Figure 23 Termopaipa XRD

3.2.4.2.2 Fabricato FA

Fabricato FA has the highest amorphous content between the local fly ashes with 69.3%. Between the crystalline phases, mullite is the one with the highest content with 20.6%; in spite of this result, for most of type F fly ashes mullite content is lower than quartz. Normally, fly ashes include in their crystalline phase quartz, mullite and hematite and in some cases hatrurite (it is assumed it was contaminated with a small

portion of cement due to C$_3$S presence); as seen in Figure 24, Fabricato has the common phases for a type F fly ash.
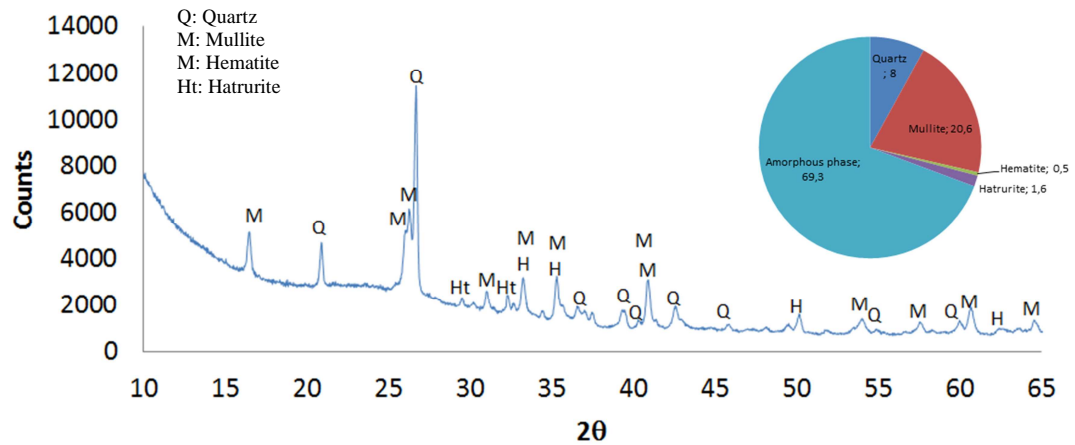

Figure 24 Fabricato XRD

3.2.4.2.3 Termoguajira FA

Termoguajira has a low vitreous or amorphous content in comparison with the other fly ashes. According to Figure 25 and the other fly ashes, Termoguajira quartz content is the highest between all of them. Magnetite and coesite are the two phases which are not present in the other fly ashes.
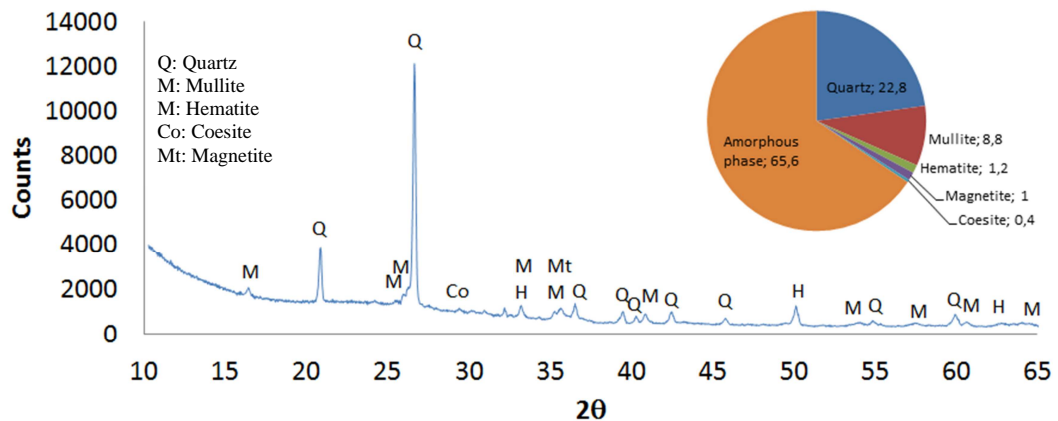

Figure 25 Termoguajira XRD

3.2.4.2.4 Tampa FA

Tampa FA has the highest amorphous content with 76%. This fly ash receives a treatment to reduce LOI content before being distributed, helping to increase the amorphous content. As can be seen in Figure 26, magnesioferrite and lime are present in the crystalline phase. Quartz, mullite and hematite are included in expected proportions.
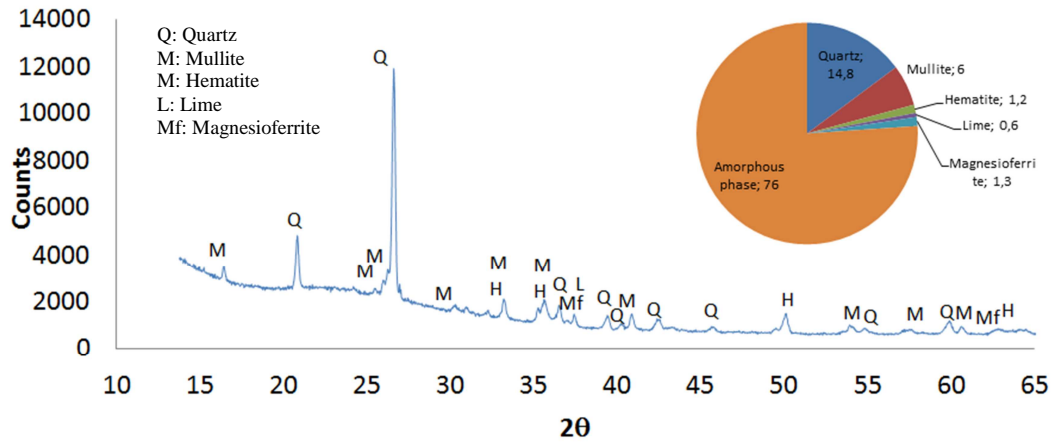
Figure 26 Tampa XRD

Figure 27 presents the complete mineralogical results of all the fly ashes; from this figure, the halo differences presented between 2θ=20° and 2θ=35° are clear. Based on the halo size it can be concluded that Tampa fly ash has the highest amorphous content while Termopaipa the lowest content. This parameter is a preliminary indicator of high pozzolanic activity.
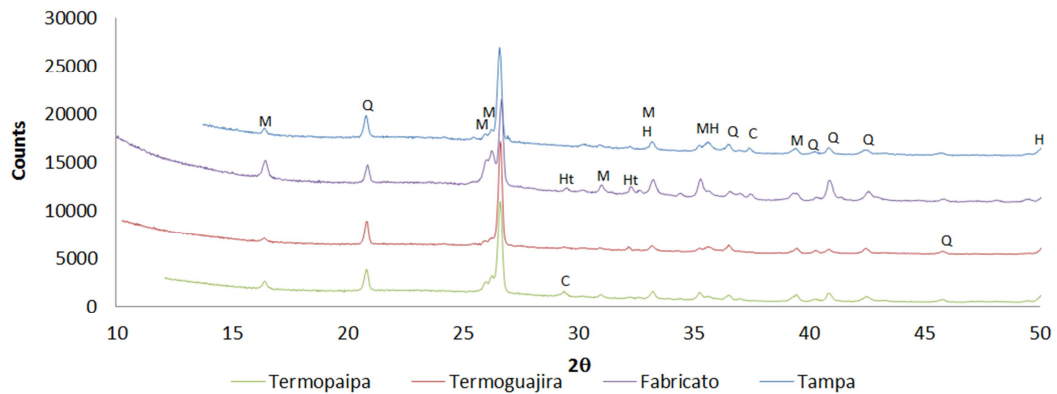

Figure 27 Fly ashes XRD

Table 4 summarizes the mineralogy of all the SCMs. The main characteristic of fly ashes is their high amorphous content.

Table 4 Mineralogy

Materials	Composition (%)									
	Quartz	Mullite	Hematite	Magnetite	Coesite	Hatrurite	Calcite	Lime	Magnesioferrite	Amorphous material
Termopaipa FA	18	15.1	0.7			0.6	1.2			64.5
Fabricato FA	8	20.6	0.5			1.6				69.3
Termoguajira FA	22.8	8.8	1.2	1.2	0.4					65.6
Tampa FA	14.8	6	1.2					0.6	1.3	76

3.2.4.3   Physical Properties

Density, granulometry, and activity index of SCMs were analysed. As can be seen from Figure 28, Termoguajira FA is the coarsest while Tampa FA is the finest fly ash.
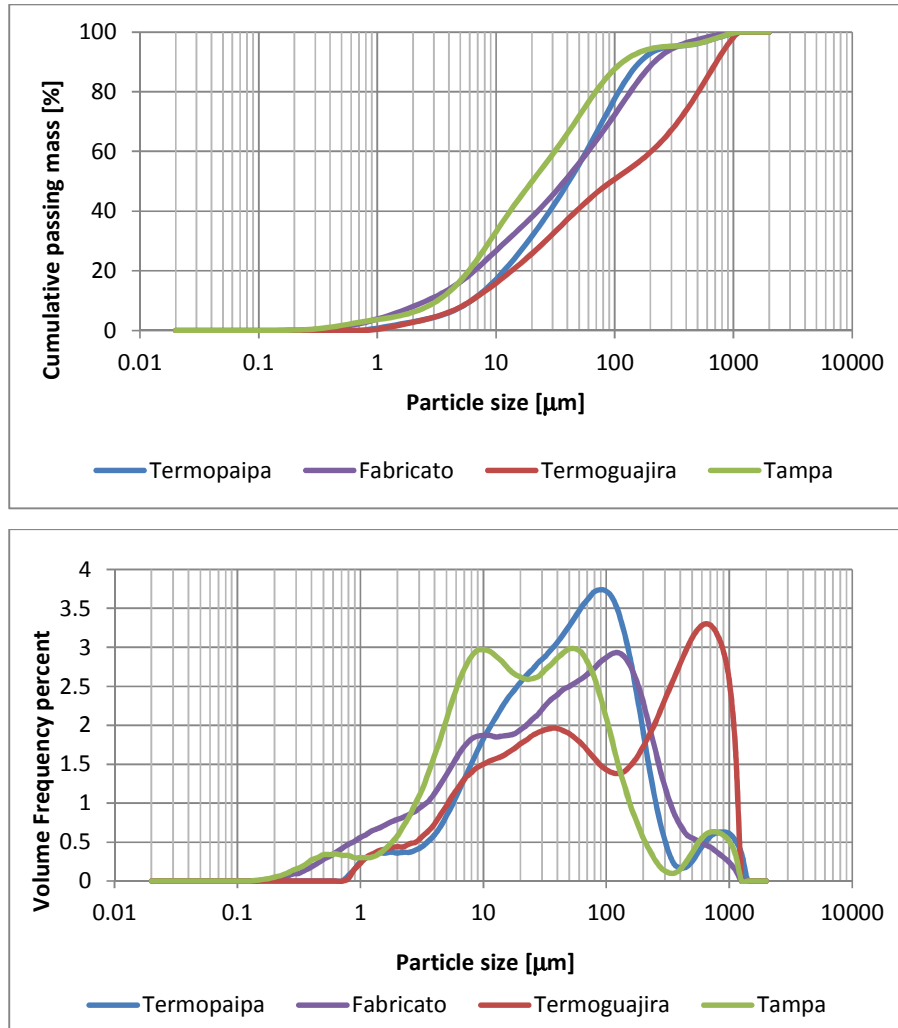

Figure 28 Granulometry of fly ashes

All the fly ashes were evaluated according to ASTM C311 (ASTM C 311, 2007). This standard includes chemical analyses and physical tests to evaluate fly ash for use in concrete. Some of the analyses considered in this standard are silicon dioxide, aluminum oxide, iron oxide, density, and activity index. Table 5 presents the density and activity index of the SCMs. Termopaipa FA has the lowest density while Fabricato FA has the highest value; it is important to mention that density of fly ash from UK varies from 1.8 to 2.4 g/cm^3 (UK Quality Ash Association, 2011) Fabricato FA also has the highest activity index.

Table 5 Physical characteristics of fly ashes

Materials	Physical characteristics (%)			
	Activity Index %		Density (g/cm^3)	Retained on # 325 sieve [%]
	7	28		
Termopaipa FA	70.20	71.60	2.09	47.57
Fabricato FA	79.20	78.20	2.11	46.32
Termoguajira FA	75.80	73.40	2.26	60.9
Tampa FA	71.60	74.30	2.32	31.07

From the physical properties presented, the need for a mechanical treatment is evident, to improve SCM fineness. By subjecting these materials to a mechanical treatment, not only their physical properties will be affected but also their chemical and mineralogical composition, depending on the treatment.

3.2.4.4 Main SCMs characteristics after mechanical treatment

When the material was sieved, not only the grading changed, but also the chemical and mineralogical characteristics. Colombian fly ashes were subjected to this process. These materials were sieved using 75 µm and 45 µm meshes. Glass composition was calculated by relating the chemical composition with minerals from XRD analysis; the glass content for each oxide is the difference between the total oxide content from the chemical analysis and its quantity calculated from XRD mineral database. The results are summarized in the following tables:

Table 6 Changes in fly ash properties a) Main parameter b) Glass composition

Fly ash	Sieve - Treatment	Main Parameters				
		LOI	Fe$_2$O$_3$	CaO	SiO$_2$	Amorphous
TP FA	As received	10.74	4.92	3.27	56.67	64.50
	< 74μm	8.67	5.90	0.57	59.50	67.30
	< 45μm	5.07	5.25	1.43	62.31	59.60
FB FA	As received	12.00	4.39	5.99	43.83	69.30
	< 74μm		3.82	3.20	44.96	60.20
	< 45μm	5.78	4.76	6.94	45.45	63.60
TG FA	As received	8.74	9.77	3.64	55.14	65.60
	< 74μm	1.54	11.15	2.57	63.12	56.10
	< 45μm	1.94	10.46	4.37	56.89	65.50
TA FA	As received	1.53	10.21	3.17	58.58	76.00
	< 74μm	1.30	10.74	2.99	57.92	75.50
	< 45μm	1.53	10.35	2.79	56.59	78.10

a)

| Glass Composition															
Materials	Fe$_2$O$_3$	MgO	SiO$_2$	Al$_2$O$_3$	CaO	Na$_2$O	K$_2$O	TiO$_2$	Mn$_3$O$_4$	SO$_3$	LOI	P$_2$O$_5$	V$_2$O$_5$	SrO	BaO
Termopaipa FA	4.22	0.62	34.04	9.81	2.04	0.07	1.59	0.93	0.01	0.06	10.74	0.27	0.04	0.04	0.07
Fabricato FA	3.89	1.74	29.65	13.32	4.76	0.89	1.28	1.17	0.01	0.09	12.00	0.06	0.10	0.02	0.22
Termoguajira FA	7.88	1.38	29.08	11.31	2.41	0.56	1.78	0.79	0.06	0.11	8.74	0.13	0.05	0.06	0.14
Tampa FA	7.97	1.26	42.02	15.65	1.28	0.76	2.29	0.93	0.05	0.50	1.53	0.22	0.05	0.03	0.08
Termopaipa FA - < 74μm	5.90	0.65	39.29	9.20	0.57	0.09	1.69	0.85	0.00	0.00	8.67	0.20	0.04	0.00	0.06
Fabricato FA - < 74μm	3.82	1.35	27.27	5.58	3.20	0.54	1.11	0.99	0.00	0.31	15.62	0.05	0.08	0.00	0.16
Termoguajira FA - < 74μm	9.71	0.89	28.90	9.23	2.37	0.60	1.58	0.71	0.05	0.33	1.54	0.12	0.04	0.04	0.00
Tampa FA - < 74μm	9.56	1.23	41.89	13.69	2.99	0.60	2.38	0.98	0.05	0.29	1.30	0.22	0.06	0.06	0.12
Termopaipa FA - < 45μm	4.63	0.65	35.54	9.49	1.05	0.12	1.66	0.99	0.00	0.14	5.07	0.33	0.04	0.03	0.09
Fabricato FA - < 45μm	4.35	1.27	30.48	12.64	5.33	1.12	1.32	1.20	0.00	0.00	4.89	0.06	0.12	0.06	0.23
Termoguajira FA - < 45μm	5.76	1.48	35.51	13.30	2.36	0.64	1.96	0.90	0.06	0.37	1.94	0.16	0.00	0.06	0.15
Tampa FA - < 45μm	9.24	1.33	42.70	14.99	2.79	0.65	2.55	1.06	0.05	0.64	1.53	0.25	0.06	0.06	0.12

b)

76

Based on these results, it was decided to use these granulometries for the next phase of the project. Three finenesses will be used: 100% passing #325 sieve (45 µm), 100% passing #200 sieve (75 µm) and the original granulometry.
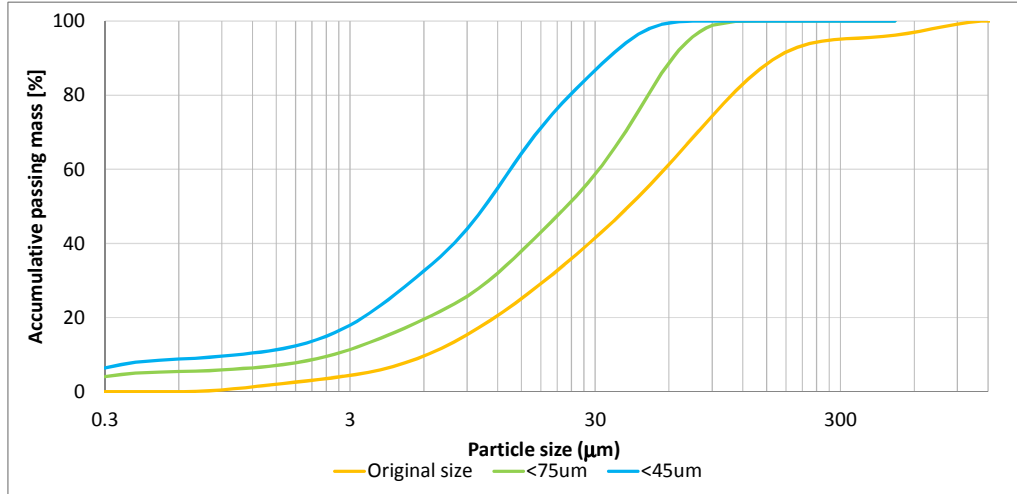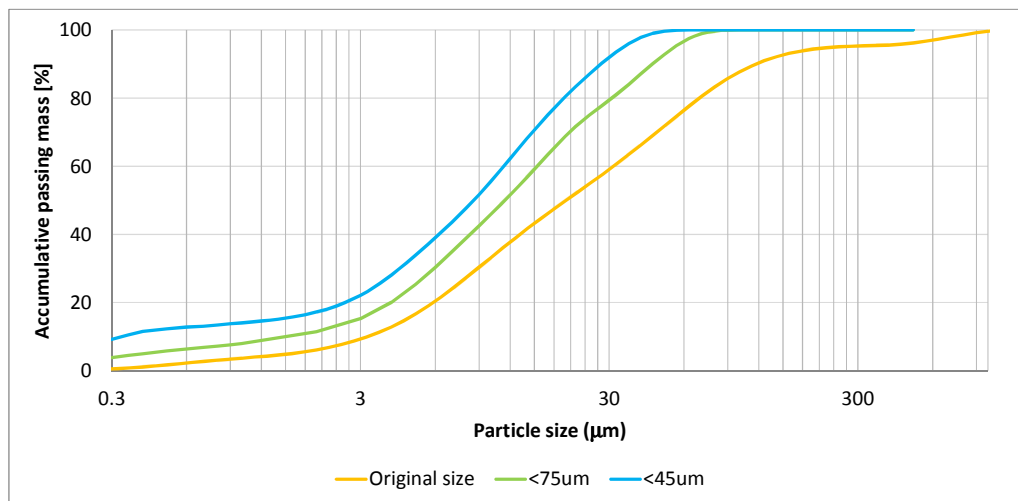

a) Termopaipa FA
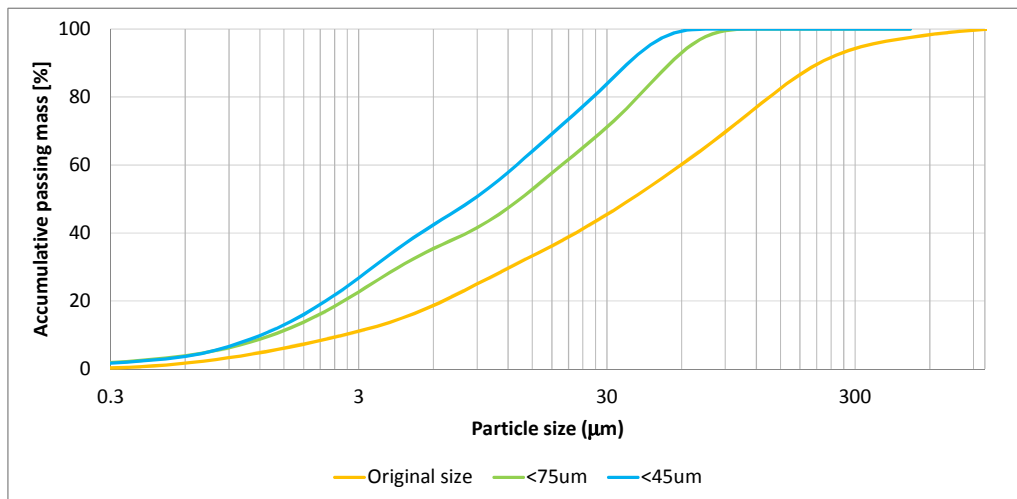
b) Fabricato FA
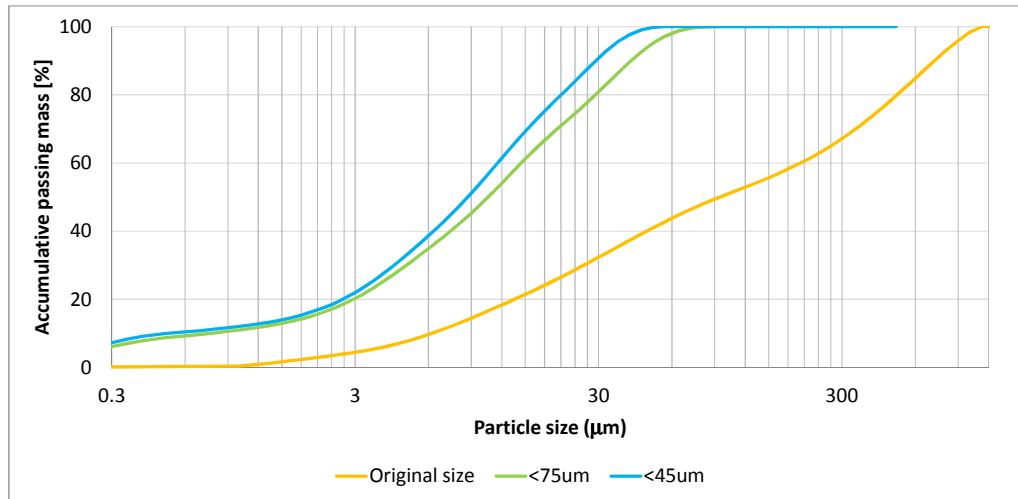
c) Termoguajira FA

d) Tampa FA

Figure 29 Fly ashes granulometry

As seen from Figure 29 and Table 7, Termoguajira fly ash has the largest particles compared to the others; however, after sieving, the values for D_{50} and D_{90} are close to the fly ash from Tampa. It is clear how the largest particles in this fly ash are due to the presence of LOI.

Table 7 D_{50} and D_{90} values

Fly ash	D	Original size	<75µm	<45µm
Termopaipa	D50	41	23	11
	D90	163	62	34
Fabricato	D50	38	13	9
	D90	224	54	37
Termoguajira	D50	94	11	9
	D90	719	41	29
Tampa	D50	20	11	9
	D90	117	45	28

3.3   Cement

The cement selected for this study is Type III according to ASTM C150 (ASTM C150, 2009) and classified as CEM I 42.5N according to BS EN 197-1 (BS EN 197-1, 2011). This cement is used for Argos ready mixed concrete production. Table 8, 9 and 10 present the chemical, mineralogical, physical and mechanical properties of the cement.

Table 8 Cement chemical composition

XRF	Chemical Composition of Cement (%)								
	LOI	CaO	SiO_2	Al_2O_3	Fe_2O_3	SO_3	MgO	K_2O	Na_2O
Argos Cement	1.4	65.82	21.53	4.73	3.56	1.91	0.9	0.57	0.06

Based on its chemical and mineralogical characterization, it can be assumed that this cementitious material is useful to be blended with any pozzolanic material. The high C_3S and C_3A amounts help to increase the pozzolanic activity.

Table 9 Mineralogical composition of cement determined using X-ray diffraction

Mineralogical Composition of Cement (%)							
C_3S	C_2S	C_4AF	C_3A (Aluminate cubic)	C_3A (Aluminate ortho)	Anhydrite	Calcite	Quartz
52.1	30.5	10.2	3.3	0.8	1.8	1.0	0.3

From Table 9, it can be deduced that this cement will produce a high amount of heat, has short setting time periods and high early and 28 day strengths. In fact, Table 10 confirms what is deduced from Table 9; all the compressive strengths are high if they are compared with a type I cement.

Table 10 Physical and mechanical properties

Blaine [cm²/g]	Setting time [min]		Density [g/cm³]	Compressive strength [MPa]			
	Initial	Final		1 day	3 days	7 days	28 days
4382	122	190	3.10	16.7	29.0	37.9	48.7

Cement granulometry (Figure 30) and Blaine fineness affect the strength positively; according to its mineralogical, chemical and physical characteristics, it is possible to use this cement with SCMs in high proportions to accomplish normal compressive strength at 28 days.
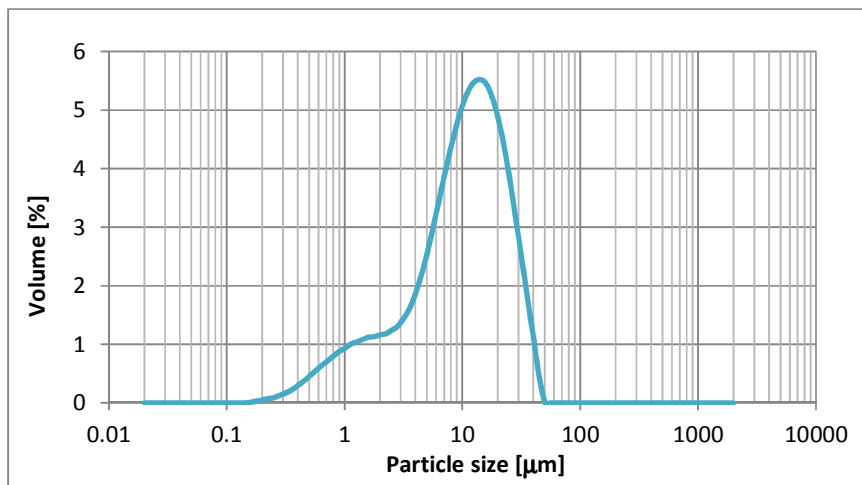
Figure 30 Cement granulometry

3.4 Activators

The main activators to be considered are Sika Activator (Activator 1), hydrated lime, quicklime and Na_2SO_4.

Table 11 Activator 1 chemical composition

Chemical Composition			
Fe_2O_3	Na_2O	SO_3	LOI
0.53	45.48	49.49	4.52

3.5   Summary

The following is a summary based on materials characterization:

- Colombian fly ashes are characterized by their high LOI content. The type of fly ash available in Colombia is a type F. Most of Colombian bituminous coal is used for energy generation in cement and thermoelectric plants. Four different fly ashes will be considered in the study including one from USA.

- The highest value of (SiO_2+Al_2O_3+Fe_2O_3) was for Tampa fly ash and the lowest for Fabricato fly ash. The latter had the highest LOI value of 12% while the other Colombian fly ashes were between 8% and 10%. Tampa fly ash had the lowest LOI content due to the treatment it receives before being commercialized.

- Tampa fly ash had the highest amorphous content of 76% before being sieved while Termopaipa fly ash had the lowest value (64.5%). In terms of percentage retained on # 325 sieve, the lowest value was for Tampa and the highest for Termoguajira fly ash.

- SiO_2 content was the highest for Termopaipa fly ash before and after being sieved while Fe_2O_3 content was the highest for Tampa and Termoguajira fly ash. The amorphous content and LOI changed with fly ash fineness. Although the LOI content decreased when the fineness increased, there was not a trend with respect to the amorphous content.

4 Evaluation of fly ashes and activators in mortar and paste systems

4.1 Introduction

The main objective of this part is to select the materials, combinations and dosages based on mortars and pastes; the main evaluations are strength, calorimetry, thermogravimetry, XRD and SEM.

4.2 General procedures for mortar and paste preparation and testing

4.2.1 Mortar and paste preparation

The procedures presented in ASTM C 109 were followed as far as possible, and modified where necessary. The following general aspects were considered for mortar and paste preparation:

- The activator was added to water; it was mixed until it was completely dissolved. Cement was added to the mix of water and activator; it was mixed for 30 seconds at the lowest velocity (level 1; 140 min^{-1}) using an epicyclic type mechanical mixer. After that, sand was added and mixed for 30 seconds. After that, it was left for 1.5 minutes, then mixed again for 1.5 minutes at a velocity of 285 min^{-1} (level 2).

- Activator 1, lime and sodium sulfate had good solubility, while quicklime in contact with water increased the temperature and formed white solid forms. This effect increased when dosages increased.

- Samples were left in the curing room with a temperature of 23°C

Mortars mix design

The following table includes the quantities to make 6 cubes. Although the quantities changed depending on the number of cubes, the proportions were constant.

Table 12 Mix proportions

w/cm	0.484			
Fly ash [%]	0%	20%	50%	50%
Cement [g]	500	400	250	200
Fly ash [g]		100	250	200
Sand [g]	1375	1375	1375	1375
Water [ml]	242	242	242	242
				+ Activator

4.2.2   Process to stop sample hydration

- 50 mg of paste per sample was used for this process.
- This material was ground in order to increase the specific surface.
- The sample was submerged in acetone for 5 minutes.
- After five minutes, the acetone was replaced by absolute ethanol. The sample was sealed in special plastic buckets until the day of the test.

4.2.3   XRF procedure

- The sample was dried at 40°C for 4 hours.
- It was then ground in a tungsten mortar at 400 rpm for 3 minutes. Between 20 to 30 grams of sample was used in this test.
- Moisture content of the sample was determined by drying the sample.
- When loss of ignition was evaluated, it was done by drying a sample for 3 hours at 110°C. After obtaining the weight of the sample at 110°C, it was taken to a temperature of 1000°C.
- To obtain a pressed pellet, a pressure of 100 kN was applied for 20 seconds.
- The instrument used was a PANalytical's Axios sequential wavelength dispersive XRF (WDXRF)
- Results of XRF evaluation were obtained using the SUPERQ software.

4.2.4   XRD procedure

General considerations
- Sample drying and grinding were done following the same procedures as described for XRF.

- In order to evaluate the amorphous content, rutile was used as the internal standard mixed with the sample. A spike of 0.5 g of rutile was included per each 4.5 g of sample.

Analysis method and process

The mineralogy was evaluated with an XRD diffractometer. The results were obtained using a PANalytical XRD with an X 'PERT-PRO MPD system. Each sample was measured with a Bragg-Brentano optical configuration including an X'celerator data collector.

The method used for this analysis was the Rietveld method. The software which helped to perform this analysis was X'Pert HighScore Plus. The following is the process which was used to perform this analysis:

- To determine the background: the software used proposes an initial curve. Manually, this background was then modified in order to improve the accuracy of the results. This is important as it also affects the amorphous content quantification (the amorphous content is higher than 60% for fly ash).
- Find the main peaks.
- Select the possible compounds which are part of the material structure.
- Check the chemical composition of the compounds.
- Include the crystalline phases in the inputs in order to start the refinement control.
- Determine the global parameters of all compounds before Rietveld refinement.
- Perform Rietveld refinement using the software.
- Determine the global parameters of all compounds after Rietveld refinement.

4.2.5   Thermogravimetry procedure

- The Instrument used is a Thermogravimetric Analyzer TGA 2950.
- 60 mg of samples were used for the thermogravimetry procedure

- Tests were performed with a controlled nitrogen atmosphere with a 40 mL/min flow. The temperature was increased from ambient to 950°C at a rate of 10°C/min.
- The final results included weight loss relative to temperature and their respective derivatives. These results were analysed using TA Universal Analysis software.

The main equations followed for the portlandite and non-evaporable water calculation were:

$$\% \, CH = \frac{w_{T1}-w_{T2}}{w_{942°C}} * \frac{74.03}{18}$$ (50)

Where,

$\% \, CH$: Portlandite content

w_{T1}: Sample weight where a change in the slope starts (450°C - 550°C).

w_{T2}: Sample weight where a second change in the slope occurs (450°C and 550°C).

w_{942}: Sample weight at 942°C (Argos Procedure - The maximum reading from the equipment is from 940°C – 950°C)

$$\% \, W_n = \frac{w_{110}-w_{942}-(w_{loi})}{w_{942°C}}$$ (51)

Where,

$\% \, W_n$: non evaporable water

w_{110}: Sample weight at 110°C.

(w_{loi}) : LOI weight. It is calculated following the methodology described in section 4.2.3.

This method is the Argos procedure to calculate portlandite content and non-evaporable water. The temperatures mentioned for each calculation follow Argos criteria.

4.3   Mortar and paste combinations

Figure 31 describes the initial main variables of mortars and pastes, which are fly ash, fineness and activator dosage. Although fineness values, dosages, SCMs and activators were defined already, they could change depending on the results from the experimental data analysis. Alkali activators, hydrated lime and quicklime are some of

the activators considered. The preparation and evaluation of mortars follow ASTM C 109 and the procedure presented in section 4.2.1.

Mortars evaluation			Pastes evaluation		Activity	Phase 2
SCM: 50%					Constants	
SCMs: Termopaipa FA, Fabricato FA, Termoguajira FA, Tampa FA **SCMs particle size:** Original size, <75um, <45um **Activator 1 SIKA (0%, 0.5%, 1%, 1.5%, 3,5%):** Na_2SO_4 **Activator 2 (0%, 1%, 3%, 5%):** Hydrated lime **Activator 3 (0%, 1%, 3%, 5%):** Quicklime **Activator 4 (0%, 1%, 3%, 5%):** Na_2SO_4					Variables	
Compressive strength	**Heat of hydration**	**Mineralogy**	**SEM**	**Thermogravimetry**	Evaluation	

Figure 31 Mortar and paste variables

4.3.1 Fineness evaluation without including any activator

As it was mentioned in the literature review of this study, one of the ways to activate fly ash is by increasing fly ash fineness (Paya, *et al.,* 1995, 1996, 1997). It is important to highlight that its activity increases due to the increment of both the specific surface area and the reactive sites of fly ash (Shi and Shao, 2002); however, water requirement increases if a grinding process is used instead of the sieving process (Chindaprasirt, *et al*., 2004). Therefore this parameter was evaluated using a sieving treatment.

The effects of the sieving process on the chemical and mineralogical characteristics of the fly ash were presented in the previous chapter in Table 6. Walker and Pavia developed a complete study evaluating the influence of the fineness, amorphous and total silica content of different SCMs (Walker and Pavia, 2011); the results from that study showed that the specific surface area affected water demand, and the amorphous content influenced compressive strength. Based on the previous studies, different comparisons were developed in order to find the parameter which influenced the performance of the mortar the most, and to compare these results with published data.

For this initial part, the effect of the fineness on the compressive strength of blends of PC with 20% fly ash was evaluated without including any activator; it was done with the purpose of identifying the effect of the fly ash itself, making it easier to understand the main influencing factors after introducing an activator. From Figure 32, it is evident that Tampa fly ash was affected positively by the fineness; local fly ashes did not have the same pattern due to the variation of the amorphous content.
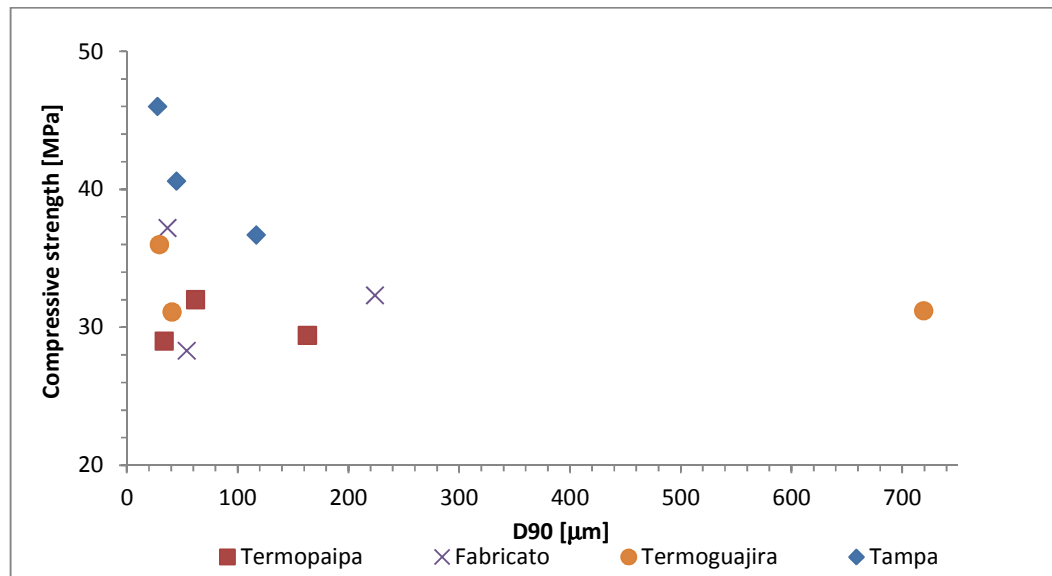
Figure 32 Fineness effect on the 28-day compressive strength for different size fractions of each ash (represented by D_{90})

The compressive strength is expected to decrease upon increasing the LOI content (Atiş, 2005). This general behaviour was observed, but there were also some unexpected trends; by decreasing the LOI content of a given ash, the compressive strength was not always seen to be improved; Figure 33 presents this for three of the fly ashes (Tampa FA, Termoguajira FA and Termopaipa FA). This behaviour means that it is necessary to also consider the other fly ash components. It is important to mention that the w/b of 0.484 was the same for all the mixes.
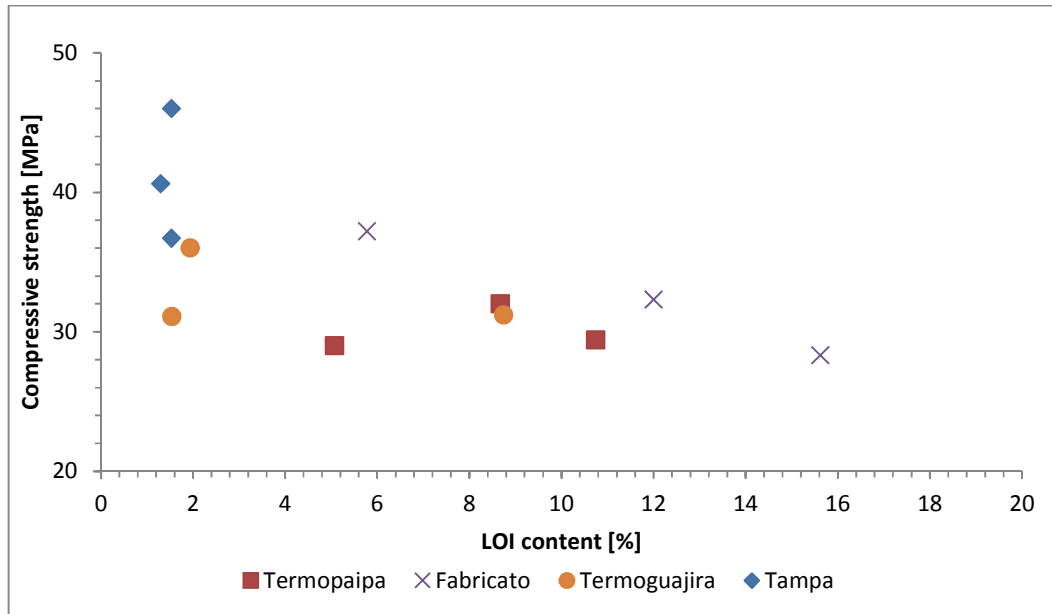
Figure 33 LOI effect on the 28-day compressive strength

The calculated reactive silica content of all of the fly ashes is plotted in Figure 34, and the compressive strength seemed to be more influenced by this parameter than the LOI content. It is important to mention that the approximate reactive SiO_2, Al_2O_3 and Fe_2O_3 values were calculated by using the total amorphous content, XRF data for the bulk ash composition, and the composition and quantities of all crystalline products presented in the fly ash according to XRD Rietveld analysis. The difference between the total XRF values and the chemical components of the crystalline products was defined to be the amorphous content. The composition of each crystalline product was obtained from each mineral description from the XRD database. Walker and Pavia plotted the total SiO_2 and in their data, there was not a trend of improving compressive strength by increasing the content of this parameter (Walker and Pavia, 2011); this was not the reactive SiO_2 value, making it difficult to compare with the results here.
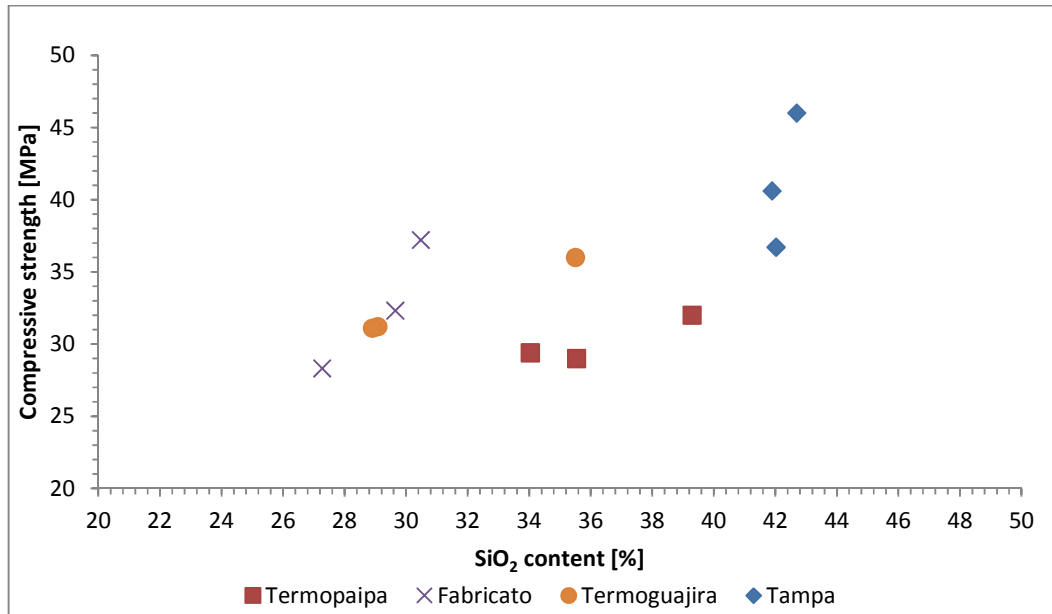
Figure 34 Reactive SiO$_2$ effect on the 28-day compressive strength

The reactive Al$_2$O$_3$ was calculated in the same way the SiO$_2$ was done. Figure 35 shows how the compressive strength was also influenced significantly, at least more than the effect of the LOI. This did not occur with Fe$_2$O$_3$, where there was not any trend in Figure 36. Some authors such as Fernández-Jimenez and Palomo evaluated fly ash with high Fe$_2$O$_3$ content; main reaction products did not present any iron content (Fernandez and Palomo, 2003).
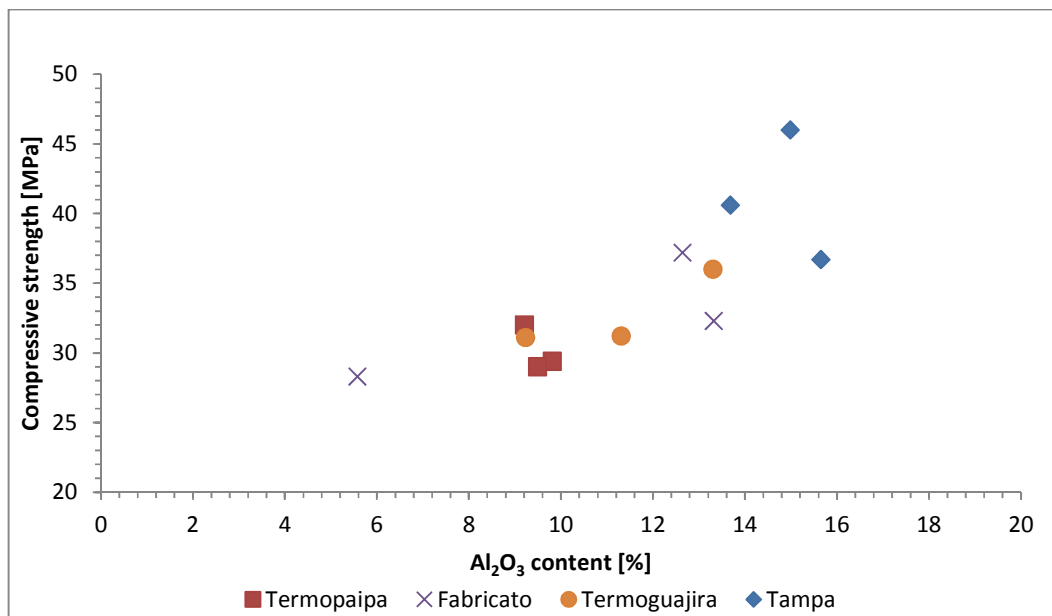
Figure 35 Reactive Al$_2$O$_3$ effect on the 28-day compressive strength
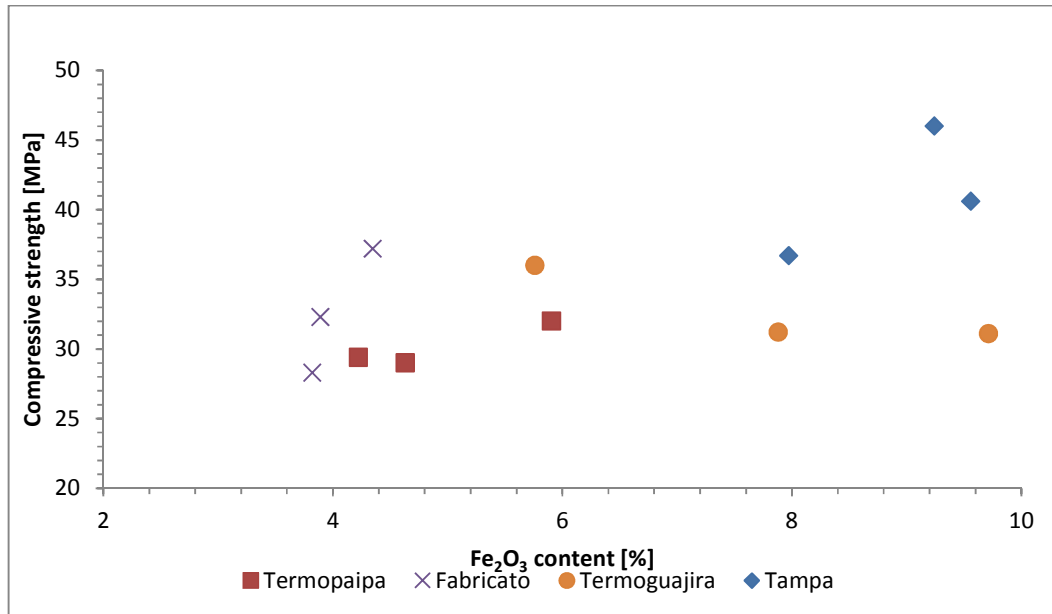
Figure 36 Reactive Fe$_2$O$_3$ effect on the 28-day compressive strength

When SiO$_2$ and Al$_2$O$_3$ were added and plotted in Figure 37, the influence of these two components over the compressive strength was significant. Berry, *et al.* studied the influence of both materials describing the processes they are involved in, ending with insoluble silicate and aluminate hydrates which improve compressive strength (Berry, *et al.,* 1990; Berry, *et al.,* 1994).
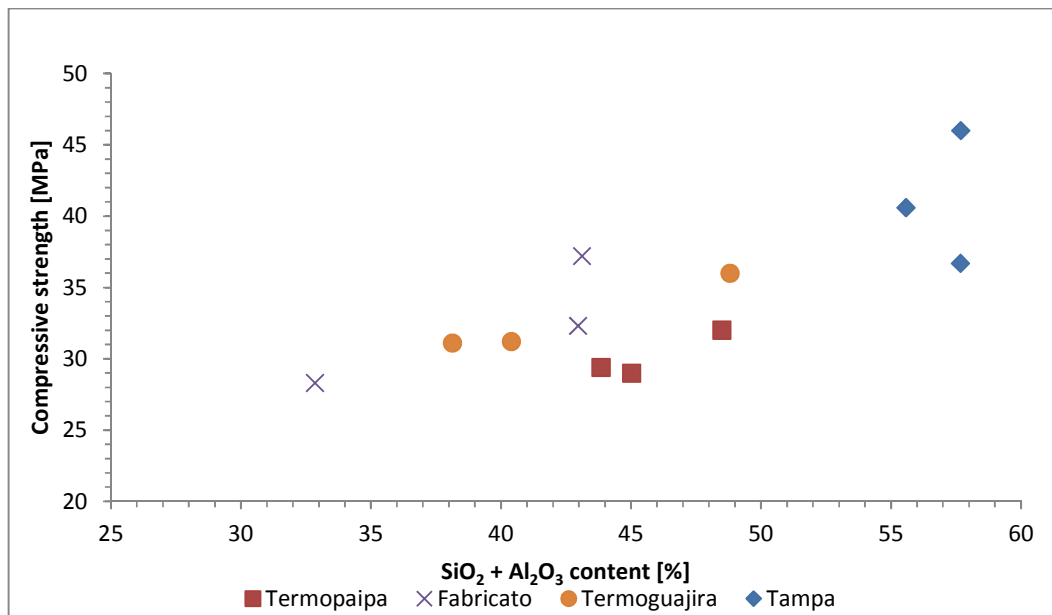
Figure 37 Reactive SiO$_2$ + Al$_2$O$_3$ effect on the 28-day compressive strength

For all the fly ashes, the amorphous content changed with the fineness (D90) but without following a distinct pattern. The compressive strength was improved by increasing the amorphous content. Based on the previous results including the reactive

90

calculated values of SiO_2 and Al_2O_3, the amorphous content was one of the most relevant characteristics related to the 28-day compressive strength; this is evident in Figure 38 and 39. Although the majority of LOI particles were among the largest size ranges, it did not present a key influencing role on the compressive strength as the amorphous content did. Walker and Pavia also found that for different SCMs the amorphous content was one of the most relevant factors to control for compressive strength evolution (Walker and Pavia, 2011).
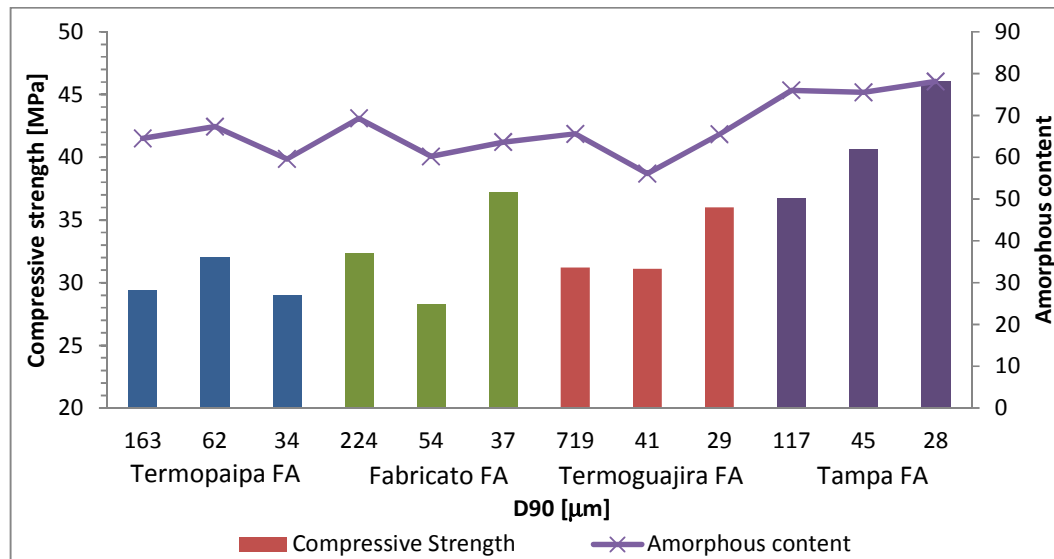
Figure 38 Effect of the fineness and the amorphous content on the compressive strength
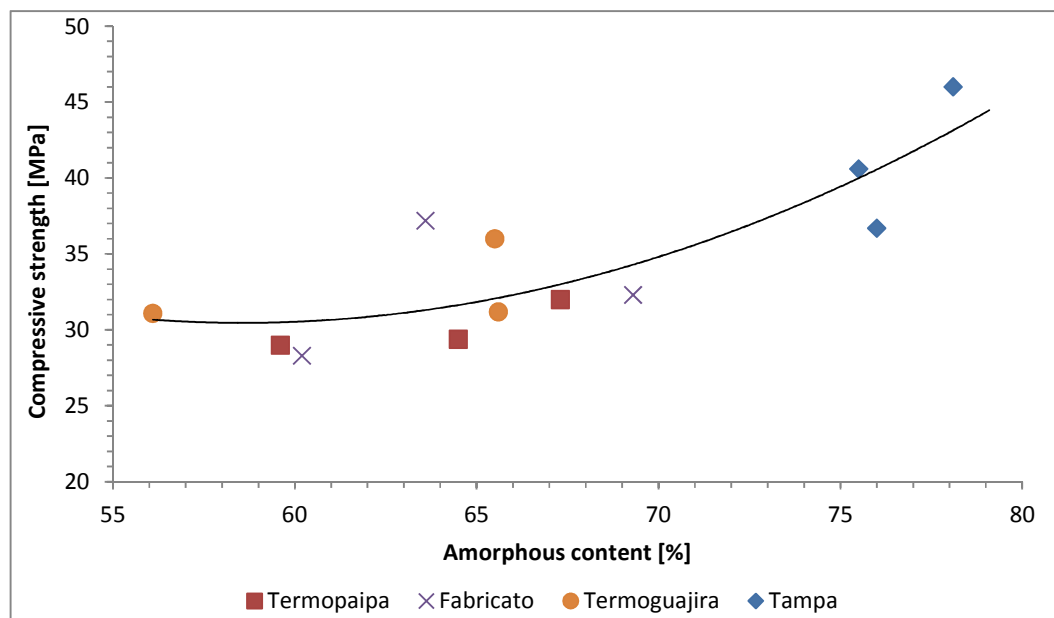
Figure 39 Effect of the amorphous content on the compressive strength

91

4.3.2 Activated mortars and pastes evaluation

This evaluation considered all the activators, fly ashes and fineness variation. Every set of samples included 100% PC, 80% PC - 20% FA, and three mixes with 50% PC - 50% FA and three different dosages (mass). Table 13 presents the variables considered in the project.

Table 13 Variables in activators study

FA Fineness	Fly ash	Activator	Activator Dosage
Original size / <74 µm / <45µm	Termopaipa / Fabricato / Termoguajira / Tampa	Activator 1	0%, 0.5%, 1%, 1.5%, 3%
		Quicklime	0%, 1%, 3%, 5%
		Lime	0%, 1%, 3%, 5%
		Na_2SO_4	0%, 1%, 3%, 5%

Considering these initial variables, the total number of mortar mixes is 612; in the same way for some of these mixes, there are some pastes which are included for additional testing. The order followed to test all the variables starts with the original size (OS) Termopaipa FA evaluation including every activator and dosage; this is followed by OS Fabricato FA, Termoguajira FA and Tampa FA evaluation. After this, the next step is to evaluate these fly ashes with a lower D90.

The analysis methodology followed the structure presented in Table 14. In this table all the variables were included; four different analyses were developed in order to find the most important influencing parameters in mortar behaviour.

Table 14 Analysis structure

Analysis number	Size	Fly Ash	Activator	Dosage
1	Constant	Constant	Variable	Variable
2	Constant	Variable	Variable	Optimum
3	Variable	Constant	Variable	Optimum
4	Variable	Variable	Constant	Optimum

Due to the number of variables and mixes developed along this phase, it was necessary to consider a Mix ID. Each mix had a code where all the variables were included. The following tables present the Mix ID components.

Table 15 Mixes ID a) Order/Description b) Code per variable

Mix ID (1/2/3/4/5/6)	
Letters and numbers order	**Description**
1	Cementitious material name
2	Fly ash size
3	Fly ash percentage
4	Activator
5	Dosage
6	Age

a)

1 - Cementitious Material Name	
CE	Cement
TP	Termopaipa FA
FB	Fabricato FA
TG	Termoguajira FA
TA	Tampa FA
2 - Size	
OS	Original Size
75	<75 µm
45	<45 µm
3 - Fly ash percentage	
0	0%
20	20%
50	50%
100	100%
4 - Activators	
A	Activator 1
Q	Quicklime
L	Lime
S	Sodium sulfate

b)

4.3.2.1 Original size evaluation

4.3.2.1.1 Termopaipa FA

As can be seen in Figure 40, the compressive strength of the sample with 50% Termopaipa FA using activator 1 (Na_2SO_4 from Sika) was improved about 50% compared to the sample without activator (Average TP/OS/50). The compressive strength improvement occurred in the first 3 to 7 days. Although the compressive strength was lower compared to the sample with 20% fly ash (TP/OS/20), it could be improved by reducing the water to cementitious material ratio. This part will be evident in the following phase where the concrete mixes are evaluated. Although the mix with 3% activator 1 had the best behaviour, the mix with 1% was close in performance.

When quicklime and lime were added to the mix, there was little effect on the compressive strength. The optimum dosage using quicklime and lime was the same (3%) for both of these compounds. Comparing quicklime and lime, the former gave a higher compressive strength at 3 days, even passing the control sample (Average TP/OS/50); at 7 and 28 days the lime mix had a higher compressive strength and only after 56 days the quicklime mix improved its strength. Considering the compressive strength evolution using lime and quicklime, Shi found that there was an optimum

portlandite level and when it was passed, the $Ca(OH)_2$ not involved in any reactions would weaken the matrix; Shi also found that the initial heat released from the quicklime and water reaction helped to accelerate the pozzolanic reaction, and the $Ca(OH)_2$ thus formed could be more soluble than manufactured lime (Shi, 2001).

According to XRF results, activator 1 (Sika activator) and the last activator are composed mainly of the same component: Na_2SO_4. The plain Na_2SO_4 had a positive effect at every age; the most relevant effect was from 7 to 28 days. The effectiveness of Na_2SO_4 with high volume fly ash mixes was evaluated by Qian, *et al.*; fly ash dissolution is accelerated due to alkalinity increase when reacting Na_2SO_4 with $Ca(OH)_2$. The density of mixes is increased by ettringite formation when sodium sulfate is included in the matrix (Qian, *et al.*, 2001).
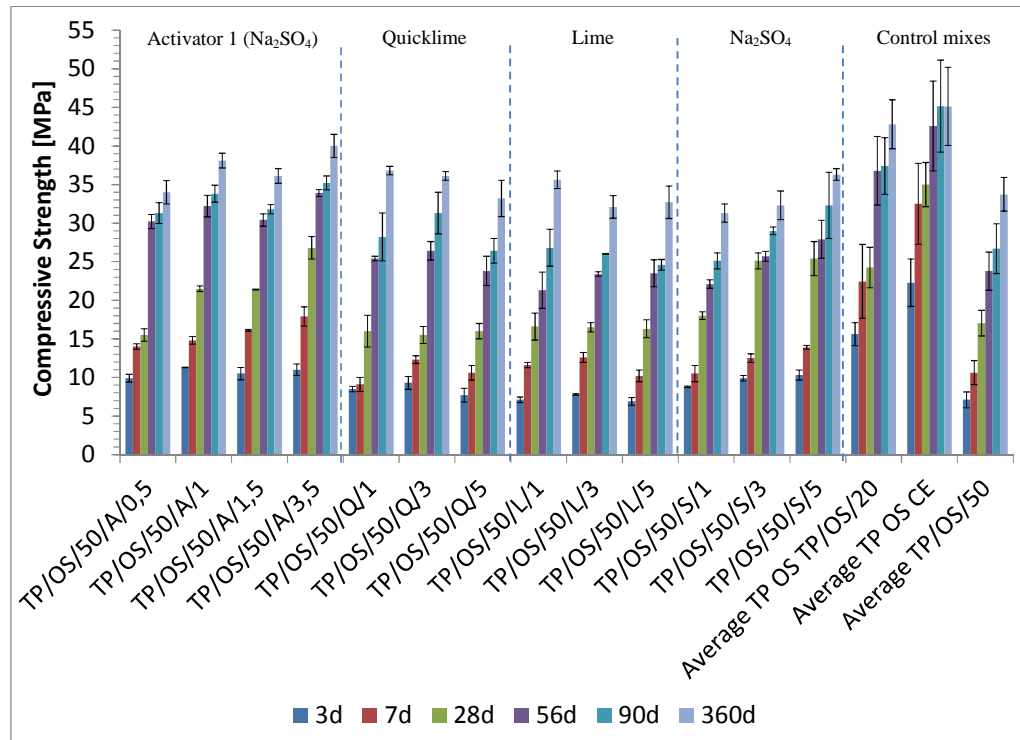
a) Compressive strength evolution
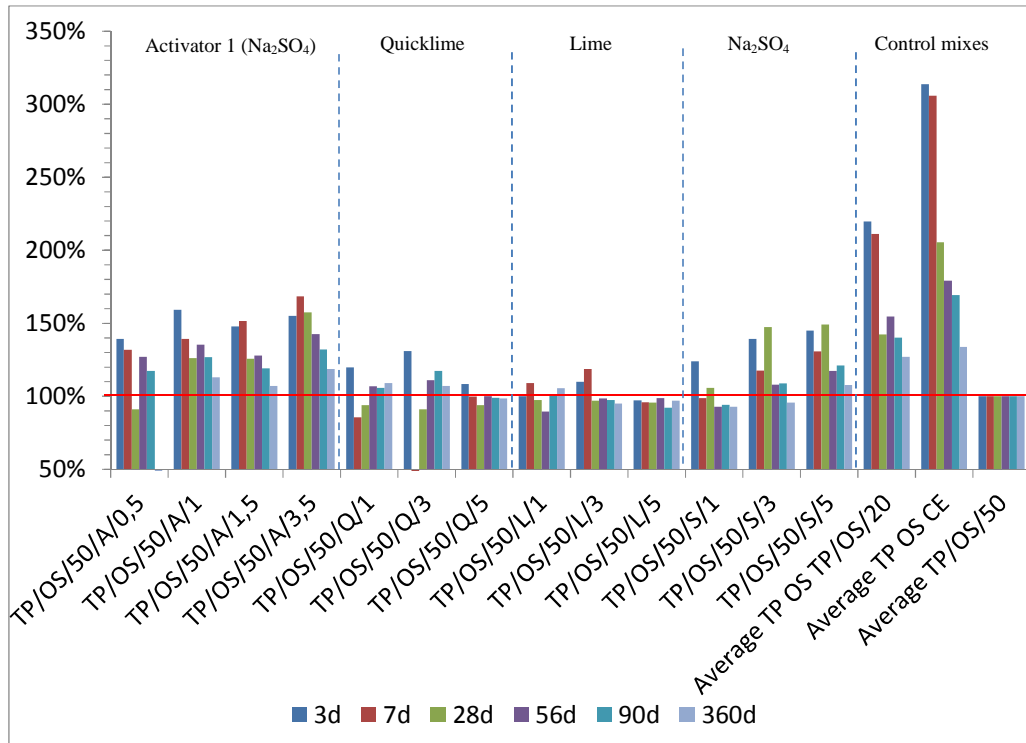
b) Percentage evolution relative to the control mix (Average TP/OS/50)

Figure 40 Compressive strength

According to the isothermal calorimetry data presented in Figure 41, the sample with 50% of fly ash decreased in heat flow and increased in setting time by about two hours, compared with the 100% cement mix (CE/10/100). Quicklime had the highest peak in the first minutes. The induction period for the 100% cement sample started after an hour, while the others about two hours later. The acceleration period started after two hours for the 100% cement sample and the others after four hours; this was probably due to the delay in the C-S-H formation. Generally, delays in reactions can increase by increasing fly ash content due to an increase in the effective water to cement ratio and the dilution of the reactive cement. There is a possible delay due to the reaction of the Ca of the solution with the aluminium of the fly ash surface (Wei, *et al.,* 1985). However, it is important to consider that the filler effect can help to accelerate the reaction when the W/CM is very low; additional nucleation sites are available (Deschner, *et al.*, 2012). Mixes with lime and quicklime presented the same behaviour as the one without any activator. The presence of a peak in the deceleration period was not evident; this peak is related to a second aluminate and calcium sulfate reaction ending in ettringite or AFm (alumininate-ferrite mono) phase; generally it is more evident when fly ash is used due to the seeding effect (Deschner, *et al.*, 2012).
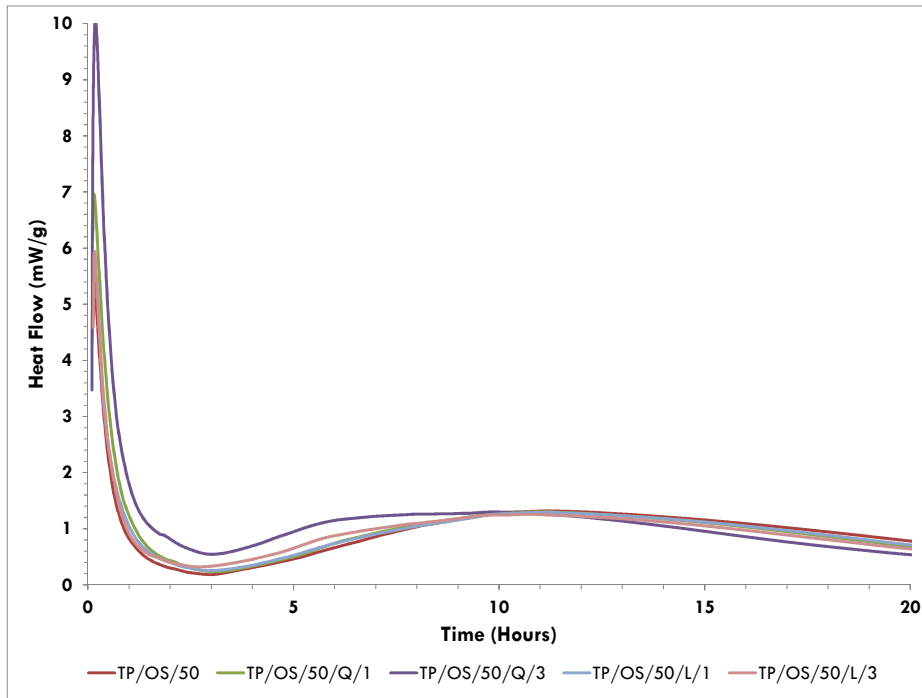
Figure 41 Heat Flow – Termopaipa FA OS – 20°C

As seen in Figure 42 pastes with quicklime released more energy than the others. The sample with 3% of quicklime had a positive energy delta of 20 J/g compared to the rest of the mixes at the beginning of the curve. According to these curves quicklime reduces the setting time; a combination of quicklime and activator 1 could be an alternative in order to guarantee the setting time. It is important to combine different quicklime and activator 1 proportions to find a standard setting time depending on the concrete application.
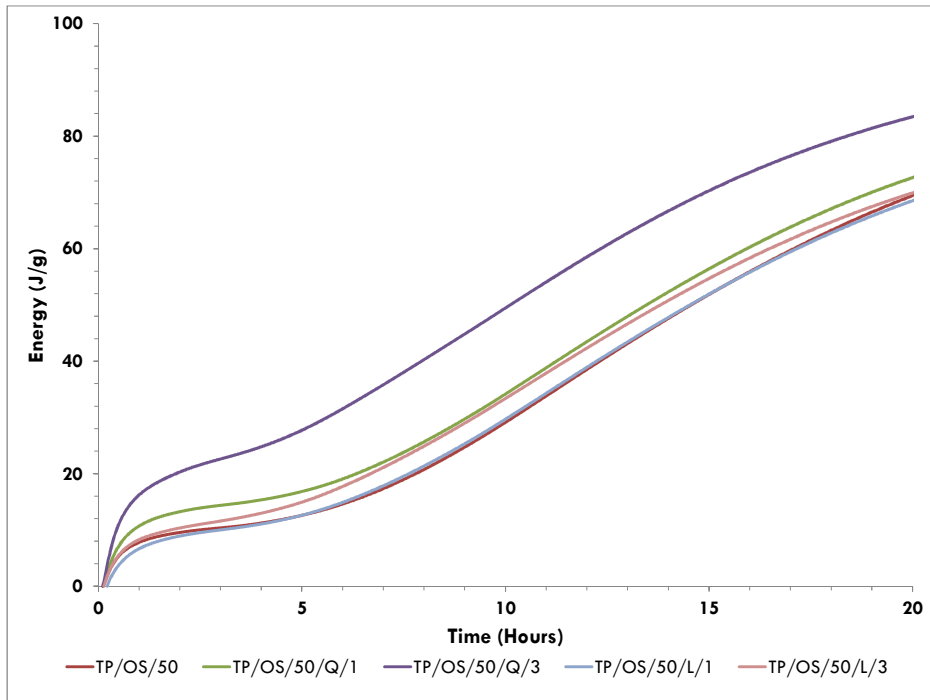
Figure 42 Energy (Pastes) – Termopaipa FA OS

Figure 43 includes the thermogravimetry data for samples with different activators. As is seen in this figure and as mentioned before in the TGA procedure, the slope change takes place at around 450°C and 550°C, becoming a reference for portlandite calculation. The total non-evaporable water is also calculated from this figure using the reference weights at 110°C and 942°C.
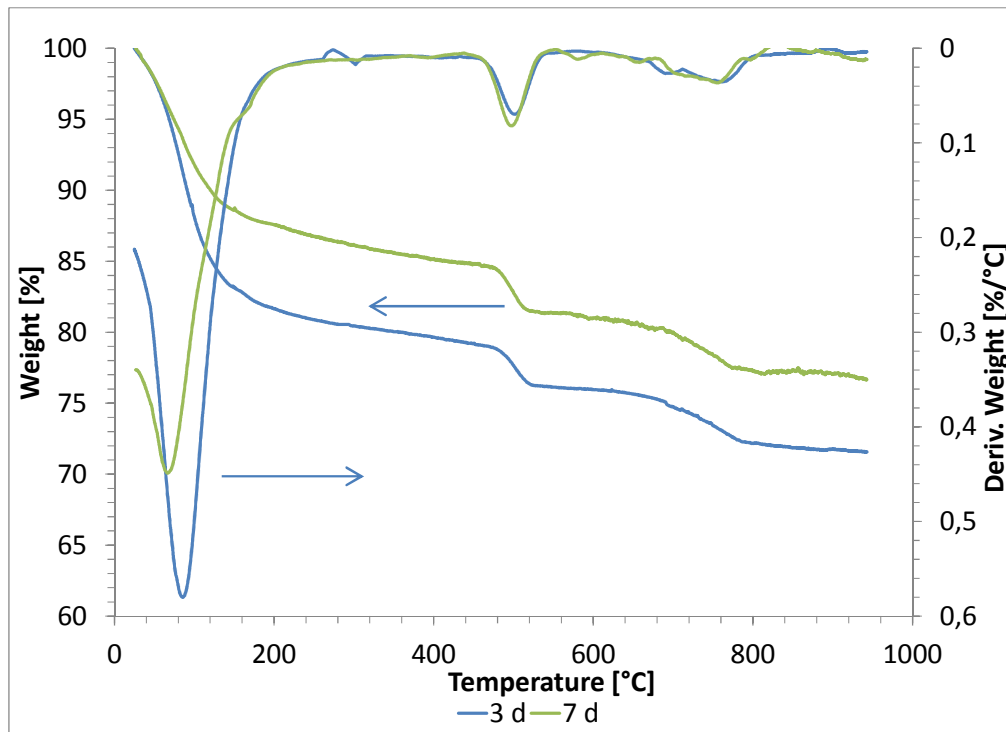
a) CE/10/100
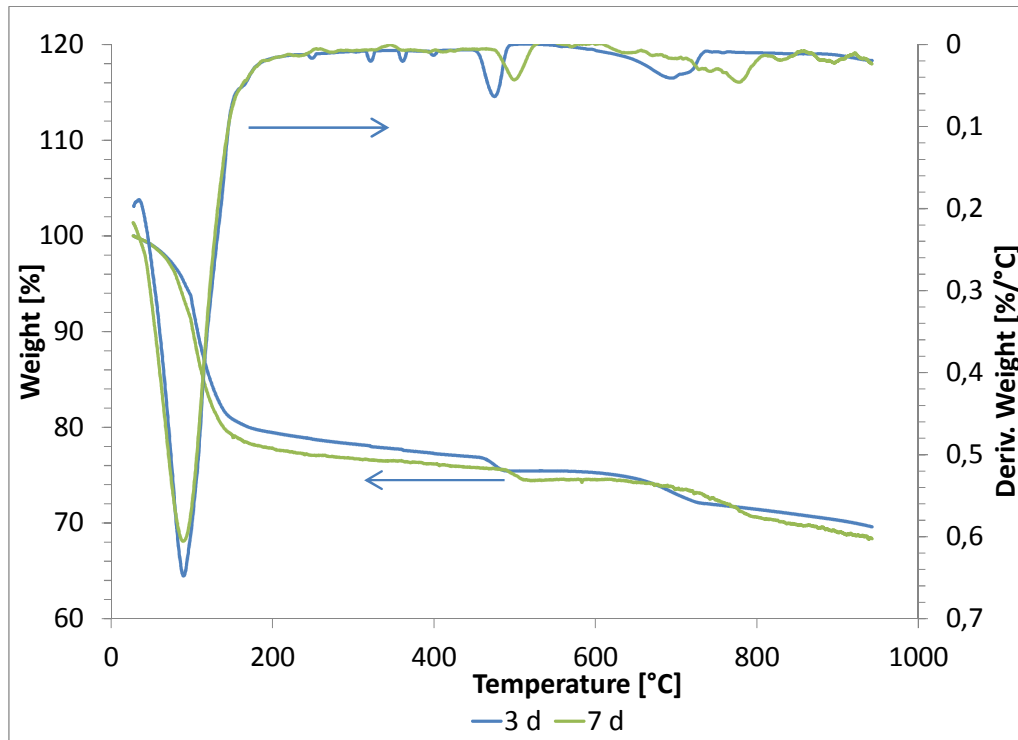
b) TP/OS/50/A
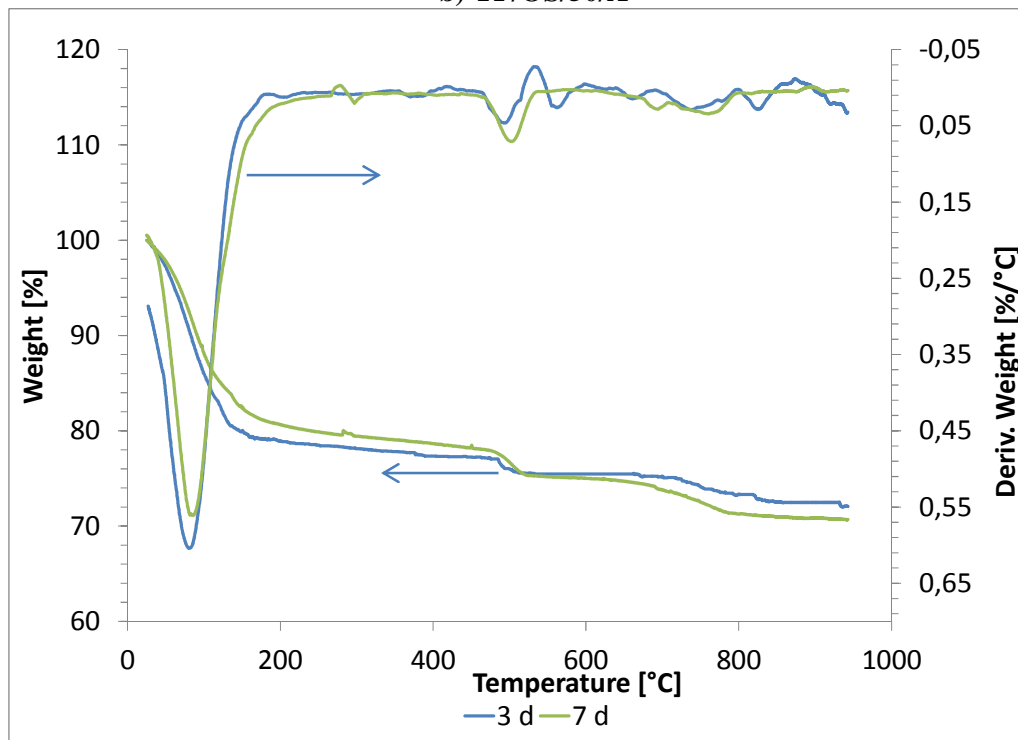
c) TP/OS/50/Q
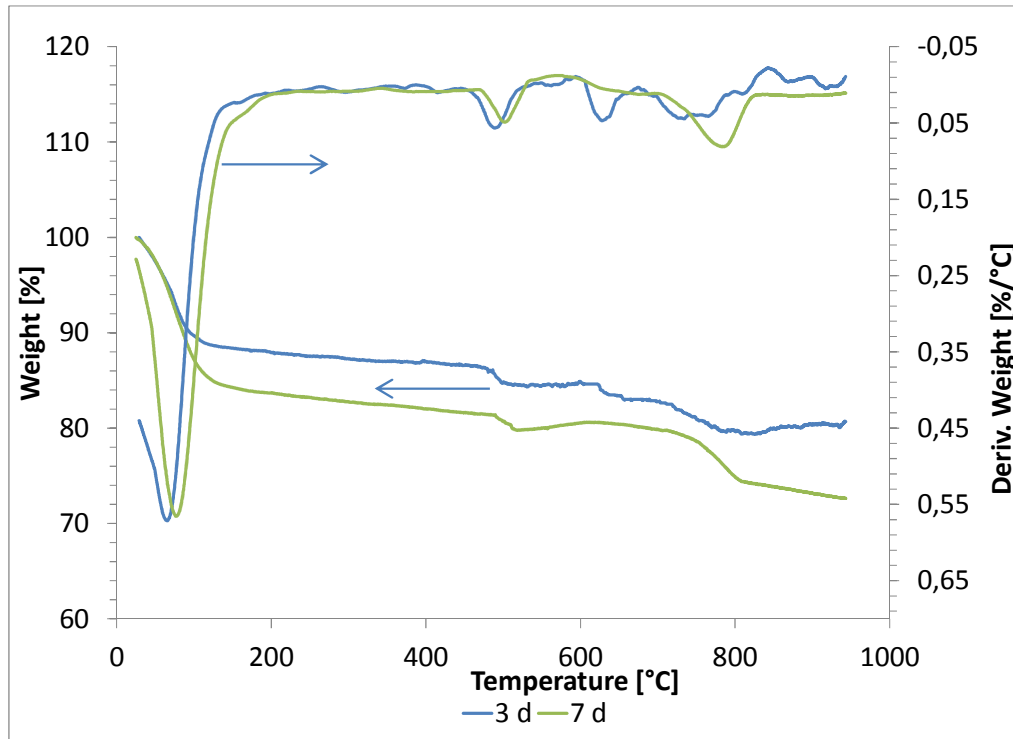
d) TP/OS/50/L
Figure 43 TGA using different activators at 3 and 7 days

The Ca(OH)$_2$ content decreased using activator 1 before 7 days (TP/OS/50/A/1/7), while for quicklime and the control mix with 20% fly ash (TP/OS/20/0/0/7), it occurred after this period; the amount of Ca(OH)$_2$ increased with time for quicklime mixes in the first days, where quicklime reacted with water forming Ca(OH)$_2$. Portlandite consumption started earlier using activator 1 showing its influence on fly ash; this is shown in Figure 43 and 44. Due to nucleation and the seeding effect the amount of the Ca(OH)$_2$ per gram of cement for mixes including 50% fly ash was higher than the mix with 100% cement. After 7 days it is evident how lime reacts with fly ash, reducing the lime amount significantly.
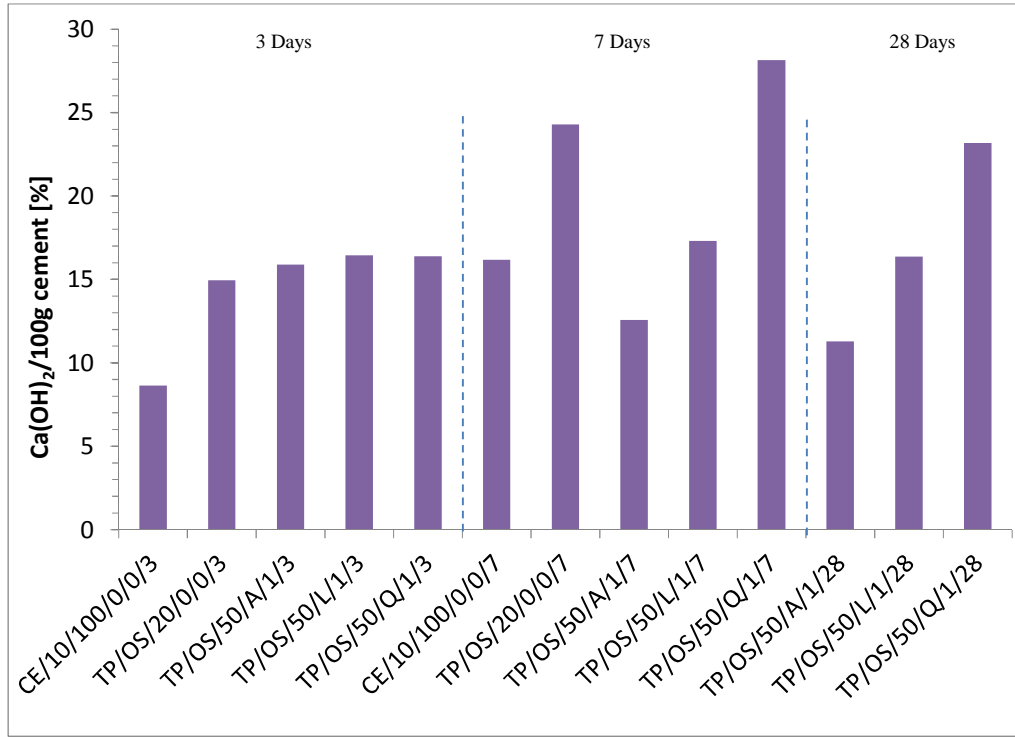
Figure 44 Ca(OH)$_2$ / 100g cement

As seen in Figure 45, the bound water increased more from 3 to 7 days for the mix with activator 1 than the mix with lime; this parameter decreased for the mix with quicklime at this range of time. At the age of 28 days the bound water values for all the mixes were similar.
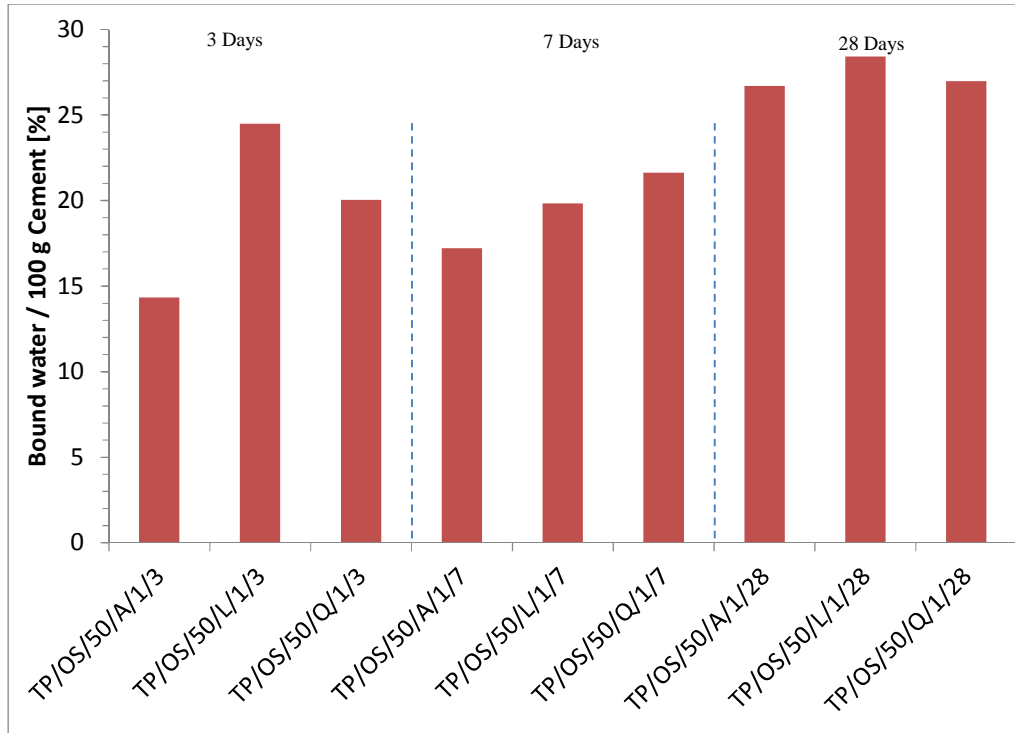
Figure 45 Bound water / 100 g cement

100

In the XRD evaluation the amorphous content was included in order to have the most accurate values of all the phases; some of the C-S-H was amorphous, while some was more ordered and able to be described separately. It is important to make clear that rutile was used as an internal standard for the amorphous content quantification. The content of well ordered C-S-H (fitted as tobermorite) was the highest in the sample with 100% cement at 3 and 7 days. The activator 1 (Na_2SO_4) mixture had a higher tobermorite content at the first three days compared to the mix with lime but it became lower at 7 days; after 28 days tobermorite content increased for mixes with activator 1, quicklime and lime, getting closer to the mix with 20% fly ash.

Portlandite content as measured by XRD was the highest for the mix with 100% cement followed by the mix with lime. Portlandite content was almost halved for mixes with activators at the first 3 days. At 7 and 28 days, portlandite for the mix with activator 1 decreased significantly, while for lime it kept increasing up to 7 days and then decreased at 28 days through the pozzolanic processes. Comparing these results with those obtained with TGA, the portlandite consumption is similar with time; the activator effect is seen from the first days while mixes with lime have a reduction in portlandite after 7 days.

A	Alite
B	Belite
E	Ettringite
C	Calcite

M	Mullite
Q	Quartz
R	Rutile

P	Portlandite
T	Tobermorite
MC	Monocarbonate

MS	Monosulfate
G	Gypsum
Ha	Hatrurite

Legend: —— CE —— TP/OS —— CE/10/100/0/0/3 —— TP/OS/100/A/1/3 —— TP/OS/50/A/1/3 —— TP/OS/50/L/1/3

a) 3 days

A	Alite
B	Belite
E	Ettringite
C	Calcite

M	Mullite
Q	Quartz
R	Rutile

P	Portlandite
T	Tobermorite
MC	Monocarbonate

MS	Monosulfate
G	Gypsum
Ha	Hatrurite

2θ

CE — TP/OS — CE/10/100/0/0/7 — TP/OS/20/0/0/7 — TP/OS/50/A/1/7 — TP/OS/50/L/1/7

b) 7 days

103

A	Alite	M	Mullite	P	Portlandite	MS	Monosulfate
B	Belite	Q	Quartz	T	Tobermorite	G	Gypsum
E	Ettringite	R	Rutile	MC	Monocarbonate	Ha	Hatrurite
C	Calcite						

c) 28 days

Figure 46 XRD Diffractograms

104

Activator 1 had an effect on ettringite formation; as is shown in Figure 46, the mix with activator 1 had the highest content at all ages. Monocarbonate, dicalcium silicates and tricalcium aluminate were present in all the mixes in low proportions. As expected, some phases such as quartz, mullite and even the amorphous content appeared in high proportion for mixes including fly ash.

Quartz and mullite content was proportional for mixes including 50% fly ash, comparing it with the total content of Termopaipa OS, indicating that these phases are unreactive. The majority of amorphous content in each mix is composed of the combination of C-S-H and fly ash amorphous content itself. The reference amorphous content for a mix with 50% of fly ash at 3 and 7 days is 51.3% and 53.96% respectively; these values are obtained by adding half of the amorphous content of the 100% cement mix with half of the amorphous content of the fly ash. Comparing these initial values with the real ones, the mix with lime had the highest value and passed the calculated one at 3 days; on the other hand the mix with activator 1 had the highest value at 7 days, exceeding the precalculated one. This can be seen in Figure 47.
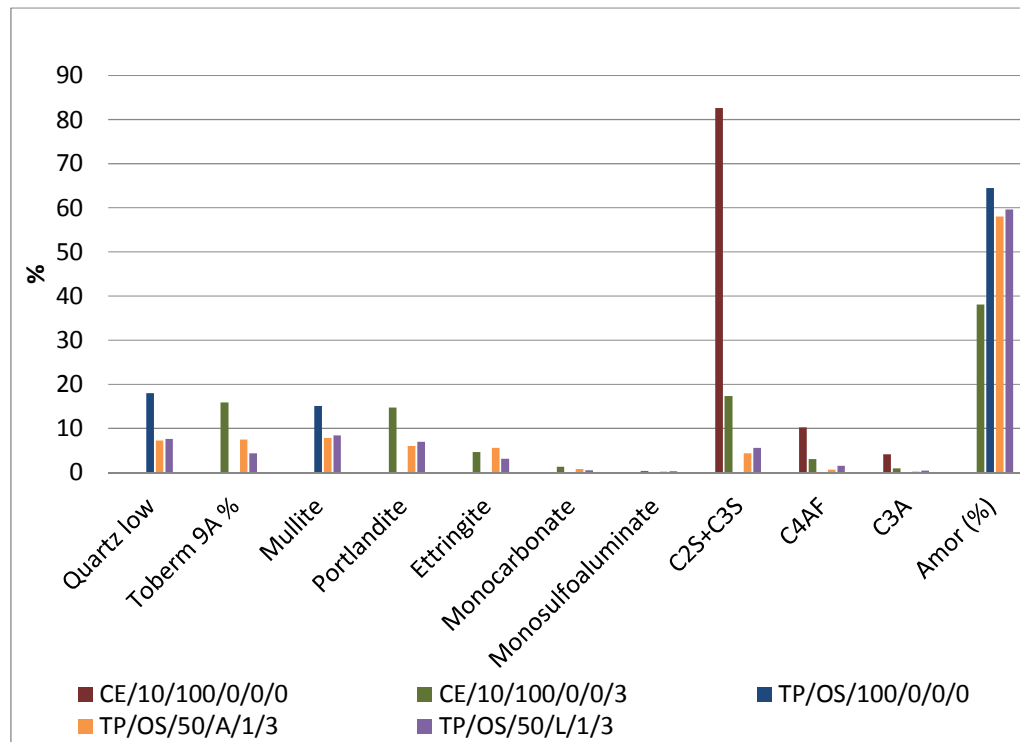
a) 3 days
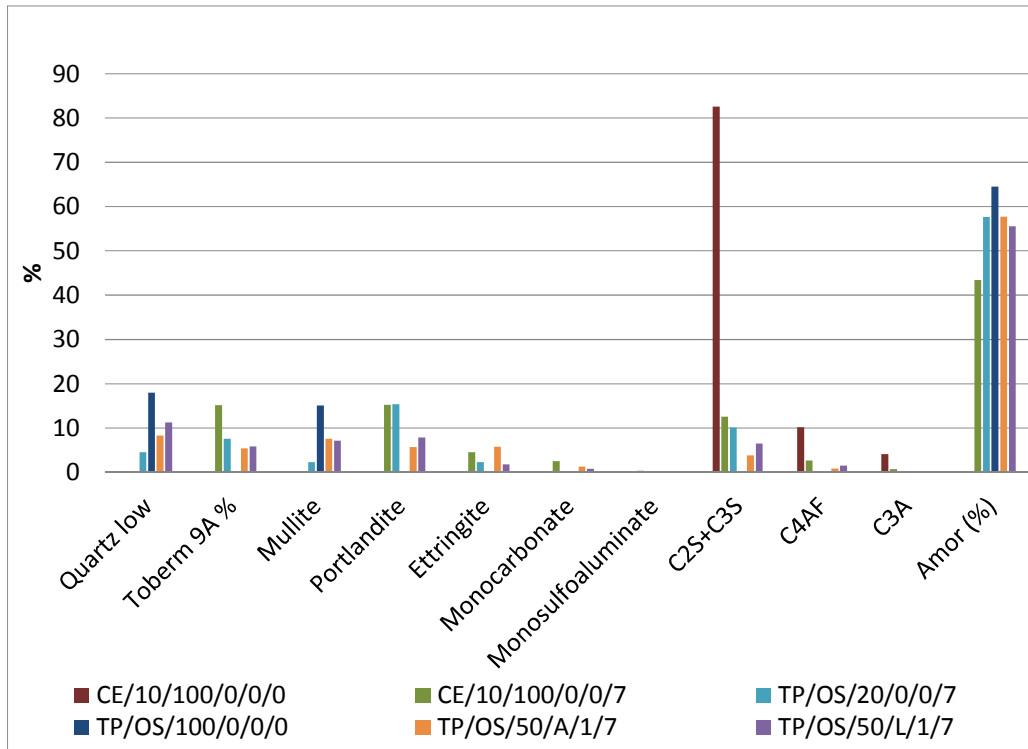
b) 7 days
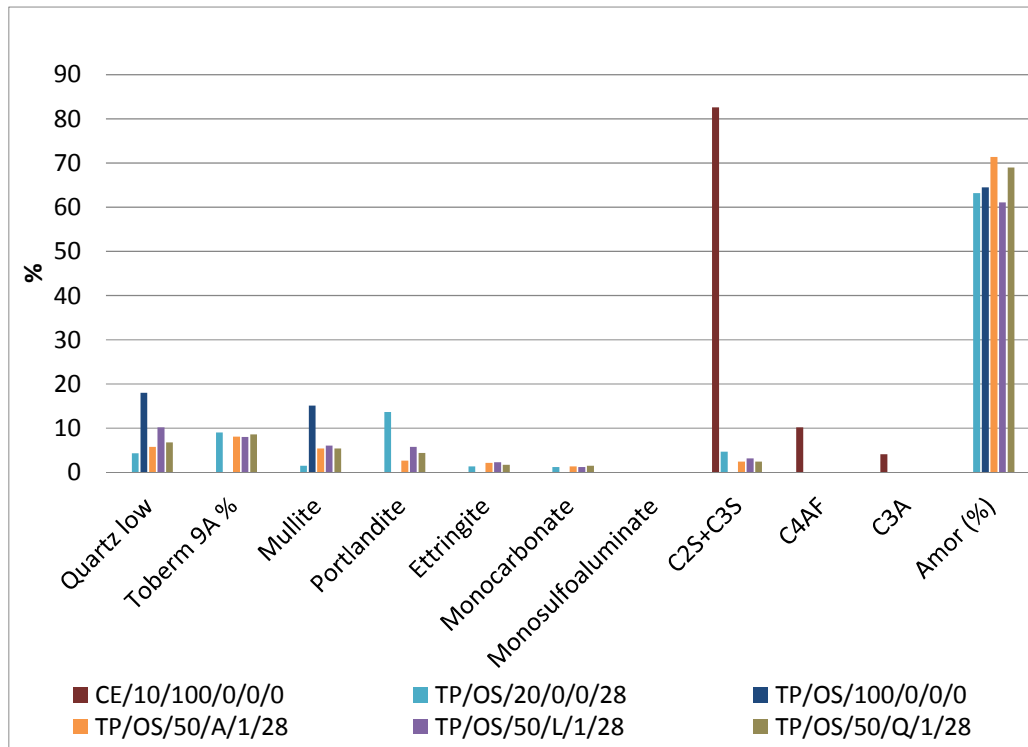
c) 28 days

Figure 47 XRD

4.3.2.1.2   Fabricato FA

Activator 1 increased the compressive strength simultaneously as the activator dosage increased. These results were compared against FB/OS/50 samples and the highest strength with activator was almost double that of the non-activated mix; OS Fabricato fly ash has a high amorphous content which could influence the activation process. Activator 1 dosage had the same effect on both Termopaipa FA and Fabricato FA; there was not a significant variability in the strength with 1% and 1.5% and it was improved after increasing the dosage to 3%. Activator 1 increased strength with 3% significantly passing sample FB/OS/20 at 56 days.

Although quicklime increased the compressive strength with a dosage of 3%, it did not have the same effect as activator 1. Figure 48 presents a trend where after 28 days it had a significant increment. There was an unexpected effect with 3% of quicklime, not only with Fabricato but also with Termopaipa FA. Considering lime mixes, they had low strengths compared with the control one at most of the ages tested. Although quicklime and lime mixes had a delayed effect compared to activator 1 mix, strengths seemed to be improved at later ages.
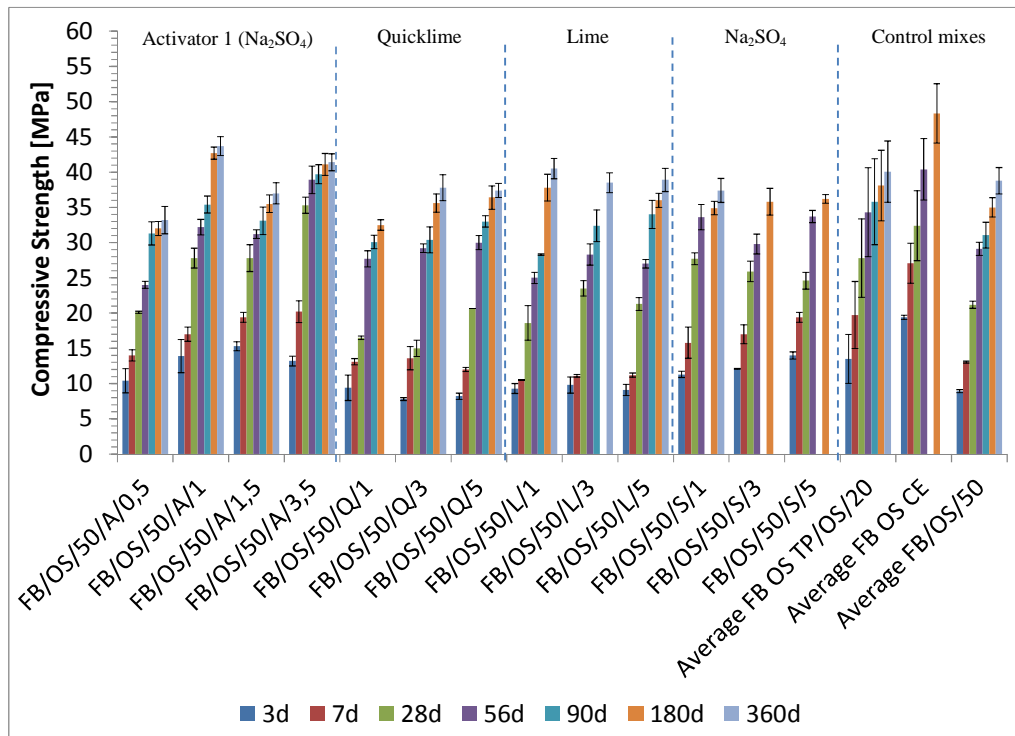
a) **Compressive strength evolution**
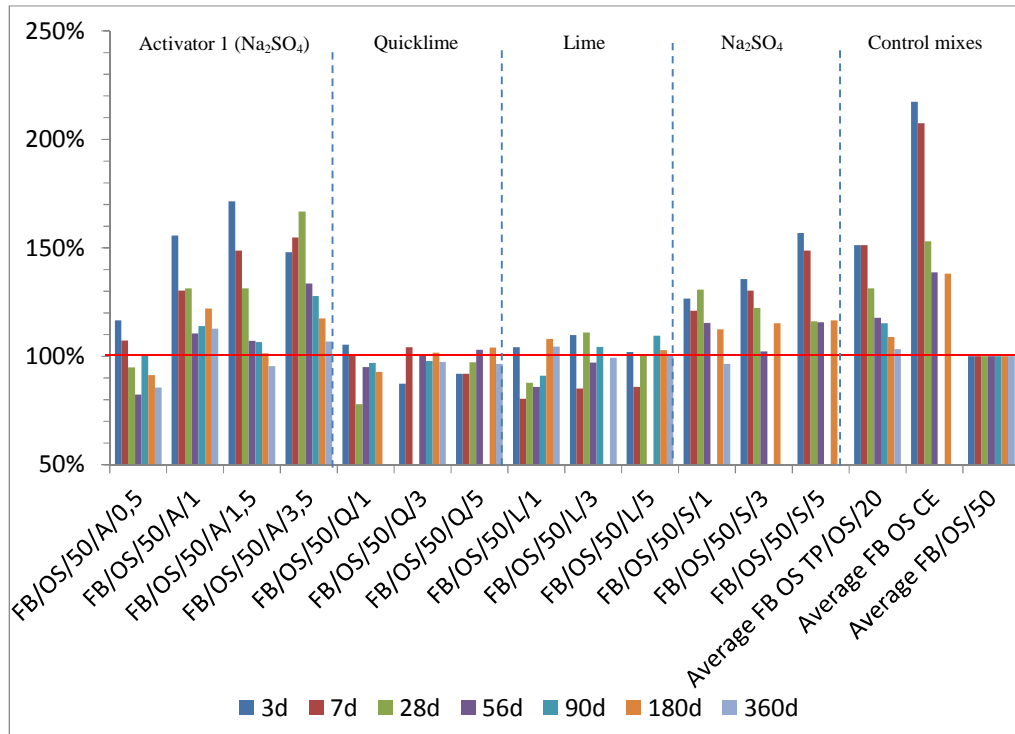
b) Percentage evolution relative to the control mix (Average FB/OS/50)

Figure 48 Compressive strength

Fabricato FA had almost the same effect as Termopaipa FA in terms of calorimetry as shown in Figure 49. The induction and acceleration period had about an hour delay for all the mixes with 50% of fly ash compared to the 100% cement mix. As was seen with Termopaipa FA, Fabricato FA had the highest first peak (mixing peak) with quicklime. When quicklime and lime were included, the setting time decreased. Activator 1 increased the peak of the heat flow by 0.4 mW/g but there was a delay in the final setting time of about 2 hours compared to the mix FB/OS/50; as this activator introduced sodium and sulfate to the mix, it was expected to react with aluminium supplied by the fly ash.
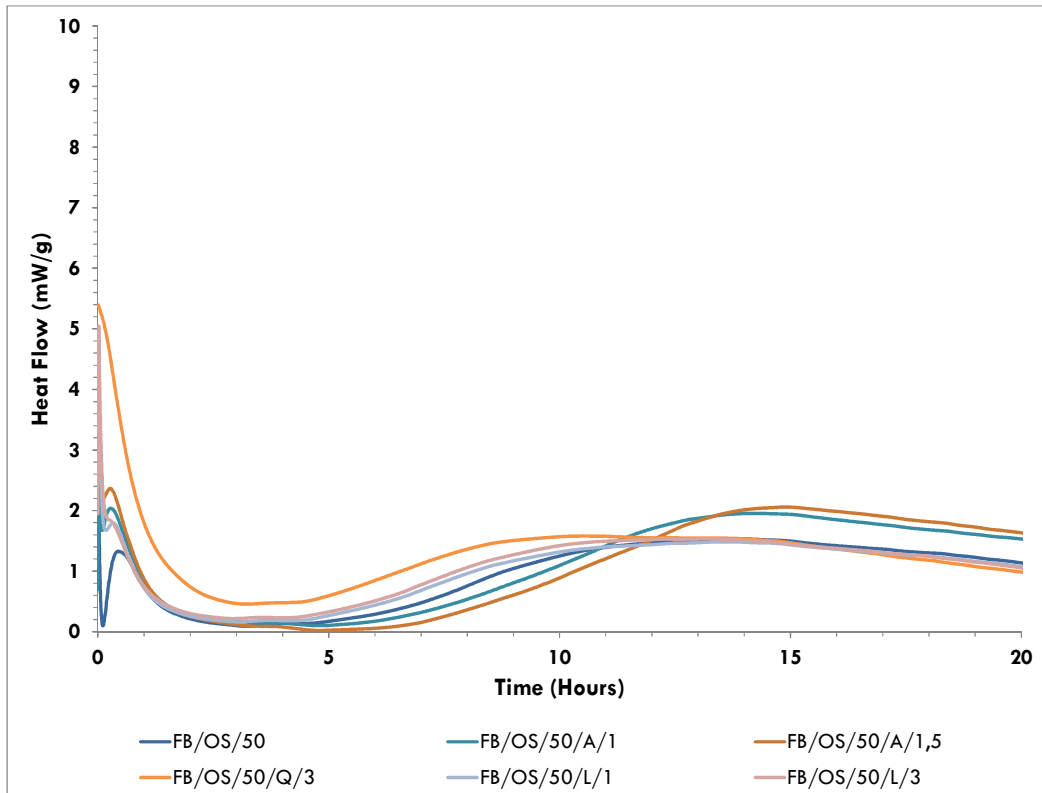
Figure 49 Heat Flow – Fabricato FA OS
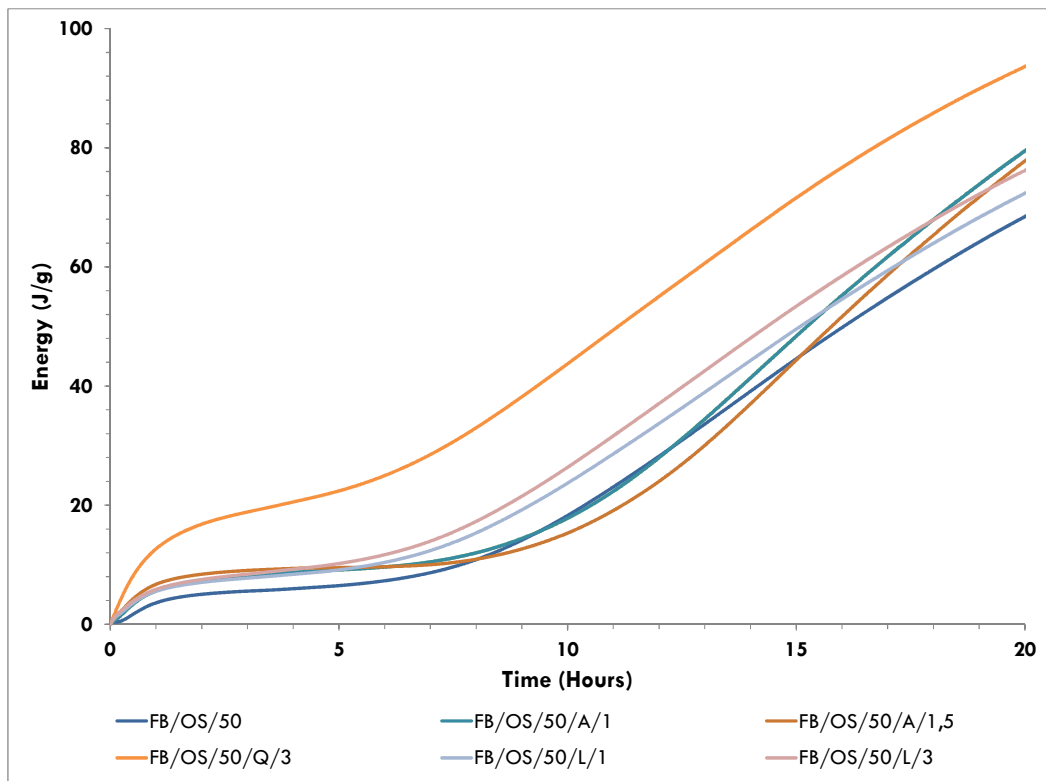
Figure 50 Energy (Pastes) – Fabricato FA OS

The mix with quicklime had the highest energy release compared to the other mixes with activators at the first 20 hours. Figure 50 shows that activator 1 and lime

did not have an effect in the first hours; these mixes released a similar amount of energy in the first 20 hours compared to the mix without activator.
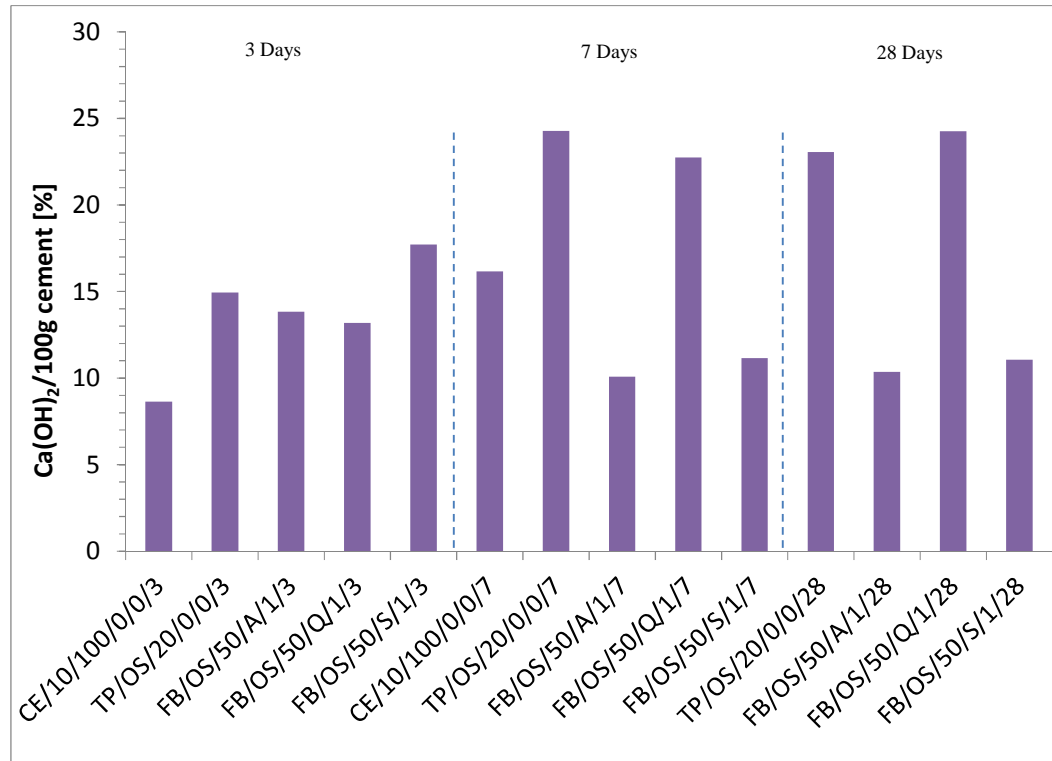
Figure 51 Ca(OH)$_2$ / 100g cement

It is important to mention that the quantification considers total mass loss in certain temperature ranges as referenced in the procedure included at the beginning of this chapter. The total Ca(OH)$_2$ content for samples with fly ash decreased as the fly ash content increased. As seen in Figure 51, after the first 3 days, the amount of Ca(OH)$_2$ per 100g of cement was higher for mixes with fly ash than the 100% PC sample; this was a result of the seeding effect on the mix of the fly ash (Deschner, *et al.*, 2012). The Ca(OH)$_2$ of the control sample with 20% fly ash TP/OS/20/ and samples with quicklime FB/OS/50/Q/1 started to decrease after 7 days; this was delayed compared to the mixes with activator 1 FB/OS/50/A/1 and sodium sulfate FB/OS/50/S/1, where after 3 days the portlandite content decreased. As occurred with Termopaipa fly ash in the previous section, during the first days lime content increased due to quicklime and water reaction while sodium sulfate accelerated the process for the reaction of the fly ash with portlandite for mixes with this activator.

The amount of bound water with activator 1 was the lowest at 3 and 7 days but after 28 days it was the highest; Figure 52 presents how the formation of hydration

products for the mix with activator 1 at the early days was not significant as at 28 days. The mix with quicklime made little difference compared with the other activators.

Figure 52 Bound water / 100 g cement

A	Alite		M	Mullite		P	Portlandite		MS	Monosulfate
B	Belite		Q	Quartz		T	Tobermorite		G	Gypsum
E	Ettringite		R	Rutile		MC	Monocarbonate		Ha	Hatrurite
C	Calcite

2θ

CE   FB/OS   CE/10/100/0/0/3   FB/OS/100/A/1/3   FB/OS/50/A/1/3   FB/OS/50/L/1/3
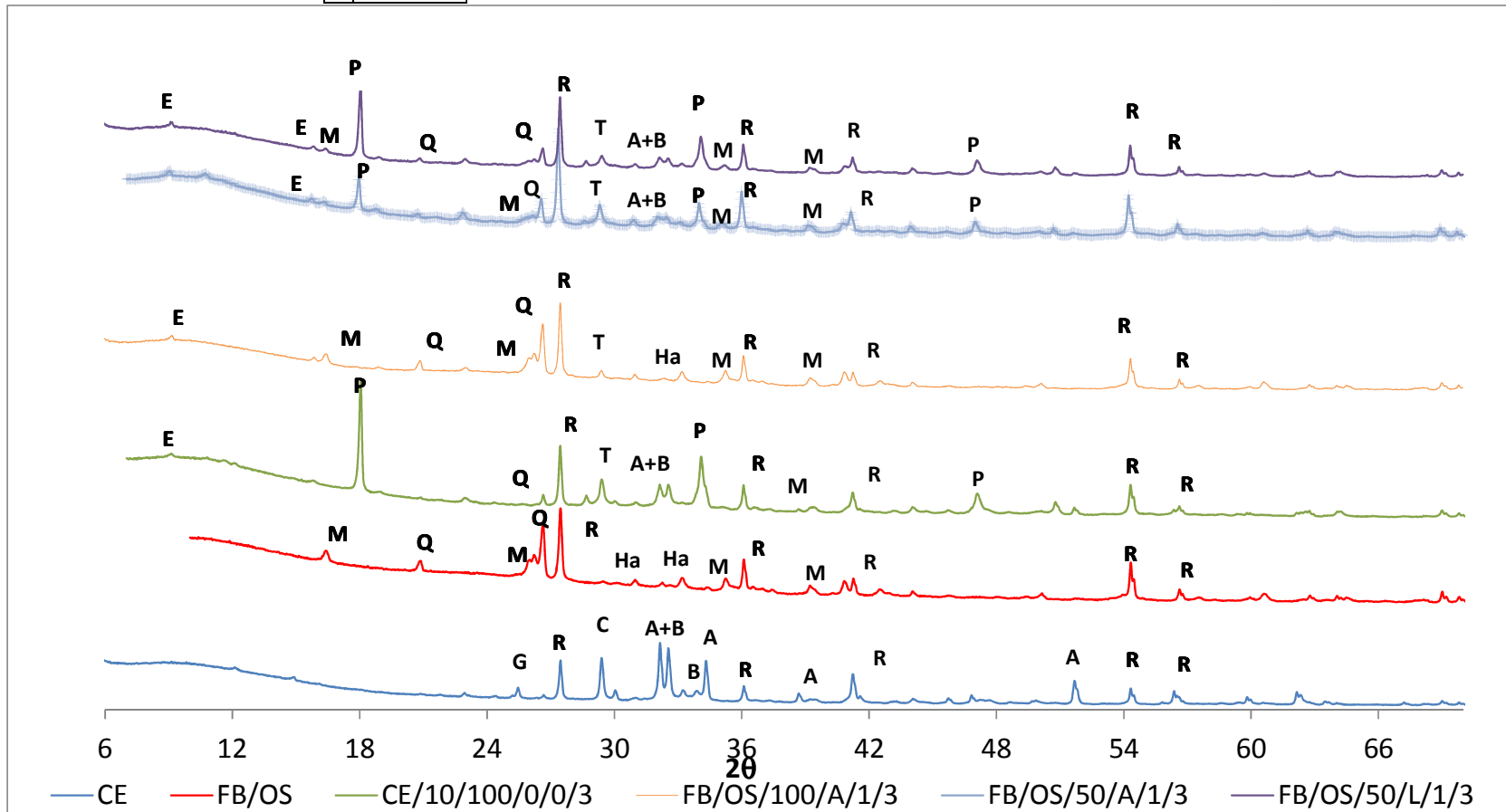
a) 3 days

A	Alite
B	Belite
E	Ettringite
C	Calcite

M	Mullite
Q	Quartz
R	Rutile

P	Portlandite
T	Tobermorite
MC	Monocarbonate

MS	Monosulfate
G	Gypsum
Ha	Hatrurite

b) 7 days

A	Alite
B	Belite
E	Ettringite
C	Calcite

M	Mullite
Q	Quartz
R	Rutile

P	Portlandite
T	Tobermorite
MC	Monocarbonate

MS	Monosulfate
G	Gypsum
Ha	Hatrurite
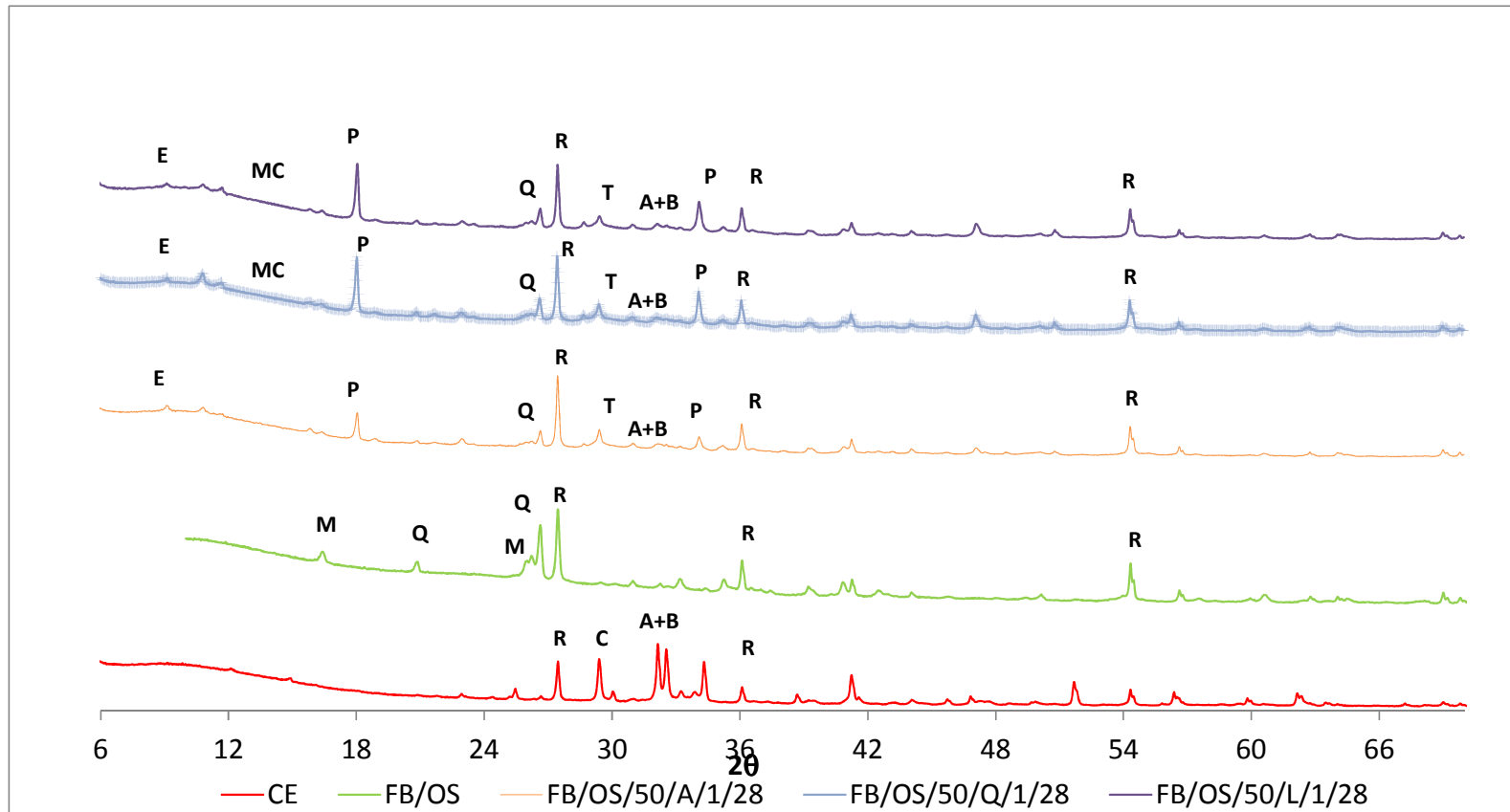
c) 28 days

Figure 53 XRD Diffractograms

114

According to Figure 53 and 54 the presence of quartz and mullite in mixes with activators was due to the presence of fly ash. The amount of the amorphous content for the mix with Activator 1 was higher compared to 53.7% which is a reference value; this value is obtained by adding half of the amorphous content of the 100% cement mix with half of the amorphous content of the fly ash. The reference value makes it possible to observe a general variation of the amorphous content after adding the activator to the system. The amorphous content for the samples with quicklime and lime was lower compared to the calculated value. For all the mixes the amorphous content decreased with time. Portlandite consumption started after three days for mixes with activator 1, and after 7 days for mixes with lime and quicklime. Tobermorite was always the highest for the mix with lime compared to the other mixes including activators. Ettringite increased slightly for mixes with activators and it increased with time; the amounts were similar or higher to those of the control mixes (CE/10/100/0/0 and TP/OS/20). There was a reduction in the tricalcium silicate peak for all the mixes; the levels of this phase were lower for mixes with lime and quicklime. It is important to mention that in section 4.3.2.2, there is an additional analysis comparing all the fly ashes simultaneously.
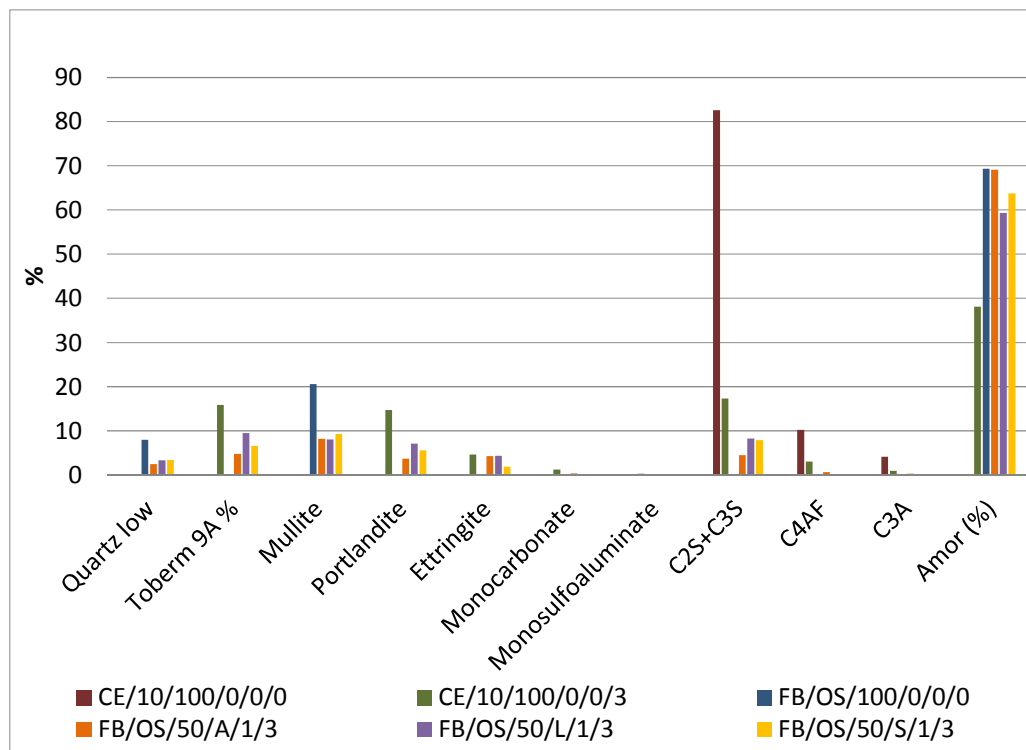
a) 3 days
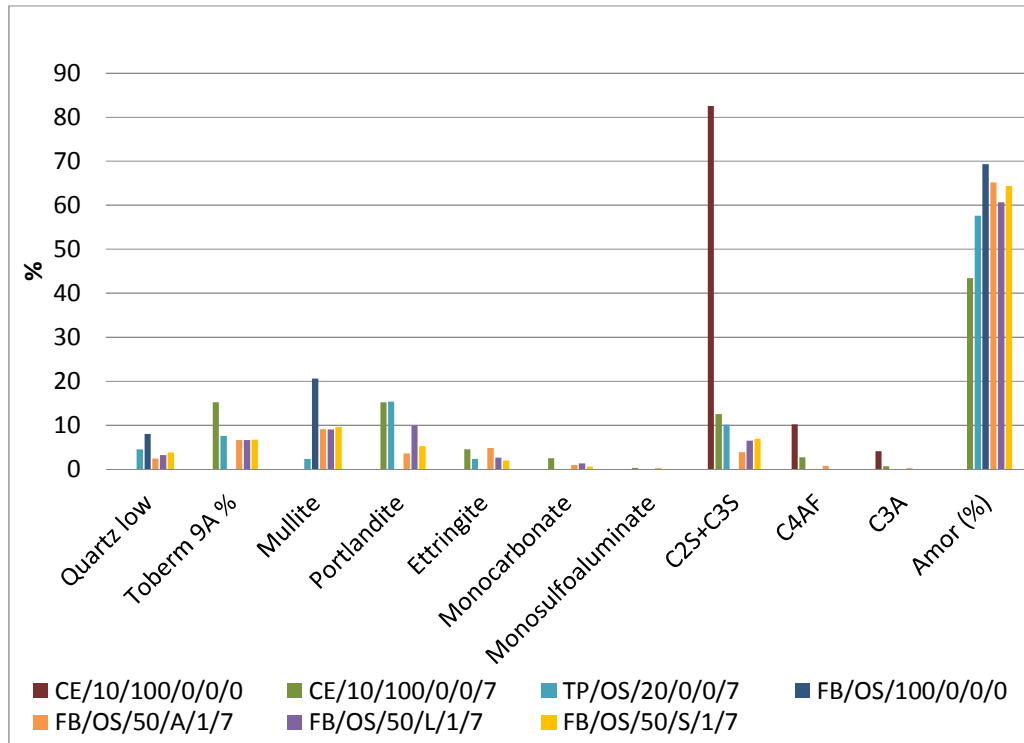
b) 7 days
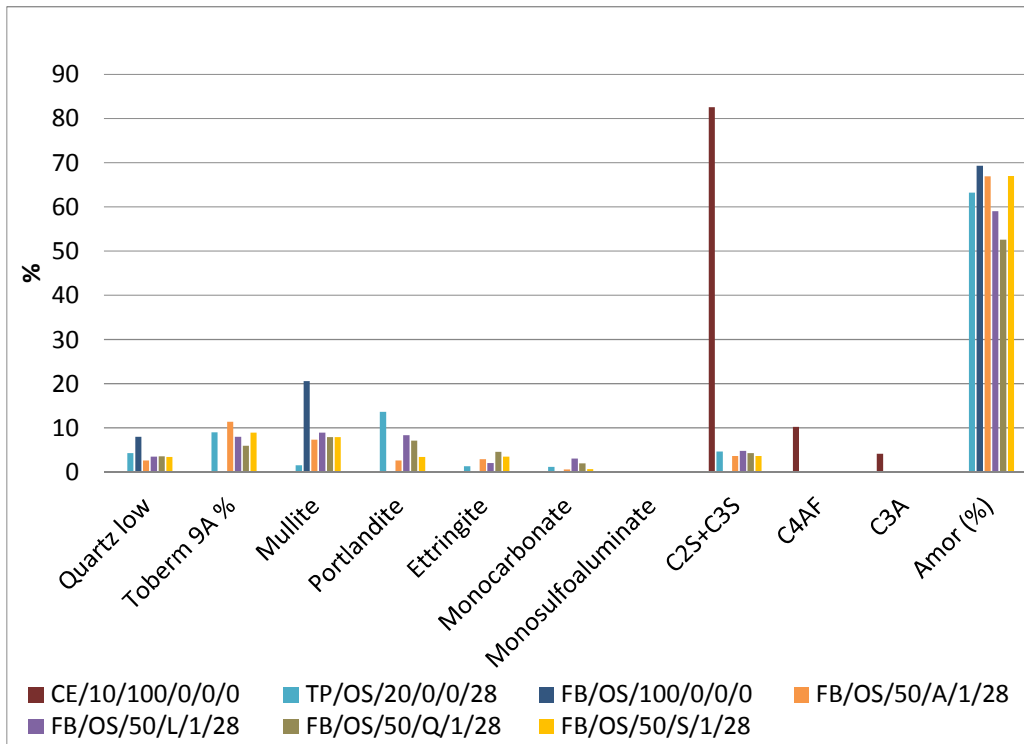
c) 28 days

Figure 54 XRD

4.3.2.1.3   Termoguajira FA

For most of the activators used in combination with Termoguajira FA, the highest dosage was the most effective one. Mixes with activator 1 (TG/OS/50/A) had a high variability between results at different ages as presented in Figure 55. Mixes with quicklime (TG/OS/50/Q/5) and lime (TG/OS/50/L/5) had the best performance with 5% activator dosage; although in some cases the compressive strength could not exceed those of the control samples, the evolution from 7 to 28 days was significant. Mixes with sodium sulfate presented the best performance between activators; the optimum dosage was with 3% having a significant effect at 3 and 7 days. Mixes with sodium sulfate also passed the compressive strength of the control TG/OS/50 at 28 days. After 28 days, compressive strength is still higher than the control but the latter gets closer with time. In this case and comparing with the previous fly ashes, the effect of sodium sulfate is not only present at 3 and 7 days but also at 28 days.
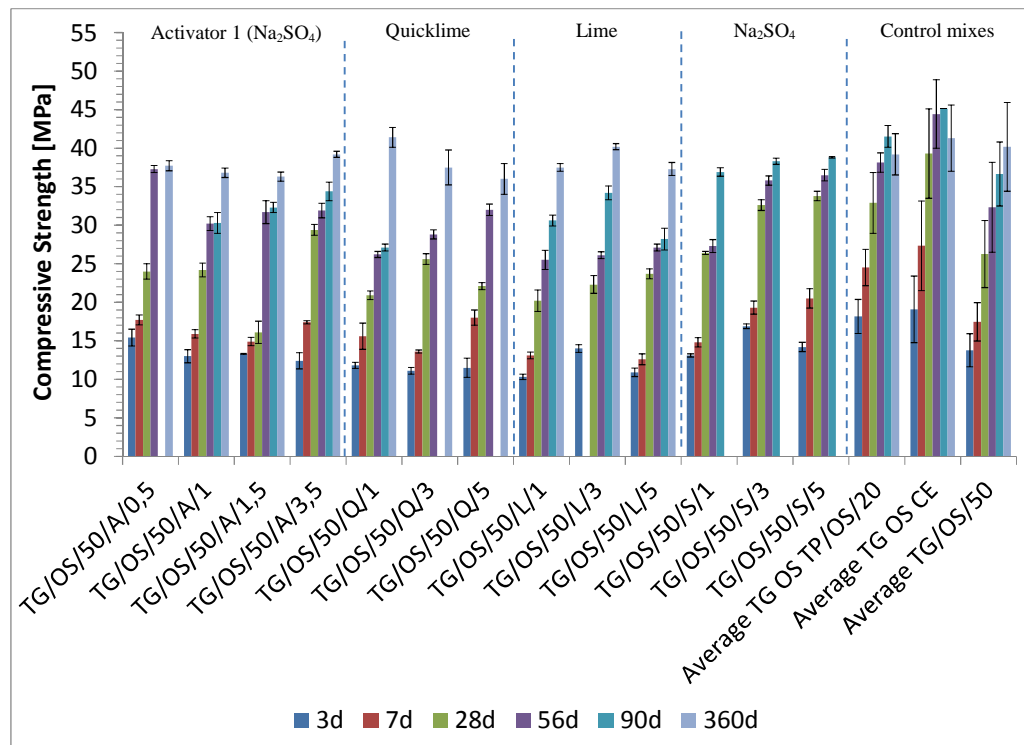
a) Compressive strength evolution
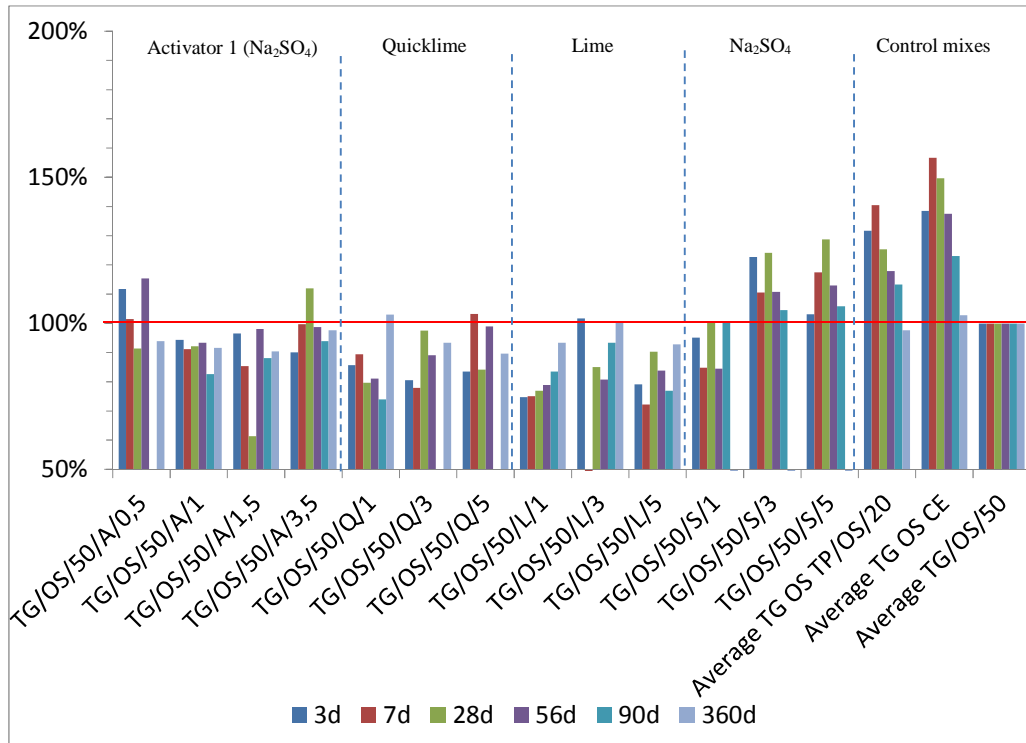
b) Percentage evolution relative to the control mix (Average TG/OS/50)

Figure 55 Compressive strength

The portlandite content for the mix with activator 1 always increased, even at 28 days. Using this activator with the previous fly ashes (Termopaipa and Fabricato), the portlandite content always decreased before 28 days; in Figure 56 this sample behaved similar to the mix without activator where portlandite content increased at every age. This is probably due to the amount of iron in the fly ash which did not allow this SCM to react with the activator as fast as did Termopaipa FA and Fabricato FA.

In relation to the bound water and according to Figure 57, it was lower for the mix with activator 1 than the mix without activator; it means activator 1 was not contributing to the formation of hydrates. The filler effect was more evident in terms of bound water; the formation of hydrates per 100 g of cement was higher for the mix with 50% of fly ash than the mix with 20%.
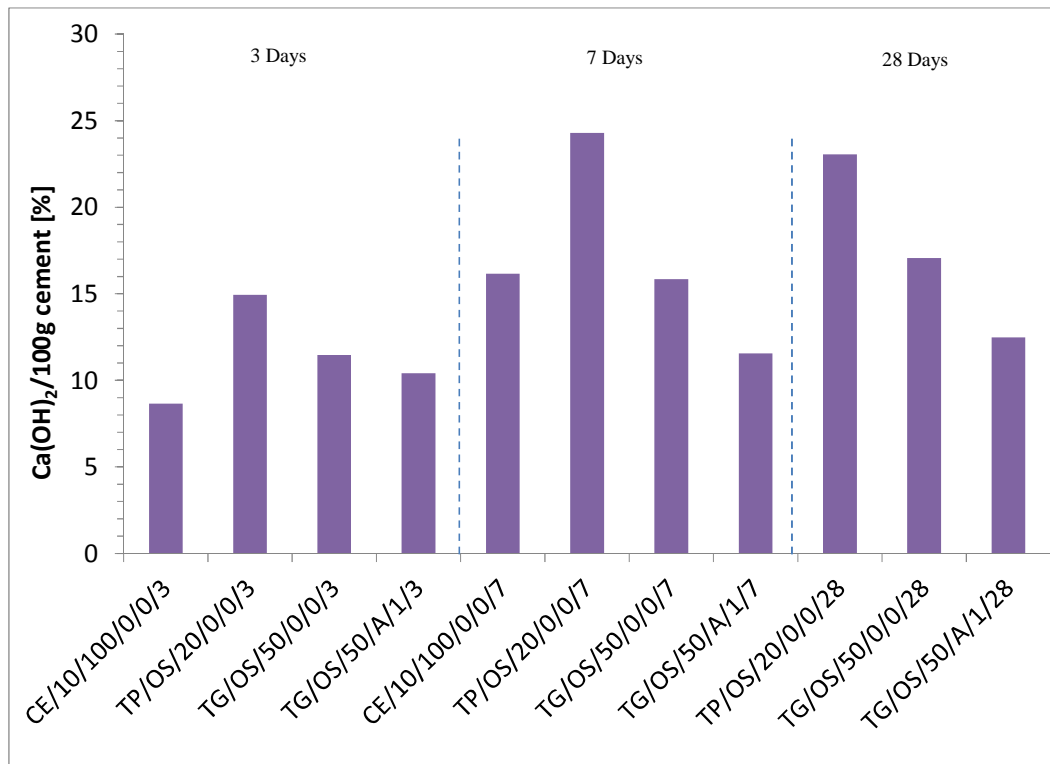
Figure 56 Ca(OH)$_2$ / 100g cement

Figure 57 Bound water / 100 g cement

A	Alite		M	Mullite		P	Portlandite		MS	Monosulfate
B	Belite		Q	Quartz		T	Tobermorite		G	Gypsum
E	Ettringite		R	Rutile		MC	Monocarbonate		Ha	Hatrurite
C	Calcite									

2θ

CE — TG/OS — CE/10/100/0/0/3 — TG/OS/50/L/1/3

a) 3 days

A	Alite		M	Mullite		P	Portlandite		MS	Monosulfate
B	Belite		Q	Quartz		T	Tobermorite		G	Gypsum
E	Ettringite		R	Rutile		MC	Monocarbonate		Ha	Hatrurite
C	Calcite									

b) 7 days

A	Alite		M	Mullite		P	Portlandite		MS	Monosulfate
B	Belite		Q	Quartz		T	Tobermorite		G	Gypsum
E	Ettringite		R	Rutile		MC	Monocarbonate		Ha	Hatrurite
C	Calcite									

c) 28 days

Figure 58 XRD Diffractograms

According to Figure 58 and 59, the amorphous content for the sample with activator 1 was always higher than the others with quicklime and lime. The minimum amorphous theoretical value was passed at 3 and 7 days with activator 1. The amount of portlandite for the mix with lime was the highest between mixes with activators. The sample with activator 1 had a lower amount of portlandite compared to the mix without any activator; anyway the effect of activator 1 was not significant in terms of portlandite consumption. Only after 28 days a decrease in portlandite content for the mix with lime was evident. Ettringite content for the mix with activator 1 was higher at seven days compared to the mix without activator, helping to improve initial compressive strengths.
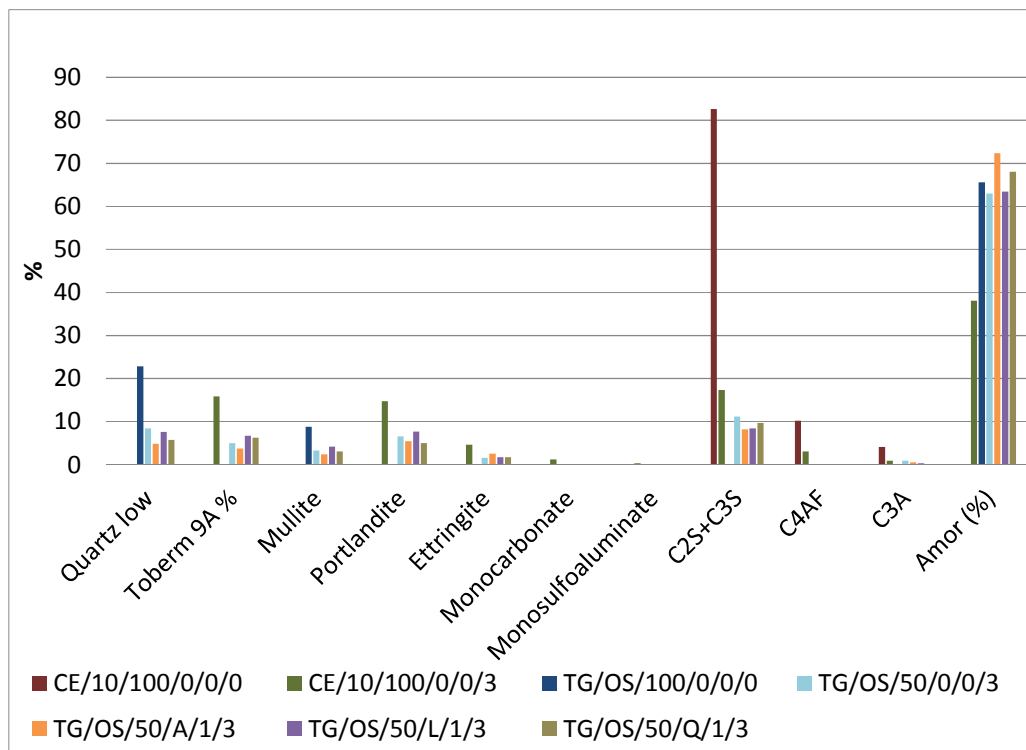
a) 3 days
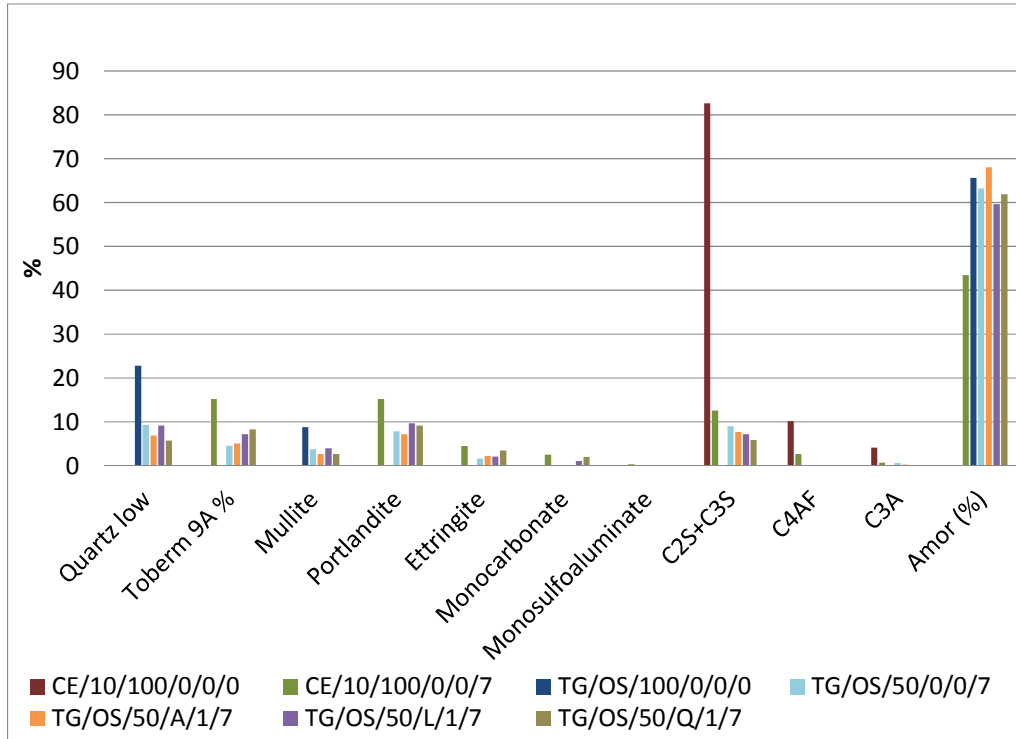
b) 7 days
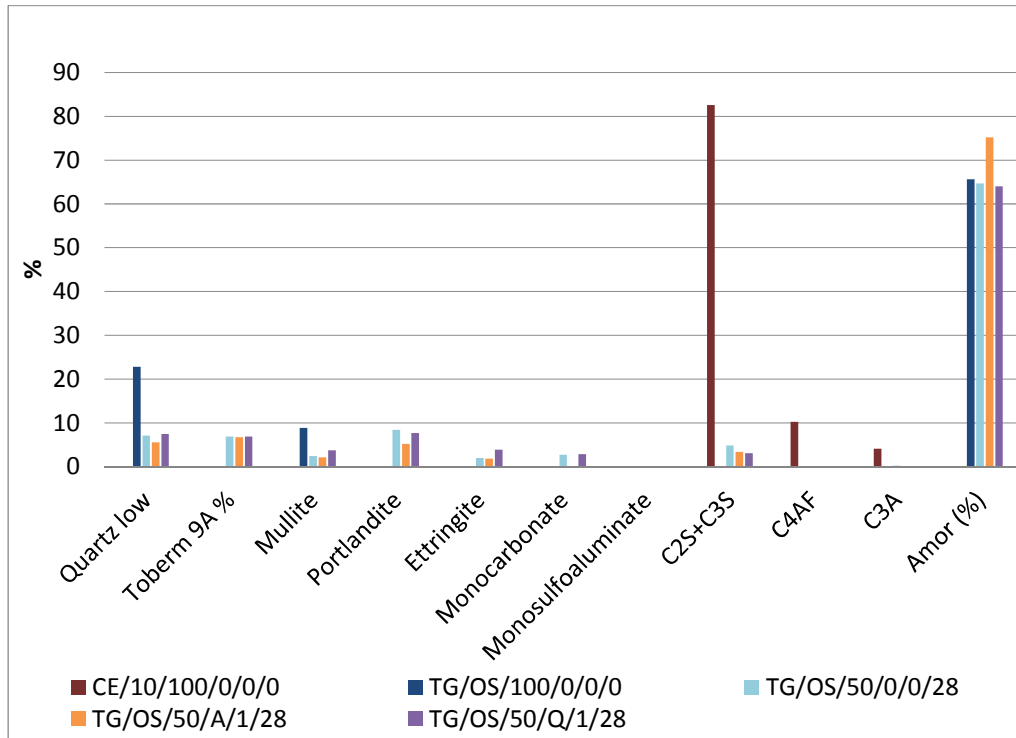
c) 28 days

Figure 59 XRD

4.3.2.1.4   Tampa FA

Activator 1 and sodium sulfate at certain dosages improved the compressive strength of mixes containing Tampa FA relative to the control mix (TA/OS/50). This is seen in Figure 60. The mix with 1% of activator 1 had a similar performance than the control mix with 20% fly ash. These two activators seemed to react at early ages. Although mixes with sodium sulfate (TA/OS/50/S) had a positive effect at different dosages, it did not have the same effect as it did with the other fly ashes. Lime and quicklime did not result in strengths matching those of the control mix; the effect with these activators was similar using different fly ashes.
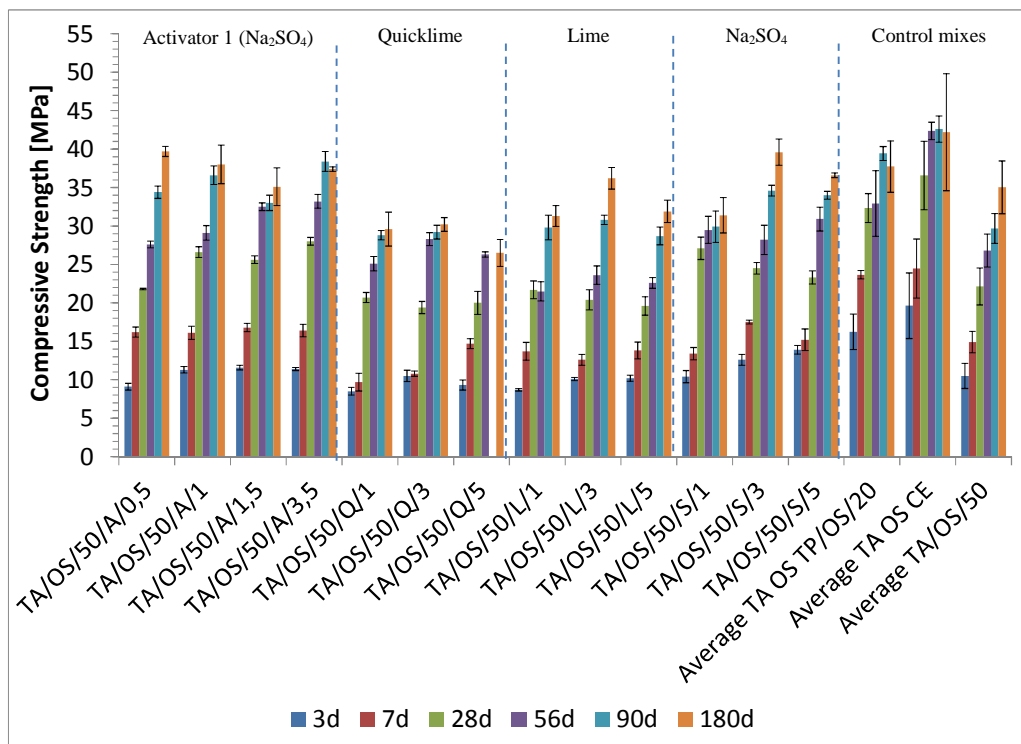
a) Compressive strength evolution

125
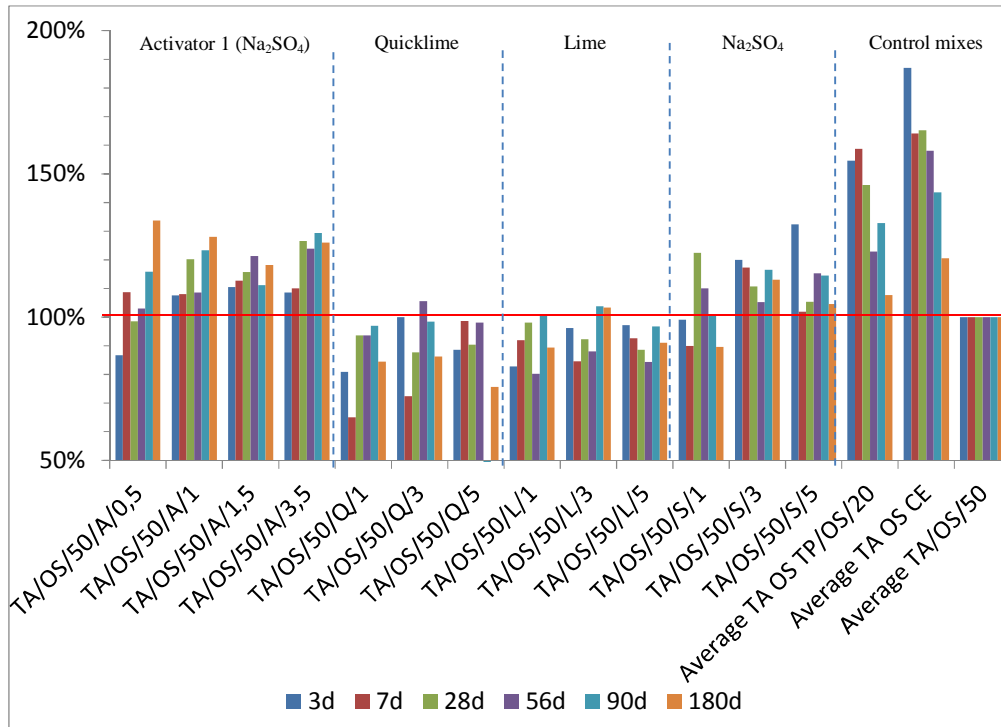
b) Percentage evolution relative to the control mix (Average TA/OS/50)

Figure 60 Compressive strength

The amount of portlandite for the mix with activator 1 was lower than in the mix without activator; in Figure 61 the amount of portlandite for this mix increased at 7 days which means there was not any influence of the activator in accelerating the process of portlandite consumption. The behaviour of Tampa fly ash in terms of portlandite formation was similar to Termoguajira FA. The amount of bound water was higher for the mix with activator 1 compared to the mix without activator; Figure 62 presents how the formation of hydrates per 100 g of cement was the highest for the mix with this activator.
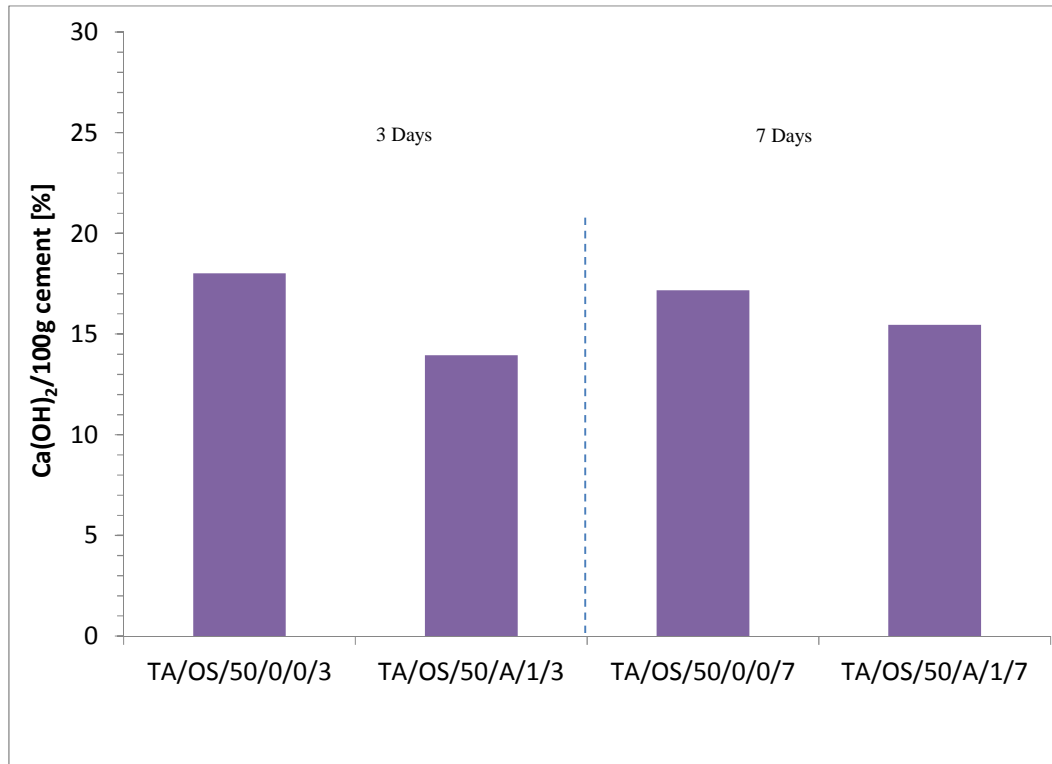
Figure 61 Ca(OH)₂ / 100g cement
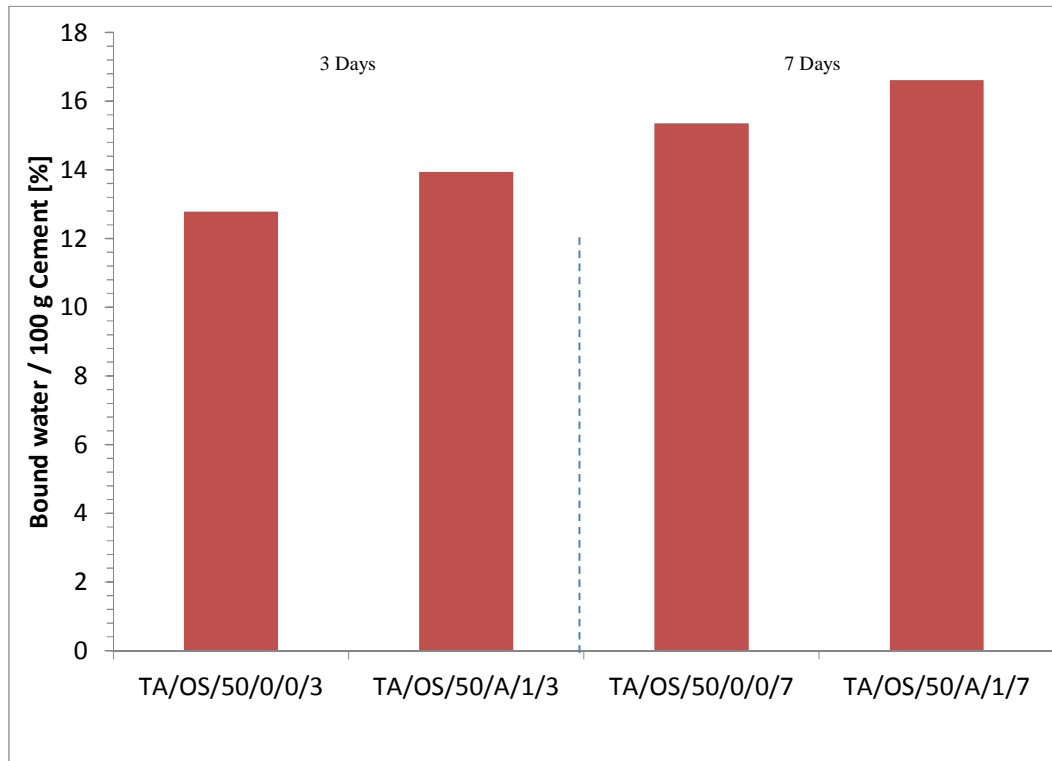
Figure 62 Bound water / 100 g cement

A	Alite
B	Belite
E	Ettringite
C	Calcite

M	Mullite
Q	Quartz
R	Rutile

P	Portlandite
T	Tobermorite
MC	Monocarbonate

MS	Monosulfate
G	Gypsum
Ha	Hatrurite

a) 3 days

128
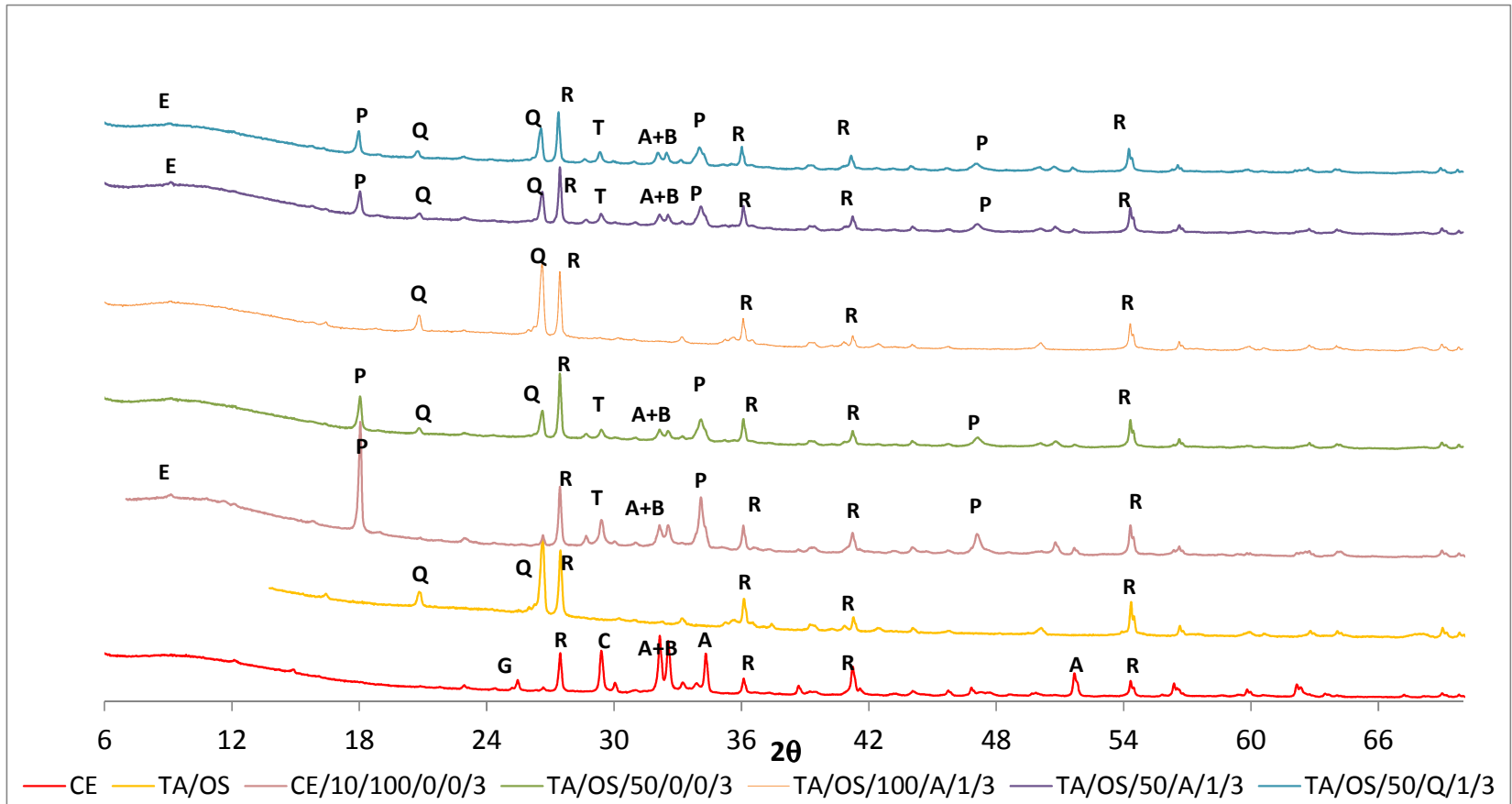
A	Alite		M	Mullite		P	Portlandite		MS	Monosulfate
B	Belite		Q	Quartz		T	Tobermorite		G	Gypsum
E	Ettringite		R	Rutile		MC	Monocarbonate		Ha	Hatrurite
C	Calcite									

b) 7 days

Figure 63 XRD Diffractograms

129

There was a small difference in the amorphous content for the control mix including 100% of fly ash (TA/OS/100/A/1/3) and Tampa FA itself (TA/OS) at 3 days; based on Figure 63 and 64 it was deduced that activator 1 had little effect on fly ash when it was used without cement. On the other hand, the mix with activator 1 TA/OS/50/A/1 produced more amorphous content than the calculated value at 3 days (57.05%); at 7 days, this value was the lowest between mixes with activators. Although the ettringite value was always low for all activated mixes, the highest value was with activator 1. The mix with 20% of fly ash (TP/OS/20/0/0) had a similar content of C_3S compared to samples with activators.

a) 3 days
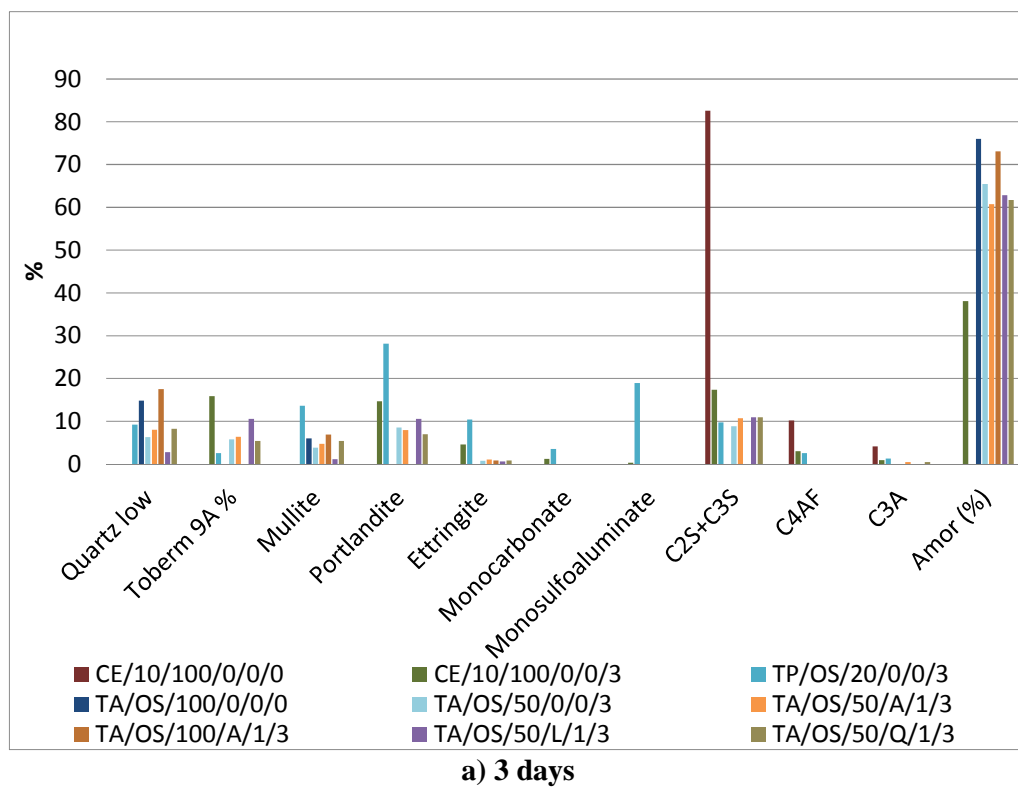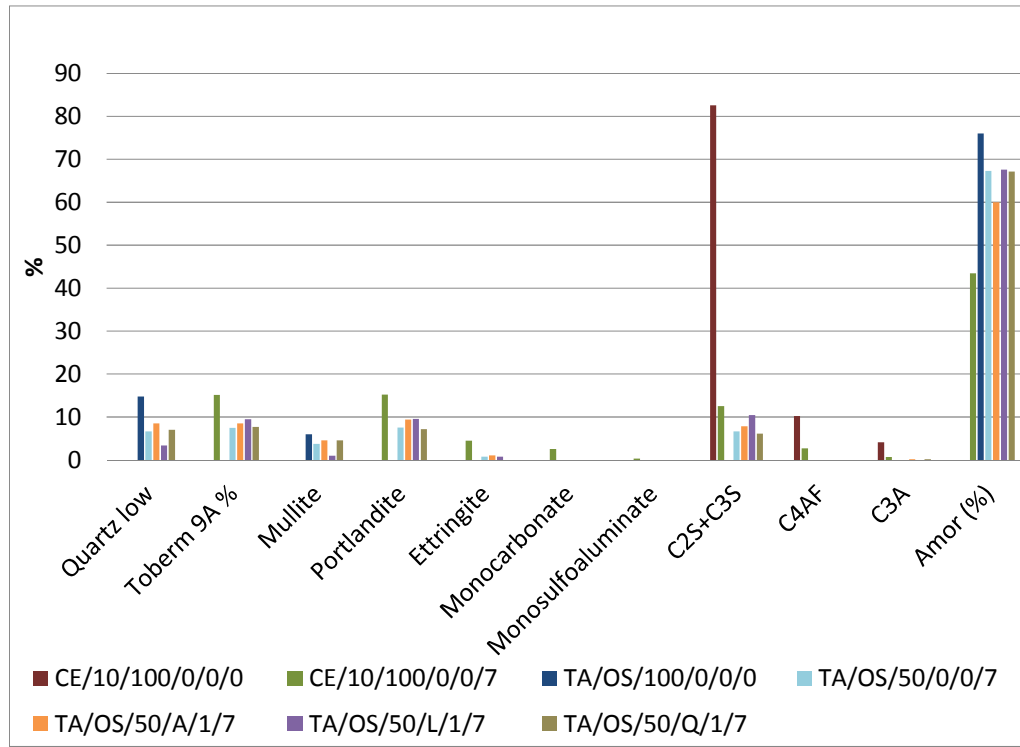
b) 7 days

Figure 64 XRD

4.3.2.2 Analysis considering all original size fly ashes and activator 1 at a dosage of 1%

The effect of activator 1 or sodium sulfate on mixes with different fly ashes was significant at early ages (Figure 64). Termopaipa FA and Fabricato FA were affected positively by the inclusion of sodium sulfate. As was seen before, the amount of ettringite and the accelerated portlandite consumption were reflected in the compressive strength evolution. On the other hand, sodium sulfate did not have the same effect on Termoguajira FA and Tampa FA. The amount of ettringite formation and portlandite consumption was not significant as it was with the first two fly ashes; the main difference between these fly ashes was the higher amount of Fe_2O_3 for the last two.

a) Compressive strength evolution

b)
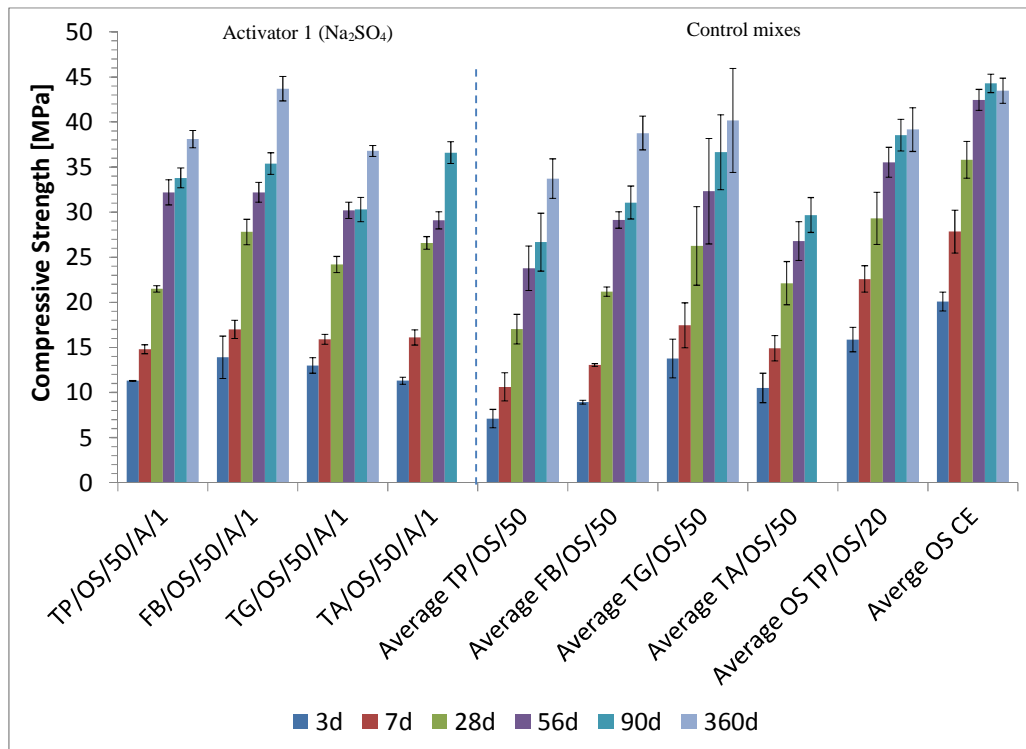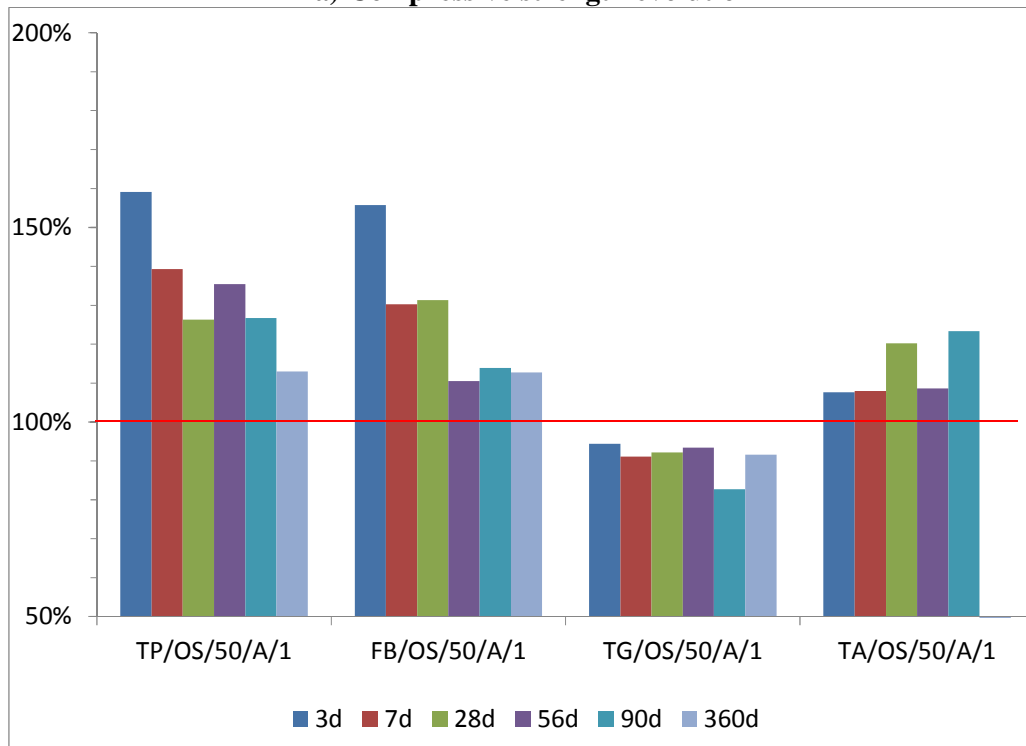
b) Percentage evolution relative to the control mixes with 50% of fly ash and without activator

Figure 64 Compressive strength

As seen in Figure 65, portlandite decreased considerably for Termopaipa FA from 3 to 7 and from 7 to 28 days. It only occurred for Fabricato FA from 3 to 7 days. For Tampa FA and Termoguajira FA the amount of portlandite always increased; it

means there was not any influence of the activator in accelerating the process of portlandite consumption. The bound water always increased significantly for Termopaipa FA and Fabricato FA. The increase in bound water for Tampa FA and Termoguajira FA was limited which means that activator 1 was not contributing to the formation of hydrates. This is seen in Figure 66.
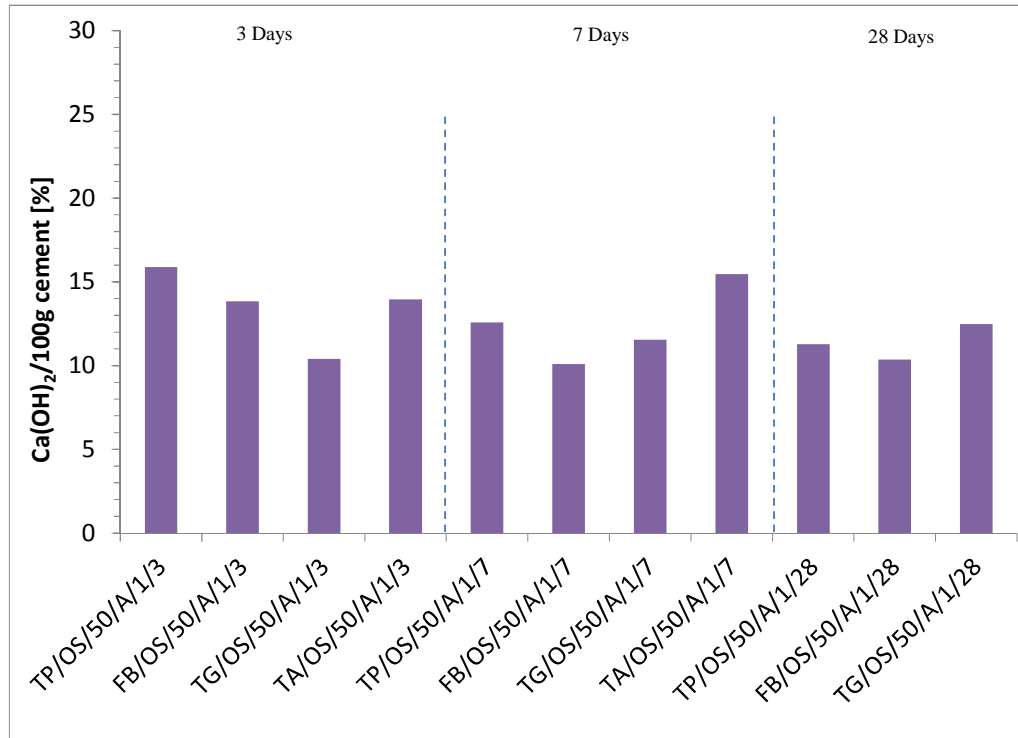
Figure 65 Ca(OH)$_2$ / 100g cement
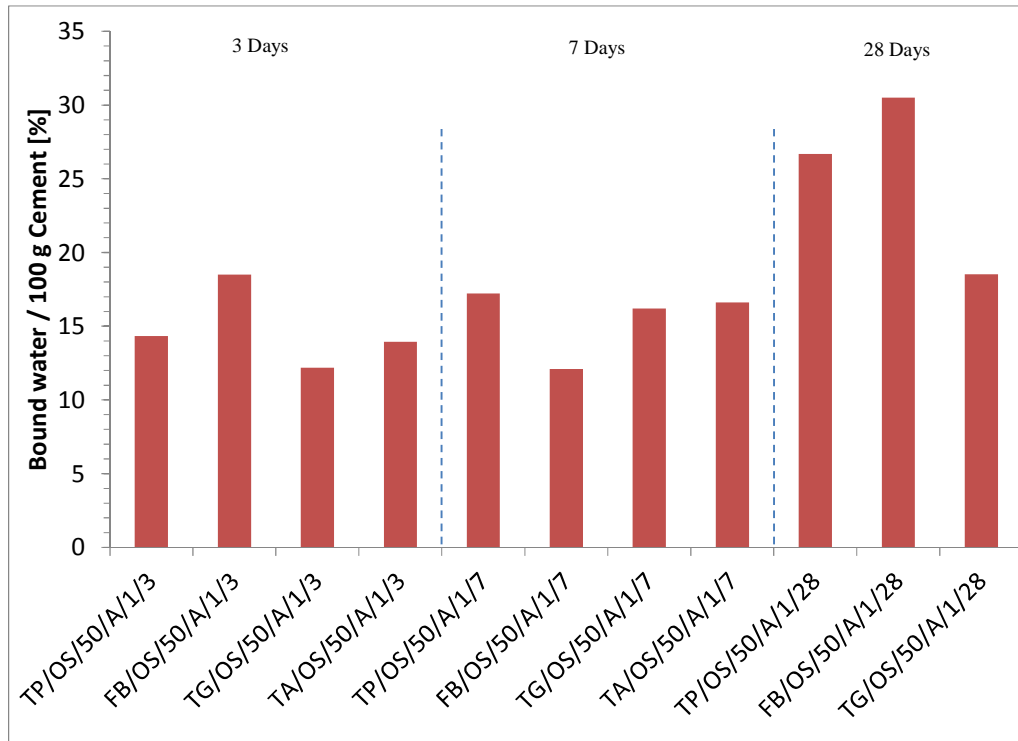
Figure 66 Bound water / 100g cement

Ettringite levels for mixes with Termopaipa FA and Fabricato FA were always higher than those with Termoguajira FA and Tampa FA; in some cases it doubled the amount of ettringite. In the case of portlandite, this trend was the same as presented in TGA results; achieving a higher consumption with Termopaipa FA and Fabricato FA.

From SEM images it can be deduced that sodium sulfate promoted ettringite formation. Figure 67 presents how ettringite was formed using 100% of OS Fabricato FA with activator 1. The cubic shapes presented over the fly ash surface could be related to portlandite or AFm. Appendix 1 includes the complete SEM/EDS analysis.
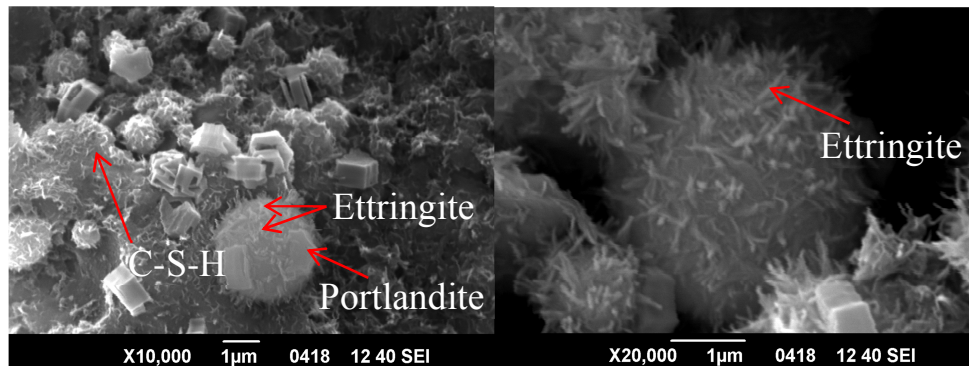
Figure 67 FB/OS/100/A/1/28

134

Figure 68 shows ettringite formation over Termopaipa FA surface at an age of 7 and 28 days. In this case a mix with 50% of fly ash and activator 1 was analysed. The presence of portlandite and C-S-H is also evident in these SEM images.
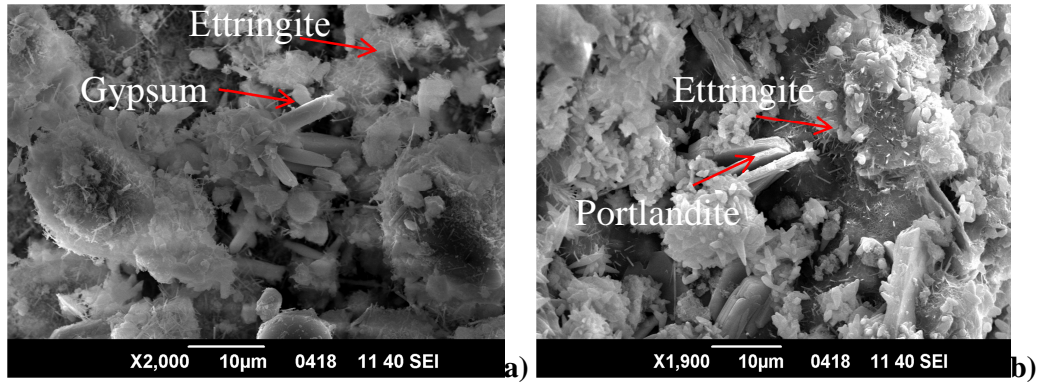
Figure 68 TP/OS/50/A: a) 7 days, b) 28 days

4.3.2.3 Analysis considering all the fly ashes and activators at optimum dosages

From Figure 69 it is evident that activators have a better performance when the fineness is improved; the material passing the 75µm sieve for Termopaipa FA, Fabricato FA and Termoguajira FA had a better reaction with the activators. In the case of Tampa FA, it occurred with the material passing the 45µm sieve.

Termopaipa FA always had the highest compressive strength with Activator 1 at a dosage of 1% (Figure 69 (a)). As mentioned before, the effect of sodium sulfate was evident in the first days. It also occurred for Tampa FA passing 45 µm as seen in Figure 69-d, where sodium sulfate at a dosage of 3% exceeded the strength of the control sample with 80% PC – 20% FA at every age. Figure 69-b shows lime performance at a dosage of 3% with Fabricato FA, where after a year, the compressive strength passed all the mixes including the control. The mix of quicklime with Termoguajira FA presented a significant strength development at later ages passing the strength of all the control samples.
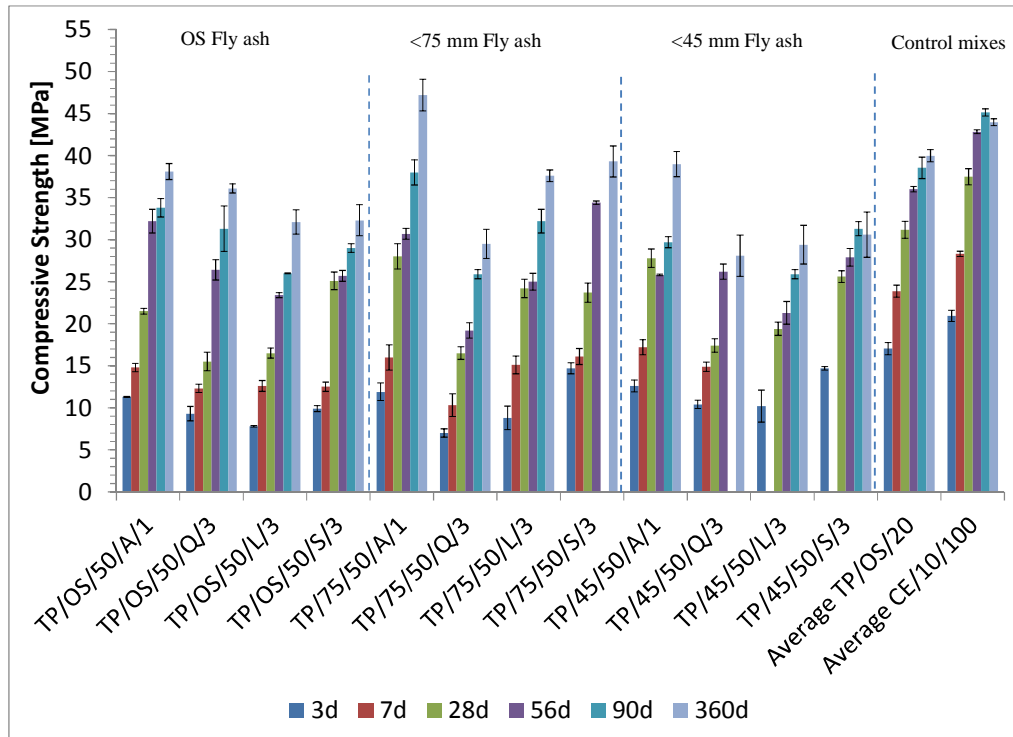
a) TP FA
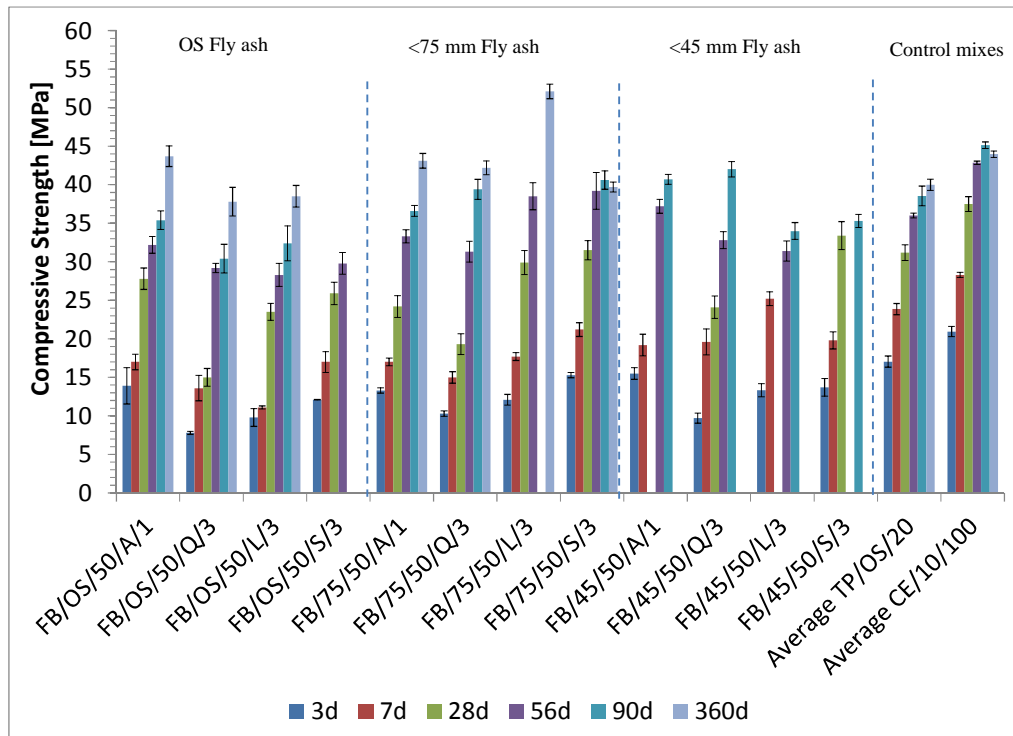
b) FB FA
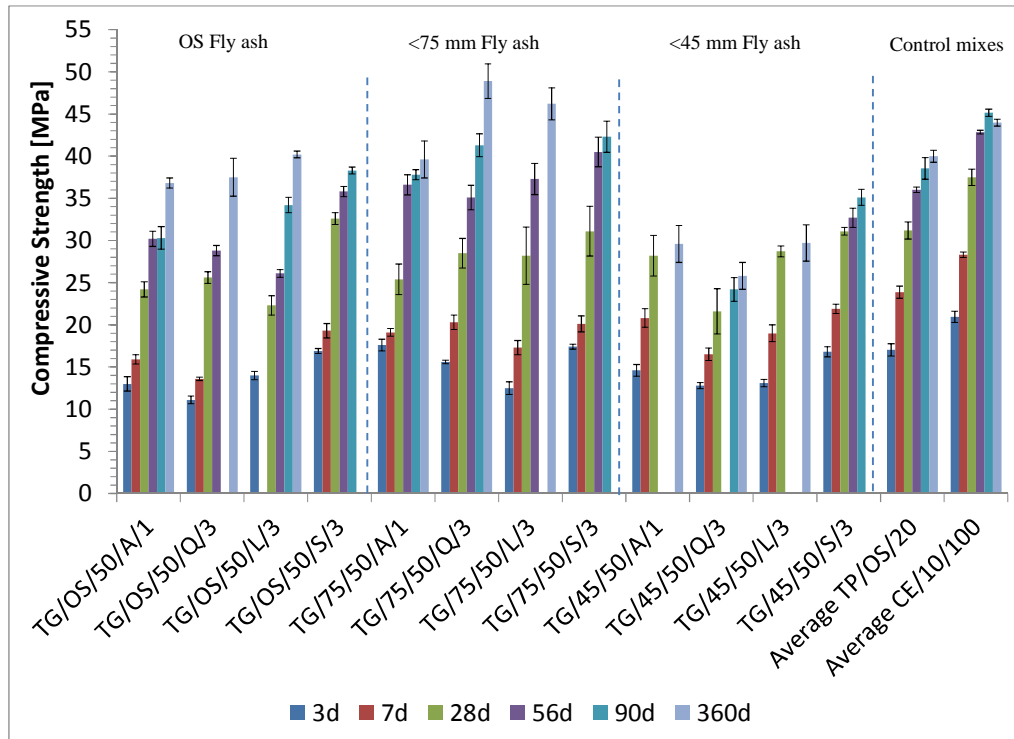
c) TG FA
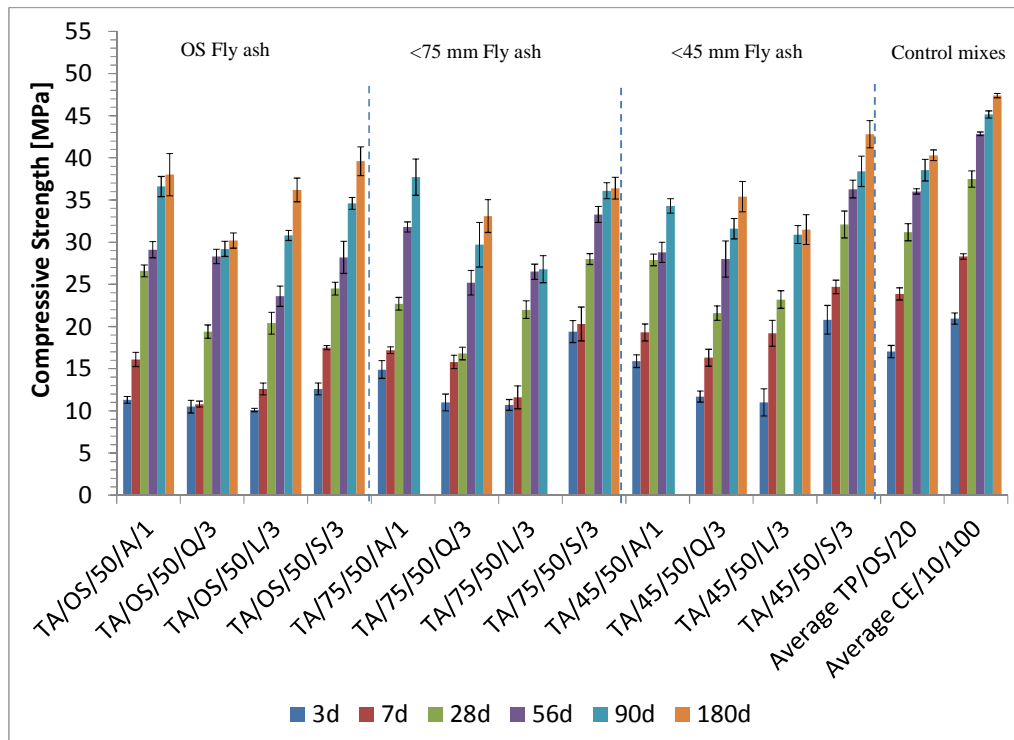
d) TA FA

Figure 69 Compressive strength evolution of mixes with optimum dosages of different activators

Figure 70 presents how the effect of lime and quicklime became significant at later ages, reacting with the remaining fly ash in the system. As mentioned before, in
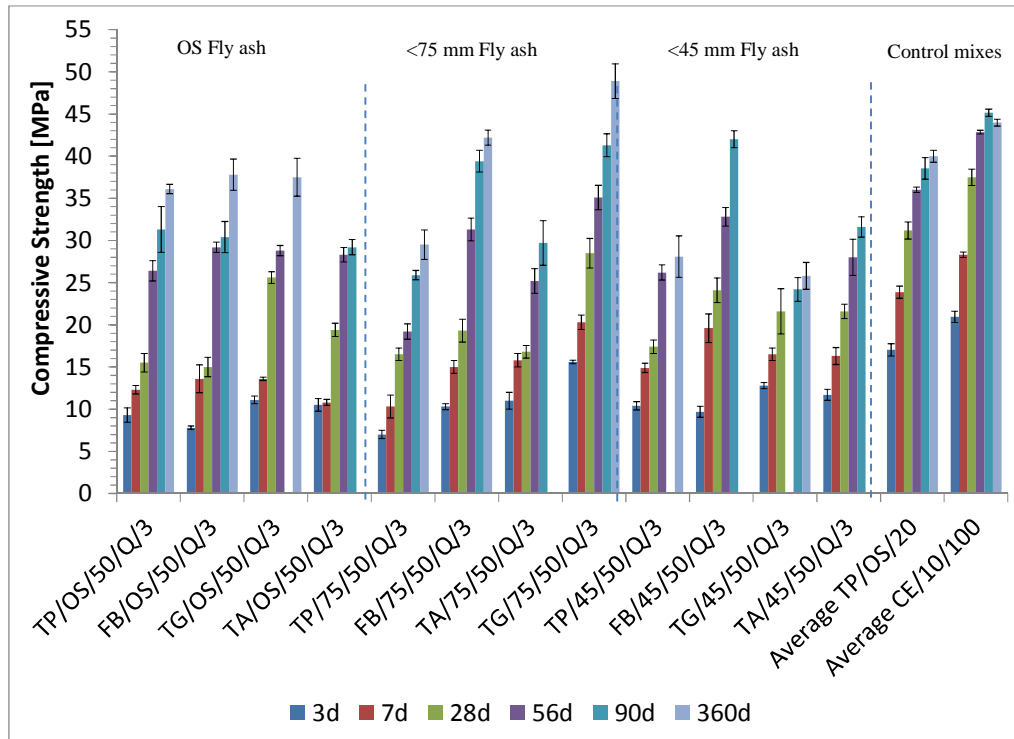
the case of sodium sulfate, the amount of ettringite present at initial ages played a relevant role for the compressive strength at early ages.
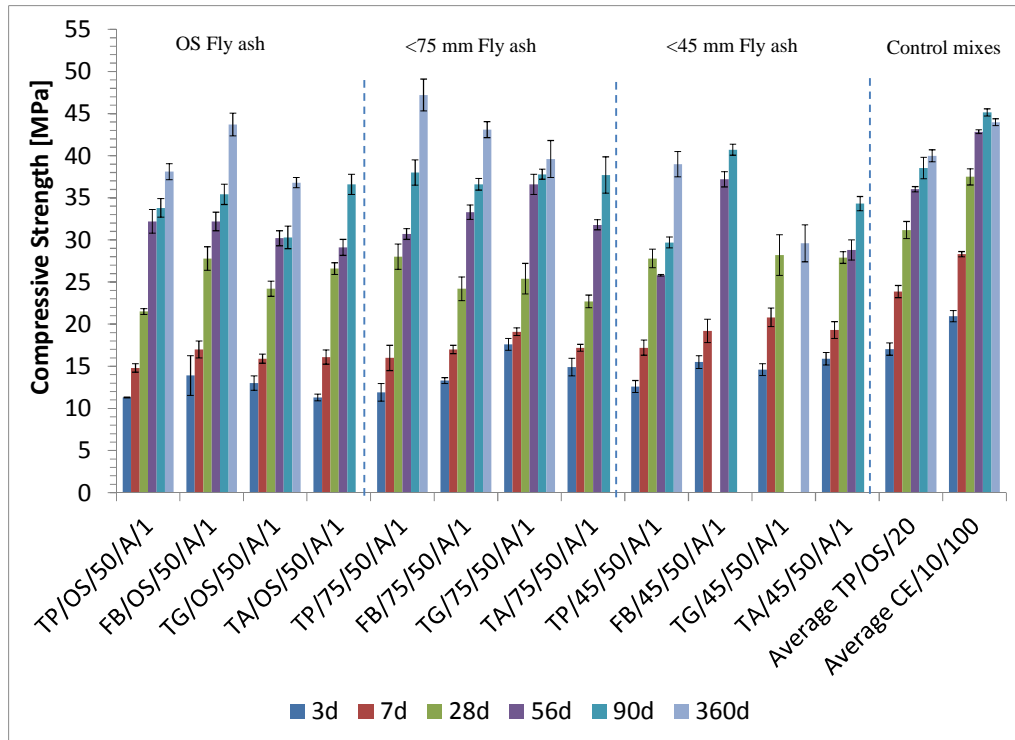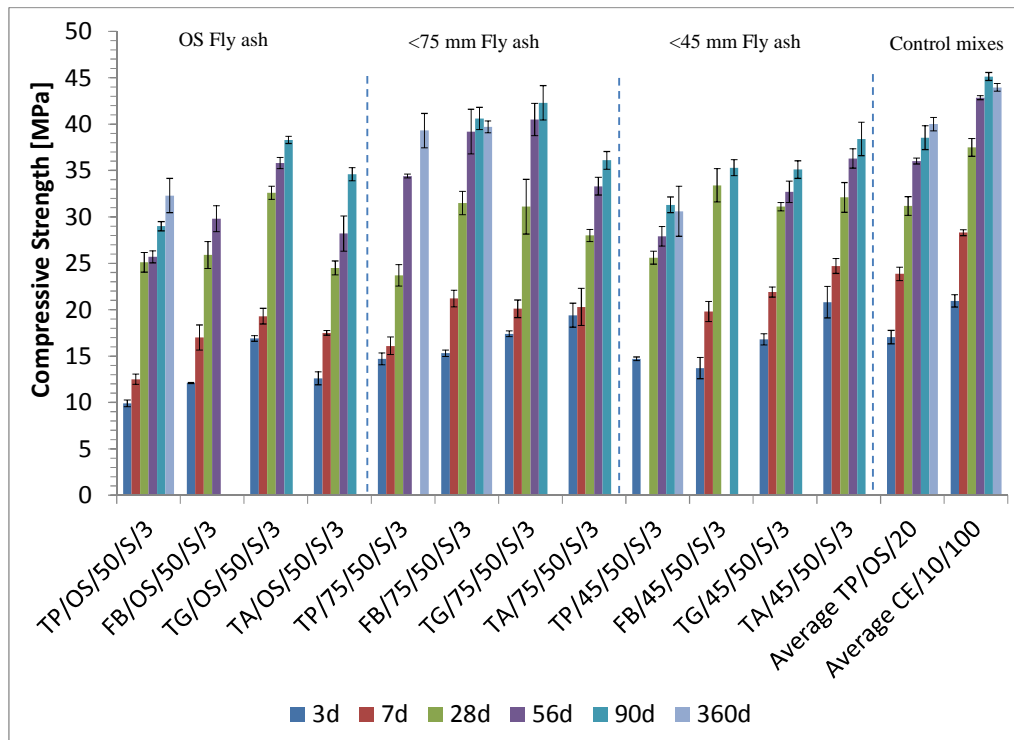

a) Activator 1
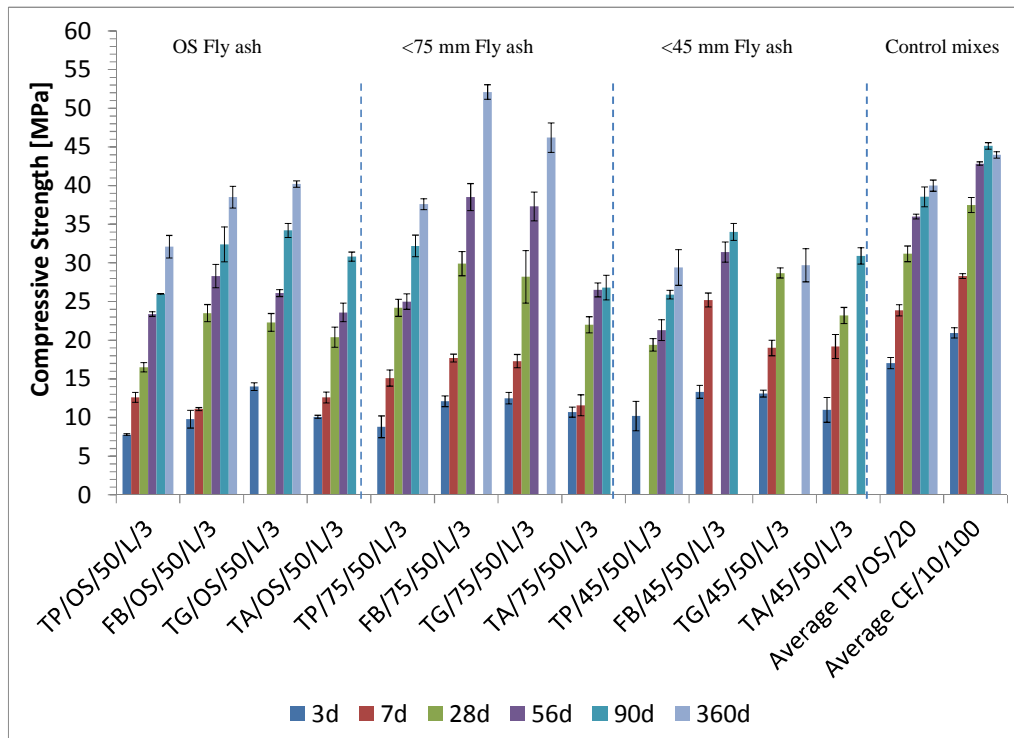
b) Lime

c) Quicklime

d) Na₂SO₄

Figure 70 Compressive strength evolution of mixes with different fly ashes and one activator

Figure 71 summarizes the data in Figure 69 and 70; this figure shows how lime and quicklime with a fly ash with a fineness increment, presented a significant evolution at later ages.
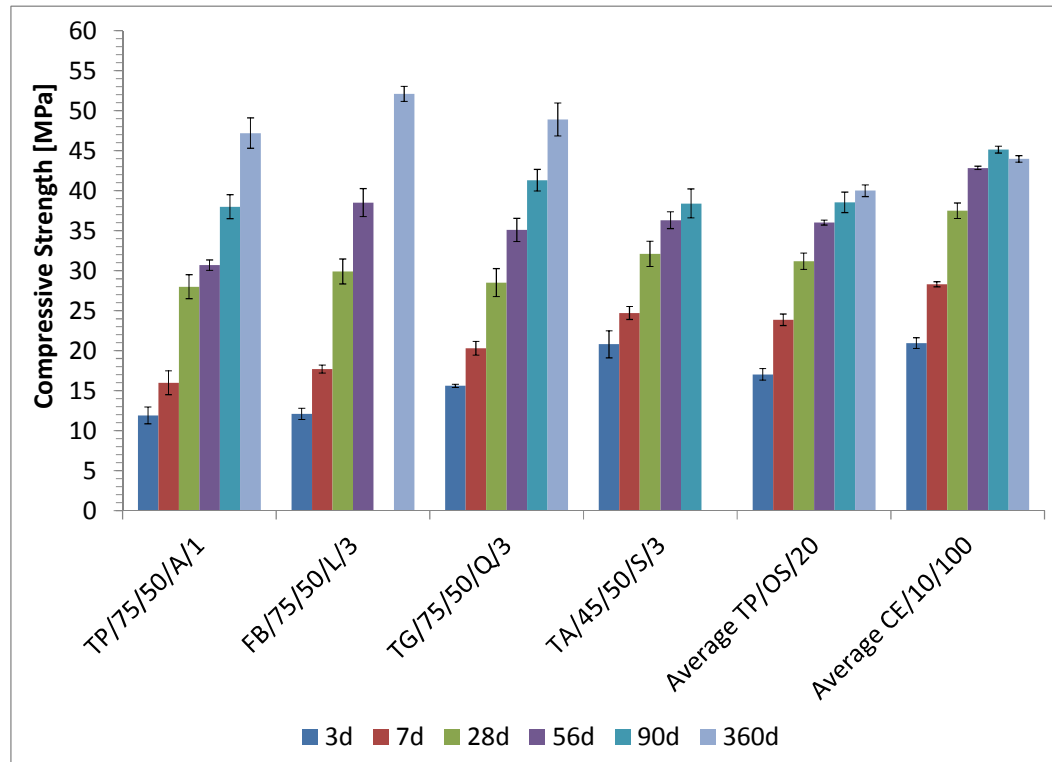
Figure 71 Compressive strength evolution of mixes with the optimum activator per fly ash

It is important to mention that by comparing the performance between OS fly ashes as presented in the previous section, Activator 1 presented the best performance compared to control samples. Due to the performance in mortars and availability of materials, the following chapters include the complete analysis on concretes produced using OS Termopaipa FA and Activator 1.

4.4 Summary

The following are some of the findings based on paste and mortar evaluations:

- When the amorphous content of fly ash increased, the compressive strength increased. Some fly ashes would not need any mechanical treatment due to the initial amorphous content as this could be reduced with detrimental effects due to sieving.

- Mixes with activator 1 produced more ettringite than the others; this helped to increase initial compressive strengths. Correspondingly, the amount of portlandite

consumption was higher for these mixes at an early age. The previous scenario occurred for mixes with Termopaipa FA and Fabricato FA while for mixes with Termoguajira FA and Tampa FA this did not occur. One of the main differences between these fly ashes is the high Fe_2O_3 content for Termoguajira FA and Tampa FA. The effect of Fe_2O_3 content must be studied with more detail due to the negative influence that it could have in hybrid cementitious systems with sodium sulfate.

- For mixes with lime and quicklime, the compressive strength became important at later ages. Although for the first days mixes with these activators had low compressive strengths, their performances were improved at a later age. As it is known, fly ash keeps reacting and in this case the fact of including lime and quicklime helped to increase compressive strength with time.

- Calorimetry curves were influenced by the inclusion of fly ash. Quicklime mixes released more heat than the others. The peak of the calorimetry curves for mixes with sodium sulfate was moved by two hours. While setting time for mixes with quicklime was reduced, it was increased with sodium sulfate.

- Comparing OS fly ashes, Termopaipa FA and activator 1 had the best performance in terms of compressive strength. Based on these results and the fact of being a close source, Termopaipa FA was selected to be used for performance evaluation in concrete.

5 Properties of Fresh and Hardened Concrete

5.1 Introduction

Mixes with Termopaipa FA and activator 1 were used for this part of the study. As previously presented and as shown in Figure 72, slump, setting time and air content were evaluated; slump loss was also considered in order to assess the effect of the activator (sodium sulfate), plasticizer (lignosulfonate) and superplasticizer (polycarboxylate). In the hardened state, compressive strength and shrinkage were evaluated.

5.2 Concrete combinations

Concrete samples were developed using Termopaipa FA and activator 1 (sodium sulfate). Figure 72 presents all the parameters considered in the mix designs for this phase. All the different fresh and engineering properties evaluated in this phase are also presented in this figure. Durability results are presented in the next chapter.

Concrete evaluation	Activity	
OS Termopaipa FA, optimum activator, plasticiser and superplasticiser	Constants	
W/CM: 0.557, 0.483, 0.426 **Fly ash content:** Control (0%, 20% and 50%), 50% + Act 1 **Curing:** Laboratory curing, outdoor curing	Variables	
Slump, Setting Time, **Air Content**	Fresh Properties	Phase 3
Compressive Strength (1, 3, 7, 28, 56, 90, 360 days)	Engineering Properties	
Drying shrinkage (4, 7, 14, 28, 56, 112, 224, 448 days) **Water permeability** (90, 180, 270, 360 days) **Chloride permeability** (28, 90, 180, 270, 360 days) **Carbonation** (28, 90, 270, 260 days) **Sorptivity** (28, 90, 360 days) **Diffussion Coefficient** (90, 180, 270, 360 days) **ASR, Sulphate attack**	Durability	

Figure 72 Concrete parameters and tests conducted

5.3 General procedure for concrete preparation and tests

5.3.1 Concrete mix design

Concrete designs were developed to obtain a slump of 225 mm. The input variables are considered in Table 16; all of these proportions were obtained for 1 m^3 and adjusted to the laboratory mixer capacity.

Table 16 Mixes evaluated

w/cm	0.554				0.482				0.427			
f/agr	0.539				0.54				0.541			
Fly ash [%]	0%	20%	50%	50%	0%	20%	50%	50%	0%	20%	50%	50%
fa/agr	0.462	0.460	0.459	0.459	0.449	0.448	0.446	0.446	0.437	0.435	0.432	0.432
Paste Volume [l]	277	286	301	301	292	303	320	320	307	320	339	339
Cement [kg]	316	253	158	158	363	290	182	182	410	328	205	205
Fly ash [kg]		63	158	158		73	182	182		82	205	205
Fine Aggregate 1 (#4 - 4.75 mm) [kg]	696	683	667	667	663	650	631	631	631	616	594	594
Fine Aggregate 2 (#50 - 0.3 mm) [kg]	174	171	167	167	166	163	158	158	158	154	149	149
Coarse Aggregate (1/2" - 12.5 mm) [kg]	1013	1003	983	983	1017	1002	981	981	1016	1001	977	977
Water [kg]	175	175	175	175	175	175	175	175	175	175	175	175
Admixture 1 (Lignosulfonate)	0.45%	0.45%	0.45%	0.45%	0.45%	0.45%	0.45%	0.45%	0.45%	0.45%	0.45%	0.45%
Admixture 2 (Policarboxilate)	0.6%	0.6%	0.85%	0.85%	0.6%	0.6%	0.85%	0.85%	0.6%	0.6%	0.85%	0.85%
Activator (Sodium sulfate)				1%				1%				1%

Description of each mix by Mix ID is needed due to the number of parameters studied in concrete; all of these parameters are mentioned in Table 17, including the water to cementitious material ratio and curing type.

Table 17 Mixes ID a) Order/Description b) Code per variable

Mix ID (1/2/3/4/5)	
Letters and numbers order	Description
1	W/CM
2	Cementitious Material
3	Cementitious Material Percentage
4	Curing type
5	Activator

a)

1 - W/CM	
0.675	
0.557	
0.483	
0.426	
2 - Cementitious Material Name	
CE	Cement
TP	Termopaipa FA
3 - Cementitious Material Percentage	
0	0%
20	20%
50	50%
100	100%
4 - Curing type	
L	Lab Curing
O	Outdoor Curing
5 - Activator	
A	Activator 1

b)

5.3.2 Concrete preparation

Each batch of concrete prepared in the laboratory mixer was 30 L. Each mixing process took 7 minutes. The materials were mixed in the following order:

143

1. Coarse aggregates
2. Fine aggregates
3. Cement and fly ash
4. Activator
5. ¾ of water
6. $\frac{1}{8}$ of water with lignosulfonate (plasticizer)
7. Remaining water with polycarboxylate (superplasticizer)

5.3.3 Concrete tests

Table 18 includes the standards followed for each test. In order to test the slump loss, slump testing was performed again after 30 and 60 minutes. Figure 72 presents the ages of evaluation for compressive strength and drying shrinkage.

Table 18 Tests for fresh and engineering properties

CONCRETE EVALUATION	STANDARD TEST METHOD	
Slump	Standard Test Method for Slump of Hydraulic-Cement Concrete	ASTM C 143
Air content	Standard Test Method for Air Content of Freshly Mixed Concrete by the Pressure Method	ASTM C 231
Setting time	Standard Test Method for Time of Setting of Concrete Mixtures by Penetration Resistance	ASTM C 403
Compressive Strength	Standard Test Method for Compressive Strength of Cylindrical Concrete Specimens	ASTM C 39
Maturity	Standard Practice for Estimating Concrete Strength by the Maturity Method	ASTM C 1074
Shrinkage	Standard Test Method for Length Change of Hardened Hydraulic-Cement Mortar and Concrete	ASTM C 157

The ASTM standards were followed to evaluate fresh and engineering properties of samples. The same evaluations were performed for specimens in the curing room and outdoors under ambient conditions (Figure 73). In order to understand the variation of the ambient conditions, they were tracked with a Kestrel® weather meter. The variables tracked in the ambient environment were temperature, relative humidity, heat index, evaporation point, wind speed and CO_2 concentration. Figure 74 shows the variation of these parameters. Some CO_2 concentrations were missed due to the equipment calibration.

a) Curing room

b) Outdoor curing area

Figure 73 Curing conditions – Bogotá, Colombia
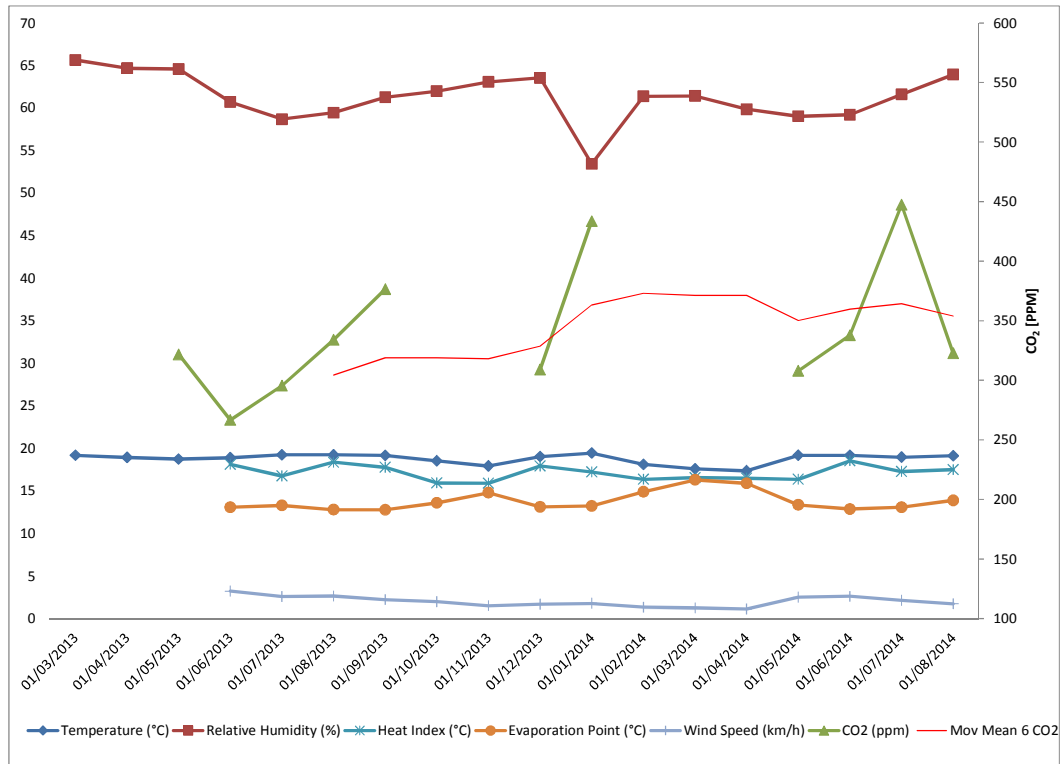
Figure 74 Variation of ambient conditions: temperature, relative humidity, heat index, evaporation point, wind speed, CO_2 concentration

5.3.3.1 Slump test

Concrete consistency is evaluated with this test. As mentioned before, the design slump was 225 +/- 25 mm.

According to the results of mixes with a water to cementitious material ratio of 0.557, the slump was always between 225 +/- 12.5 mm. There was not a negative effect of the activator on slump. Error bars are included for slump only. As shown before, these mixes used lignosulfonates and polycarboxylates as plasticizer and superplasticizer respectively. The slump loss was never higher than 12.5 mm after one hour. As seen in Figure 75, sodium sulfate did not affect slump loss.

146
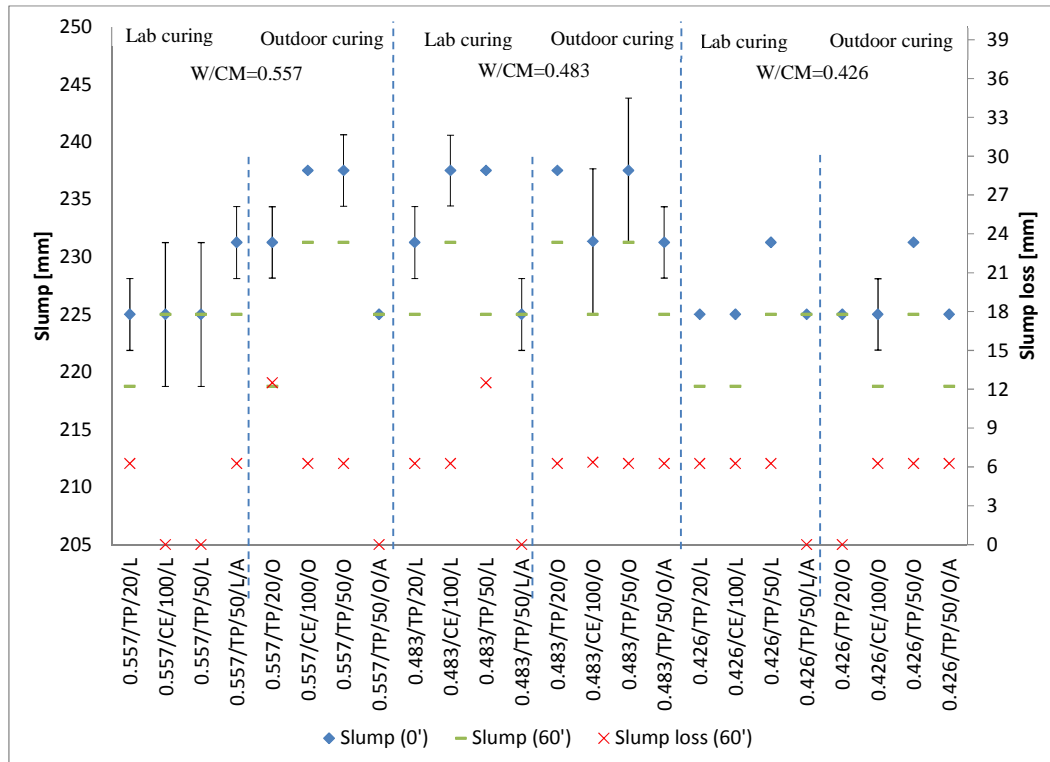
Figure 75 Slump variation

5.3.3.2 Air content

The air content measured using the ASTM C 231 (Figure 76) considers the content included inside the voids within the aggregates. The content of air for the evaluated mixes is the natural trapped air in concrete; this value was expected to be between 1% and 3%.

Figure 76 Slump cone and air content equipment

For these mixes, the air content is part of the natural trapped air. According to Figure 77, the air content always increased for mixes with 50% fly ash. This behaviour could be due to the amount of superplasticizer used in mixes with high

content of fly ash (Lazniewska-Piekarczyk, 2014); this can be seen in Table 16. Generally, polycarboxylates cause an increment in the air content, to the point that in some cases mixes with this type of admixtures require the inclusion of defoamers (Lange and Plank, 2012). Although there was an increment in the air content, the values were in the normal range for concrete production (1%-3%) (ACI 211.1, 2002). This parameter is not relevant in Colombia as in other countries where freezing and thawing affect concrete structures.
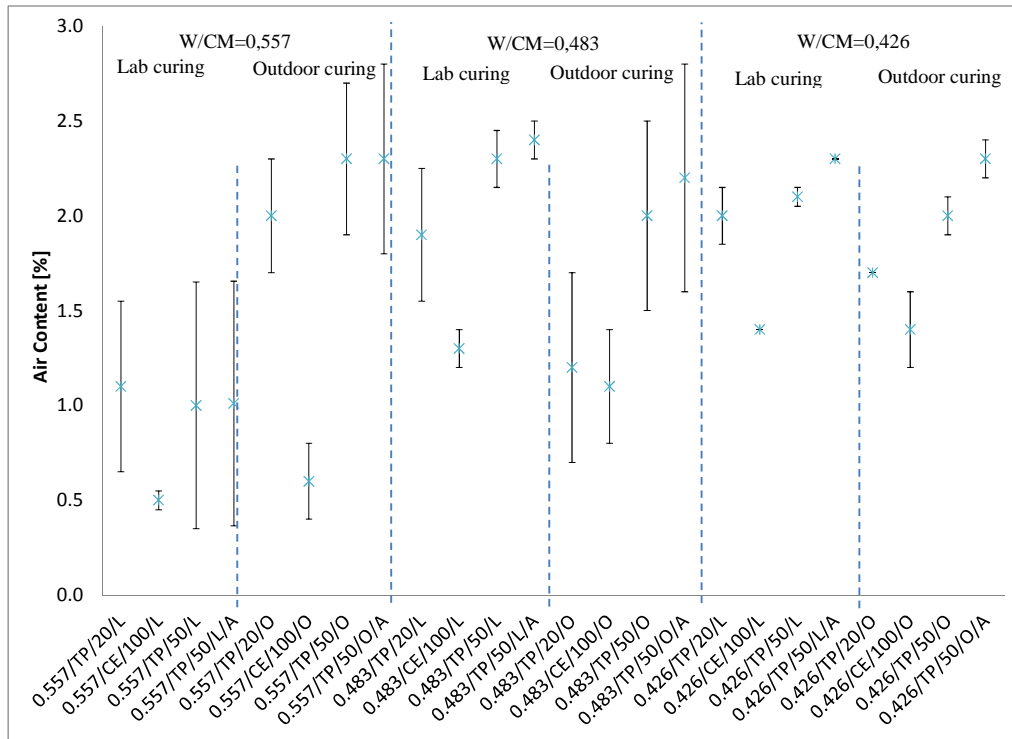
Figure 77 Air variation

5.3.3.3 Setting time

This evaluation is carried out using mortar resulting from sieving a representative quantity of concrete. As seen in Figure 78, this mortar is stored in a cylindrical container where is penetrated by needles of different sizes at different intervals of time (the Proctor method). The needle areas are 645, 323, 161, 65, 32 and 16 mm^2. The initial and final setting time occur when penetration resistance reaches 3.5 MPa and 27.6 MPa respectively.

Figure 78 Setting time test

As is seen in Figure 79, there was a delay in setting of the mix with sodium sulfate; the difference between the sample with activator and the control mix with 80% cement and 20% fly ash was from 5 to 7 hours. The difference from the 50% fly ash control sample was around 2.5 hours. In spite of the difference in setting time, concrete with sodium sulfate can be used for different applications where early demolding is not needed, for instance mass concrete. The same effect was seen in the previous chapter by using calorimetry, where different activators and fly ashes were evaluated. The main causes of the delay were the reaction between sodium and sulfate of the activator with the aluminium of the fly ash, and an additional reaction between this aluminium and calcium from the solution, delaying C-S-H formation (Wei, *et al.,* 1985). Additionally, the increment of the effective water to cement ratio could also have a relevant effect on the setting time increment (Deschner, *et al*., 2012). Depending on the application, Argos setting times vary from 13 hours to 24 hours; for instance, for industrialized constructions (Outinord and Contech) 14 hours are required while for high compressive strengths and mass concretes setting times take 24 hours due to the importance of a slow process.
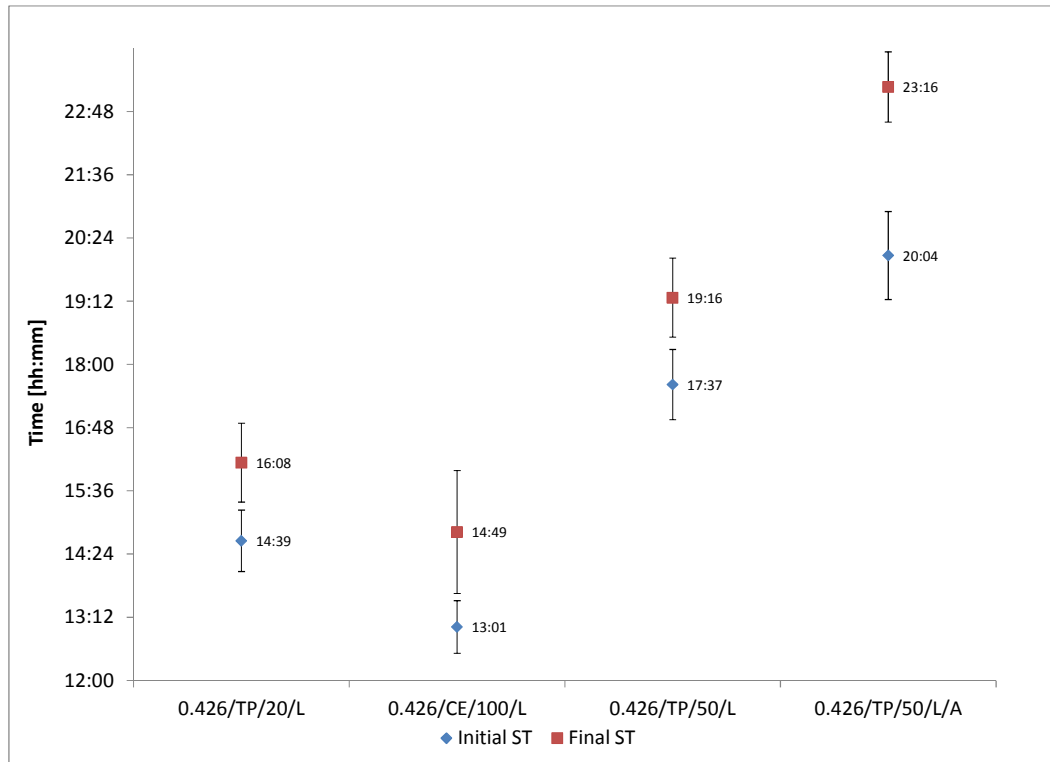
Figure 79 Setting time

5.3.3.4 Compressive strength

Although Figure 80 (a) presents how most mixes had similar behaviour when cured under different conditions, this is not a universal behaviour across the sample set. For instance, samples with 50% fly ash were affected by the curing process. For mixes with activator cured in the curing room, in most cases the compressive strength increased compared to mixes cured outside. Poon, *et al.,* studied the influence of the curing process on compressive strength evolution using mixes with 55% fly ash and calcium sulfate as activator; in this case, specimens were cured at 65°C per 6 hours before continuing a normal curing. This curing process had a positive effect (increment of 70% in compressive strength) compared to a control mix (Poon, *et al.,* 2001). In another study, pastes with sodium sulfate (1% weight of cementitious material) and 50% PC - 50% FA performed better when cured for 7 days at 20°C, than when curing them for the first day at 60°C and the remaining 6 days at 20°C (Owens, *et al.,*2010).

As seen in Figure 80, mixes with sodium sulfate at 1% had higher compressive strengths after 3 days compared to mixes with 50% fly ash without activator. This was also evident in the study presented by Qian, *et al.*, who also used Na_2SO_4 as activator

(Qian, *et al.,* 2001). As mentioned before, this activator increases the alkalinity, accelerating fly ash dissolution, and increases matrix density by increasing ettringite formation. As in the mortar characterization included in the previous chapter, the compressive strength increment was evident from 3 to 7 days compared to the control sample with 50% of fly ash. Compressive strength at 1 day was the lowest for mixes with sodium sulfate due to the possible reaction between sodium and sulfate of the activator with the aluminium of the fly ash; Delay in C-S-H formation was also another possible reason for the low 1 day compressive strength due to an additional reaction between fly ash aluminium and calcium from the solution.
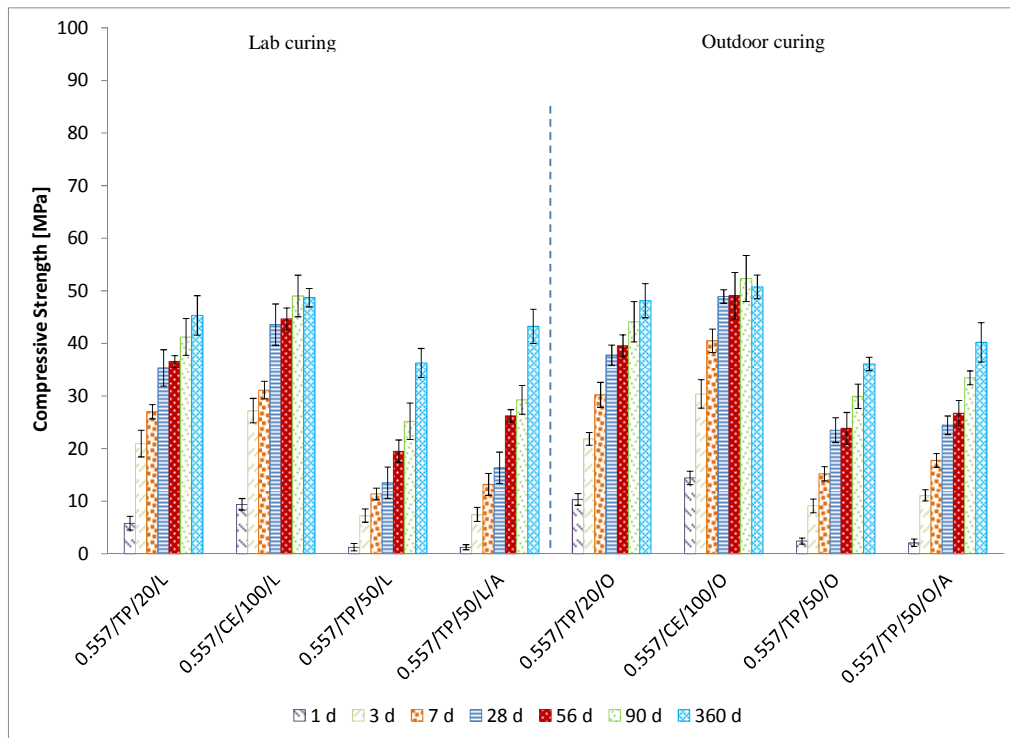
a) W/CM = 0.557
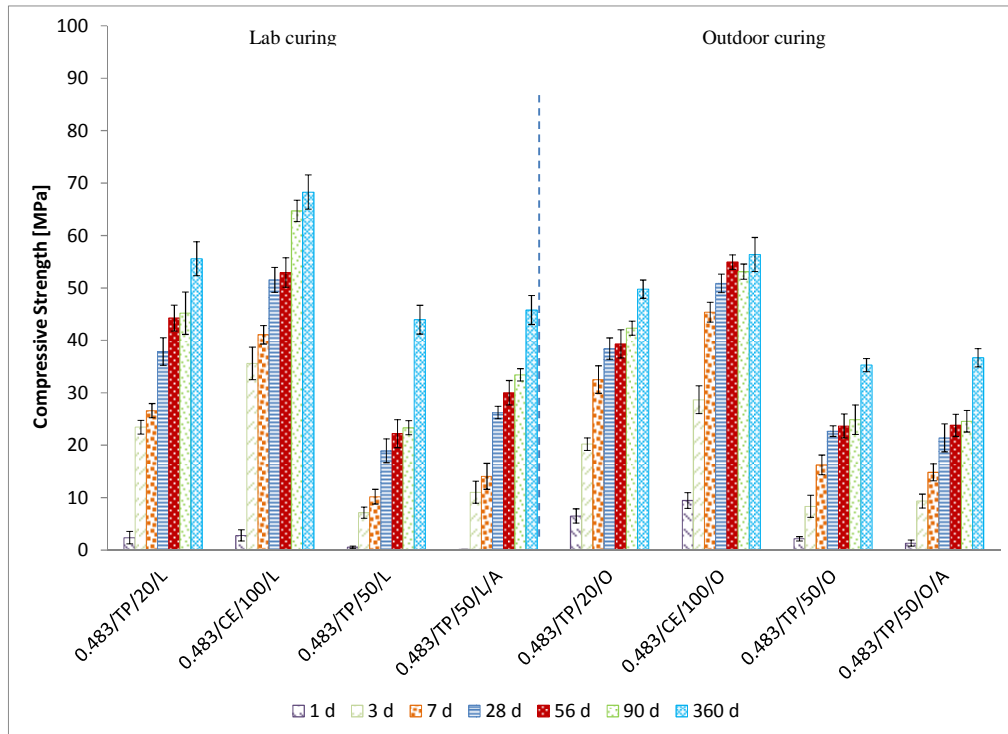
b) W/CM = 0.483
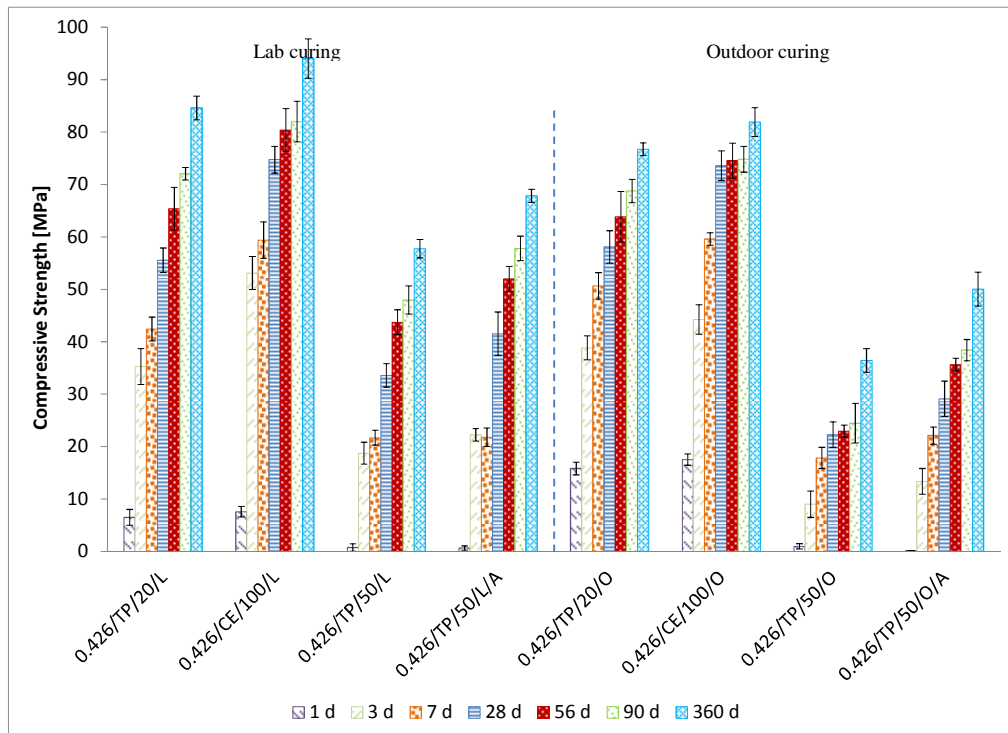
c) W/CM = 0.426

Figure 80 Compressive strength evolution

The data presented as a function of W/CM show clearly how the curing process had a significant effect on the compressive strength for mixes with 50% of fly ash; this is evident in Figures 81 and 82. Considering Figure 81, a design with a W/CM of

152

0.483, 50% of fly ash and activator, has a compressive strength (f'_c) of 24 MPa at 28 days. Additionally, it is important to consider the compressive strength after this period due to the significant evolution. On the other hand, the W/CM did not have an obvious effect at 28 days on mixes with a high volume of fly ash and cured outdoors. In this case, it was not possible to obtain a clear trend. As seen in Figure 82 and for control mixes only, the compressive strength increased by reducing the W/CM, and as mentioned before, there was not a notable effect of the curing process.
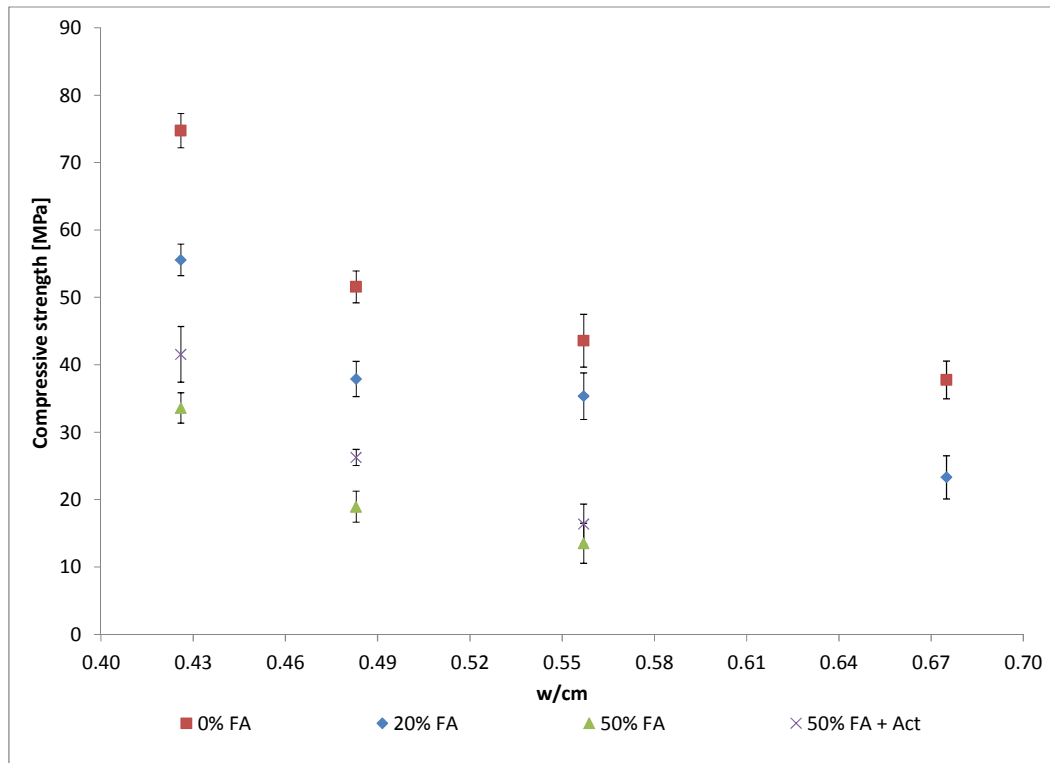
Figure 81 W/CM vs compressive strength curve – Samples cured in the curing room for 28 days
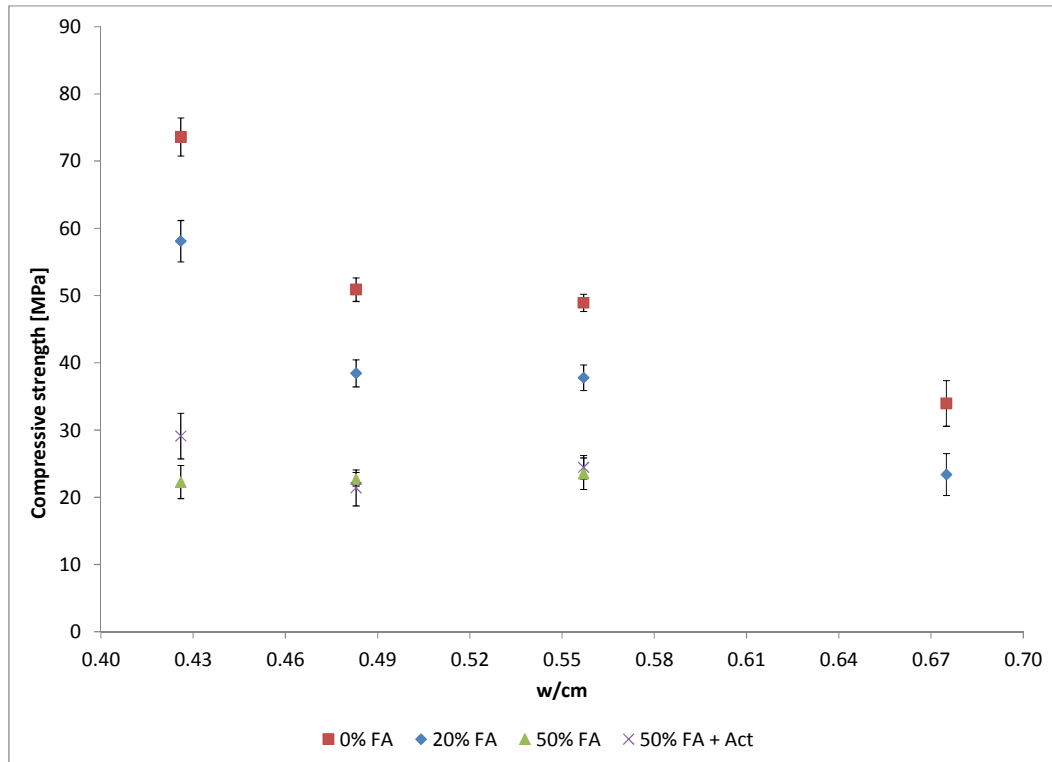
Figure 82 W/CM vs compressive strength curve – Samples cured outside for 28 days

It is important to mention that the main mix design input was the water to cementitious material ratio without considering a target compressive strength. Comparing these curves with the DOE mix design methodology (BRE, 1997), it is found that for the 0% FA curve the values are not the same (see Table 19); for instance, when a target mean strength of 40 MPa is considered, the W/CM is 0.58 for DOE and 0.63 for this study. This can be seen in Table 19. The previous scenario considers cement strength of 42.5 and crushed coarse aggregate. Although the W/CM values considered for 20% FA concretes are similar, they are different when fly ash percentage is increased to 50%, especially for 50 MPa and 60 MPa. When the methodology of the DOE mix design is reviewed, it considers that fly ash reduces total water content and in this study fly ash does not reduce water due to the LOI level.

Table 19 Tests for fresh and engineering properties

| Fly Ash [%] | Target Mean Strength [MPa] | W/CM | |
		Correlations section 7.2.1	DOE (BRE)
0%	40	0.63	0.58
	50	0.54	0.49
	60	0.47	0.42
20%	40	0.51	0.5
	50	0.44	0.42
	60	0.38	0.37
50%	40	0.39	0.38
	50	0.36	0.32
	60	0.33	0.28

Due to the effect of the curing process on small specimens (cylinders, 20 cm length, 10 cm diameter), it is important to evaluate concrete maturity using higher volume elements. In this case, the temperature rise from the larger concrete mass could improve the compressive strength of mixes with activators. The effect of the curing process on mixes with high volumes of fly ash and sodium sulfate will be evaluated using the maturity method, in elements of 120 litres.

5.3.3.5 Maturity

Maturity allows estimation of the compressive strength based on the element temperature. The correlations between strength and maturity are obtained in the laboratory. There are two specified functions to calculate maturity: Temperature - time factor and equivalent age. The function used for this project was the temperature - time factor. This curve is obtained using the following equation (ASTM C 1074).

$$M(t) = \sum (T_a - T_0)\Delta t \qquad (52)$$

Where

$M(t) =$ Temperature time factor [degree-days or degree-hours]

$\Delta t =$ Time interval [Days or hours]

$T_a =$ Average concrete temperature at each Δt [°C]

$T_0 =$ Datum temperature [°C]

Figure 83 presents the equipment and concrete elements used for maturity evaluation.

Figure 83 Maturity evaluation: a) T_0 evaluation chambers, b) Concrete temperature logger and thermocouple, c) Concrete elements with thermocouples

The maturity calculations were performed for a 0.557 water to cementitious material ratio and all the FA% replacement levels. For the T_0 calculation the temperatures were 10°C, 20°C and 39°C. The testing ages were 6 h, 12 h, 1 d, 2 d, 8 d, 16 d, 32 d. To calculate the T_0, it is important to plot first the reciprocal of strength and time for each temperature and each fly ash replacement level as seen in Figure 84.

a) 0% FA

b) 50% FA

c) 50% FA

y = 0.2327x + 0.0206

y = 0.1024x + 0.0276

y = 0.0409x + 0.0238
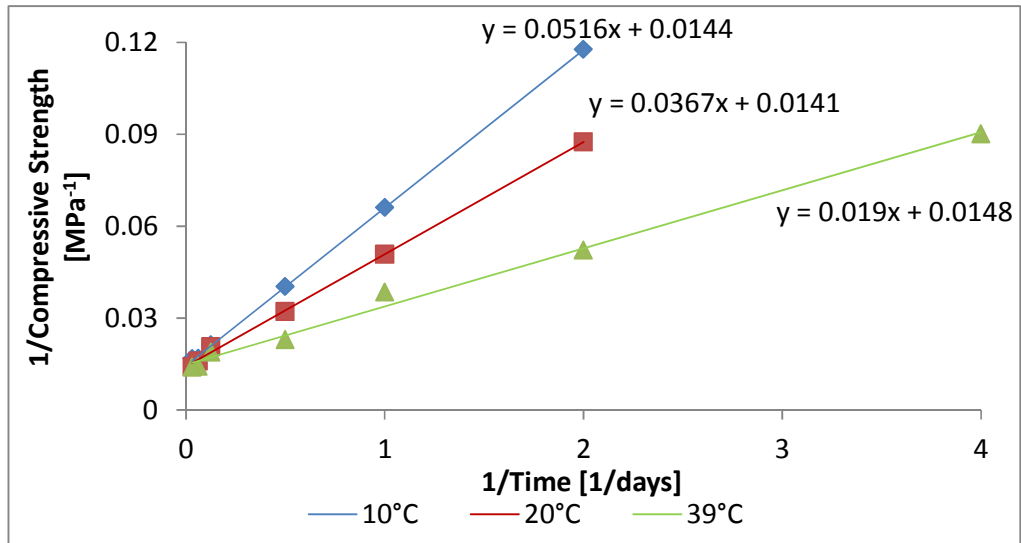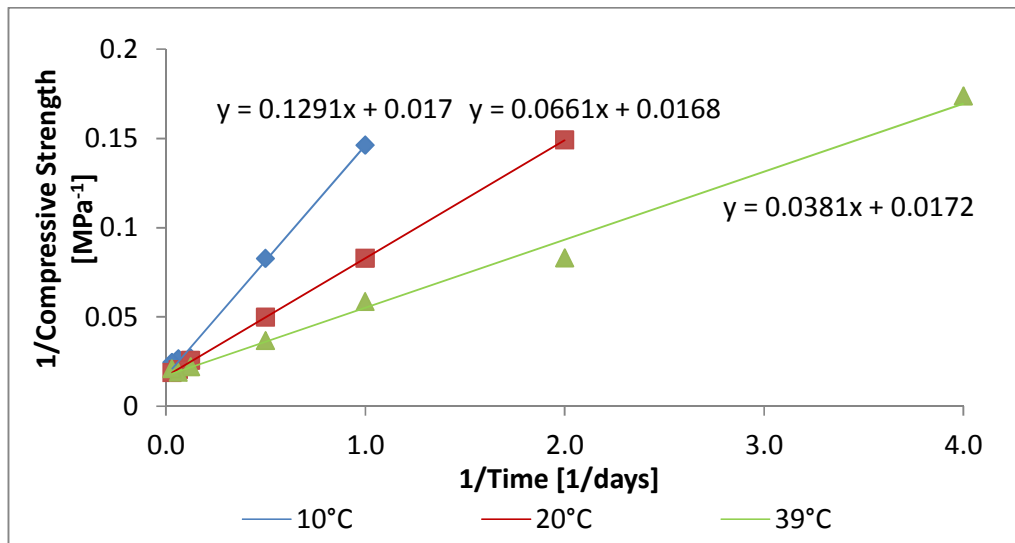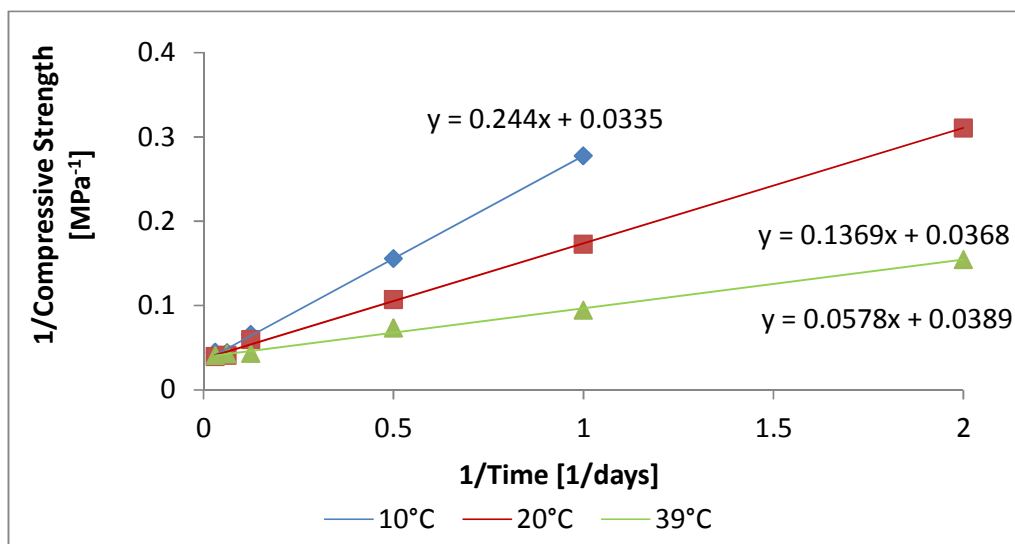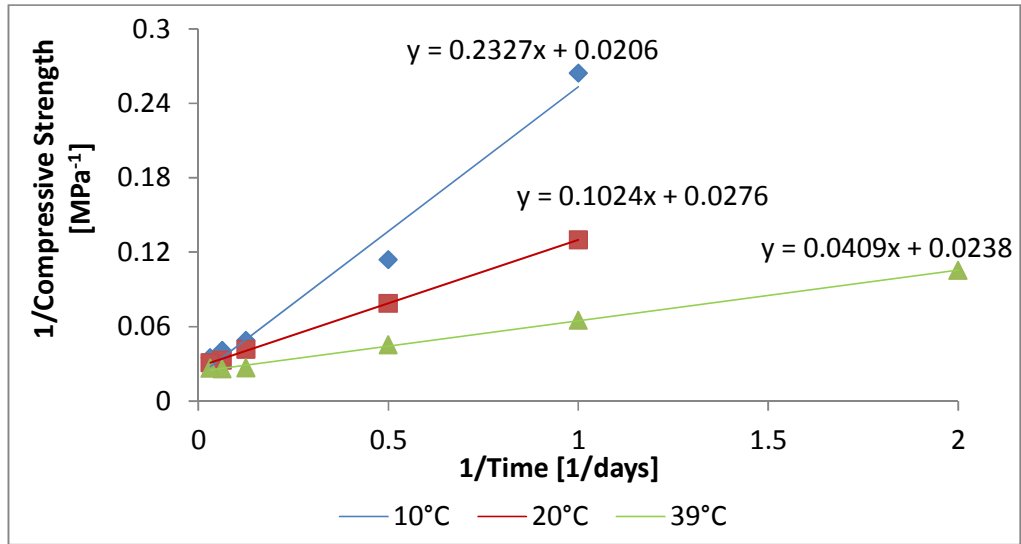
d) 50% FA + Na$_2$SO$_4$

Figure 84 *K* calculation

Based on Figure 67, the rate constant for strength development (*K*) is calculated from the slope and the *y* axis intercept of the trendlines; the intercept is divided by the value of the slope. The T$_0$ value is the *x* axis intercept from the regression between the different temperatures versus K values, for the different fly ash replacement levels. According to ASTM C 1074, the regression line must be the best fit straight line. This is presented in Figure 85.

y = 0.0177x + 0.0736

y = 0.0188x - 0.0736

y = 0.0169x - 0.0763

y = 0.0109x + 0.0274
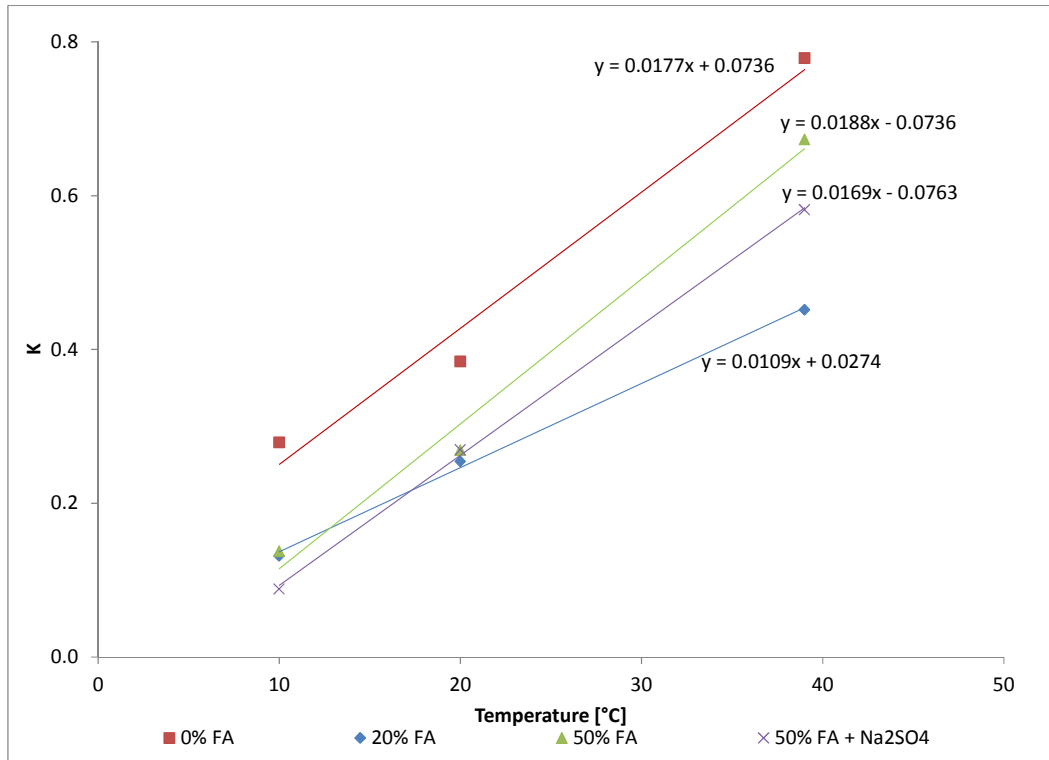
Figure 85 T_0 calculation for 0% FA, 20% FA, 50% FA, and 50% FA + Na$_2$SO$_4$

According to Nurse (1949) and Saul (1951), the datum temperature is the lowest temperature at which concrete will not gain strength (Nixon, *et al.*, 2008). As seen in Table 20, the datum temperature increases as the fly ash percentage increases; the previous effect on T_0 due to fly ash increase was also evident by Ge and Wang (Ge and Wang, 2007). The highest T_0 was for the sample with sodium sulfate. The different T_0 values are presented in Table 20.

Table 20 T_0 Values for all the different replacement levels

FA %	Temperature [°C]	K	To [°C]
0% FA	10	0.279	-4.16
	20	0.384	
	39	0.779	
20% FA	10	0.133	-2.51
	20	0.254	
	39	0.451	
50% FA	10	0.137	3.91
	20	0.269	
	39	0.673	
50% FA + Na$_2$SO$_4$	10	0.089	4.51
	20	0.270	
	39	0.582	

Considering these T_0 values, Figure 86 presents the temperature - time factor vs. predicted compressive strength for the different fly ash percentages. The predicted compressive strength is the same for all the mixes from 0 to 1000 °C-Hours. After this period, the highest compressive strength is expected for the sample with 0% fly ash and the lowest for the sample with 50% fly ash. For instance, for a maturity of 4000 °C-hours, the highest predicted compressive strength is around 40 MPa for the sample with 0% FA, or 30 MPa for the sample with 20% FA, 18 MPa for 50% FA + Na$_2$SO$_4$ and around 15 MPa for the sample with 50% FA.
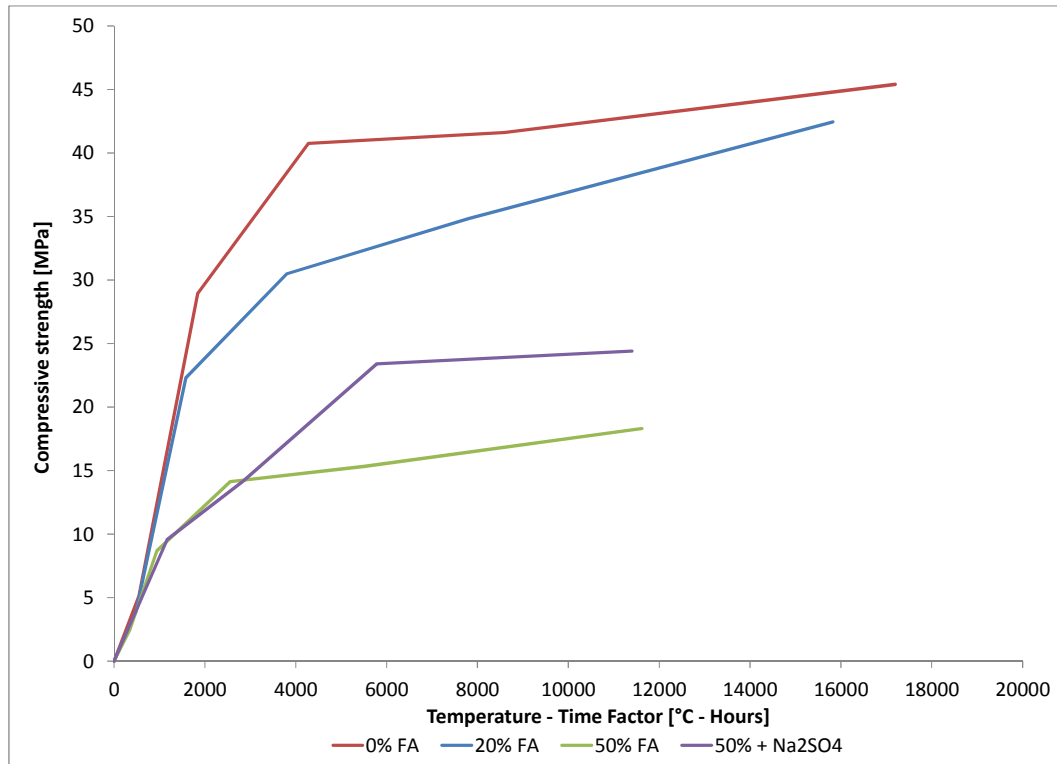
Figure 86 Temperature – Time Factor vs. Compressive Strength curves to be used under different temperature conditions

Appendix 2 presents the ambient and beam temperatures (beams presented in Figure 83). From each of the element temperatures, and using the maturity curves presented in Figure 86, the predicted compressive strength is calculated. The plots presenting the correlations for each fly ash replacement are included in Appendix 2.

Figure 87 presents the concrete element compressive strength evolution with time based on maturity for the different fly ash levels (Figure 86). Figure 87 was plotted using concrete element temperatures included in Appendix 2. According to this figure, the element with sodium sulfate had a higher compressive strength at 28 days compared to the sample with 50%; the difference between these two elements was 7.2 MPa. At early age, the compressive strength of the element with sodium sulfate was the lowest and just after the eighth day it started to pass the sample with 50% FA. The element with 0% FA had the highest compressive strengths at different ages.

As seen in the previous chapters, the water to cementitious material ratio for each replacement level could be different depending on the compressive strength

design value; for instance, based on maturity, the element with sodium sulfate has a compressive strength which classifies for a 21 MPa specification. As mentioned in section 4, delays in reaction increase as fly ash content increases due to the effective water to cement ratio increase; the reaction of Ca from the solution with aluminium from fly ash surface also delays C-S-H formation (Wei, *et al.,* 1985).

It is important to consider that some studies mention that the maturity method is accurate for early compressive strength predictions (Nixon, *et al.*, 2008); in fact, the maturity method is used for early demolding applications. Concrete with high volume fly ash is not suitable for high early compressive strength concrete. Additionally to the fact that fly ash increases the setting time (Ge and Wang, 2007), the inclusion of sodium sulfate also increases it.
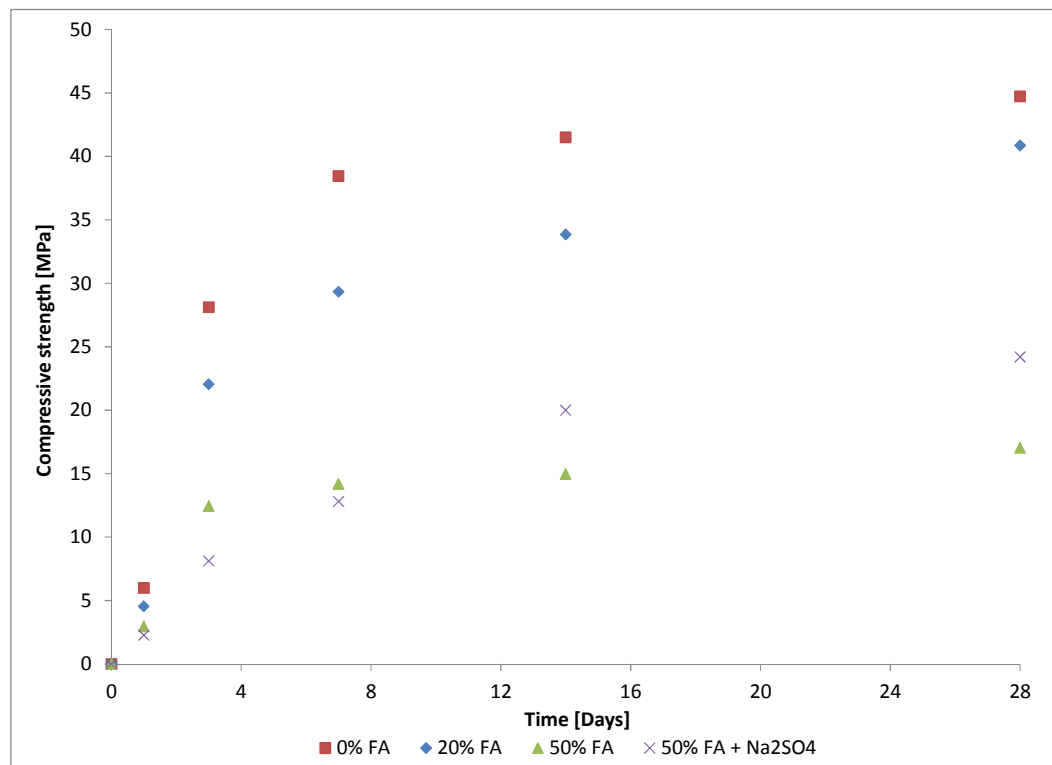
Figure 87 Time vs. Compressive Strength for 20% FA, 0% FA, 50% FA, and 50% FA + Na₂SO₄

Appendix 2 also includes all the results from cores, cylinders and maturity evaluation. According to the study of Obla, *et al*, (2008), the maturity method is more accurate than comparison of field and standard cured cylinders. From Figure 88, it is evident that cores from the elements had the highest compressive strength compared to cylinders and calculations from maturity method. Cores have the same size as

161

laboratory cylinders, becoming comparable without any correction. Nixon, *et al.* consider that the accuracy of the maturity method depends on the environment temperature; maturity evaluation for concrete elements in warm weather was not as accurate as elements in cold weather (Nixon, *et al.*, 2008).

The lowest strength value at 28 days was obtained always using the maturity method. The closest results between cores and maturity method were presented for the 50% FA + Na_2SO_4 element with a difference of 2.20 MPa at 28 days. The difference between cores and maturity method for the 0% FA element was 12.97 MPa. As considered by Nixon, *et al.*, the method is accurate at early age and this is evident in the 20% FA plot, where results are relatively the same up to 2 or 3 days (Nixon, *et al.*, 2008). The increase in long term strengths for HVFA concretes when cured at higher temperatures affect the accuracy of the maturity model (Obla, *et al.*, 2008).

It is important to mention that the points of maturity, cylinders and cores curves are not the average; there is only one result per point. In this way, more research is needed to improve maturity models for high volume fly ash concretes with sodium sulfate. Nixon, *et al.* found that the average absolute percentage error of the method is between 6% and 27% (Nixon, *et al.*, 2008). The method accuracy is reduced when long-term strength is evaluated at the point that the same author recommends to evaluate up to 7 days.
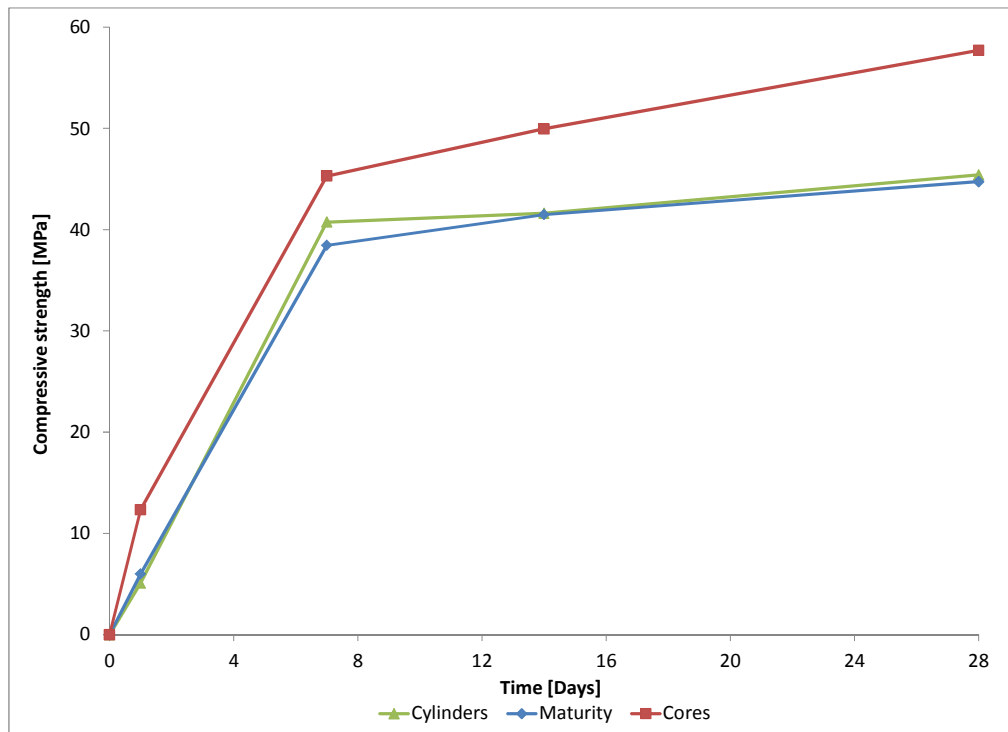
a) 0% FA
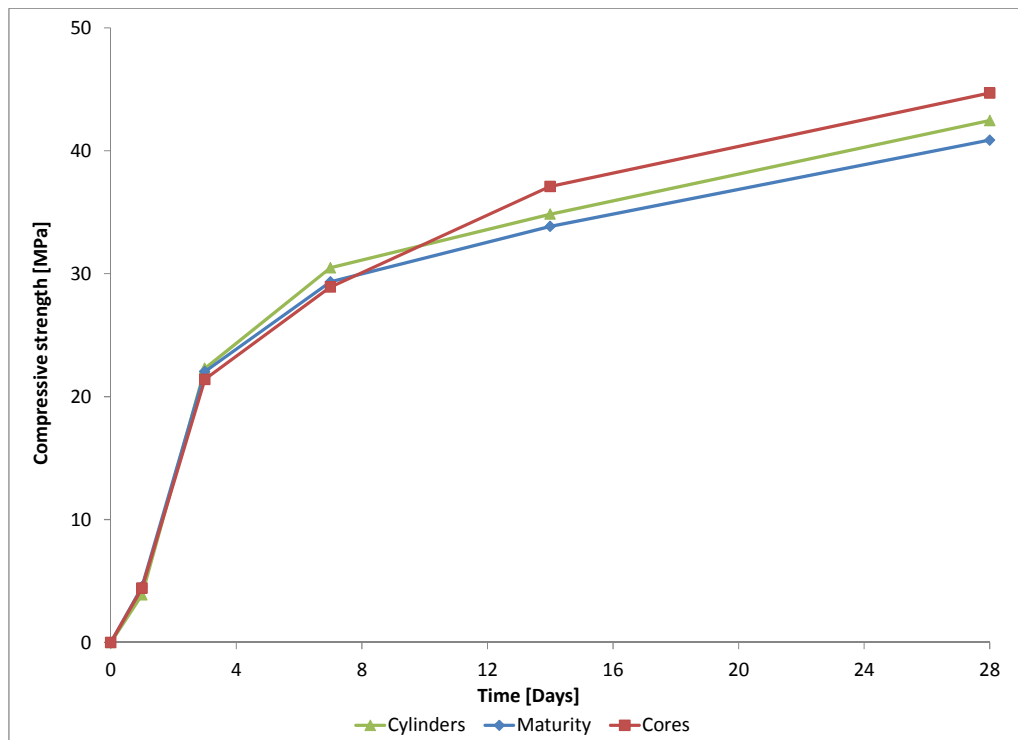
b) 20% FA
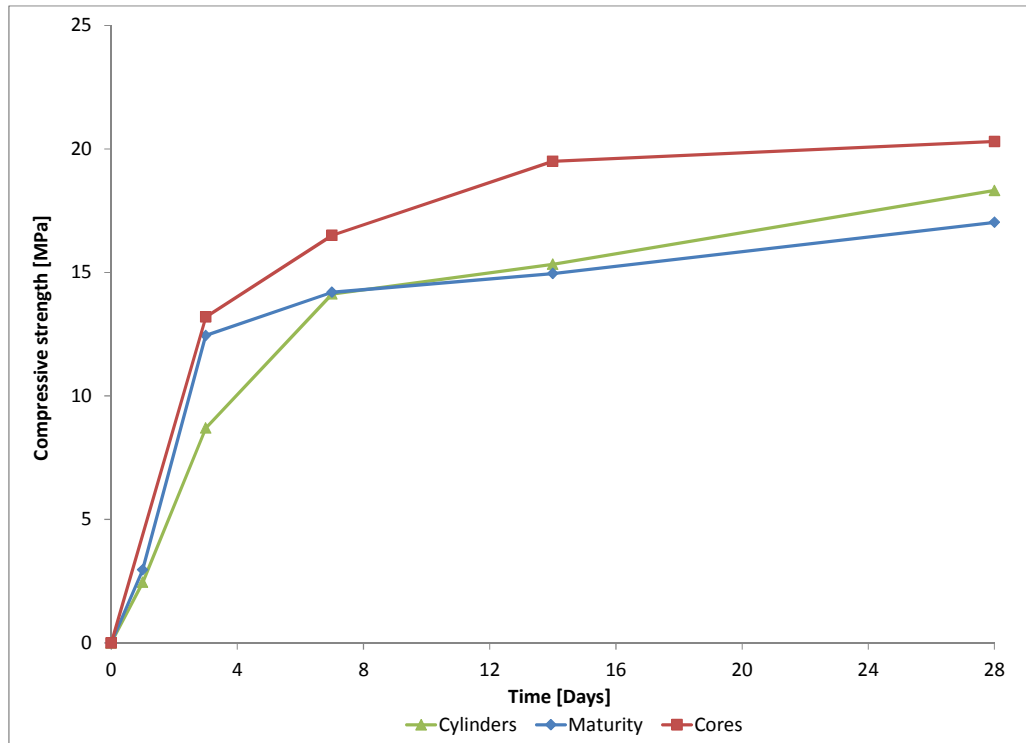
c) 50% FA
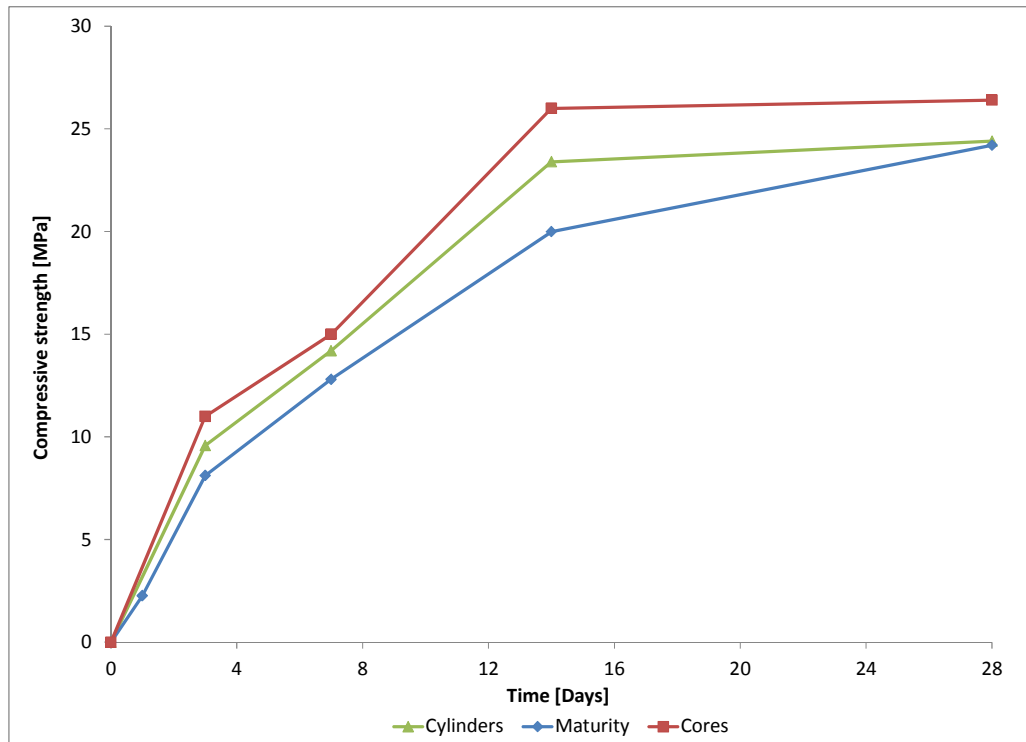
d)

d) 50% FA + Na$_2$SO$_4$
Figure 88 Compressive strength comparison using cylinders, maturity and cores

5.3.3.6 Dry shrinkage

The effect of external forces or temperatures is not considered in this evaluation; in this way, the specimen is always under a controlled temperature and moisture. In order to accomplish these controlled conditions for the specimen, a moist cabinet is used after concrete is cast, and after 24 hours the sample must be stored in lime water until accomplishing 28 days of age. After this age, the sample is stored in a drying room with a relative humidity of 50 +/- 4% and a temperature of 23 +/- 2°C (Figure 89). The readings include 3, 7, 28, 56, 112, 224 and 448 days, considering the initial reading at 1 day.
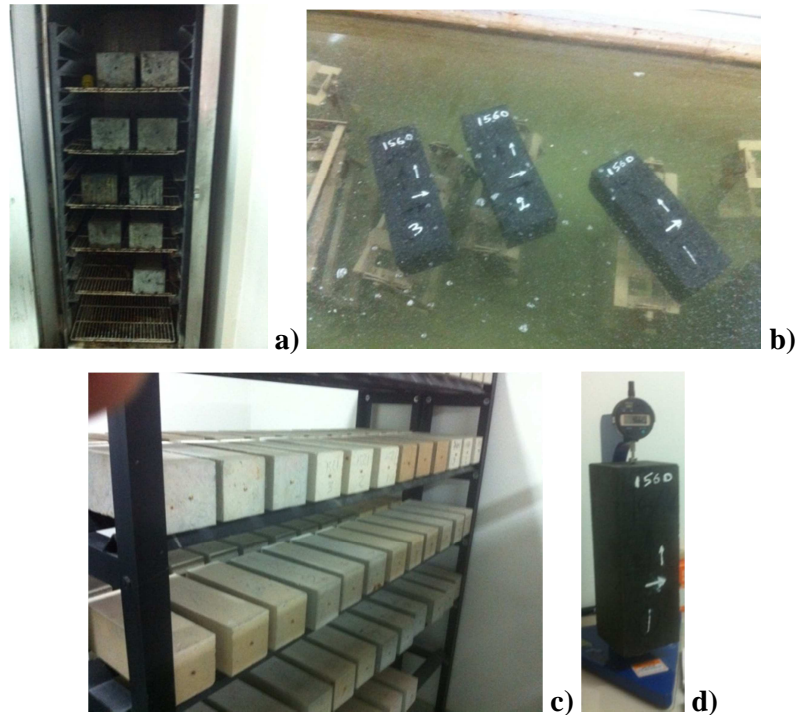
Figure 89 Shrinkage evaluation: a) Curing chamber, b) Beams under water curing, c) Drying room, c) Length comparator

According to Figure 90, the sample with the activator was the most affected sample in terms of shrinkage. This mix expanded 0.0047% (47 µε) at the first 3 days, and then it shrank -0.0747% (747 µε) at 224 days. Readings remained almost the same at 448 days. As mentioned before, the samples are under water for the first 28 days, allowing them to expand during this period; during this initial period water remains present in pores while some products from the process such as ettringite, monosulfate, monocarbonate, portlandite and C-S-H are formed causing concrete expansion. After this period, concrete is stored in a drying room allowing it to shrink under controlled

conditions. The lowest shrinkage was for the mix with 100% cement with a value of -0.0644% (644 µε) at 448 days. Shrinkage results did not agree with some of previous studies, considering that 100% cement mixes tend to have higher values; for instance, Sahmaran evaluated different mixes and found that after a year, the mix with 100% cement had the highest shrinkage (Sahmaran, *et al.*, 2009). Chindaprasirt mentioned that mixes with high volume of fly ash and a low W/CM have a lower shrinkage (Chindaprasirt, *et al.*, 2004). ACI 232.2 mentions that shrinkage increases as fly ash increases due to the paste volume increment; shrinkage could be the same as a control sample with 100% cement if the water content is reduced for the sample with fly ash. Mixes with activators also tend to shrink significantly. Collins and Sanjayan obtained higher shrinkages with waterglass-slag mixes compared with a PC concrete (Collins and Sanjayan, 1999).

Mixes with 20% and 50% fly ash shrank in a similar way. Shrinkage of the specimen with 50% of fly ash was -0.0696 (696 µε) at 224 days being relatively close to the control sample with 20% of fly ash.
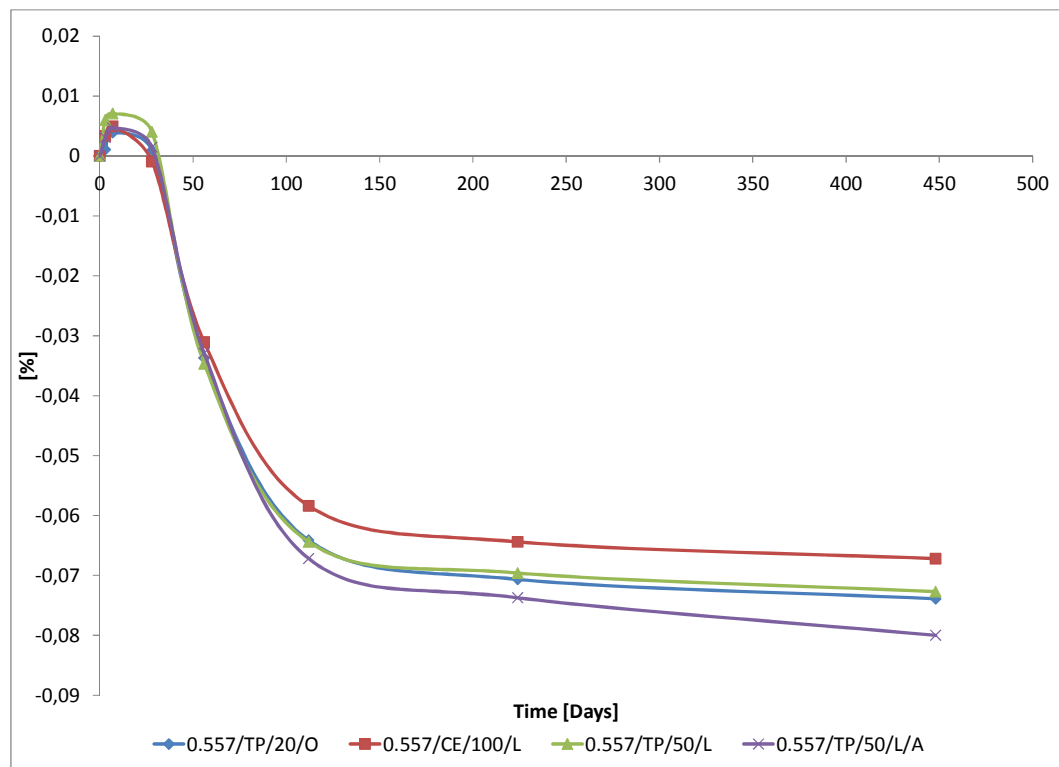
Figure 90 Shrinkage of samples with a W/CM of 0.557

5.4   Summary

Fresh and hardened properties were evaluated in this section and the following is a summary of the results:

- In general, fresh properties were not affected by the inclusion of sodium sulfate in the mix. Initial slump, slump loss and air content were in the acceptable ranges. Initial slumps were between 225 +/- 12.5 mm and slump losses were less than 12.5 mm. Although air contents increased by increasing polycarboxylate content, they were in a range of 1% to 3%. Setting time increased from 1 to 2 hours due not only to the effective W/C ratio increase but also to the reaction between sodium sulfate and fly ash aluminium.

- The curing process was important for concretes with fly ash and sodium sulfate. This type of concrete needs a curing process according to ASTM C 31 (23 ± 2 °C). The 1 day compressive strengths were low for mixes with 50% fly ash but after this time it increased significantly. Concretes with sodium sulfate always passed the control sample with 50% fly ash. The way to compare the performance of the sodium sulfate mix is by considering different W/CM. For instance, in order to achieve the same performance of a 100% PC or 80% PC and 20% FA concrete, it is necessary to reduce the W/CM. It is important to consider the W/CM and compressive strength curve at 28 days as an initial mix design input.

- Maturity test was performed for this concrete and compared with cylinders and cores taken from the element. The datum temperature increased as the fly ash percentage increased. The highest datum temperature was obtained for the concrete with the hybrid cementitious system and sodium sulfate. Predicted compressive strengths were lower by using maturity; the highest compressive strengths were obtained from the element cores.

- Shrinkage was higher for mixes with fly ash due to the paste volume. The mix with sodium sulfate had the highest shrinkage compared to the others. Although concrete with fly ash had this pattern, the values were close to each other including mixes with 100% PC.

6 Durability Properties

6.1 Introduction

Different durability tests were performed on samples cured in the lab and under outdoor conditions. Tests performed include water permeability, chloride penetration, chloride diffusion coefficient, absorption, carbonation, sulfate attack, and alkali silica reaction. It is important to mention that for carbonation, specimens were exposed to ambient conditions while for alkali silica reaction a reactive aggregate was used according to ASTM C 1260. For carbonation the phenolphthalein spray test was followed to assess naturally exposed specimens. In this chapter, one of the main objectives is to characterize transport mechanisms for the activated hybrid cementitious system and from these results the evaluation of the initiation period; this period is the time which is taken for chlorides or carbon dioxide to pass through the concrete cover and reach a concentration where steel reinforcement starts to corrode (Conciatori, 2005; Conciatori, *et al.*, 2008).

6.2 Concrete durability tests

The following table includes the standards used for each parameter evaluation. These standards allowed evaluation of transport mechanisms: absorption, permeability and diffusion. Alkali silica reaction and sulfate attack were also included in the performance evaluation. The curing treatments were the same mentioned in the previous section, including laboratory and ambient curing.

Table 21 Durability tests

CONCRETE EVALUATION	STANDARD TEST METHOD		AGE [Days]
Sorptivity	Measurement of Rate of Absorption of Water by Hydraulic-Cement Concretes	ASTM C 1585	28, 90, 360
Water permeability	Metodo de ensayo para determinar la permeabilidad del concreto al agua (Spanish) / Standard Test Method for Water Permeability Evaluation of concrete	NTC 4483	90, 180, 270, 360
Chloride penetration	Standard Test Method for Electrical Indication of Concrete's Ability to Resist Chloride Ion Penetration	ASTM C 1202	28, 90, 180, 270, 360
Chloride diffusion coefficient	Chloride Migration Coefficient from Non-Steady-State Migration Experiments	NT BUILD 492	90, 180, 270, 360
Water - Soluble Chloride in Concrete	Standard Test Method for Water – Soluble Chloride in Mortar and Concrete	ASTM C 1218	28, 90
Sulfate	Standard Test Method for Length Change of Hydraulic-Cement Mortars Exposed to a Sulfate Solution	ASTM C 1012	7, 14, 21, 28, 56, 91, 105, 168, 252
Alkali silica reaction	Standard Test Method for Potential Alkali Reactivity of Aggregates (Mortar-Bar Method)	ASTM C 1260	3, 5, 9 16, 30
Carbonation	-	-	28, 90, 270, 360

6.2.1　Water permeability

The main objective of this test is to evaluate water penetration depth in a cylindrical specimen, with a diameter and length of 10 cm. In this test, the sample is exposed under a pressure of 0.5 MPa during 4 days. After the 4 days, the sample is broken using the Brazilian method as seen in Figure 91. Water depth and permeability coefficient are measured and classified according to the following table (NTC 4483, 1998):

Table 22 Water permeability classification

Parameter	Units	Permeability		
		Low	Medium	High
Water permeability coefficient	m/s	$<10^{-12}$	10^{-12} to 10^{-10}	$>10^{-10}$
Penetration depth	mm	<30	30 to 60	>60

Penetration depth measurements apply for concretes where steady state flow is not possible to achieve. Water penetration depth is an accurate value due to the fact of being a direct measurement. When water passes through the sample (up stream to down stream), the permeability coefficient is calculated using Darcy's law (see Equation 6, Chapter 2). In the case where water does not penetrate or partially penetrates the specimen, Valenta proposed a way to calculate the coefficient considering water depth and sample porosity (Equation 8).

a)

b)

c)

d)

e)   f)
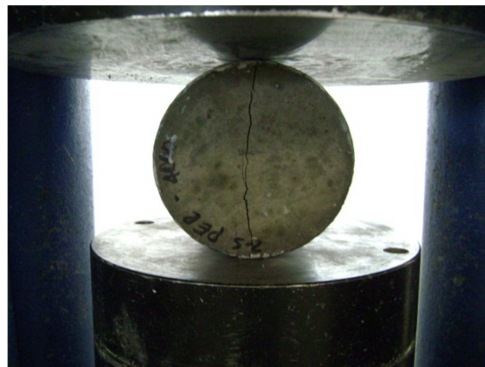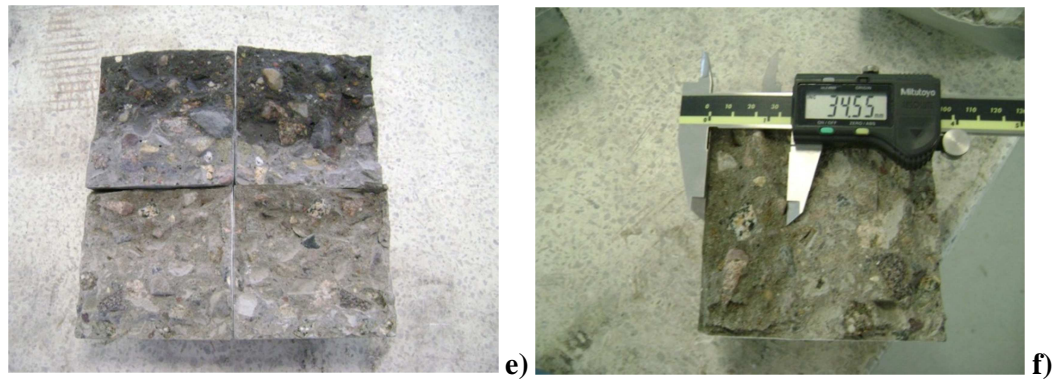
Figure 91 Water permeability test: a) Sample dimensions, b) Water permeability machine, c) Manometer, d) Sample splitting (Brazilian test), e) Split samples, f) Water penetration depth

In general terms, Figure 92 shows how the curing process had an effect on water permeability, especially in mixes with high volumes of fly ash. Samples cured outdoors had a higher water permeability. The curing room guaranteed the availability of sufficient water for the formation of all the hydration products, while conditions outdoors such as relative humidity and temperature were not favourable for hydration products formation. Different studies have evaluated the effect of the curing process for mixes with fly ash and it is evident that increasing this period reduces water permeability (Amnadnua, *et al.,* 2013). In most cases, specimens with activator presented lower water permeabilities than control samples at 180 days. The effect of water to cementitious material ratio on water permeability was significant for mixes with fly ash. Different studies have shown the same effect on mixes with PC and geopolymer concretes (Olivia, *et al.*, 2008). This was notable for mixes with lab curing; mixes under environmental conditions did not have a pattern in their behaviour.

170
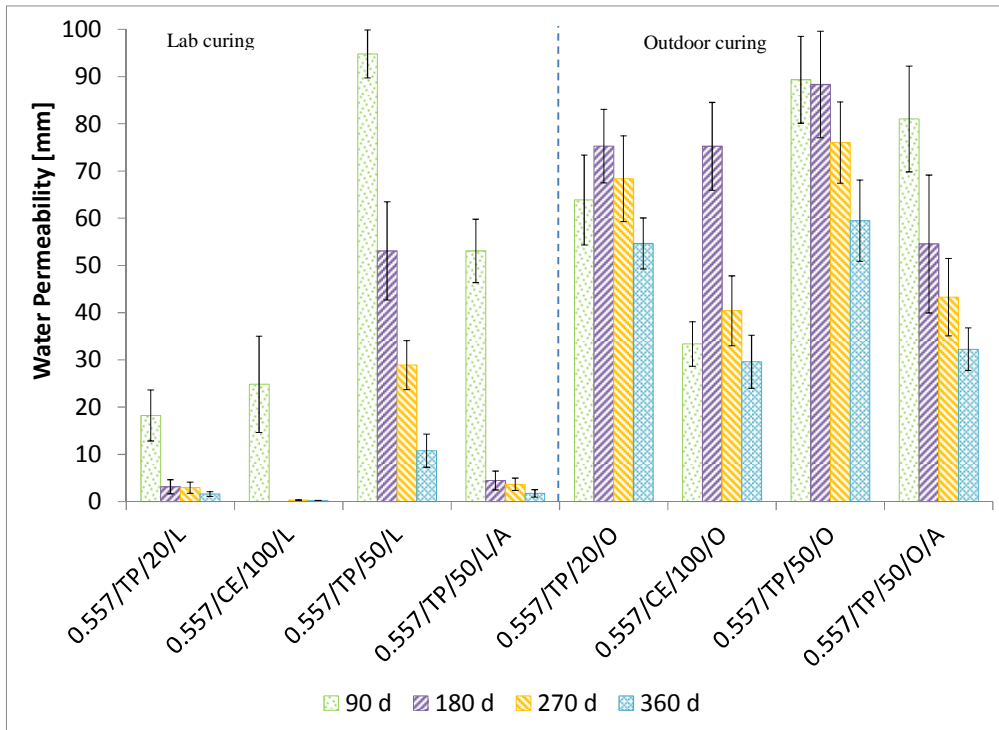
a) W/CM = 0.557
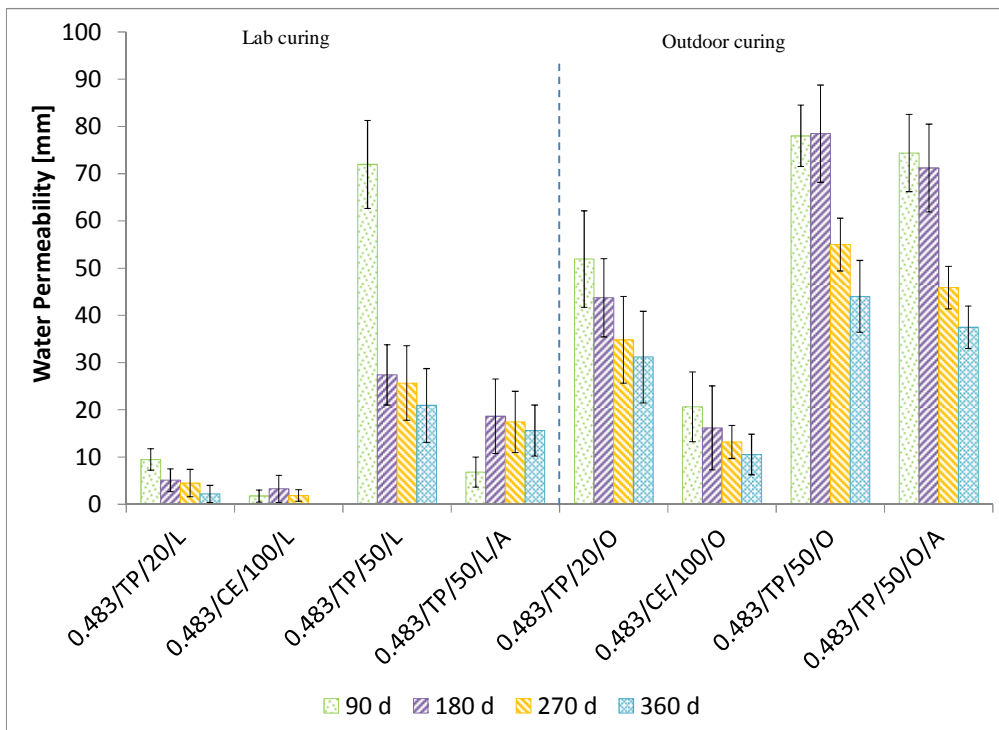
b) W/CM = 0.483
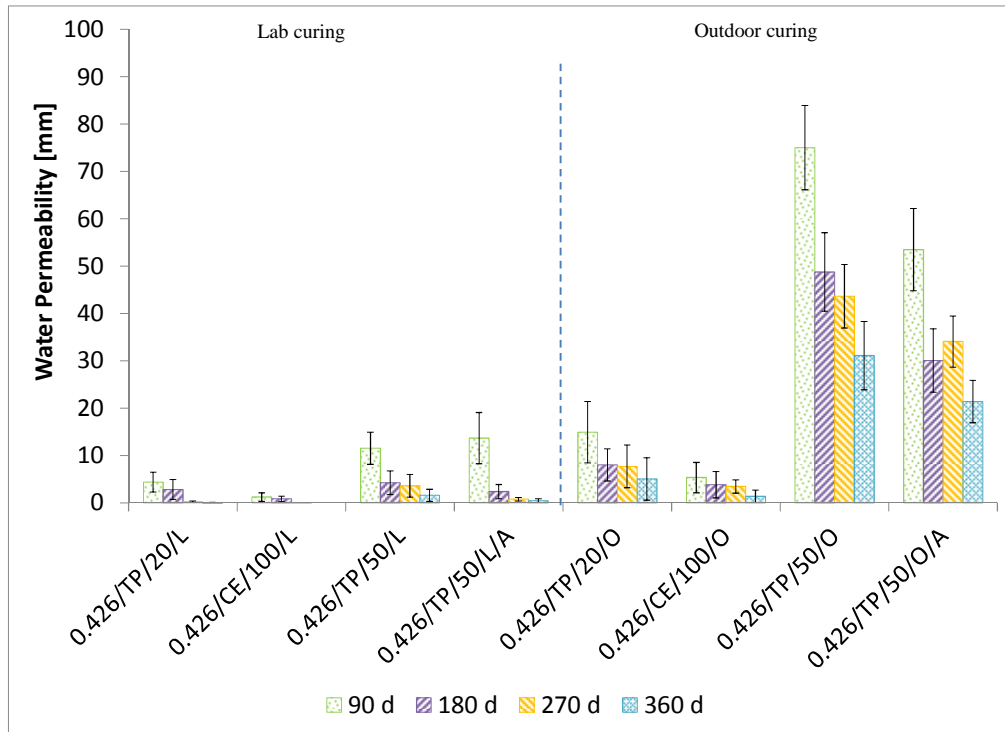
c) W/CM = 0.426

Figure 92 Water permeability

In general, most of the mixes with sodium sulfate performed better than control mixes at later ages. Following the Colombian standard and classifying penetration depths, the hybrid activated mix is classified as "low" in permeability, after 180 days for 0.557 W/CM under lab curing.

Although water permeability coefficient was not evaluated at each age, the effects of curing and the W/CM were evident. This is seen in Figure 93. Based on these results, it is important to consider the effect that hybrid mixes with sodium sulfate could have on some of the chloride and carbonation service life models such as the CEB (Comité Européen du Béton, 1997), EHE (La Instrucción Española del Hormigón Estructural, 2008) and LNEC (Portuguese National Laboratory of Civil Engineering, 2007) models; the previous models do not consider concretes with hybrid systems with sodium sulfate and the low permeability presented by this type of concretes suggests a microstructural improvement.
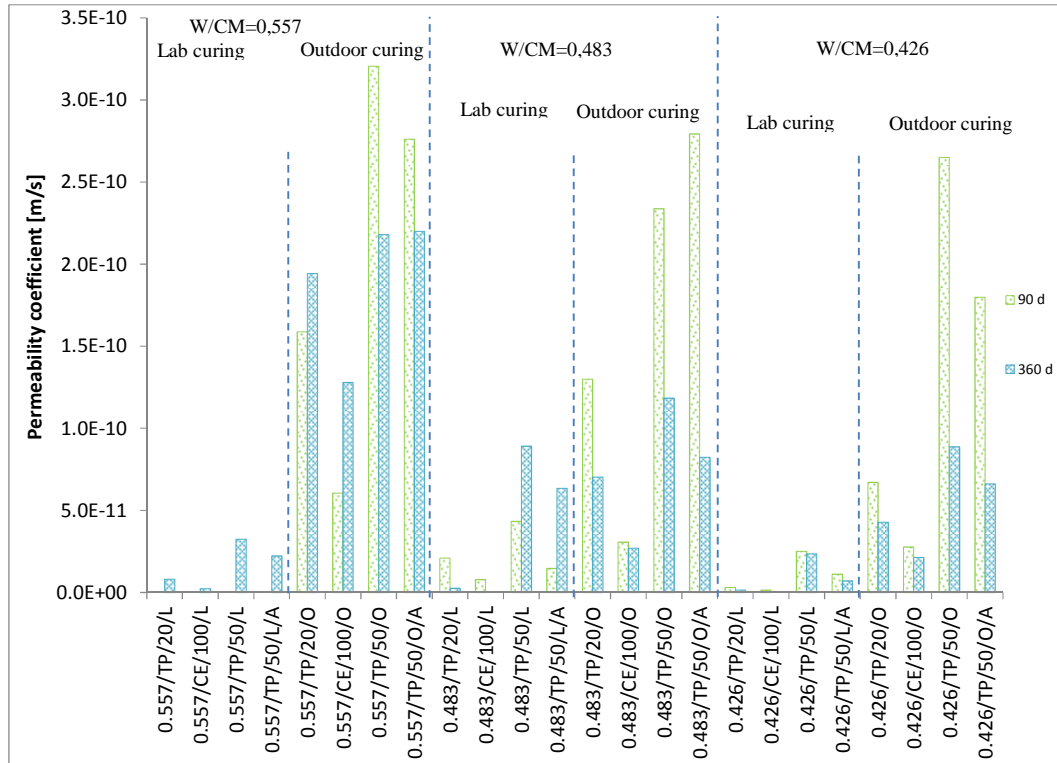
Figure 93 Water permeability coefficients

6.2.2 Rate of Absorption (Sorptivity)

Rate of absorption or sorptivity is measured by immersing in water one of the specimen sections. The rate of absorption is based on the weight variation with time due to capillary suction of the unsaturated sample. A special preconditioning for the ends of the cylindrical specimen ends (10 cm in diameter and 5 cm in length) is required before measuring concrete absorption (Figure 94). First, 3 days at 50°C and 80% RH. After that, 15 days at 23°C in a container where the RH is between 50% to 70%. After one of the sections is immersed in water, weights are recorded from 1 minute up to 8 days at different intervals. The initial and final sorptivities are obtained from this test. The initial sorptivity is obtained from the slope of the initial absorption curve in the first 6 hours and the final sorptivity is the slope of the final absorption curve from 1 to 8 days. The following are the equations used for absorption and sorptivity calculations.

$$I = \frac{m_t}{a \cdot d} \tag{53}$$

Where,

I = absorption [mm]

173

m_t = the change in specimen mass at different periods of time [g]

a = specimen exposed area [mm^2]

d = water density [g/mm^3]

The data are then fitted with a curve according to:

$$I = S_{i,s}\sqrt{t_{i,s}} + b \tag{54}$$

$$S_{i,s} = \frac{I-b}{\sqrt{t_{i,s}}} \tag{55}$$

Where

$S_{i,s}$ = initial i or secondary s sorptivity [mm/s$^{1/2}$]

$t_{i,s}$ = time for initial i (up to 6 hours) or secondary s (after the first day) absorption [s]

b = where the line crosses the y axis [mm]

Figure 94 Sorptivity test

As seen in Figure 95, the rate of absorption is strongly affected by the curing process and fly ash content. Samples with outdoor curing had higher sorptivities than samples cured in the lab. The effect of the water to cementitious material ratio was not as evident as it was expected. Although different authors reference a strong influence

of the water to cementitious material ratio, (e.g. Rabehi, 2013), there was not a clear trend in this study.
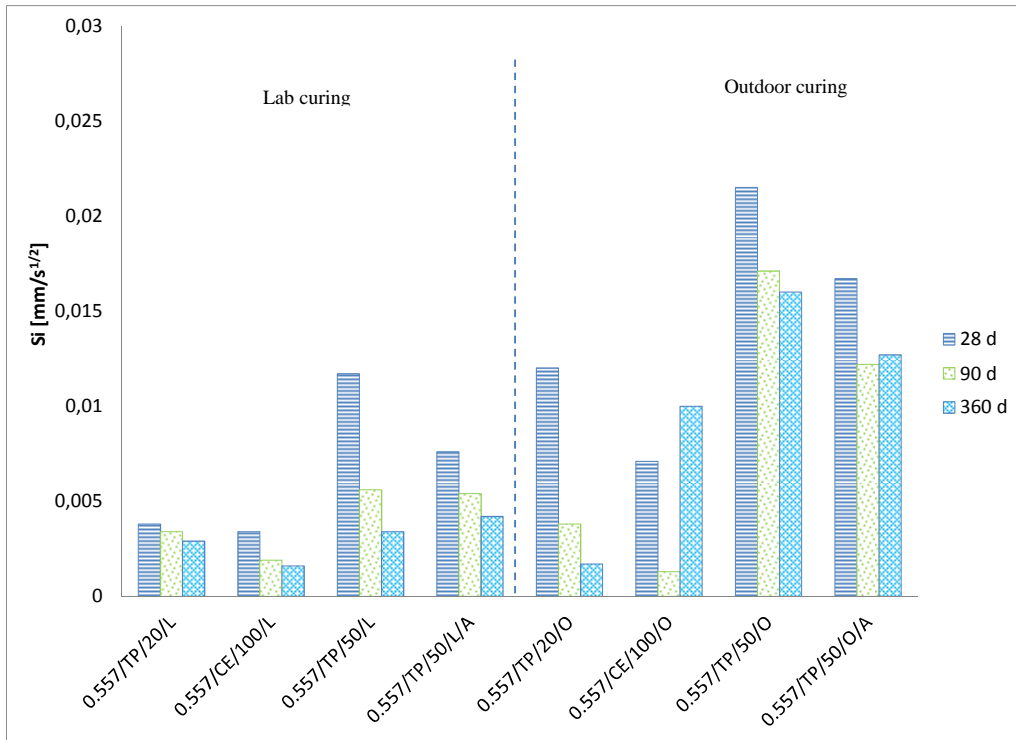
a) W/CM = 0.557
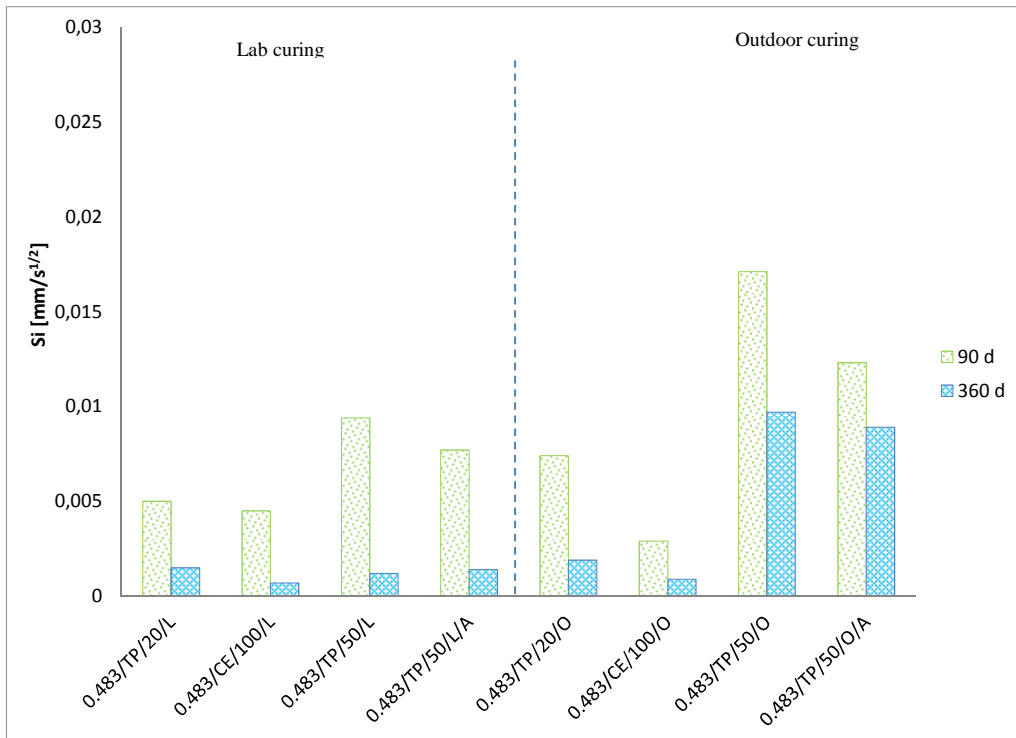
b) W/CM = 0.483
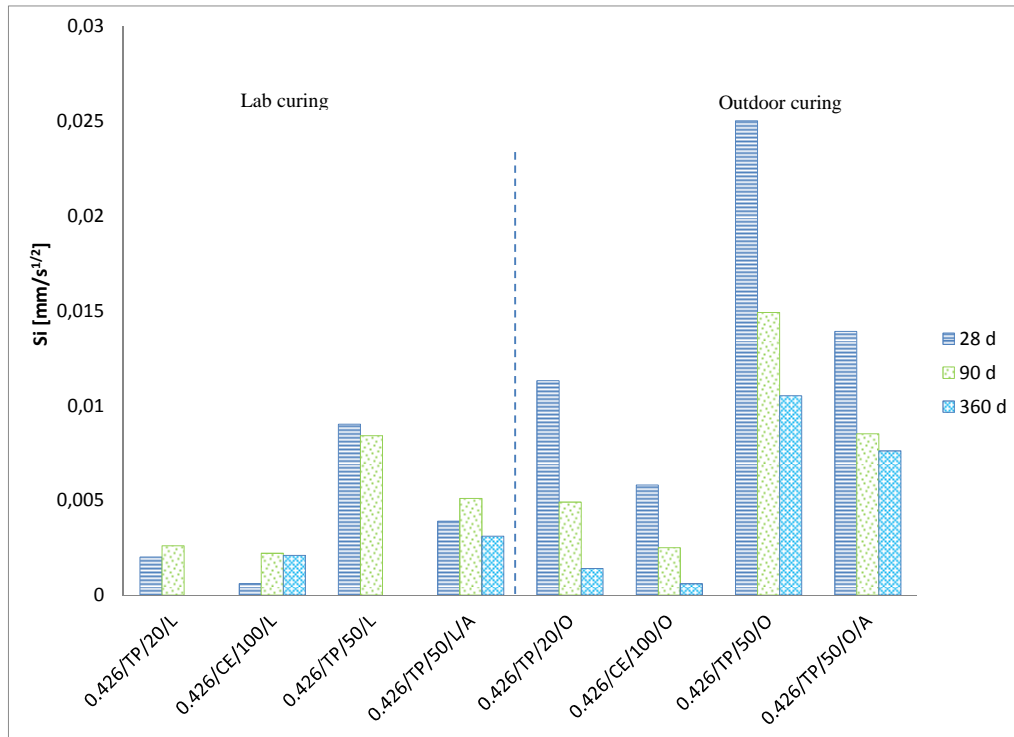
c) W/CM = 0.426

Figure 95 Initial rate of absorption

There was a higher sorptivity for mixes with 50% fly ash even at ages of 90 and 180 days; in this case, mixes with activator had a lower initial sorptivity compared to mixes with 50% fly ash only. It is important to differentiate that inclusion of fly ash on a constant-mass basis increases the total volume of paste due to its lower density than cement, increasing capillary pores (Dinakar, *et al.,* 2008). In the same way, fly ash had a high unburnt carbon content which could increase absorption of the specimens due to the porosity of these particles. The initial rate of absorption (initial sorptivity) or the slope of the initial absorption curve (first 6 hours) did not vary significantly as the secondary rate (from 1 to 8 days). In some cases under outdoor curing conditions, secondary rate of absorption was higher for alkali activator mixes than those without this admixture (Figure 96).
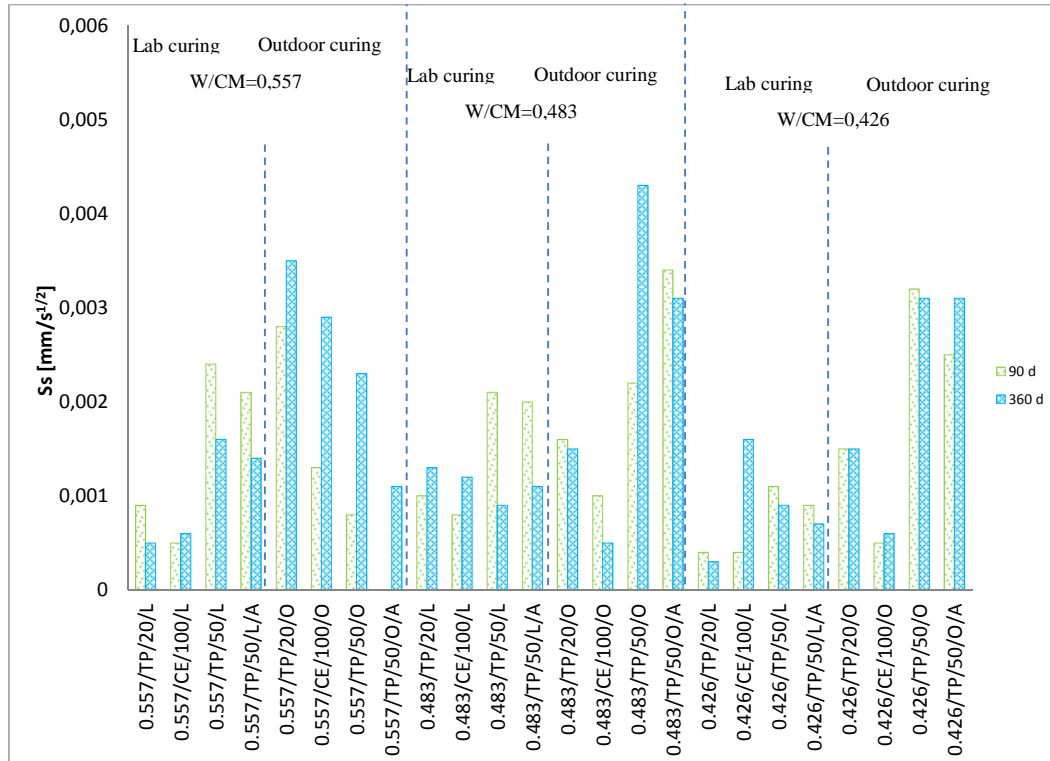
Figure 96 Secondary rate of absorption

6.2.3 Chloride penetration

Samples for this test require pre-treatment; they must have a coating at the side surface of the cylinders (thickness: 5 cm, diameter: 10 cm), and three hours of vacuum saturation is needed using de-aerated water. After this, samples are left for 18 hours in de-aerated water (Figure 97). Then samples are placed in an applied voltage cell as it is illustrated in the ASTM C 1202 figures. Electrical current which passes through the sample is monitored during 6 hours. The cell was filled with solutions, sodium chloride in one side and sodium hydroxide in the other. A voltage of 60 V dc is held constant during this period and the temperature is monitored all the time. After this period, the total charge (coulombs) can be classified according to a table present in ASTM C 1202.

Figure 97 Chloride penetration test

According to the results presented in Figure 81, the curing had a strong influence on samples with high water to cementitious material ratio. Mixes with activator and 0.557 W/CM performed better than control mixes after 180 days. These occurred earlier for lower W/CM ratios. Comparing between mixes cured outdoors, samples with activator had almost the same or lower charged passed in most of the cases.

Although chloride penetration is considered to be reduced by increasing fly ash replacements in HVFA concretes (Velandia and Echeverri, 2010), it is important to consider that this only occurs at later ages and strongly depends on W/CM level. In most cases, mixes with 50% of fly ash without activator did not perform better than control samples. For these kind of mixes, Malhotra proposed to decrease water levels by using high range water reducing admixtures (Malhotra and Bilodeau, 1999; Dinakar, *et al.*, 2008).

On the other hand, some authors consider that the chloride penetration test for mixes with activators is not an acceptable procedure due to the pore alkalinity and ionic strength (Bernal, *et al*., 2012; Puertas, *et al.,* 2004). In this case, based on the trends presented in Figure 98, there was not a negative effect on mixes with activator, probably due to low concentrations of the activator and the low mobility of sulfate ions.

Although general trends can be seen for the effects of fly ash percentages and sodium sulfate as activator in these results, the effect of the curing process is not clear. This is probably due to the low precision of the test; as considered in the standard, a maximum percentage of repeatability is 42%. Although this test is widely used in the concrete industry, it is necessary to consider some additional tests to satisfactorily evaluate concrete performance and the influence of different materials in the concrete matrix.
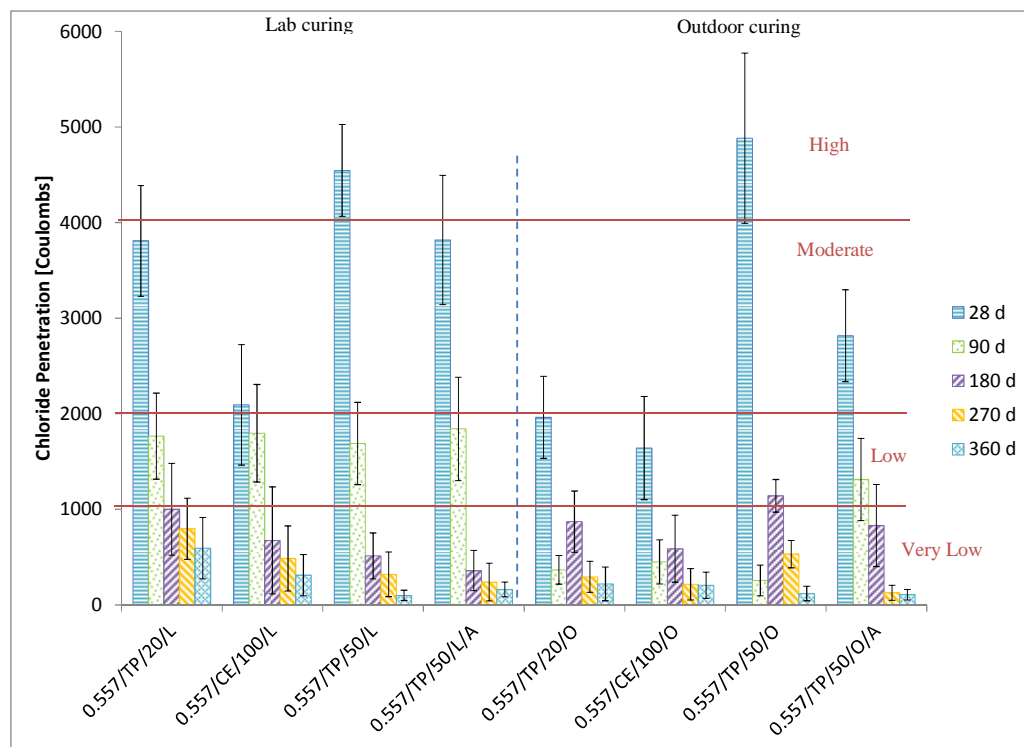
a) W/CM = 0.557
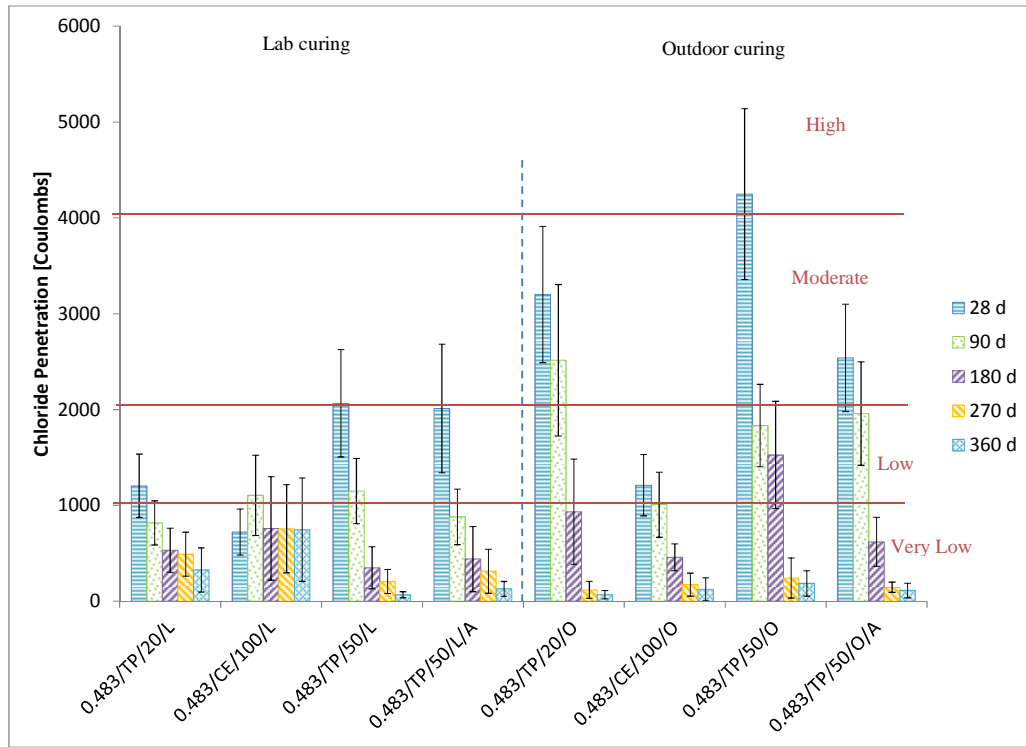
b) W/CM = 0.483
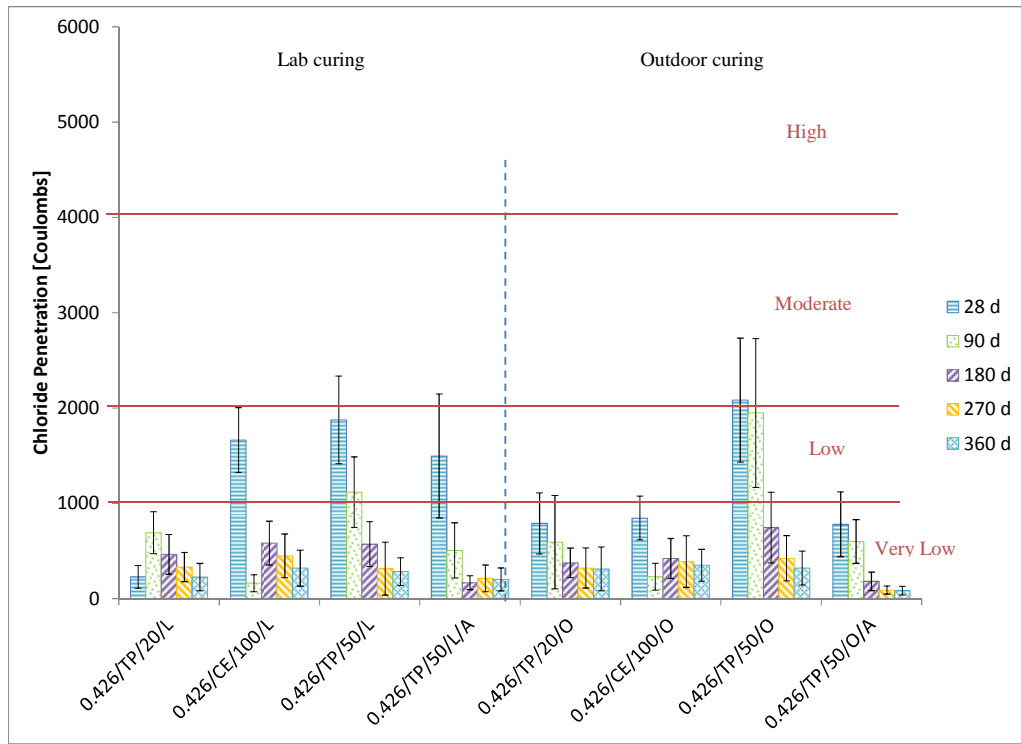
c) W/CM = 0.426

Figure 98 Chloride penetration test results

6.2.4 Chloride migration coefficient

The Nordtest Chloride migration test allows determination of concrete resistance to chloride penetration. Samples used for this test are cylindrical, 5 cm in length and 10 cm in diameter. In this test, chloride ions are forced to penetrate, and after the cylinder is split by the Brazilian method, the cross section is sprayed with silver nitrate, which allows measurement of chloride penetration based on colour variation as seen in Figure 99. In this standard, the chloride migration coefficient, represented as a diffusion coefficient, is calculated with the following equation:

$$D = \frac{0.0239(273+T)L}{(U-2)t}\left(x_d - 0.0238\sqrt{\frac{(273+T)Lx_d}{U-2}}\right) \tag{56}$$

Where:

D = Diffusion coefficient [x10^{-12} m^2/s]

U = Voltage [V]

T = Anolyte solution average temperature between initial and final measurements [°C]

L = Cylinder thickness [mm]

x_d = Average of the penetration depths [mm]

t = Test duration [hour]
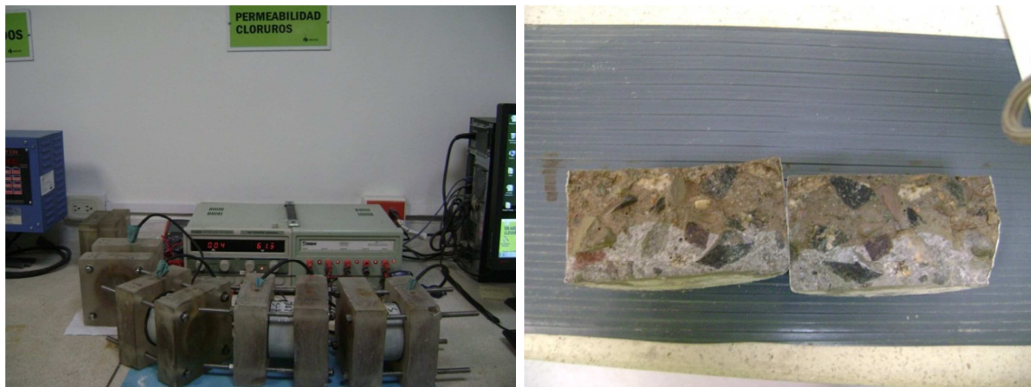
Figure 99 Diffusion Coefficient

Based on results presented in Figure 100 and as was mentioned before, curing affects significantly mixes with fly ash. In most of the cases, the 100% cement mix performed better under outdoor curing. The effect of the activator was not evident when samples were cured outdoors. According to Özbay, *et al.*, the effect is the opposite when an inadequate curing is performed and a low fly ash fineness is included in the matrix (Özbay, *et al.*, 2012). The variation of the temperature in the curing

process had an effect as mentioned by Reinhardt and Joss (1998) where a change in temperature from 20°C to 80°C for mixes with 40% FA reduced the diffusion resistance around 10% to 20%.

An increment in the chloride diffusion coefficient for mixes with fly ash was probably due to the absorption increment in the first days. In fact, Ismail, *et al.* mentioned that chloride sorption increases when fly ash is included instead of slag in alkali activated binders (Ismail, *et al.,* 2013). In this case Bernal, *et al.* also mentioned a relation between diffusion coefficient and sorptivity (Bernal, *et al.*, 2012).

From 90 to 180 days, activated mixes had a lower diffusion coefficient ($< 7x10^{-12}$ m^2/s) in comparison with control samples (Figure 100). According to Burden, the performance of high volume fly ash concrete (30%, 40% and 50%) is improved after 90 days and a year, but before this age, performance is poor (Burden, 2006). Although it is evident that the process with the activator was faster than the mix without it, the latter presented a significant improvement with time. The water to cementitious material ratio showed an influence on the diffusion coefficient, but only for mixes cured in the lab.

a) W/CM = 0.557

182

b) W/CM = 0.483

c) W/CM = 0.426
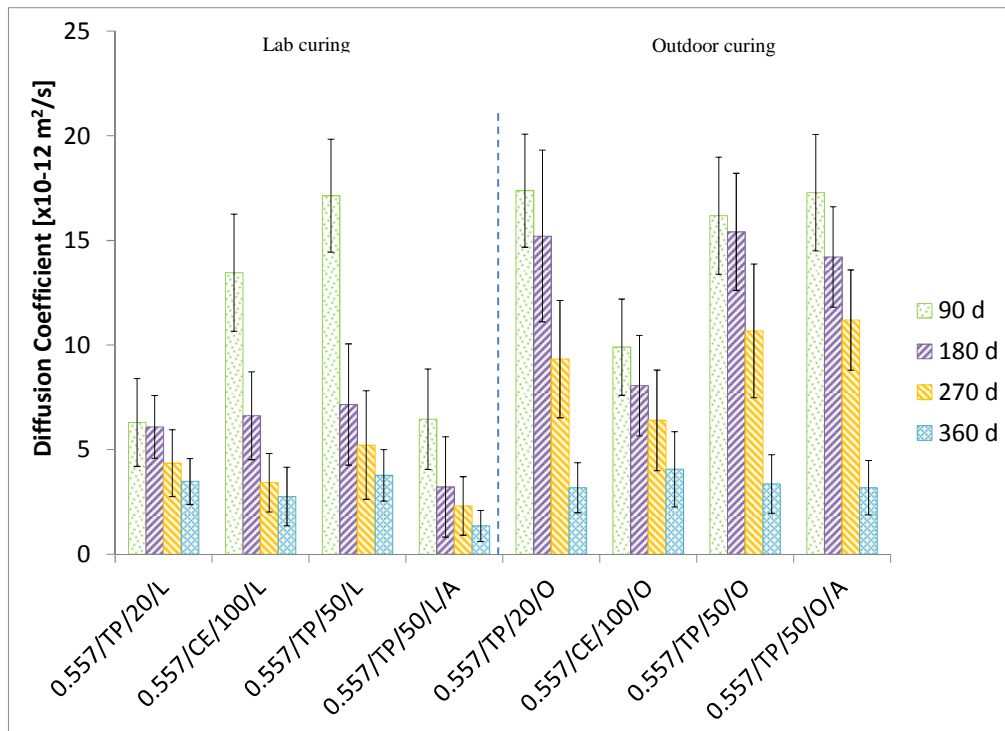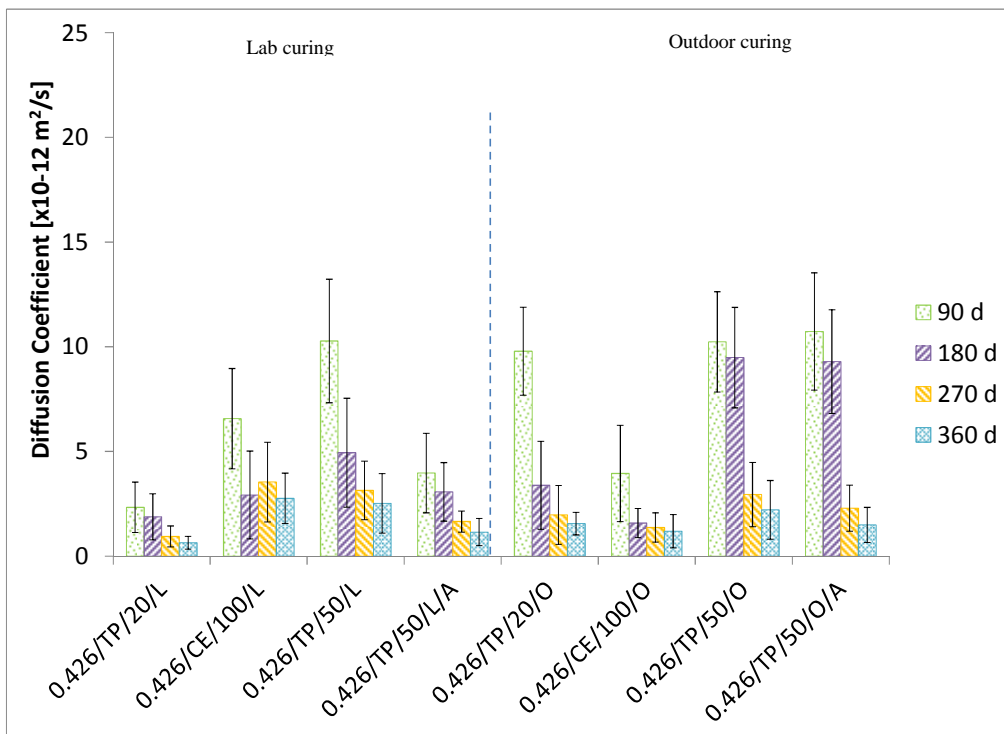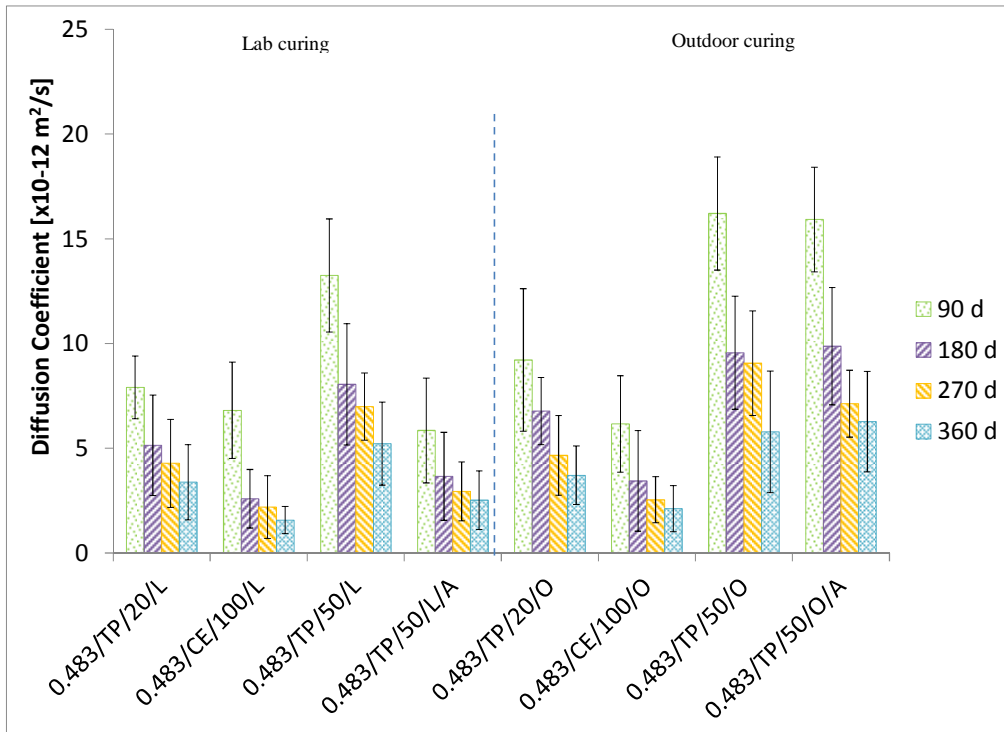
Figure 100 Chloride diffusion coefficients

6.2.5 Water - Soluble Chloride in concrete

For this evaluation, concrete cylinders were left in a solution of 3% sodium chloride. Before submerging the samples in this solution, cylinders were cured for 28 days in a curing room. After this curing process, samples were coated with an impermeable layer on all surfaces except the cross section that was immersed in the solution (Figure 101). Cylinders were always saturated during the preliminary process, before leaving them in the solution. After 28 and 90 days of being immersed, chloride concentration was evaluated at the surface and at 1 cm depth following the ASTM C 1218 – *Standard Test Method for Water – Soluble Chloride in Mortar and Concrete*.

Figure 101 Concrete in chloride concentration

Figure 102 presents the results of chloride concentration at the surface (a) and at 1 cm from the surface (b). At 28 and 90 days, the highest chloride concentrations at both depths are for samples with high fly ash percentages. As seen in diffusion coefficient results, at this age the benefit of using high volume fly ash is not evident; chloride sorption increases for fly ash binders (Ismail, *et al.,* 2013; Bernal, *et al.*, 2012). Although chloride concentrations were not evaluated after 90 days, Burden states that after this age, concrete performance is improved for high volume fly ash concrete (Burden, 2006).

In terms of water to cementitious material ratio, chloride concentration at 90 days for concrete with sodium sulfate and W/CM of 0.426 is similar to the control concrete with 20% FA and W/CM of 0.557. Although it is important to consider the effect of W/CM, in some cases the chloride concentration increment from 28 to 90 days for concrete with sodium sulfate is lower than for control concrete with 20% of fly ash.

This suggest that chloride concentration increases at a lower rate as age increases for concrete with high volume of fly ash and sodium sulfate; this is in agreement with the diffusion coefficient parameter previously evaluated.
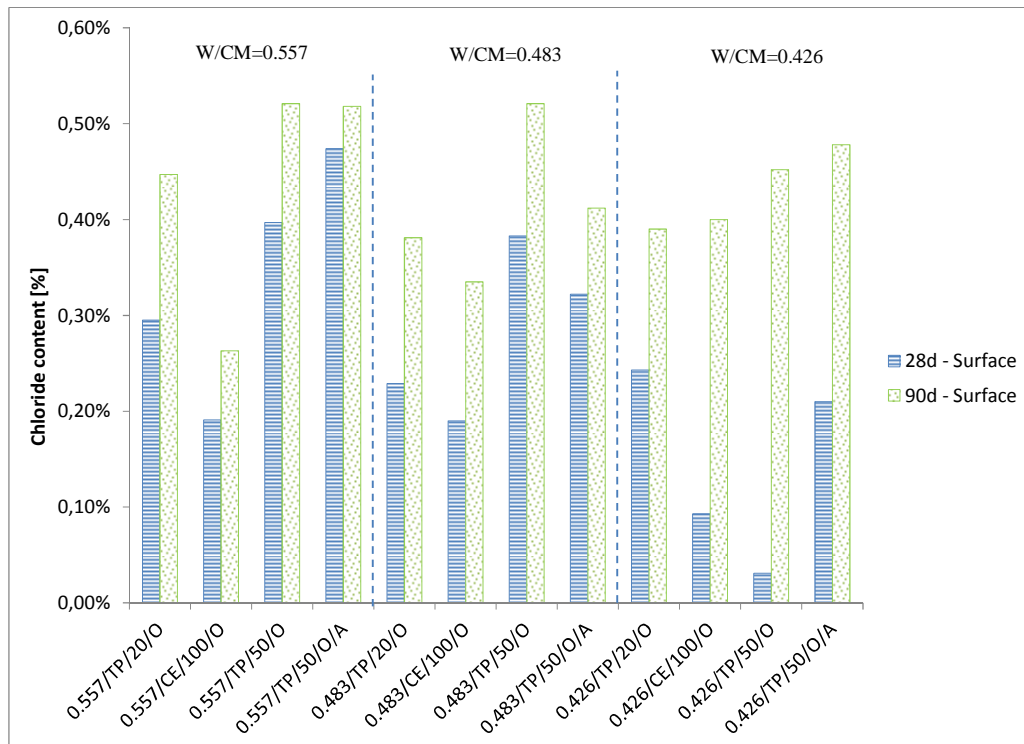
a) at the surface
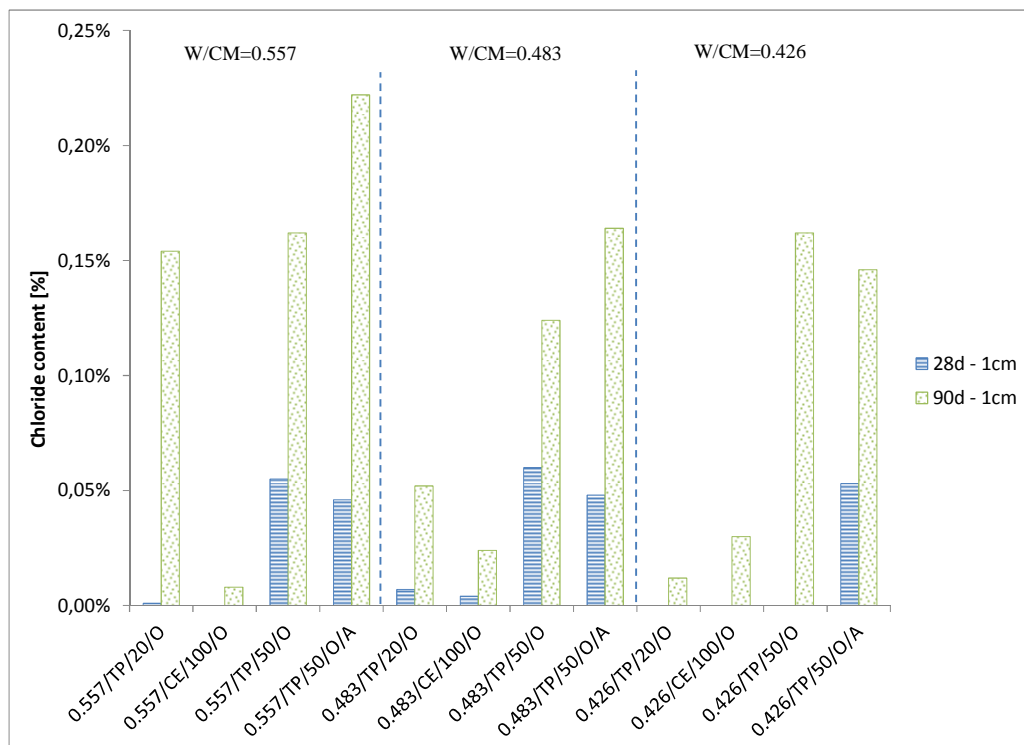
b) at 1 cm

Figure 102 Chloride concentration

6.2.6 Carbonation

Carbonation was evaluated measuring the impact of the environment directly. The average CO_2 concentration environment was 350 ppm with a relative humidity of 63%. During the evaluation period, not only CO_2 was monitored but also temperature, relative humidity, evaporation rate and wind speed, and the results were presented in Figure 74.

Cylinders exposed to ambient carbonation were 5 cm thick and 10 cm in diameter. At the end of the exposure period, the Brazilian test was performed to divide the cylinder in two sections. One of the sections was sprayed with phenolphthalein. Based on this criterion, the carbonated area was the one which retained the same grey concrete colour, while the area with a pH higher than 9 was coloured pink as seen in Figure 103.

Figure 103 Carbonation evaluation

For carbonation analysis, specimens were evaluated under lab and outdoor curing conditions. Samples cured in the curing room are not included in Figure 104 due to the zero carbonation depth presented in the specimens. This analysis therefore includes only specimens cured outdoors which were affected by the environment. Variation of humidity, dry and wet cycles and CO_2 concentration strongly affect carbonation depth (Castellote, *et al*., 2009; Parrot, 1987). There was a clear impact on high volume fly ash samples in terms of carbonation. According to Figure 104, there was not a substantial effect of the water to cementitious material ratio for high volume fly ash mixes.

Although carbonation depth was always lower for mixes with 50% fly ash and activator than those without it at 90 days, there was not a significant difference between them. Carbonation depths for mixes with 20% fly ash did not change with time significantly as 50% fly ash mixes. The average relative humidity in the environment was between 50% to 70%, which is an optimum range for carbonation (Wierig, 1984; Saeki, *et al.*, 1991). The low portlandite content in mixes with 50% fly ash led these specimens to carbonate faster than 100% cement concretes (Younsi, *et al.*, 2011). Concrete permeability reduction for 50% fly ash mixes did not have an effect on carbonation reduction.
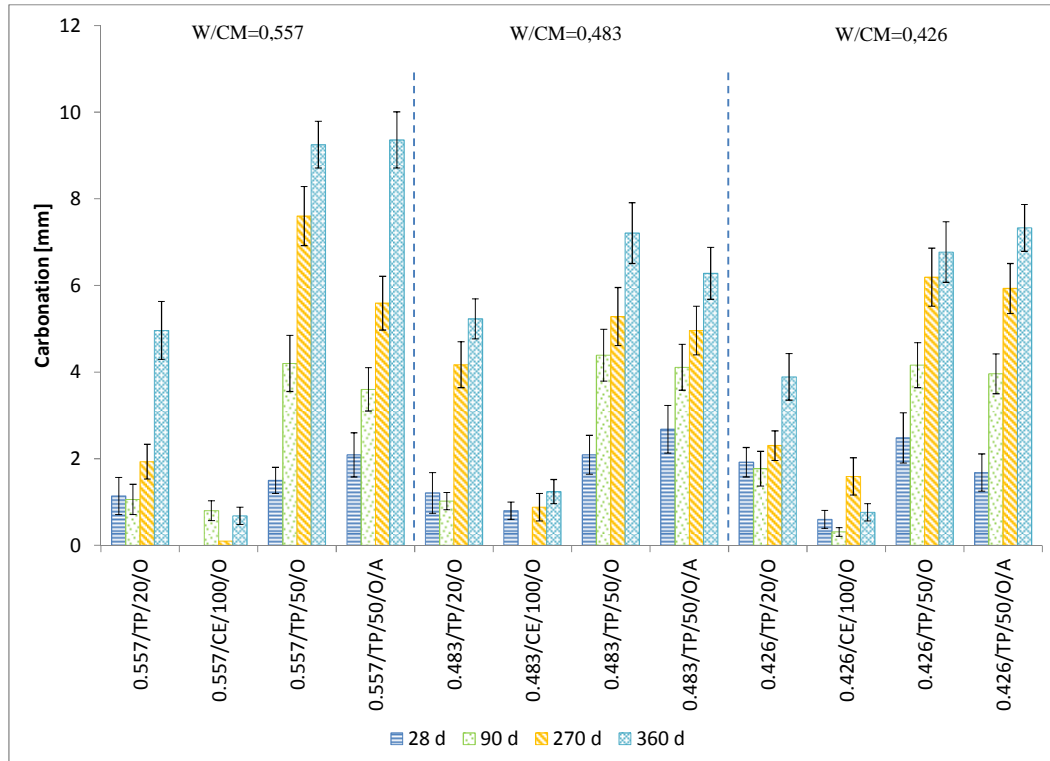
Figure 104 Carbonation depth

6.2.7   Alkali silica reaction

This evaluation is performed for 30 days using mortar bars with different cementitious materials (hydraulic cement, pozzolans, ground granulated blast-furnace slag) and aggregates. In this way, the test allows evaluation of all the possible cementitious materials. Specimens are specially handled before demolding, keeping the temperature in a range from 20°C to 27.5°C and a relative humidity higher than 50%. After demolding, samples are submerged in a sodium hydroxide solution at 80°C as seen in Figure 105. According to this standard, an expansion lower than 0.10% at 16 days is acceptable. A value higher than 0.10% is an indicative of a potential deleterious expansion.

Figure 105 Alkali silica reaction evaluation

Four additional concrete beams were cast to evaluate alkali silica reaction. The volume of each beam was 120 l. Each beam includes two steel pins to evaluate expansions with comparators as seen in Figure 106. These beams were exposed to outdoor conditions presented in Figure 74.
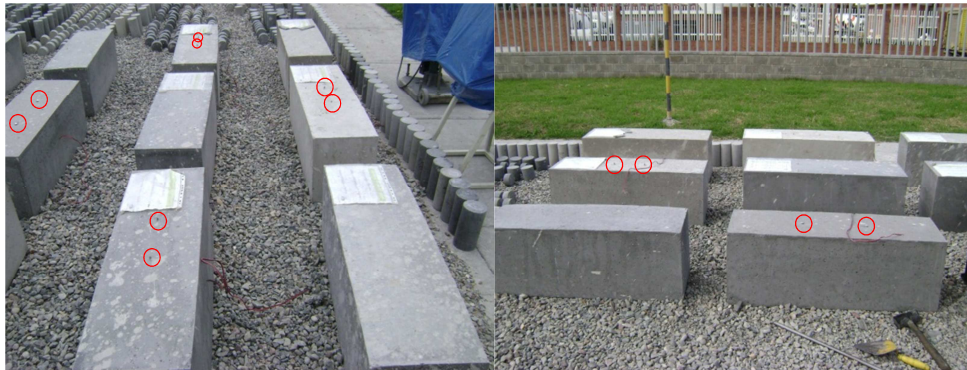
Figure 106 Outdoor concrete beams with reactive aggregate

Based on Figure 107, mixes with 50% fly ash had an expansion lower than 0.1% at 16 days. Even after 30 days, expansion was lower than 0.1% for mixes including 50% fly ash.
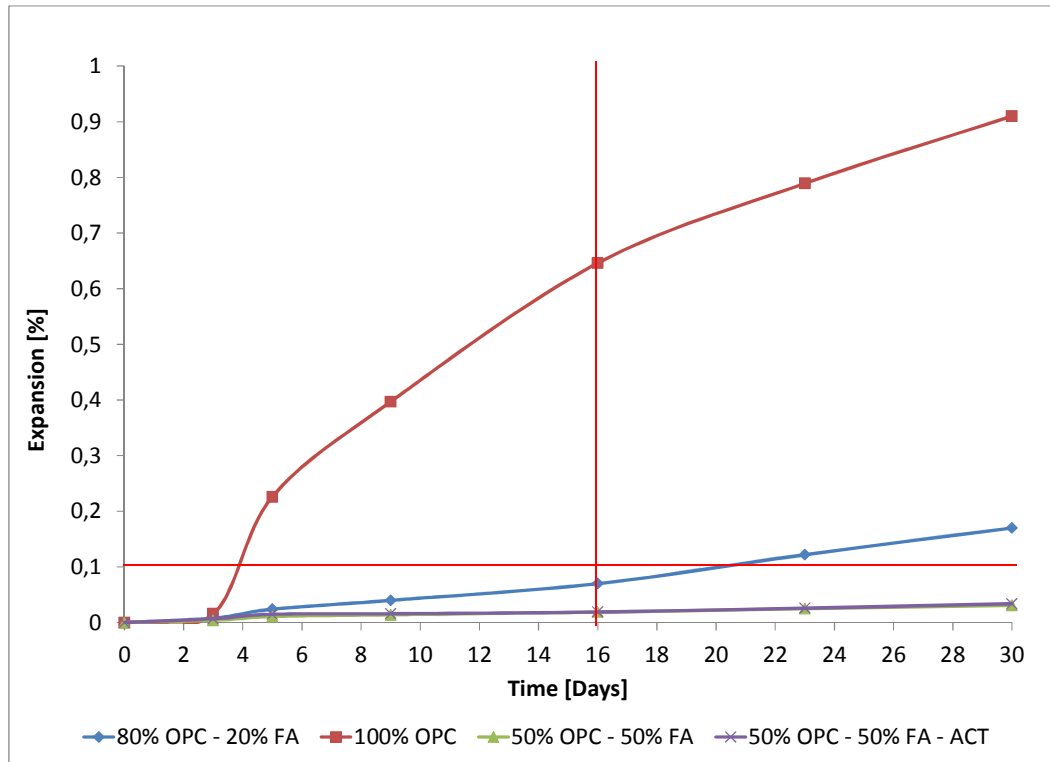
Figure 107 Alkali silica reaction evaluation

Expansion for the elements has been tracked for up to 224 days; the highest expansion is from the element with 0% fly ash; this expansion is around 0.3%. On the other hand samples with high percentages of fly ash have the lowest expansions with around 0.1% during this extended timeframe. Figure 108 shows the different expansions for the elements. Shon evaluated mixes with 58% fly ash and found a reduction in expansion using the accelerated method (Shon, 2002). According to Figure 108, the specimen with activator had a similar behaviour to the one with 50% fly ash only.
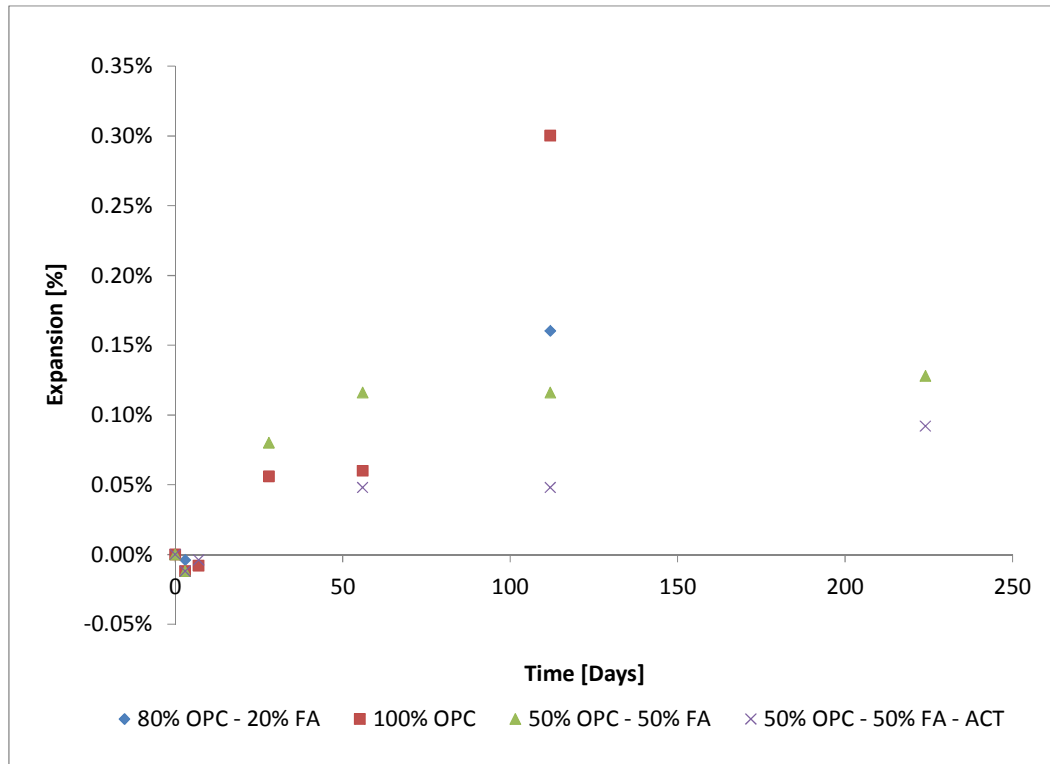
Figure 108 Elements expansion due to alkali silica reaction

6.2.8   Sulfate attack

This test allows the evaluation of the effect of sulfate using mortar bars immersed in this solution and measuring length change with time (Figure 109). It is important to mention that specimens (bars and cubes) are cured before being immersed in sulfate until they reach a compressive strength of 20 ± 1 MPa (cubes). The expansion of mortar bars is measured at 1, 2, 3, 4, 8, 13 and 15 weeks using a length comparator. After this period, length change is evaluated at 4, 6, 9 and 12 months. Different specifications or codes consider maximum expansions depending on environment conditions. For instance, the ACI 318 establishes maximum expansions at 6, 12 and 18 months from 0.05% to 0.1%, depending on the environment to which concrete will be exposed.

Figure 109 Specimens exposed to sulfate attack

Additionally, beams (10 × 10 × 28.5 cm) were left in a solution of sodium sulfate to evaluate their expansion over a period of 18 months. A concentration of 5% of sodium sulfate was used and measurements were made at 1, 2, 3, 4, 8, 13, 15 weeks initially. Figure 110 shows how beams are located in the tank outdoors. This procedure is based on Argos methodology.

Figure 110 Concrete in sulfate solution

According to Figure 111, mixes with 50% fly ash have a tendency of lower expansions than mixes with 80% and 100% cement. This effect is due to the low total C_3A in mixes with 50% of fly ash. As seen before and according to XRD results, mortars with 100% cement have higher AFm contents becoming vulnerable to sulfate attack. There is an evident difference compared to mixes with 50% fly ash. Specimens with activator had the lowest expansion. Chindaprasirt, *et al.* mentioned that a denser and stronger structure reduces expansion, in that case achieved by using a fly ash with an improved fineness (Chindaprasirt, *et al.,* 2004). In this way, probably the denser structure of the activated mix also helped to reduce the effect of the sulfate solution. It

192

is important to keep checking expansion evolution in time due to the fact that at this point it is not conclusive yet. It is important to consider that for geopolymers, the effect depends on the sulfate salt solution (Ismail, *et al.*, 2013). Sodium sulfate is not as aggressive as magnesium sulfate for alkali silicate-activated fly ash / slag geopolymer, as the Ca-rich gel present in the system is decalcified due to the magnesium present, precipitating gypsum and causing volume changes. In the same study, sodium sulfate does not have a significant effect on the paste and the positive effect of the reduction of W/CM is evident.
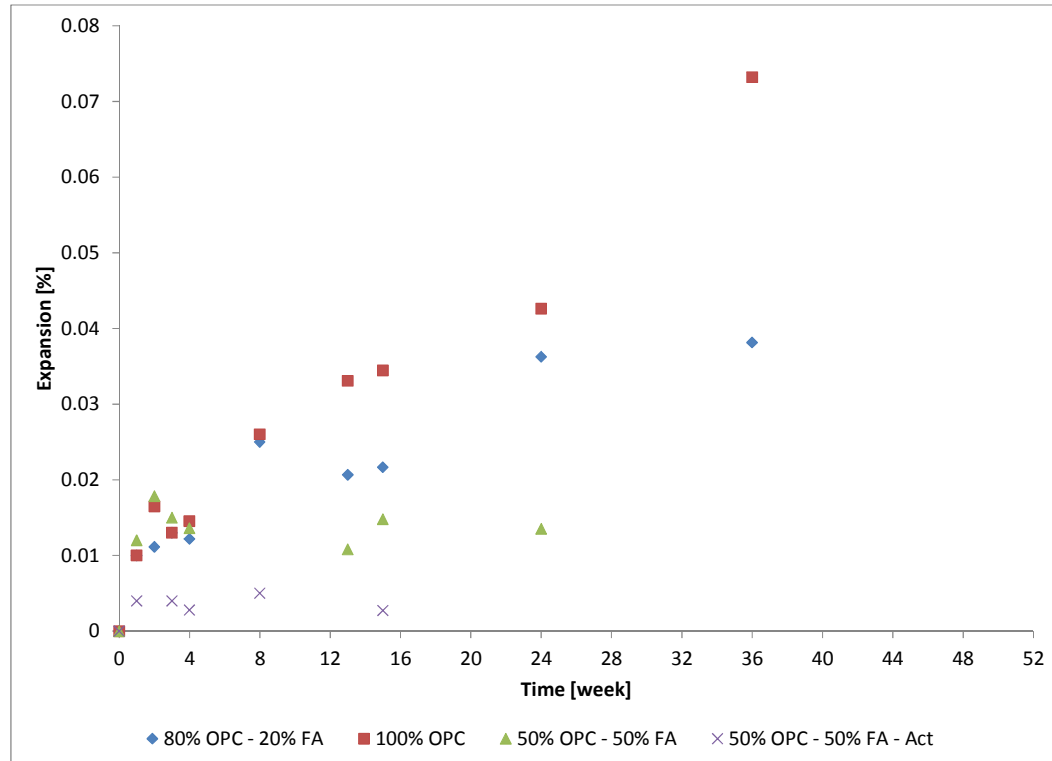
Figure 111 Expansion of specimens exposed to sulfate attack

Although there is some variability in the data presented in Figure 112, there are clear trends of the effect of sulfate attack on concrete beams. Concrete with 100% cement is the most affected, presenting the highest expansion after 15 weeks. The lowest expansion is presented by concrete including sodium sulfate. The lowest expansion is 1/3 of the highest expansion. It is important to mention that expansions present in these samples are due to sulfate attack only; no reactive aggregate was used in these beams.
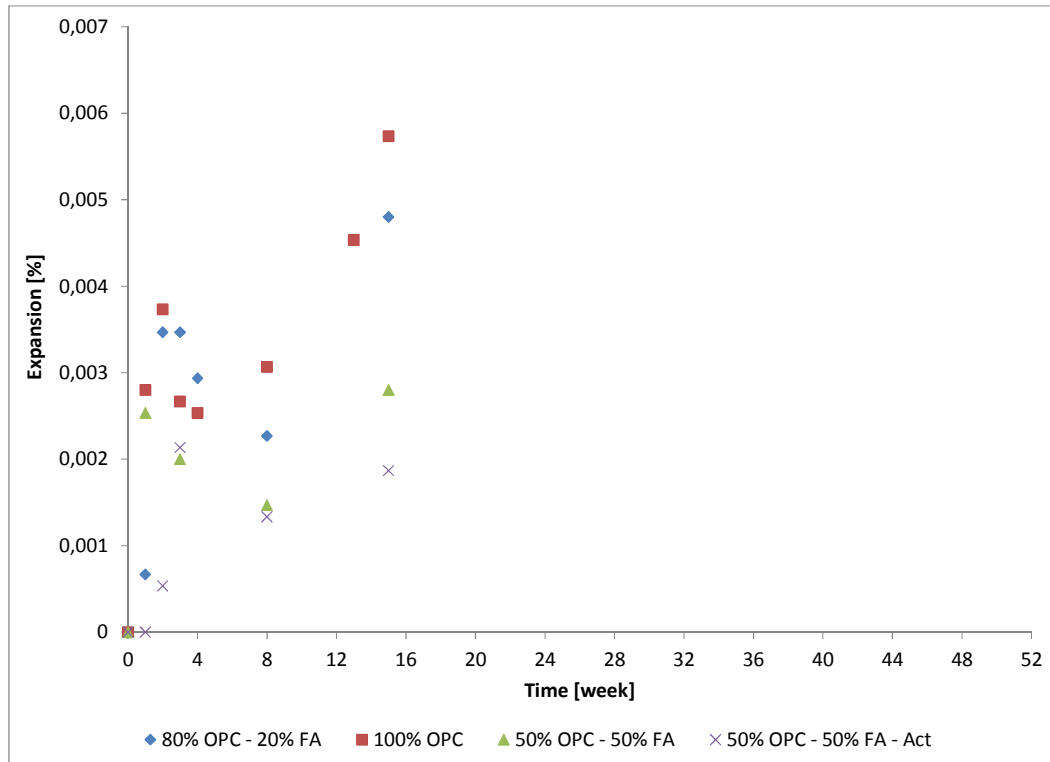
Figure 112 Beams expansion due to sulfate attack

6.3 Effect of mix design inputs and compressive strength on durability parameters

In this part, the effects of design inputs, curing type and compressive strength will be evaluated. This analysis also includes results of mixes with a W/CM of 0.675, and 0% FA and 20% FA. The objective of including results from these two mixes was to have one additional W/CM point for the 0% FA and 20% FA mixes. The mix designs and results for these two mixes are included in Appendix 3.

Although it is a repetitive analysis using Minitab and Excel software, this is needed to understand the factors influencing each durability evaluation. The following Minitab tools are used to perform the analysis.

Multi-Vari Chart: This chart considers a maximum of 4 factors. It helps to analyse the variance data with a visual evaluation. Each point of each factor is the mean for each level of analysis.

Main Effects Plot: It helps to compare the magnitudes of main effects. It plots the mean of the response variable at different levels of each factor. A line is drawn from point to point. As the slope of this line increases, the effect increases. The previous is a

194

visual analysis and the slope is an indicative of how the parameter has an effect on a specific item.

Interaction Plot: This plot helps to visualize a possible interaction between different factors. Nine factors can be included in this matrix. It includes the means for each level of a factor with the level of a second factor held constant. Parallel lines indicate no interaction. The greater the departure of the lines from the parallel state, the higher the degree of interaction.

As the compressive strength correlates with most of the durability parameters, the effect of the mix design inputs and curing type on compressive strength was evaluated first.

6.3.1   Parameters influencing compressive strength

The parameters considered in the Multi-Vari Chart are fly ash percentage, W/CM, curing and age. Each point is the mean in the specific level of analysis. As is seen in Figure 113, the compressive strength is strongly affected by the water to cementitious material ratio and fly ash percentage. When samples are cured outdoors, the effect of the water to cementitious material and FA% cannot be perceived compared to samples cured in the laboratory.
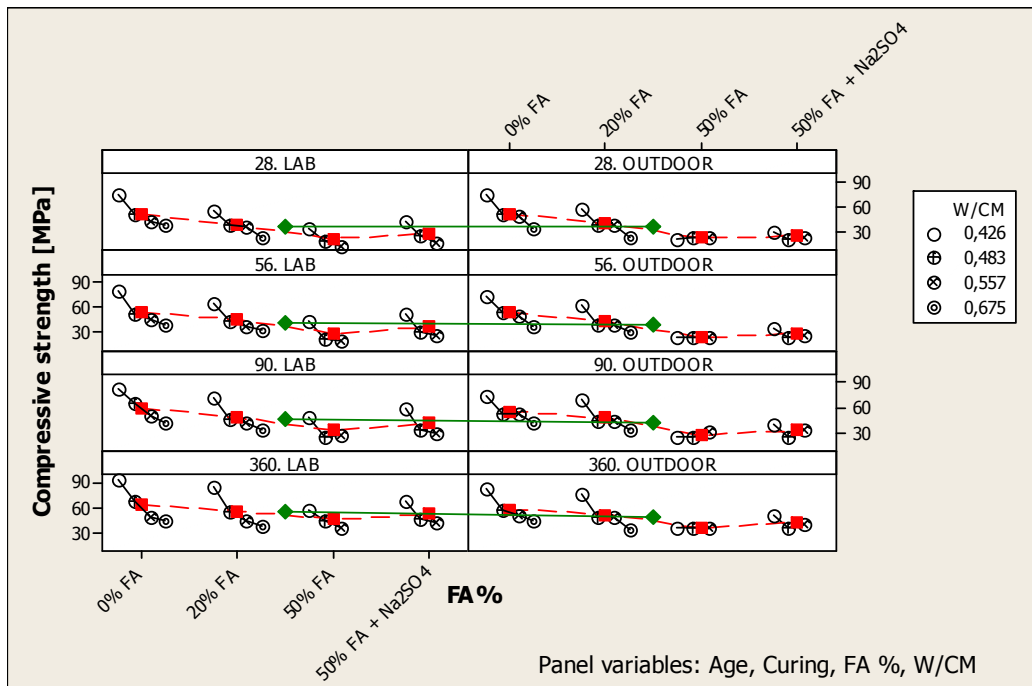
Figure 113 Multi-Vari Chart for Compressive strength by W/CM - FA % - Curing – Age

The plot for the main effects for compressive strength presented in Figure 114 allows visualization of how the variation of the water to cementitious materials and FA % affects the compressive strength. The fact of including the activator increases the compressive strength significantly.
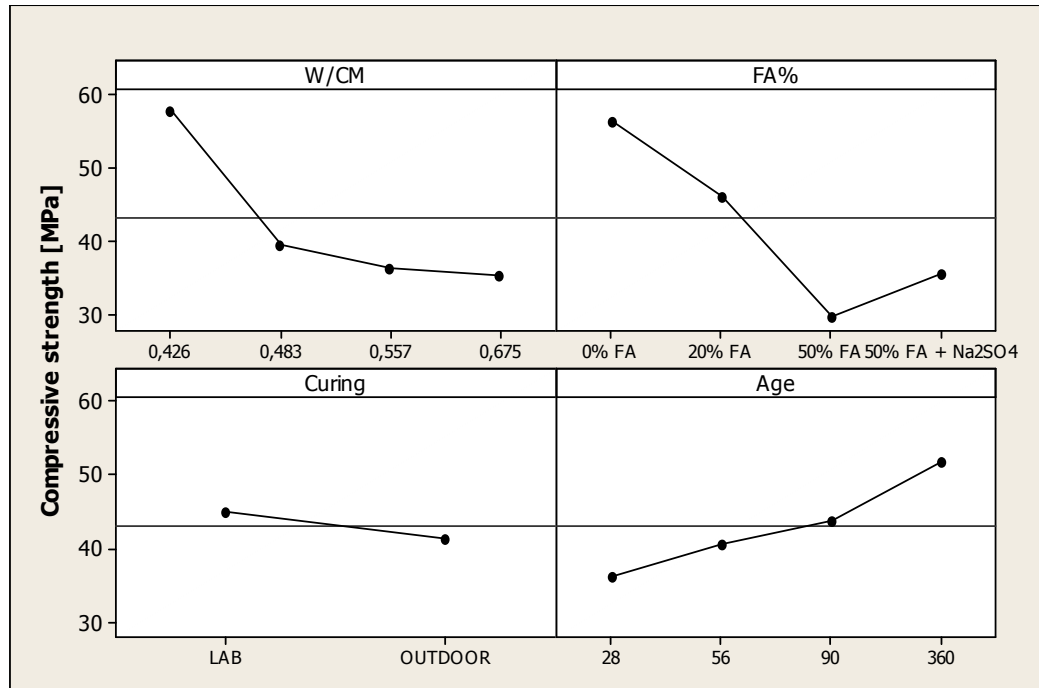
Figure 114 Main Effects Plot for Compressive strength

The interaction plot presents the influence of different parameters simultaneously; for instance, the interaction between W/CM and different fly ash content has a higher influence compared to the previous variables interacting with the curing conditions. This is presented in Figure 115. The change in the slope when sodium sulfate is included allows identification of the positive influence of this component in the matrix. The curing effect becomes more relevant with age; as the age is increased the gap between curing in the lab and outdoors increases. In the same way, concretes with 50% FA get closer to control samples from 90 to 360 days.
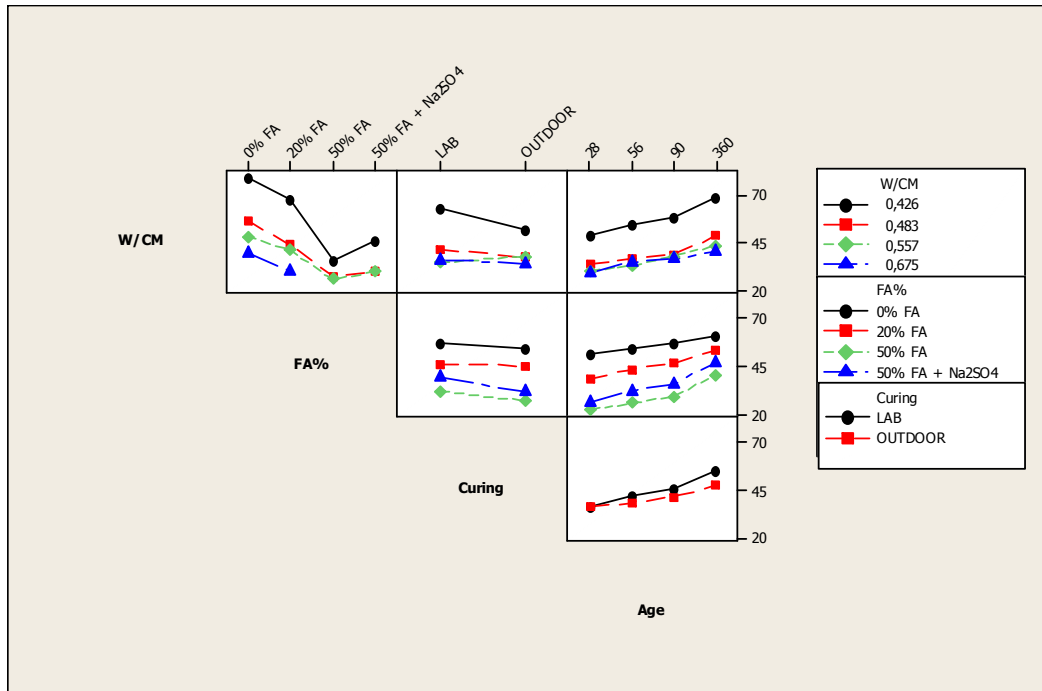
Figure 115 Interaction Plot for Compressive strength

6.3.2   Parameters influencing water permeability

Figure 116 presents the relationship between water permeability and compressive strength. Although there is a trend, the variability is seen because it compiles different water to cementitious material ratios, fly ash percentages and curing types. In this way, the fact of using compressive strength as one of the main parameters to correlate with water permeability means that it is important to consider first the influence of all the input parameters.
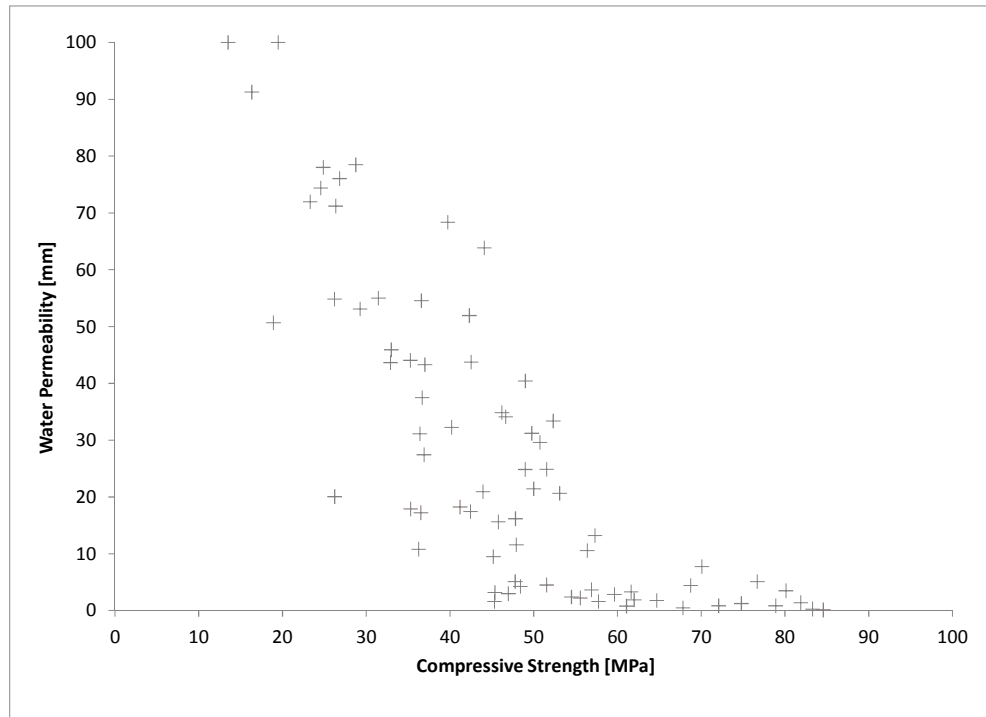
Figure 116 Water permeability vs Compressive strength

As seen in Figure 117, all the input parameters take a significant role in terms of influencing the water permeability depth. It is important to give relevance to the combined effects. For instance, without considering compressive strength and by combining the effects of W/CM, fly ash percentage and curing type, the final effect becomes relevant.
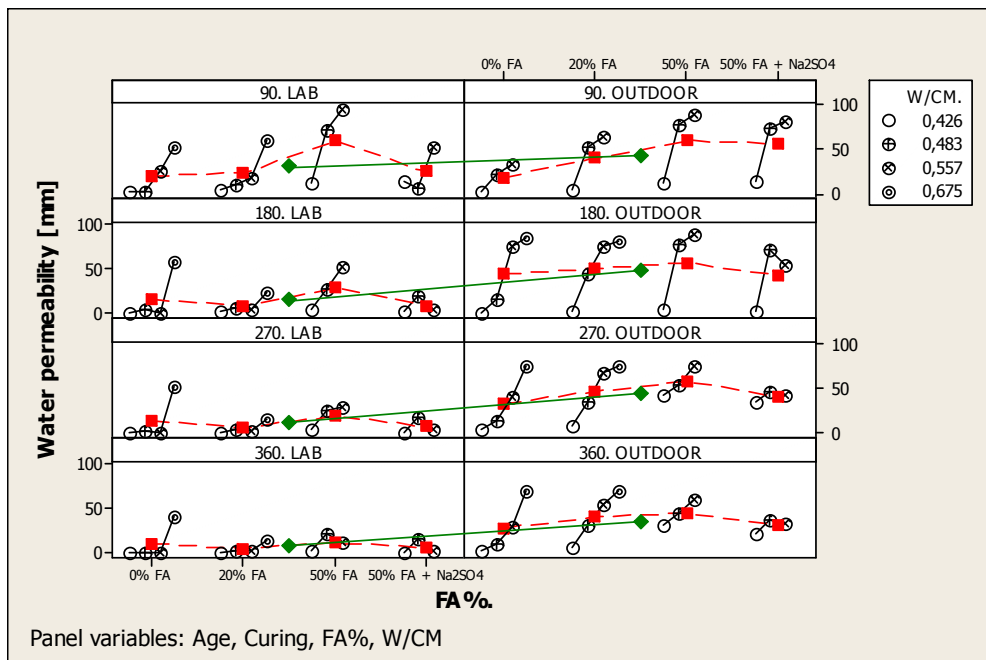
Figure 117 Multi-Vari Chart for Water permeability by Age-Curing-FA%-W/CM

The main effects plot for the different inputs uses mean values as seen in Figure 118. In this way, it allows examination of how all the variables influence water permeability. For instance, mixes with sodium sulfate reduce the water permeability at levels similar to control mixes with 20% FA. Curing and W/CM strongly affects water permeability.
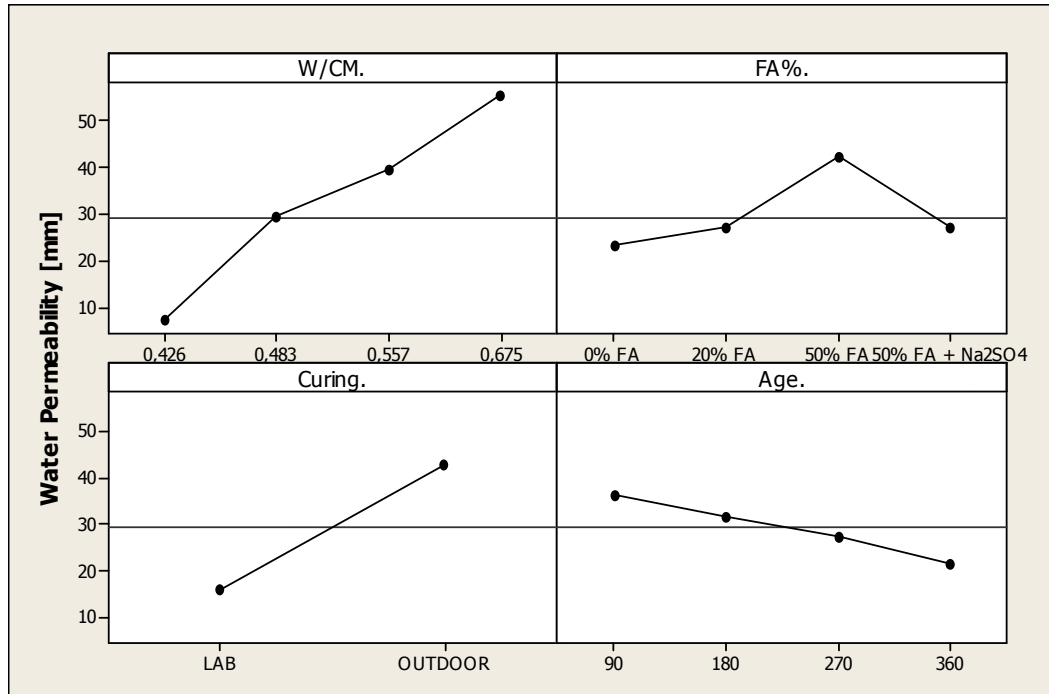
Figure 118 Main Effects Plot for Water permeability

As mentioned above, there are different parameters affecting compressive strength and water permeability causing the variability. In this way, Figure 119 allows understanding of which combinations have the major effects on water permeability. For instance, the combination of the W/CM and fly ash percentage variables shows how mixes with sodium sulfate behave similarly to control samples with 20% fly ash. From this figure, it is also evident how mixes with fly ash need a controlled curing process, as it affects water permeability significantly.
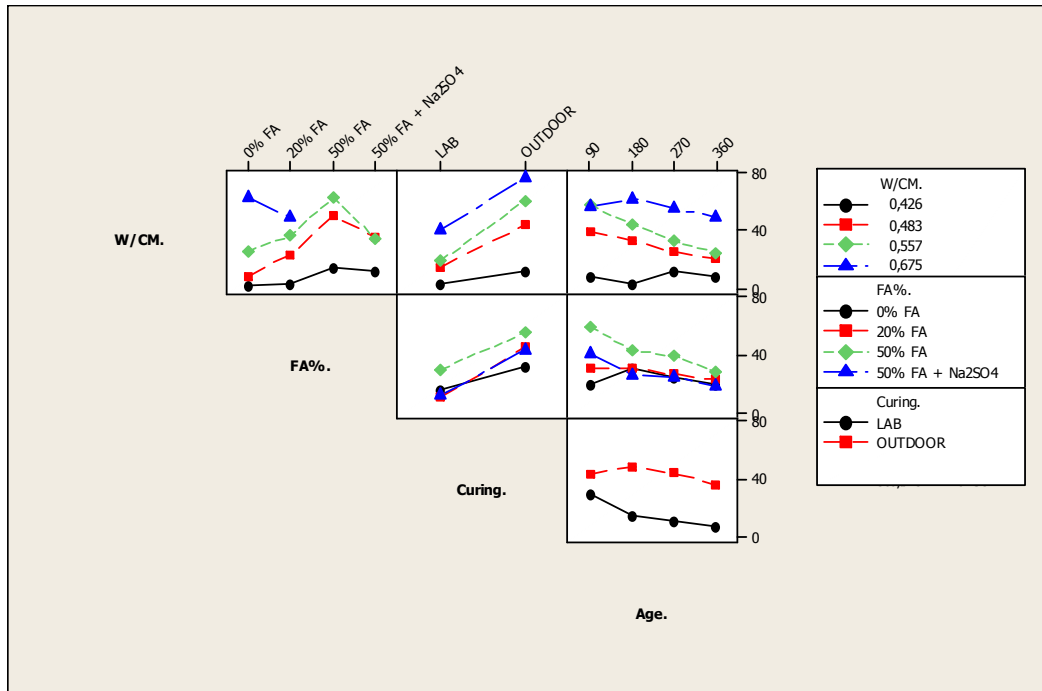
Figure 119 Interaction Plot for Water permeability

Figure 120 is obtained based on the previous analysis. According to this figure, water permeability decreases with 50% fly ash when an activator is used. In the case of the same compressive strength, water permeability is reduced as the levels of fly ash are increased. Although the compressive strength is higher, the micro structure of the samples with fly ash is less permeable due to the reduction of the $Ca(OH)_2$ content. For instance, considering lab curing, a 20 mm water permeability depth can be accomplished with a strength of around 50 MPa for a mix with 100% cement, or with 30 MPa for a mix with 50% FA and sodium sulfate.
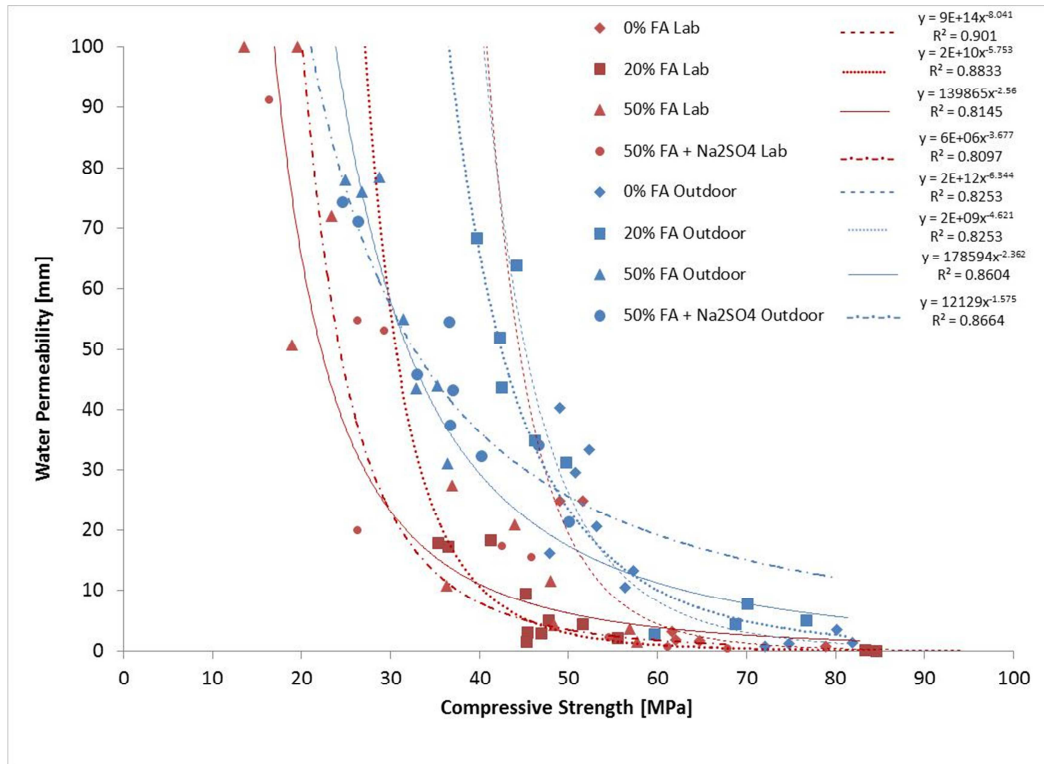
Figure 120 Water permeability vs compressive strength for 0%, 20% and 50% FA with sodium sulfate

6.3.3 Parameters influencing initial sorptivity

When the compressive strength is directly correlated to initial sorptivity, the trend is of decreasing initial sorptivity as the compressive strength is increased. Although there is a clear correlation between compressive strength and initial sorptivity (Figure 121), it is important to differentiate the influence of the W/CM, fly ash percentage and curing conditions. The multi variables chart, main effects plot, and interaction plot allow examination of the influencing parameters on initial sorptivity.
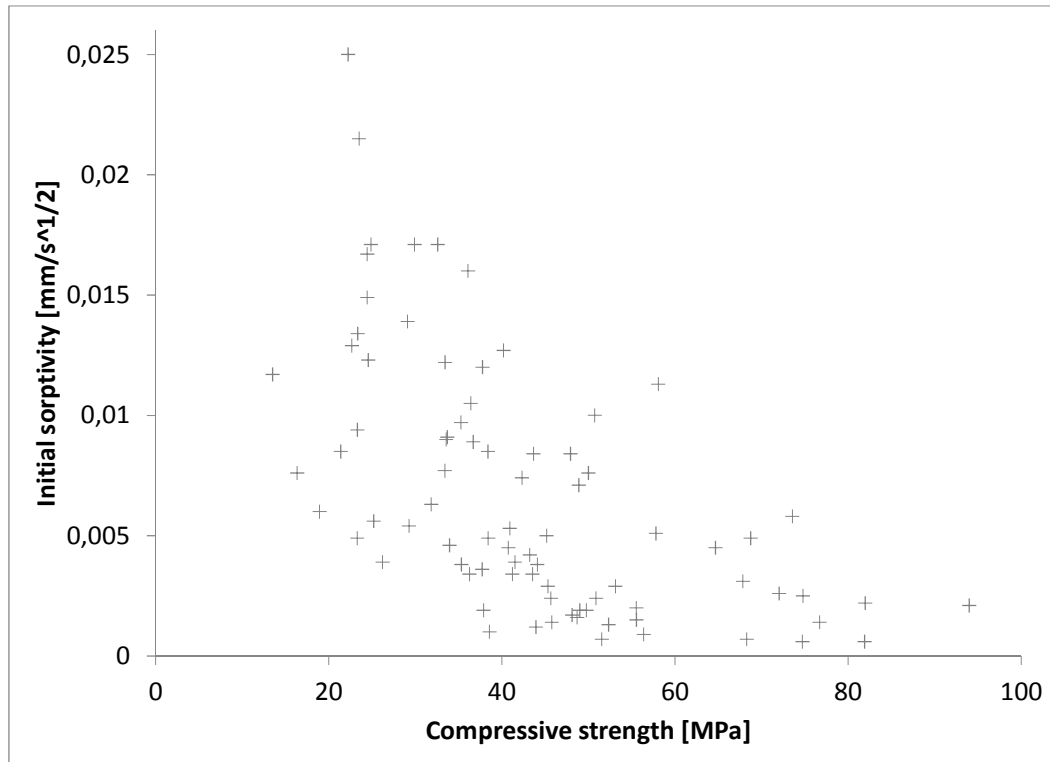
Figure 121 Initial sorptivity vs compressive strength

In terms of initial sorptivity and according to Figure 122, the curing type, FA% and age affect it. Mixes with sodium sulfate have reduced initial sorptivity close to the levels of the control sample with 20% fly ash. The pozzolanic effect is evident after 270 days, where samples with fly ash match control mixes under laboratory conditions. As can be seen in Figure 122, this is not the case for samples cured outdoors, where sorptivities are higher for 50% fly ash concretes at 360 days; samples with sodium sulfate are closer to control samples.
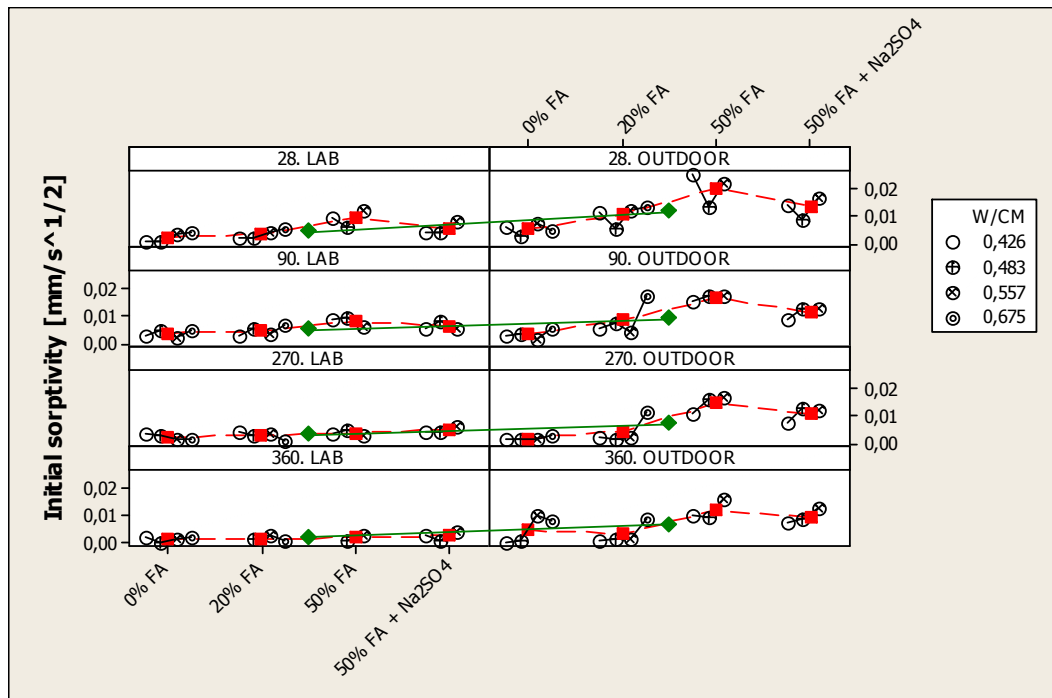
Figure 122 Multi-Vari Chart for Initial sorptivity by Age-Curing-FA%-W/CM

In the main effects plot presented in Figure 123, the curing and fly ash content are the parameters affecting the initial sorptivity. There is not a relevant effect of the W/CM on the initial sorptivity. Although age reduces the initial sorptivity, fly ash percentage seems as a key parameter to control.
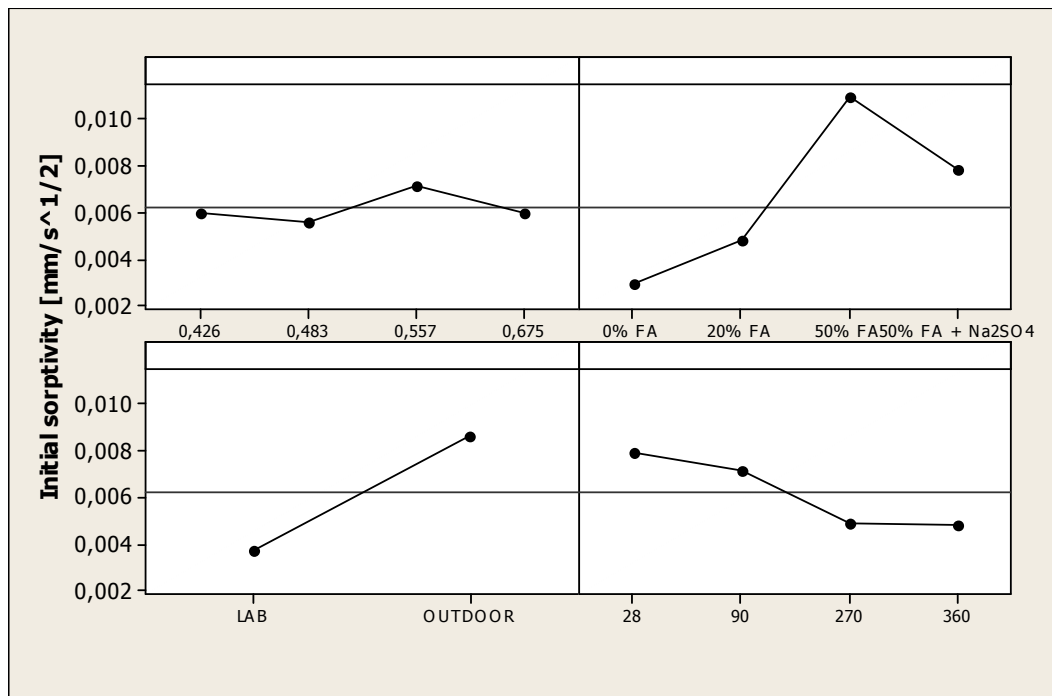
Figure 123 Main Effects Plot for Initial sorptivity

Figure 124 presents how, by considering simultaneously FA% and curing conditions, the major changes on initial sorptivity are obtained. When FA replacement level and curing type are evaluated simultaneously in the interaction plot, the latter has a higher relevance as the level of fly ash replacement is increased. Samples with high percentages of fly ash have a higher reduction with time compared to control samples with 100% cement.
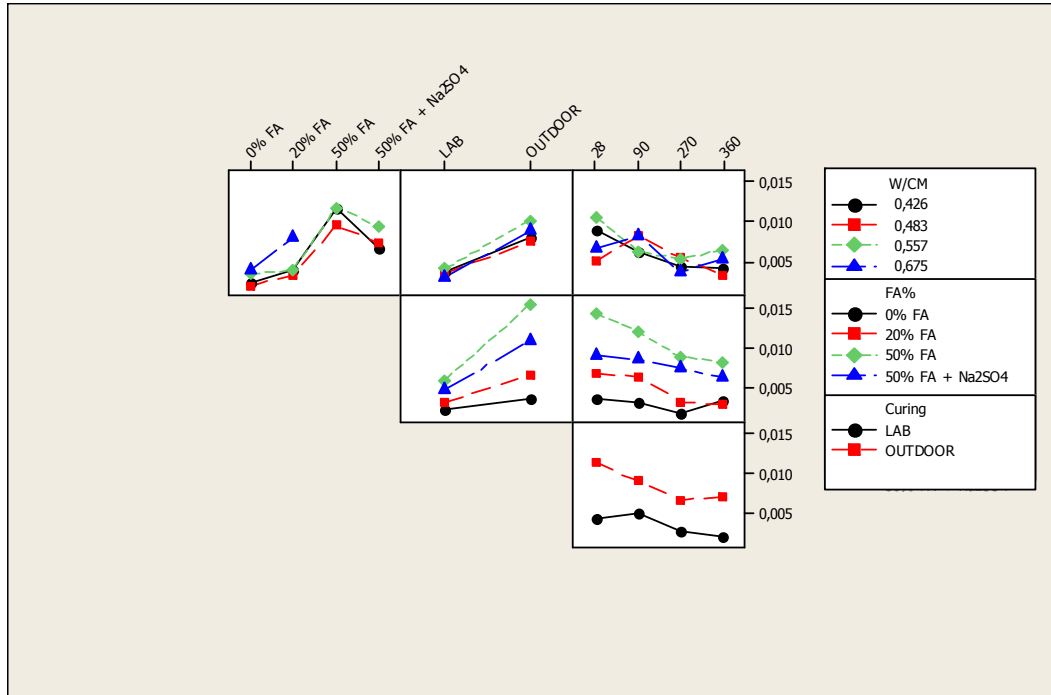
Figure 124 Interaction Plot for Initial sorptivity

Figure 125 considers previous results and the most influential parameters, such as compressive strength, fly ash replacement levels and curing conditions. This figure shows how samples cured outdoors have higher sorptivity levels. In the same way, curves of fly ash mixes have a higher slope, meaning an important correlation dependence of compressive strength on this parameter. For instance, a sorptivity close to 0.005 mm/s$^{1/2}$ could be obtained with a compressive strength of 23 MPa for a 20% FA mix or 40 MPa for a 50% FA with sodium sulfate mix. Beyond 60 MPa, the sorptivity values for all the replacement levels are close.
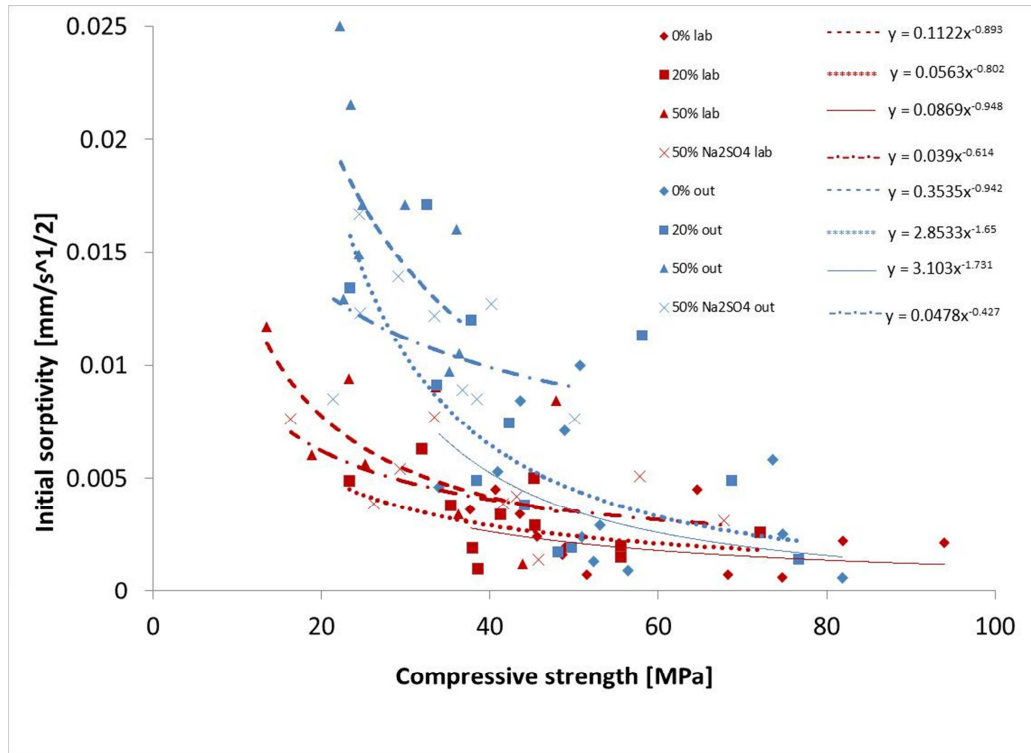
Figure 125 Initial sorptivity vs compressive strength for 0%, 20% and 50% FA with sodium sulfate

6.3.4 Parameters influencing chloride penetration

As seen in Figure 126, when compressive strength and chloride penetration (as measured by charge passed in the ASTM C1202 test) are plotted, there is a trend but with a high variability as expected according to ASTM C1202, where the results difference might be up to 42% for the same mix. As presented with the previous durability parameters, all the different input variables have an impact on chloride penetration.
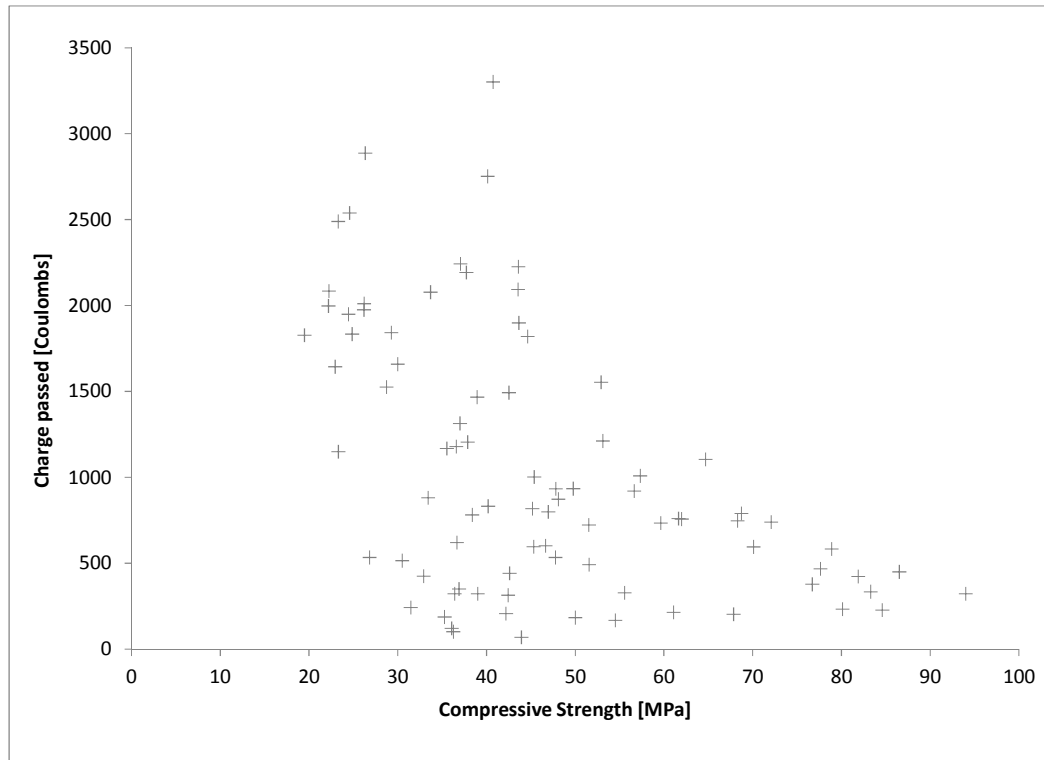
Figure 126 Chloride penetration vs compressive strength

In the multi chart plot presented in Figure 127, the effect of the curing is not evident. Effect of water to cementitious material ratio is seen at early ages only; at later ages, the values of chloride penetration are similar for all the different W/CM values. Although this behaviour is similar for different fly ash percentages, chloride penetration decreases with the inclusion of sodium sulfate when it is compared to the control sample with 50% FA.
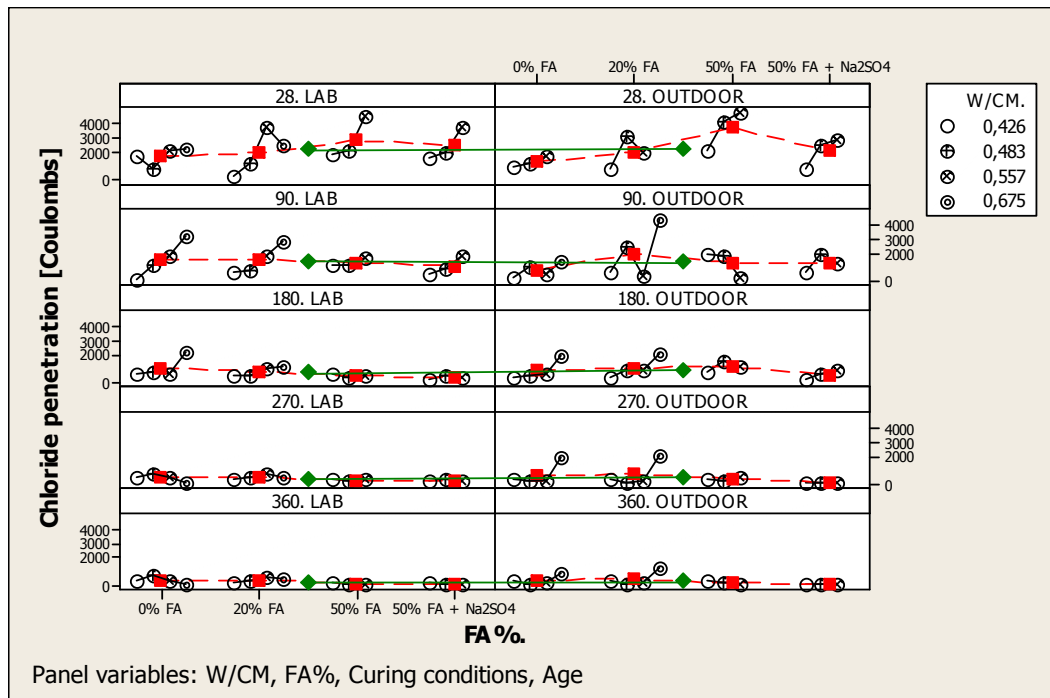
Figure 127 Multi-Vari Chart for Chloride Penetration by Age-Curing-FA%-W/CM

Figure 128 shows how the parameter affecting chloride penetration least is the curing according to the main effects plot and strongly affected by the other parameters. According to this plot, the influence of sodium sulfate is positive as the lowest value is obtained from these mixes. From the main effects plot it is possible to conclude that by decreasing the water to cementitious material and using the mix with 50% fly ash and sodium sulfate, chloride penetration could be reduced.
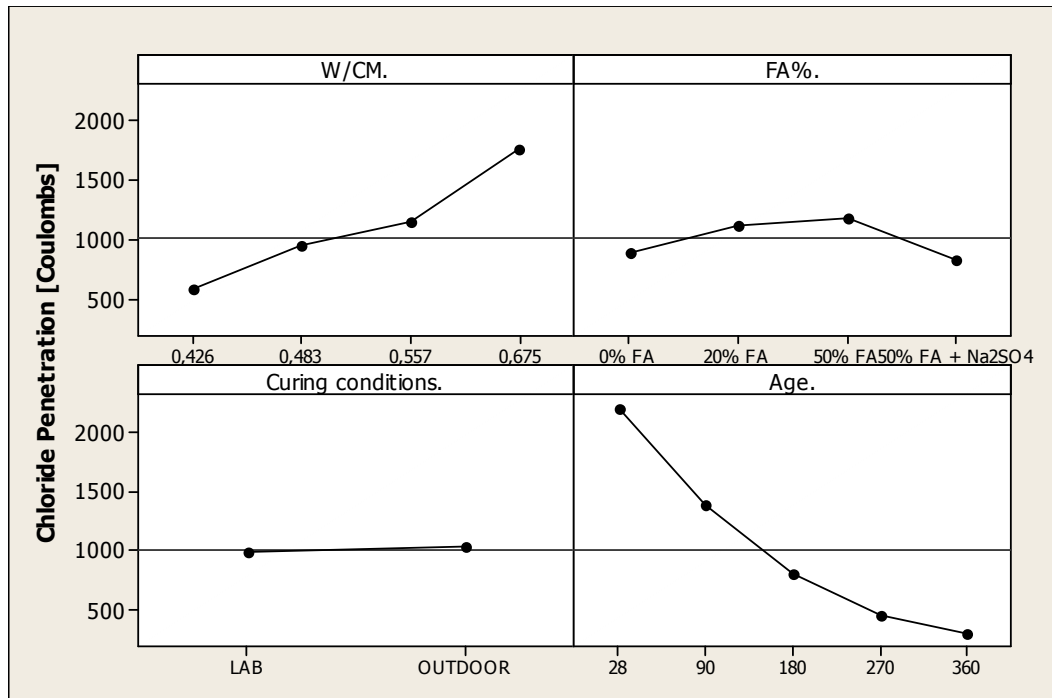
Figure 128 Main Effects Plot for Chloride Penetration

The interaction plot presented in Figure 129 shows how the increments in W/CM and fly ash increase chloride penetration, but when sodium sulfate is added this parameter is reduced. There is not a clear trend separating mixes cured in the laboratory from those left outdoors.
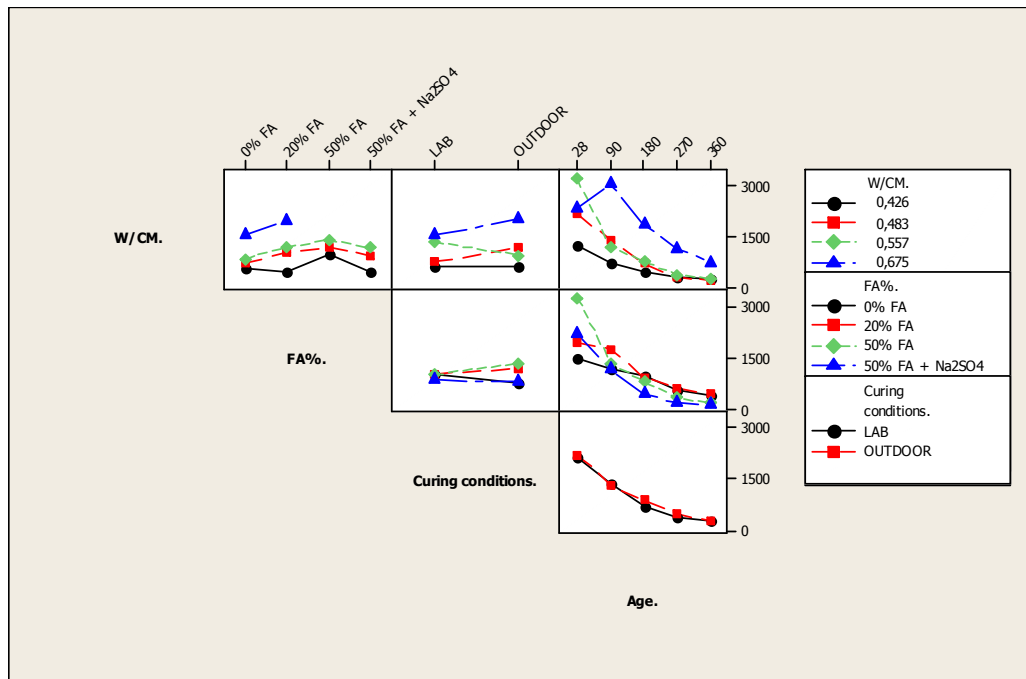
Figure 129 Interaction Plot for Chloride Penetration

208

Based on the previous results, the influencing parameters are defined and presented in Figure 130. In this way, the proposed correlations depend on compressive strength and fly ash replacement. The same value of chloride penetration can be obtained for a different compressive strength, depending on fly ash replacement and the fact of including sodium sulfate in the matrix. Mixes with high fly ash replacements and low compressive strengths are in the "Very Low" chloride penetration range, according to ASTM C 1202. The inclusion of sodium sulfate positively affects chloride penetration, with low values measured for moderate compressive strengths. For instance, around 500 Coulombs is accomplished with 80 MPa for a 100% cement mix while the same chloride penetration can be accomplished with almost half of the compressive strength by a 50% fly ash mix and sodium sulfate. The previous comparison is for samples cured in the laboratory.
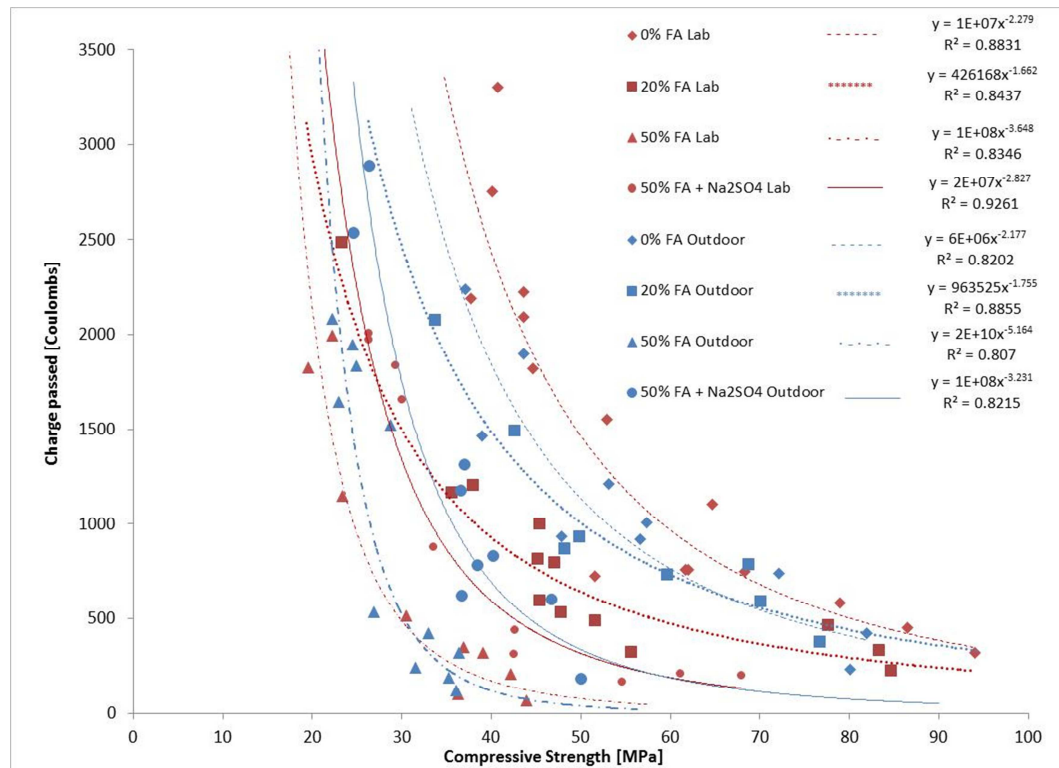
Figure 130 Chloride Penetration vs Compressive Strength for 0%, 20% and 50% FA with sodium sulfate

6.3.5 Parameters influencing diffusion coefficient

According to Figure 131, as the compressive strength increases the diffusion coefficient is reduced. This behaviour is clear and for some compressive strength

ranges, the difference in diffusion coefficient is small, compared to the other durability parameters.
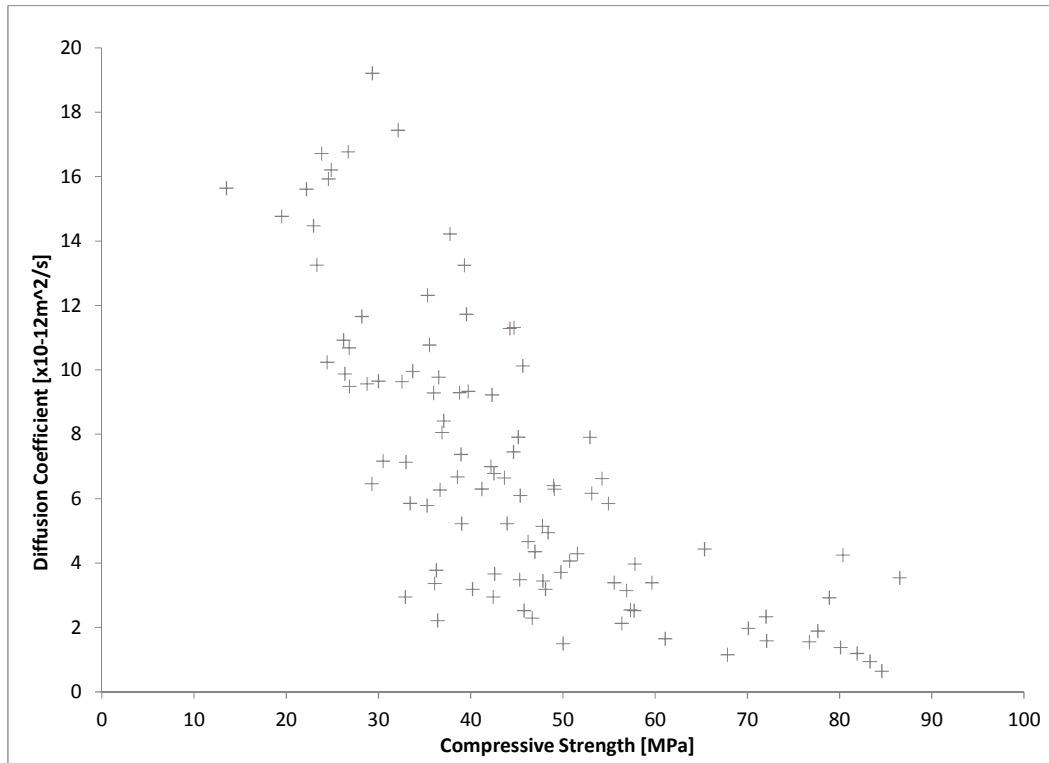
Figure 131 Diffusion coefficient vs Compressive strength

It is important to evaluate the correlation between charge passed and diffusion coefficient. As seen in Figure 132 as charge passed increases, the diffusion coefficient increases, showing that there is (as expected) a correlation between these measurements. As presented for compressive strength, the variability in the data needs to be analysed. For chloride penetration, ASTM C1202 mentions a high variability between samples from the same mix, affecting the correlation with the diffusion coefficient.
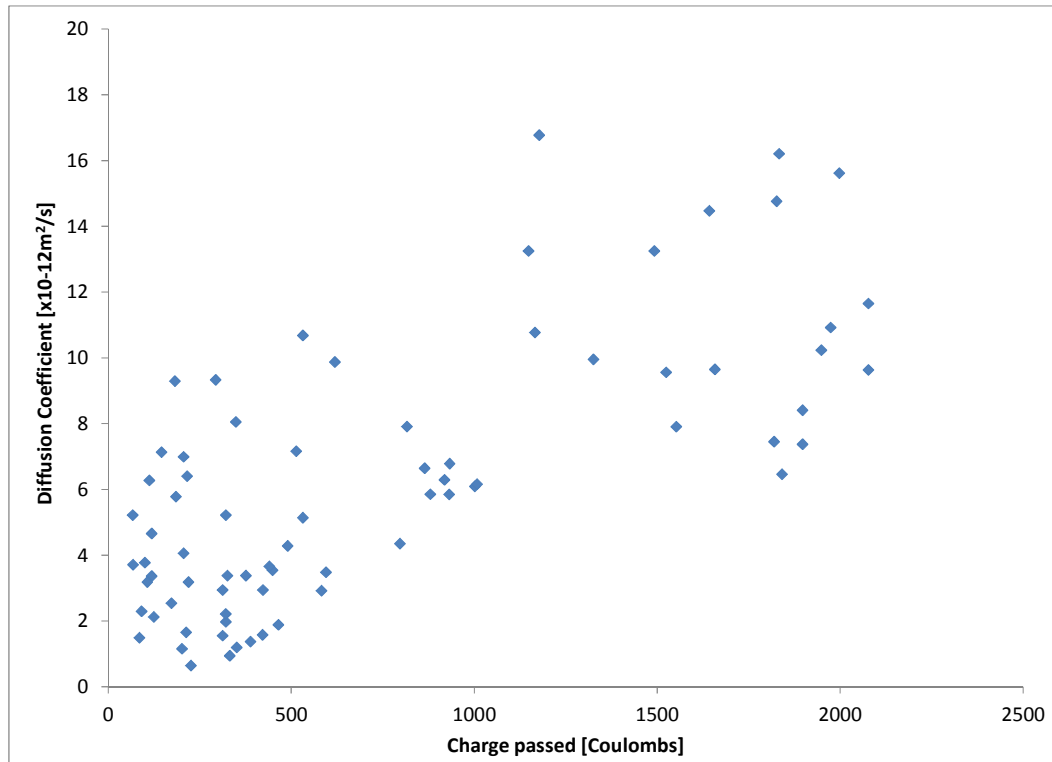
Figure 132 Diffusion coefficient vs chloride penetration

Before finding the relationship between these parameters, the effect of each variable on diffusion coefficient is evaluated as seen in Figure 133. At 90 days, the effect of sodium sulfate mix is positive for laboratory curing and the effect is the opposite when cured outdoors. The reduction of the W/CM reduces the diffusion coefficient for most of the samples. The curing has a significant impact at early ages. After a year, the diffusion coefficient is low for the activated mixes for laboratory and outdoor curing.
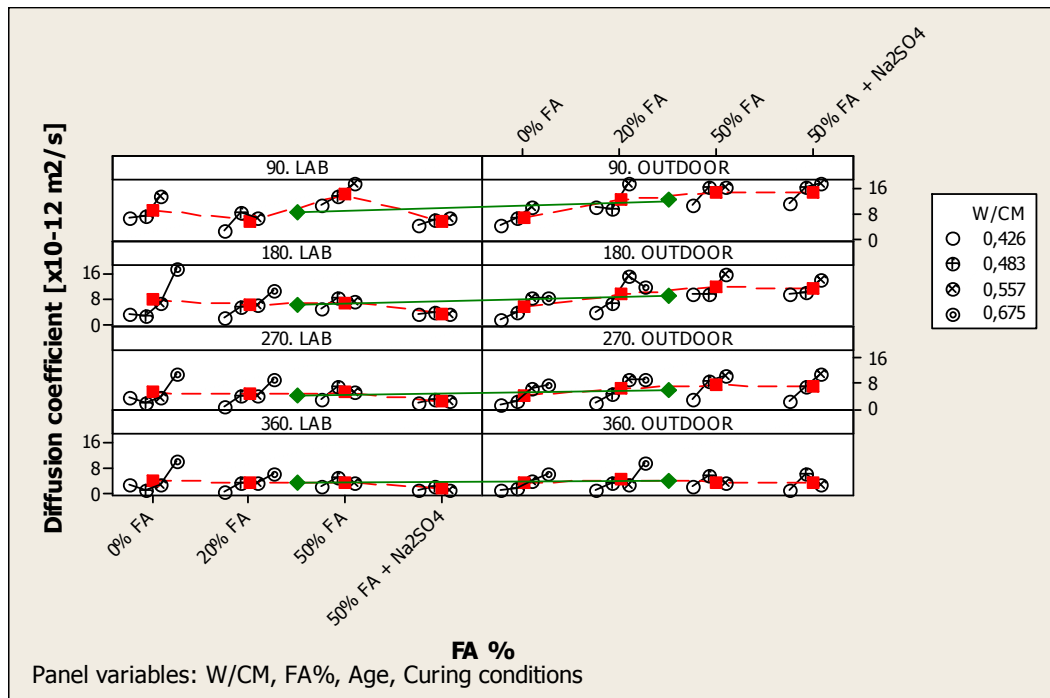
Figure 133 Multi-Vari Chart for Diffusion Coefficient by Age-Curing-FA%-W/CM

As mentioned, the main effects plot does not include the interaction of additional parameters; instead, each parameter is evaluated separately. Figure 134 shows how W/CM, fly ash percentage, curing and age have a significant effect on the diffusion coefficient.
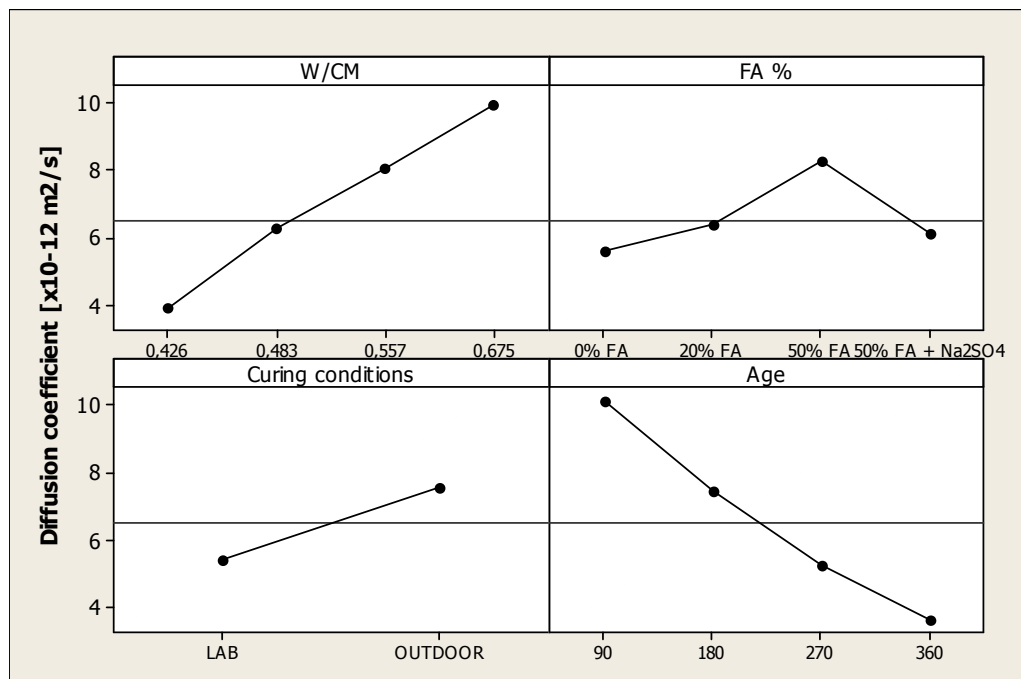
Figure 134 Main Effects Plot for Diffusion coefficient

According to the interaction plot presented in Figure 135, by considering the W/CM and FA% simultaneously, the effect of mixes with sodium sulfate is clear, reaching the diffusion coefficient levels of samples with 20% FA. It is important to consider that the positive effect in samples with high volume fly ash can be seen at later ages. For instance, mixes with 50% fly ash have a greater decreasing slope from 90 to 360 days than mixes with 0% FA and 20% FA.
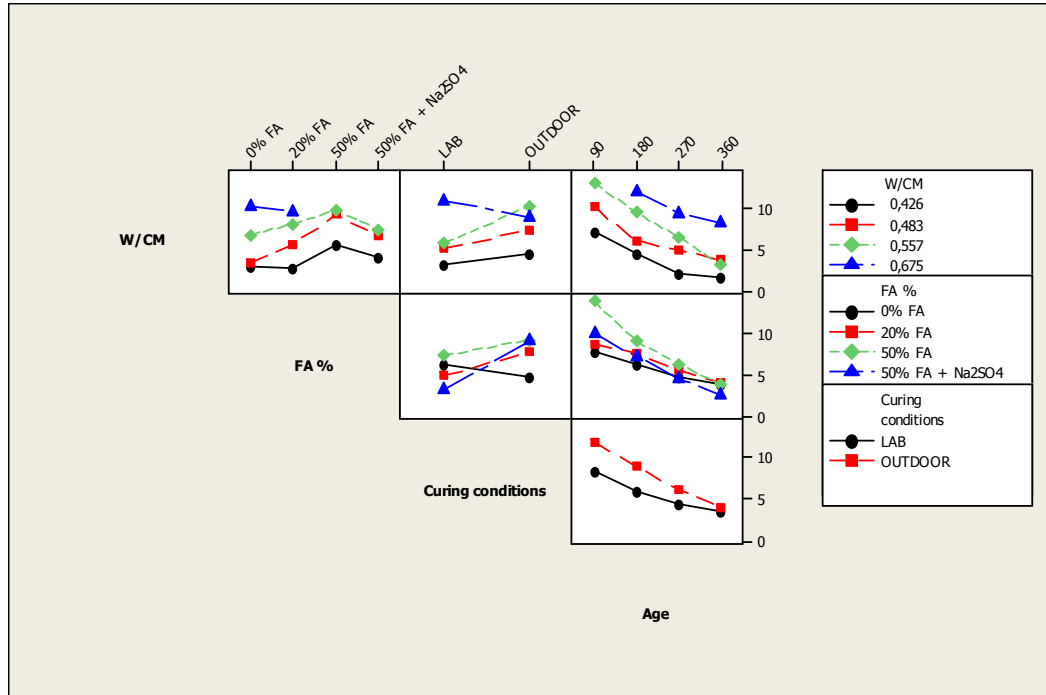
Figure 135 Interaction Plot for Diffusion coefficient

The variation of the diffusion coefficient is connected to the variation of the compressive strength and the fly ash content. Similar to the water permeability case, keeping constant the cementitious material type (with or without sodium sulfate), as the compressive strength is increased the diffusion coefficient is reduced. When fly ash is increased and sodium sulfate included, and keeping constant the compressive strength, the diffusion coefficient can be reduced. This behaviour can be seen in Figure 136. For instance, a chloride diffusion coefficient of 4×10^{-12} m^2/s for a 0% FA mix is accomplished with a compressive strength of 80 MPa, and for a 50% FA and sodium sulfate mix with around 40 MPa.
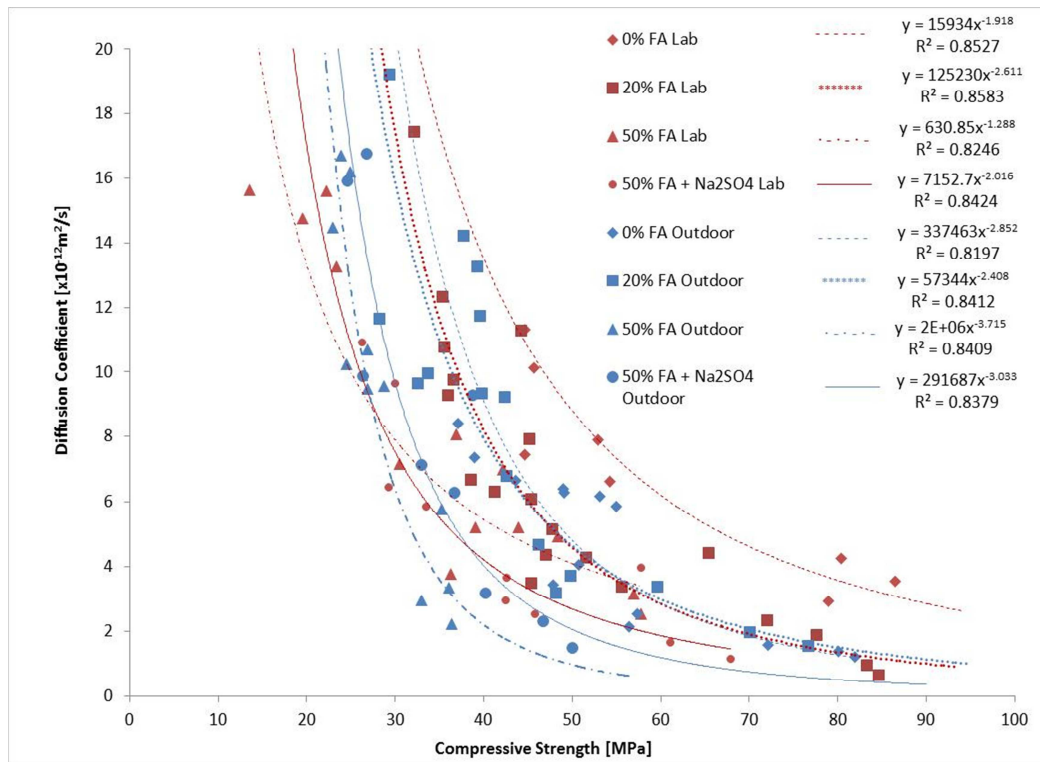
Figure 136 Diffusion coefficient vs compressive strength for 0%, 20% and 50% FA with sodium sulfate

According to Figure 137, the correlation is more accurate for laboratory curing; in this case, concretes with 50% FA and sodium sulfate have the lowest diffusion coefficient for most of charge passed values. In the case of outdoor curing the trend for concretes with 50% FA and sodium sulfate presents the opposite behaviour; the highest diffusion coefficients are present for different charge passed values. This shows the importance of the curing process for this hybrid system. It is important to highlight that ASTM estimates the variability in the chloride penetration test results to be as high as 42% between two samples from the same batch. When chloride penetration was evaluated, the highest variability between two set of samples of the same mix design but different batch was 33%. It is important to mention it occurred for samples cured outdoors with 50% fly ash. The variability decreased with age.

These correlations become important when they are applied in different projects where diffusion coefficient or chloride penetration is specified. It allows the user to predict any of these parameters considering fly ash percentage and curing conditions. For instance for port foundations some constructors specify a diffusion coefficient lower than 10×10^{-12} m^2/s while others specify a passing charge lower than 1000

Coulombs, and Figure 137 shows that a number of the mixes tested will pass one of these criteria and fail the other.
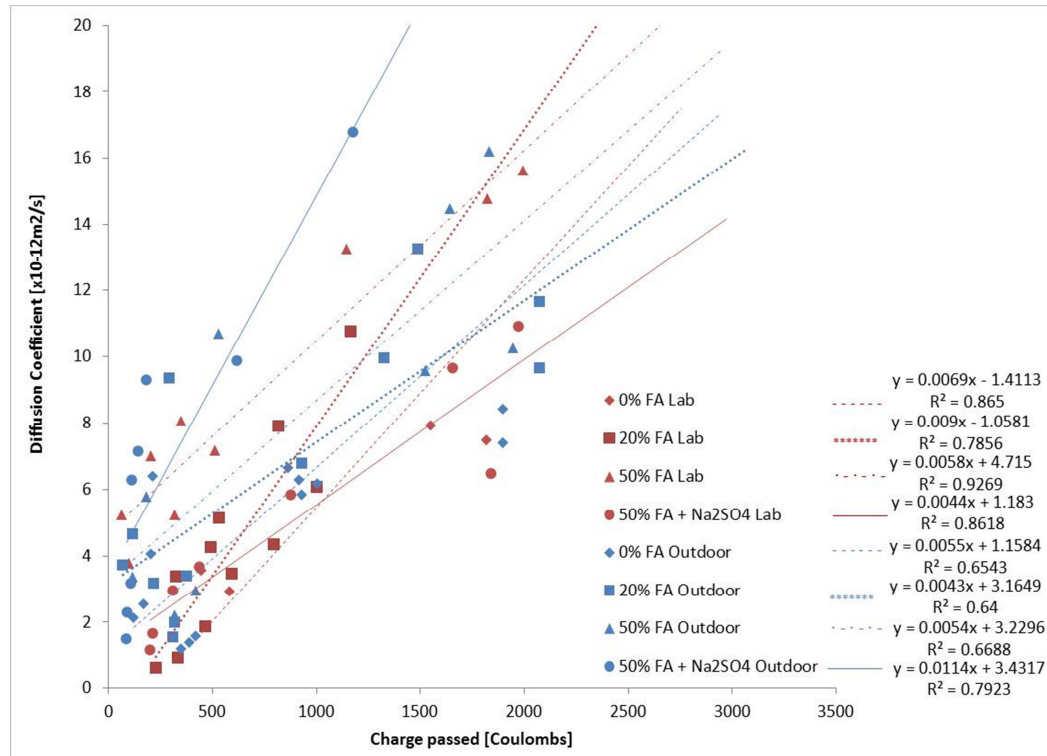
Figure 137 Diffusion coefficient vs chloride penetration for 0%, 20% and 50% FA with sodium sulfate

6.3.6   Parameters influencing carbonation

As seen in Figure 138 (a), presence of fly ash increases the carbonation levels. Inclusion of sodium sulfate reduces carbonation levels compared to the sample with 50% fly ash. The effect of the water to cementitious material ratio is not clear. Carbonation increases as the age increases. The carbonation coefficient is constant at different ages for each fly ash replacement level as presented in Figure 138 (b). This coefficient was calculated using Equation 12 from Chapter 2.
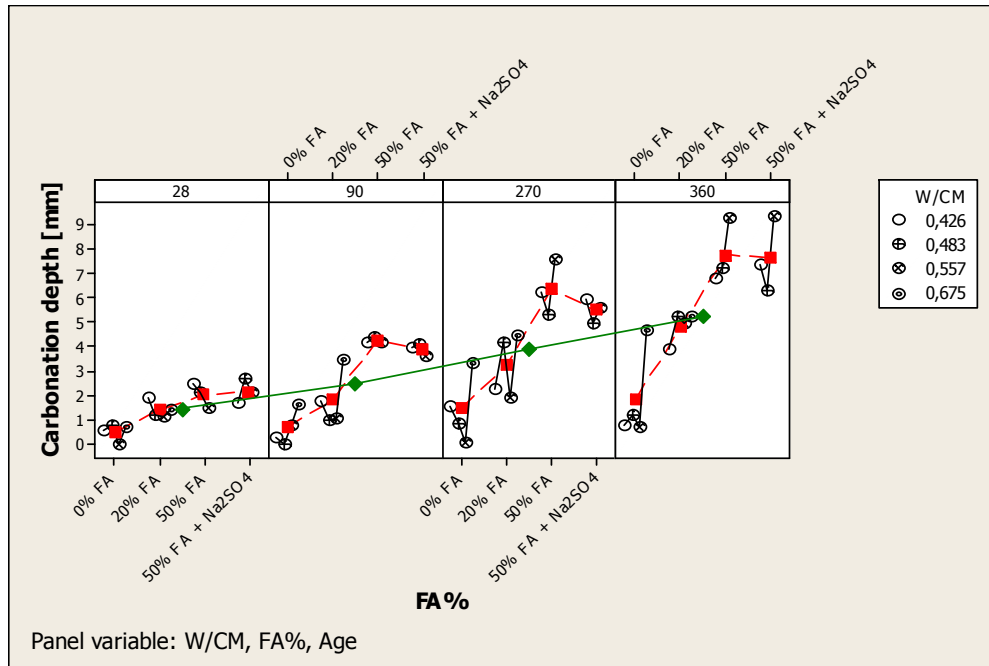
a) Carbonation depth
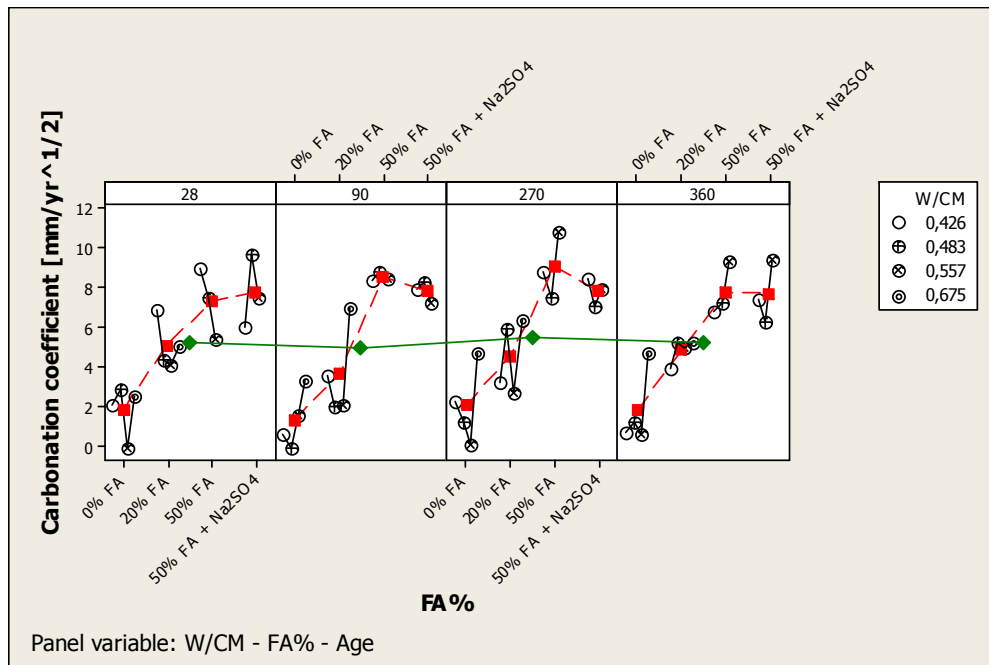
b) Carbonation coefficient
Figure 138 Multi-Vari Chart for Carbonation by Age-Curing-FA%-W/CM

Considering the main effects plot from Figure 139 (a) W/CM does not have as significant an influence as the other parameters. As is seen in Figure 139 (a) and Figure 139 (b), the carbonation depth and carbonation coefficient do not change significantly as the W/CM changes. The other parameters have an influence on carbonation depth increment. In terms of carbonation coefficient as presented in Figure

139 (b), the increase of fly ash content increases carbonation coefficient but with sodium sulfate it decreases.
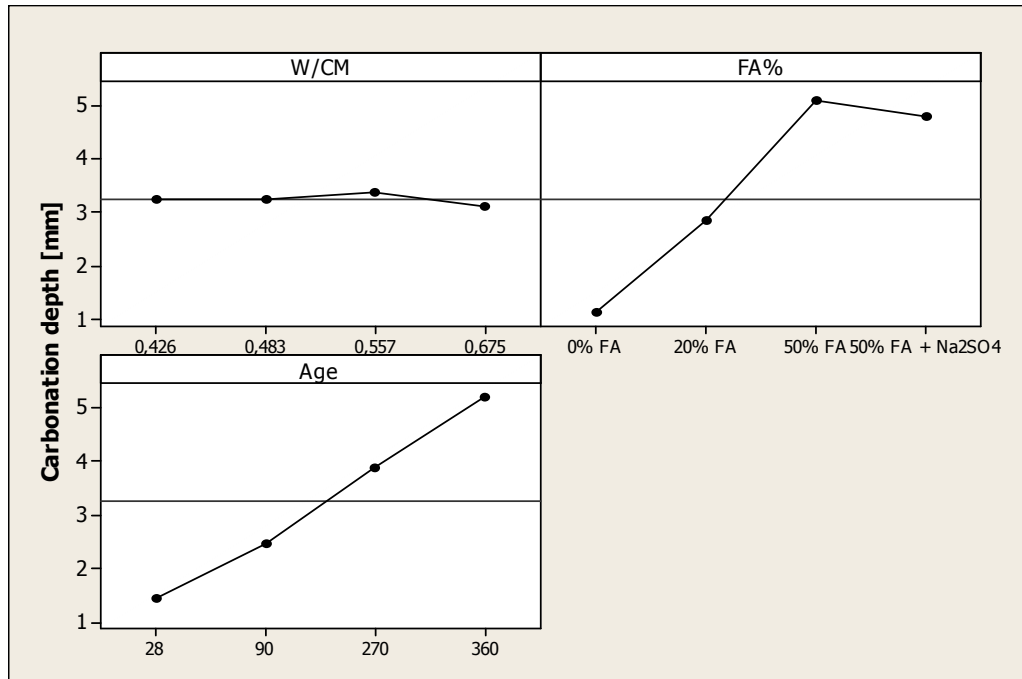
a) Carbonation depth
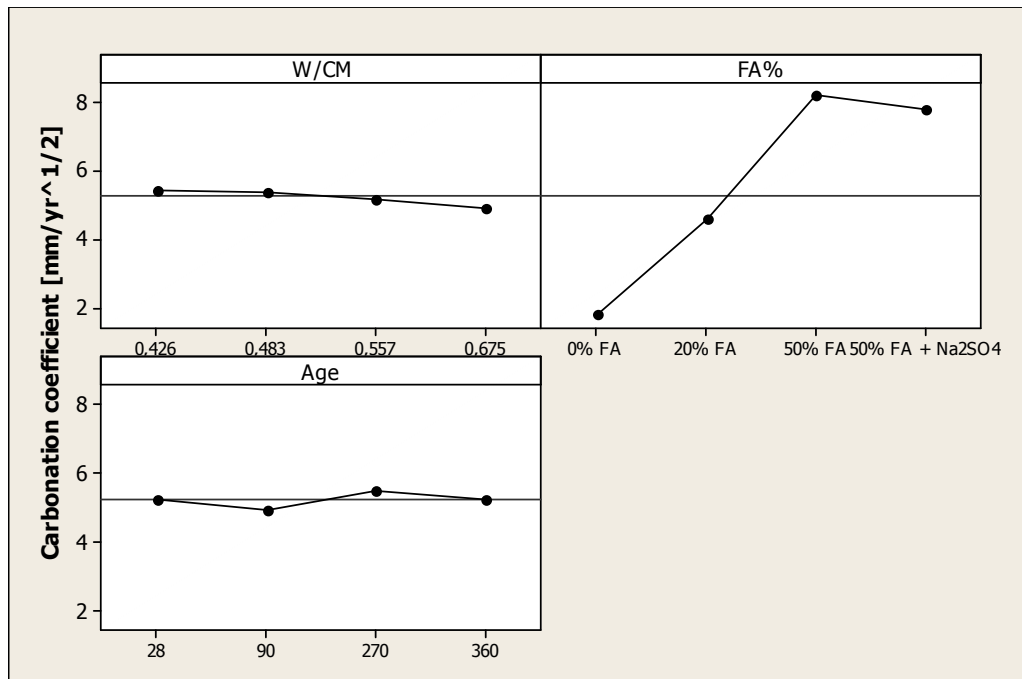
b) Carbonation coefficient
Figure 139 Main Effects Plot for Carbonation

Figure 140 (a) and (b) shows how the influence of the combination of factors such as the W/CM with age does not present a strong influence on the carbonation

depth and carbonation coefficient as FA% does. The carbonation coefficient is constant at different ages but varies depending on the cementitious system.
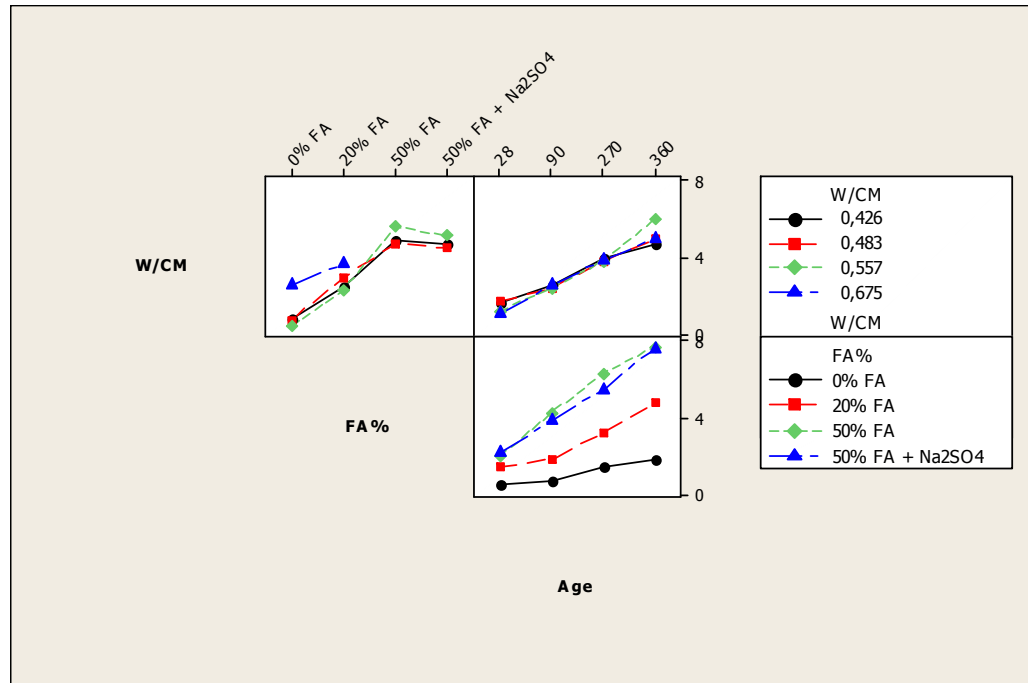
a) Carbonation depth
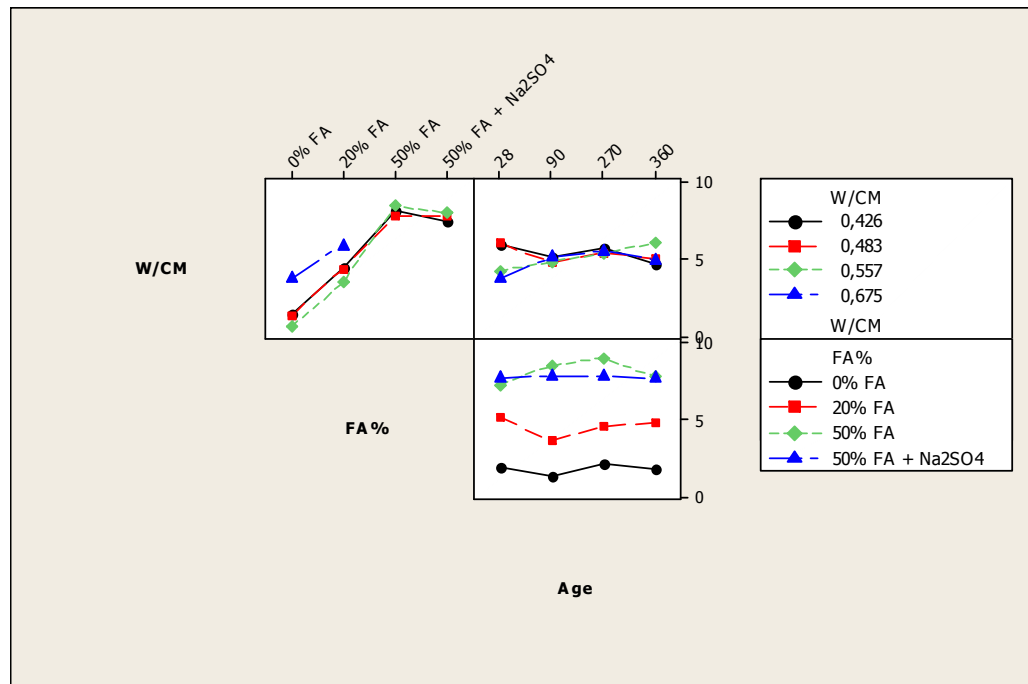
b) Carbonation coefficient

Figure 140 Interaction Plot for Carbonation

Based on the previous analysis, the carbonation coefficient is constant at different ages and strongly influenced by the cementitious material composition. The

benefits of activating a high volume fly ash concrete with sodium sulfate is evident in Figure 141. It is evident that the only relationship is between PC content and carbonation rate; the increase of fly ash content does not help to reduce carbonation rate.
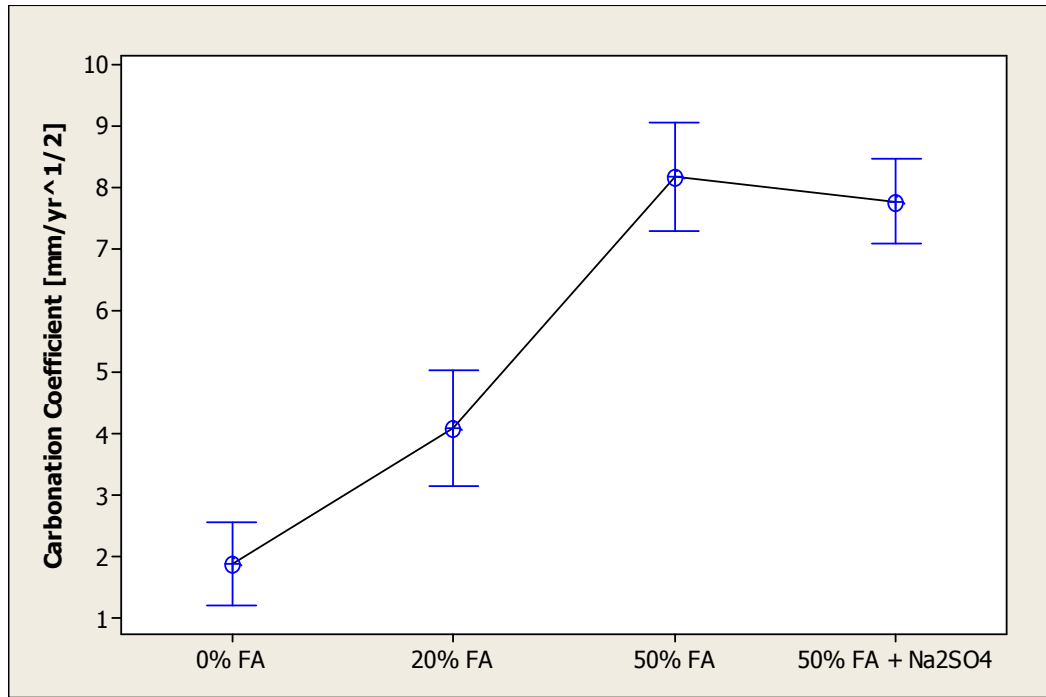
Figure 141 Carbonation coefficient vs fly ash percentage

When fly ash percentage and W/CM are considered simultaneously to estimate carbonation coefficient, there is an increase in this parameter as the FA% and W/CM are increased; this is presented in Figure 142 (a) and (b). Although the increase of fly ash increases the carbonation coefficient, this trend was not followed for mixes with sodium sulfate. The difference in terms of carbonation coefficient between the sample with 0% FA and 50% FA + Na_2SO_4 reaches levels close to 5.5 mm/yr$^{1/2}$.
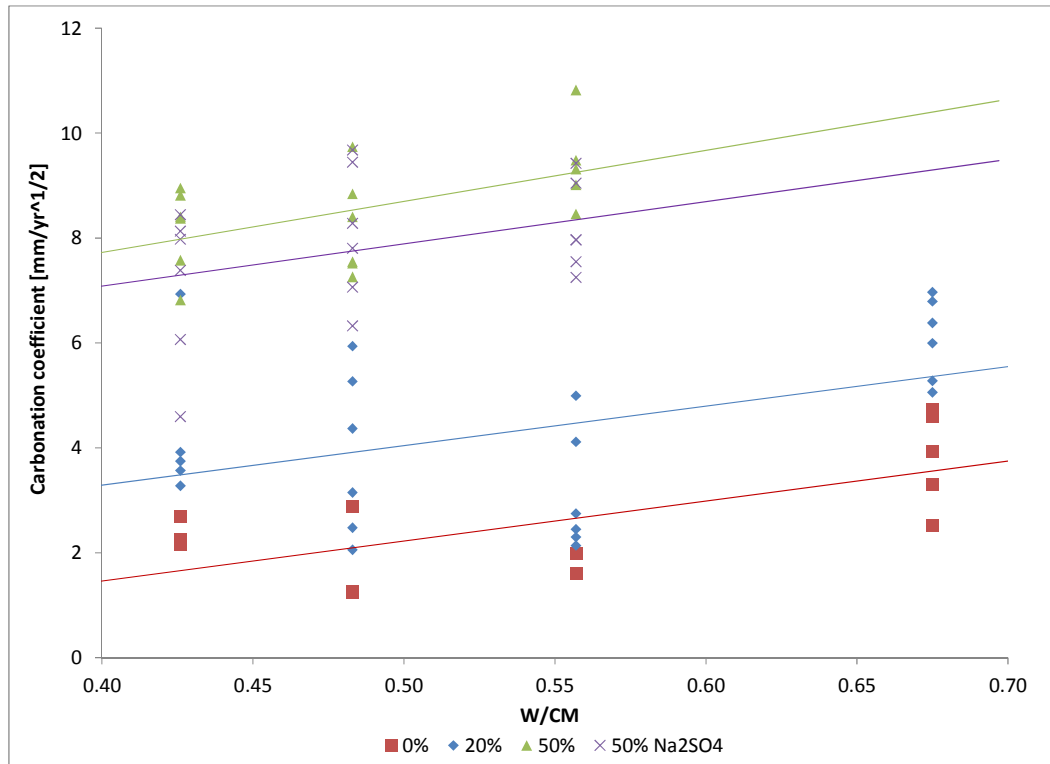
Figure 142 Carbonation coefficient vs W/CM and fly ash percentage: Correlation curves

6.4 Evaluation of large outdoor concrete elements

To evaluate and compare results and correlations seen in the previous section, beams of $0.3 \times 0.4 \times 1$ m were cast as seen in Figure 143. These elements were exposed to ambient conditions and cores were taken to be evaluated in the lab as presented in Figure 144. The evaluated beams had a W/CM of 0.557 with 0% FA, 20% FA, 50% FA and 50% FA + Na_2SO_4. The age of evaluation was 360 days. It is important to mention that only one result for each mix and test was obtained due to number of cores available.

Figure 143 Elements left outdoors: a) front view, b) back view

Figure 144 Cores extraction process

Figure 145 presents the compressive strength from cores. These compressive strength results were applied in the correlations obtained in the previous section from lab specimens to predict water permeability, initial sorptivity, chloride penetration, diffusion coefficient and carbonation. These predicted values are compared with results from large specimens.
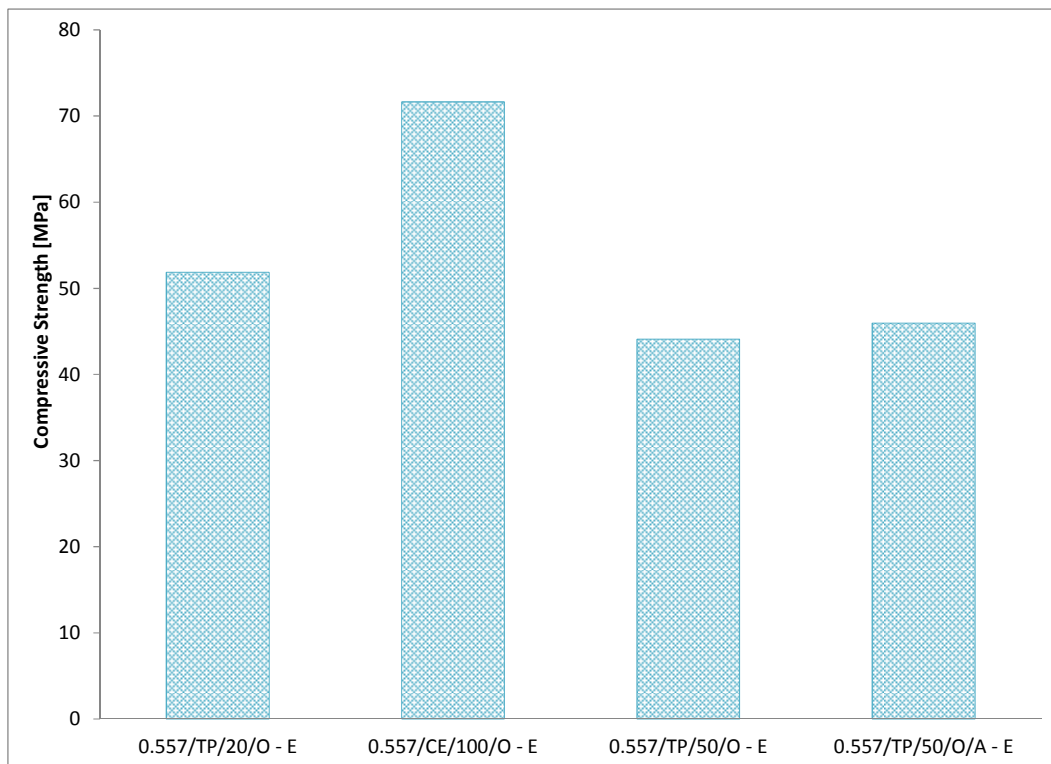
Figure 145 Compressive strength of cores from large elements at 360 days

Results from correlation equations are presented in the right-hand side of the following figures. These are compared to the left-hand results obtained directly from measurements on cores from the large outdoor specimens. As seen in Figure 146 (a), water permeability calculated values were close to the concrete element values. The calculated values were obtained from compressive strength and water permeability correlation equations. Initial sorptivity calculated values were similar to cores with the exception of 50% fly ash which was higher for the calculated one. Figure 146 (c) shows that all the samples are under 1000 Coulombs, classified as 'Very Low' chloride penetration, according to ASTM C 1202. Predicted results are similar to those presented for the element with the exception of the control sample with 20% FA, which was higher. In general, the elements had higher diffusion coefficients compared to correlations results. In the same way, all the diffusion coefficient values were lower than $10x10^{-12}$ m^2/s. In both cases 50% FA mixes had the lowest diffusion coefficients. Diffusion coefficients from correlations were in a range from $2 x10^{-12}$ to $4x10^{-12}$ m^2/s while for elements from $4x10^{-12}$ m^2/s to $7x10^{-12}$ m^2/s; calculated values were almost half of the actual elements values. As seen in Figure 146 (e), carbonation trends are similar for all the set of results; the calculated values from correlations are similar to results from cores. It is important to mention that environment conditions are presented in Figure 74 becoming relevant for samples under carbonation.

In order to keep testing the correlations, it is necessary to obtain more data for each evaluation due to the fact that in this study only one core per mix was used for each test.
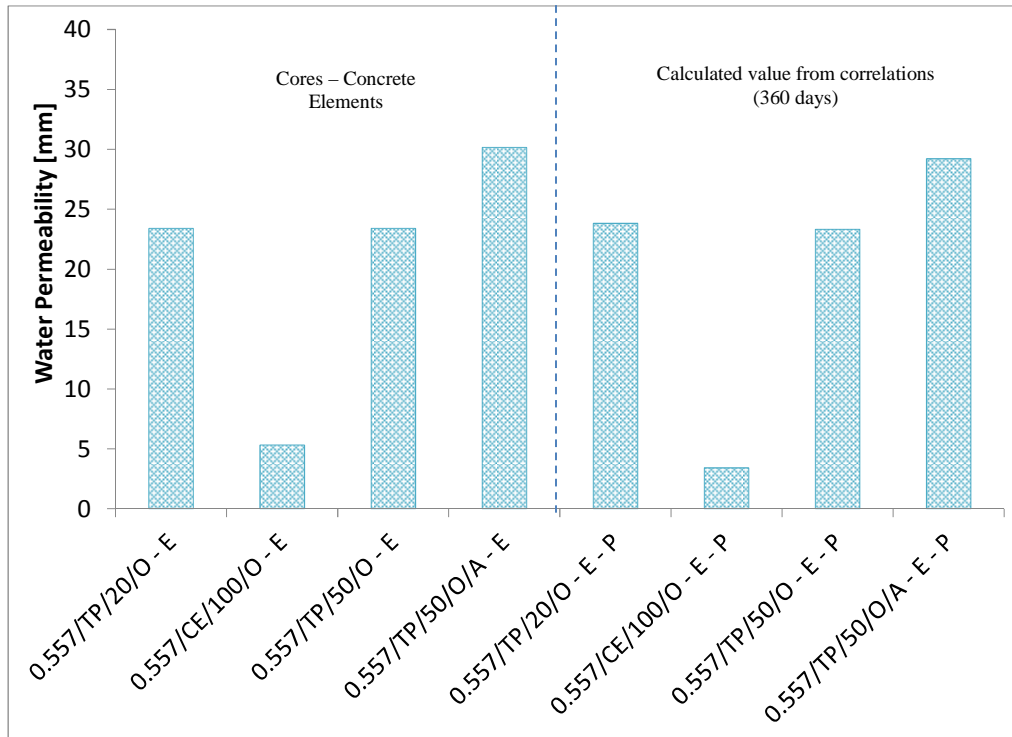
a) Water permeability
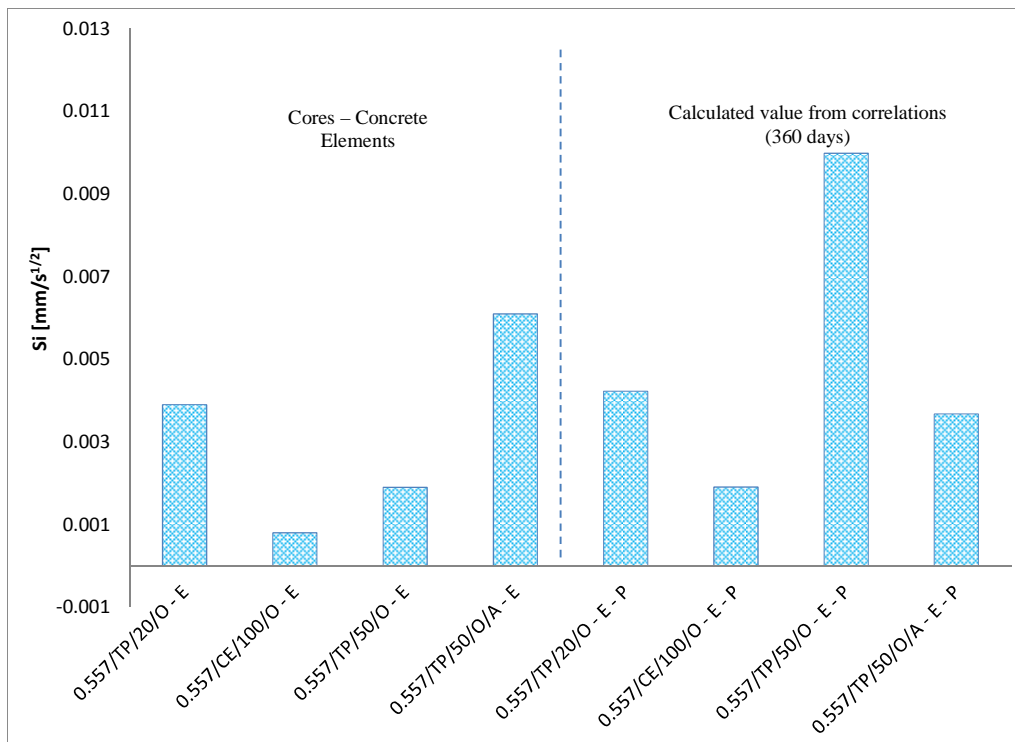
b) Initial sorptivity

223
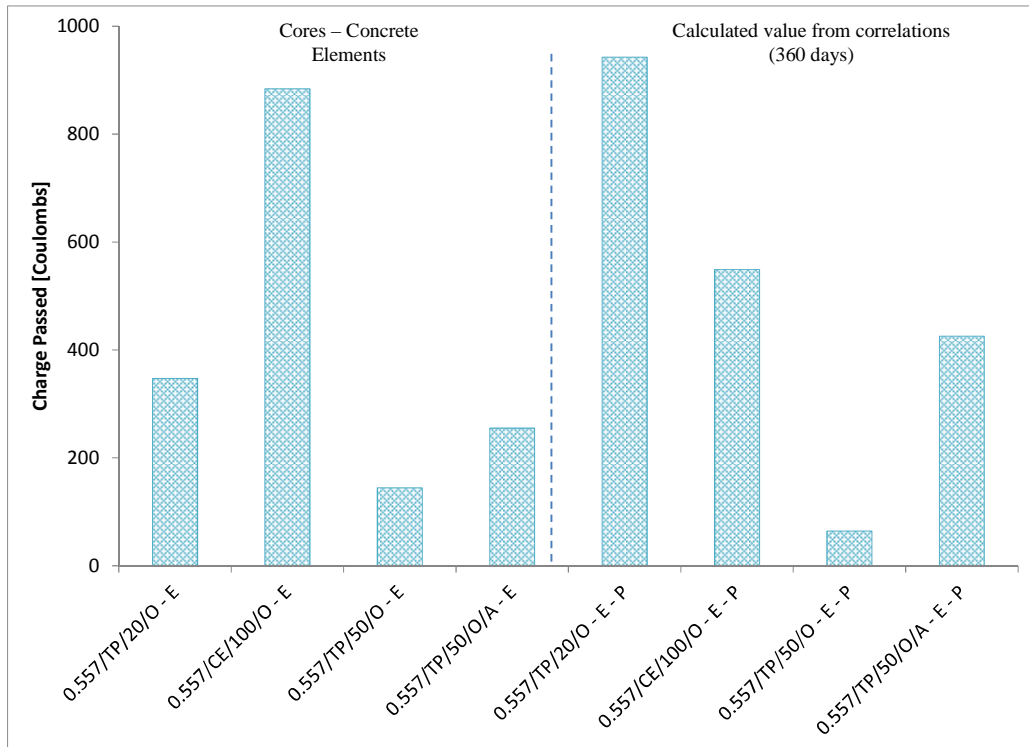
c) Chloride penetration
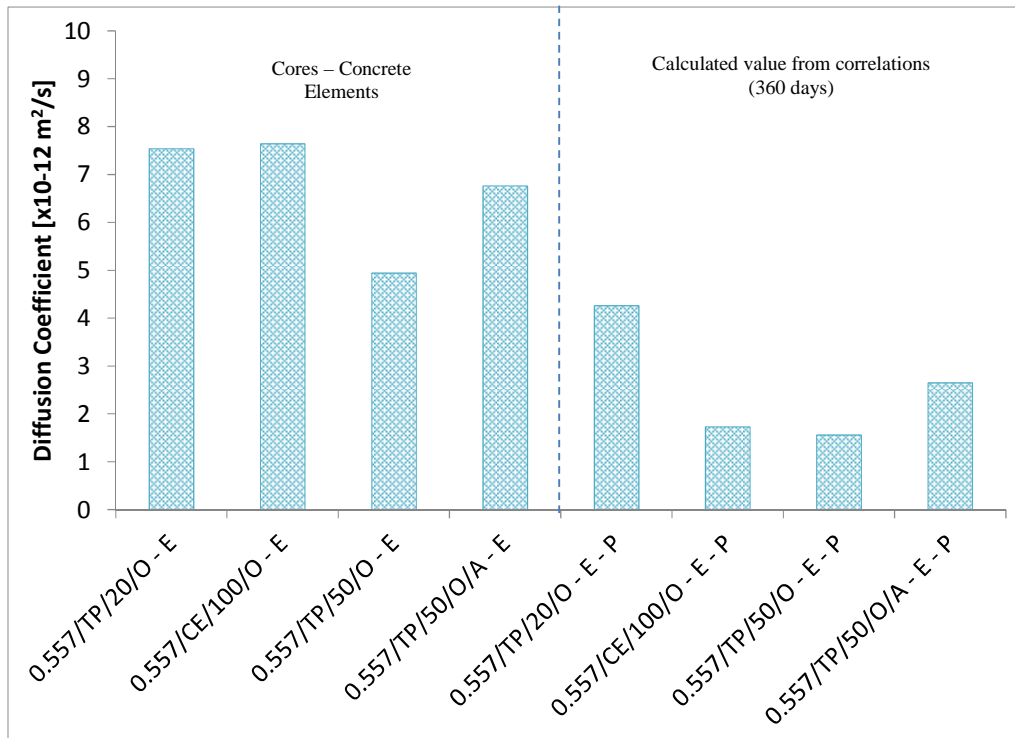
d) Diffusion coefficient
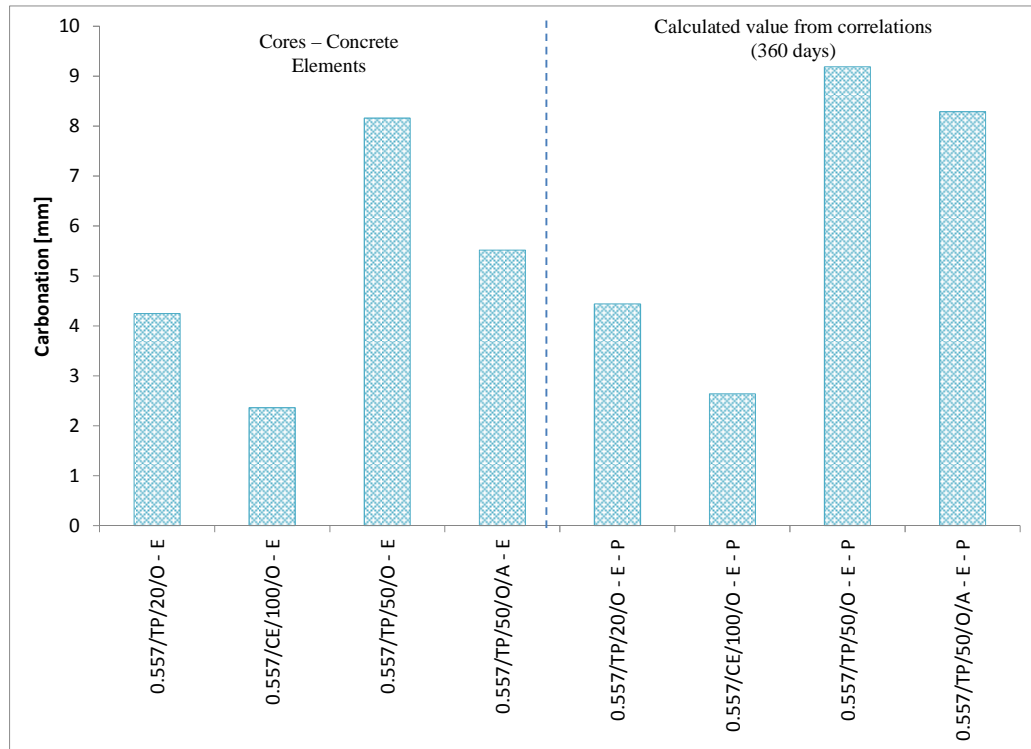
e) Carbonation
Figure 146 Elements evaluation

6.5   Summary

The following summary includes the main findings related to durability properties of the hybrid cementitious system with sodium sulfate:

- Curing under controlled conditions reduced initial and secondary absorption, water permeability, chloride penetration and chloride diffusion. These parameters also reduced as W/CM was reduced. The hybrid cementitious system needs a curing process due to the high volume of fly ash present in the matrix. It is important to guarantee the hydration process of the system and hence the pozzolanic reaction. It is important to mention that comparing all the samples with the same W/CM, the hybrid cementitious system with sodium sulfate had a better performance than control samples in most of the cases. The previous scenario was completely different when concrete was exposed to CO_2; carbonation was always higher for concretes with fly ash. As fly ash increased the carbonation depth increased. On the other hand, alkali silica reaction and sulfate attack were mitigated by increasing the fly ash volume of the mix.

- Compressive strength was correlated with all the durability parameters. As the compressive strength increased the durability parameters improved. Although it

225

was possible to evidence trends, there was some variability; this variability was reduced by also including curing conditions, fly ash levels, and activators simultaneously.

- In order to evaluate correlations, large specimens were left outdoors. Results were similar to those obtained from correlation equations. Results from water permeability, initial sorptivity, chloride penetration and diffusion coefficient were similar for the mix with 50% FA and sodium sulfate, and the mix with 20% FA at 360 days. In this way, the pozzolanic effect of the mix with 50% FA was improving its performance with time; this mix had poor performance at early age.

- Alkali silica reaction was also measured using large specimens. The 0% FA concrete had the highest expansion. The lowest expansion was for the mix with 50% FA and sodium sulfate due to the higher level of Al released by the fly ash.

- The lowest expansions were also obtained for 50% FA and sodium sulfate concrete when exposed to sulfates. The fact of having a low total C_3A helped to reduce expansions.

- Chloride penetration data showed similar penetrations for the mix with 50% fly ash and sodium sulfate, and the mix with 20% fly ash.

7 Service Life

7.1 Introduction

Based on the literature review and the results presented in the previous chapters, initiation periods for degradation are modelled considering chloride diffusion and carbonation. The mix design parameters and compressive strengths are included in each model. A nomogram is obtained at the end as a carbonation model, while an algorithm is programmed using Matlab to calculate concrete initiation period for chloride diffusion.

7.2 Carbonation model

In order to model carbonation for concretes evaluated under Bogota's environmental conditions (Figure 74), the following procedure was considered based on the previous results and correlations obtained: correlations were calculated based on trends between W/CM, compressive strength, carbonation coefficient and carbonation depths. In this way, the main objective is to present the influence of input design parameters on carbonation initiation period. The following procedure was considered.

1. Calculation of the compressive strength at 28 days based on the water to cementitious material ratio and fly ash percentage, or calculation of the water to cementitious material ratio from the compressive strength and fly ash percentage.

2. Calculation of the carbonation coefficient from the water to cementitious material ratio and different fly ash replacement levels.

3. Correlation of the carbonation coefficient with the carbonation depth and the initiation period.

7.2.1 Water to cementitious material ratio vs compressive strength at 28 days for different fly ash replacement

As discussed in the previous section, Figure 147 correlates the compressive strength with the concrete mix design W/CM and fly ash percentage. The previous inputs also apply for the mix design with 1% sodium sulfate. This curve is essential not only to know the mix design inputs for a specific concrete compressive strength,

but also to correlate the final initiation period of the element with the selected 28 day compressive strength. Although mixes with fly ash or sodium sulfate could present significant residual compressive strength evolution, most concrete specifications and codes consider 28 days as the age to use in structural design. The correlation functions are based on Duff Abrams' law published in 1919 (Sear, 2001).
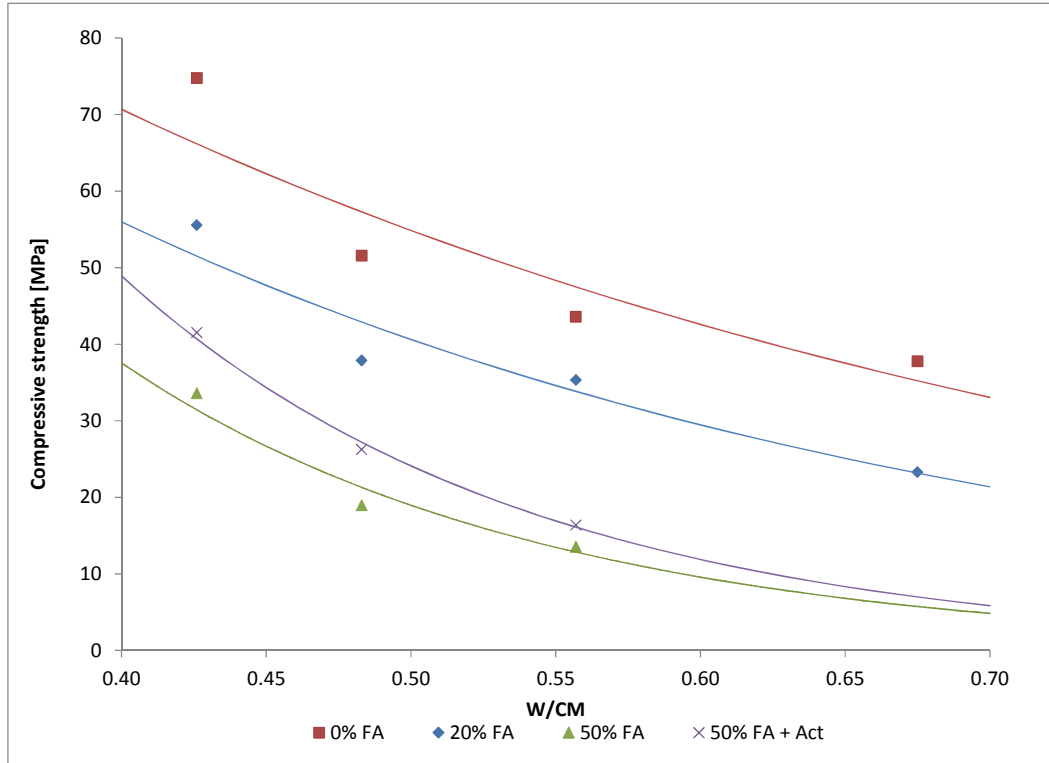
Figure 147 Compressive strength at 28 days vs Water to cementitious material ratio for different fly ash replacement levels

The following are the correlations for the different fly ash replacements:

For 0% FA

$$F = \frac{194.54}{12.58^{\frac{W}{CM}}}$$
(57)

For 20% FA

$$F = \frac{202.07}{24.75^{\frac{W}{CM}}}$$
(58)

For 50% FA

$$F = \frac{576.50}{924.06^{\frac{W}{CM}}}$$
(59)

For 50% FA+Na₂SO₄

$$F = \frac{828.32}{1180.05^{\frac{W}{CM}}}$$
(60)

228

7.2.2 Carbonation coefficient vs W/CM and FA content

There is a linear correlation between W/CM and carbonation coefficient for different fly ash contents. As seen in Figure 148, the carbonation coefficient increases by increasing the levels of fly ash. This was also evidenced by Ho and Lewis, where carbonation for concrete with fly ash was faster than Portland cement concrete; the variation of this parameter depended on PC content only (Ho and Lewis, 1987; Burden, 2006). As mentioned in the literature review section, a reduction in the water to cementitious material ratio reduces carbonation due to pore reduction (Claisse, 2005; Helene and Castro-Borges, 2009; Rabehi, *et al.*, 2013). The complete analysis of this graph was presented in the previous section 6.3.6.
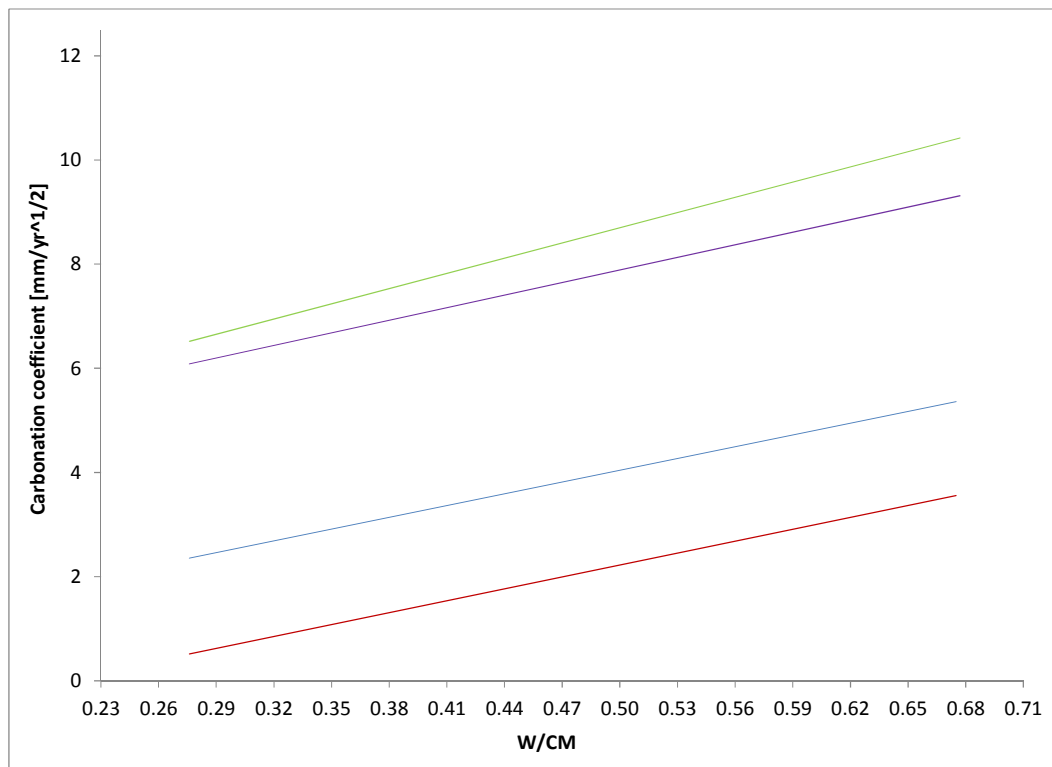
Figure 148 Carbonation coefficient, W/CM and fly ash percentage

The following are the carbonation coefficient (k) equations for the different water to cementitious material ratios $\left(\frac{W}{CM}\right)$ and fly ash percentages, obtained from Figure 148:

For 0% FA

$$k = 7.6222 \frac{W}{CM} - 1.5875 \tag{61}$$

For 20% FA

$$k = 7.53 \frac{W}{CM} - 0.2769 \tag{62}$$

For 50% FA

$$k = 9.7347\frac{W}{CM} - 3.8312 \tag{63}$$

For 50% FA+Na₂SO₄

$$k = 8.0503\frac{W}{CM} - 3.8644 \tag{64}$$

7.2.3   Carbonation coefficient vs carbonation depth and time

By calculating the carbonation coefficient, the carbonation depth is obtained for different periods using Tutti's model (Tutti, 1982). Figure 149 presents the variation of carbonation depth and carbonation coefficient with time.
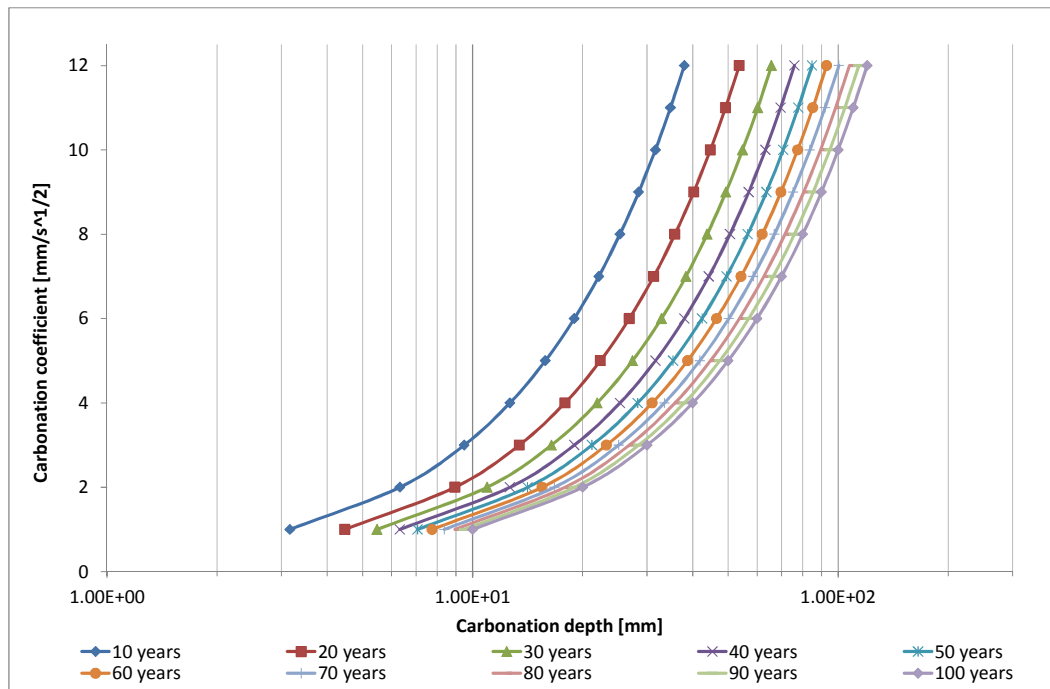
Figure 149 Carbonation coefficient vs carbonation depth and time

7.2.4   Initiation period nomogram

The nomogram is developed based on Figures 147, 148 and 149. The main objective of the nomogram presented in Figure 150 is to correlate all the different parameters with the initiation period. In this way, the carbonation depth and time is correlated to compressive strength, W/CM, fly ash percentage and activator and carbonation coefficient. This nomogram applies for Bogotá's conditions. In order to

see the influence of each parameter, it is important to consider the following procedure for Figure 150:

1. Select the required compressive strength, W/CM and fly ash percentage.
2. Draw a line, keeping constant the W/CM and finding the selected fly ash percentage.
3. Draw a line from the FA% and carbonation coefficient curve to the selected period of time.
4. Different periods of time are correlated to carbonation depths.

This procedure could also be applied in the inverse order from the last to the first step.
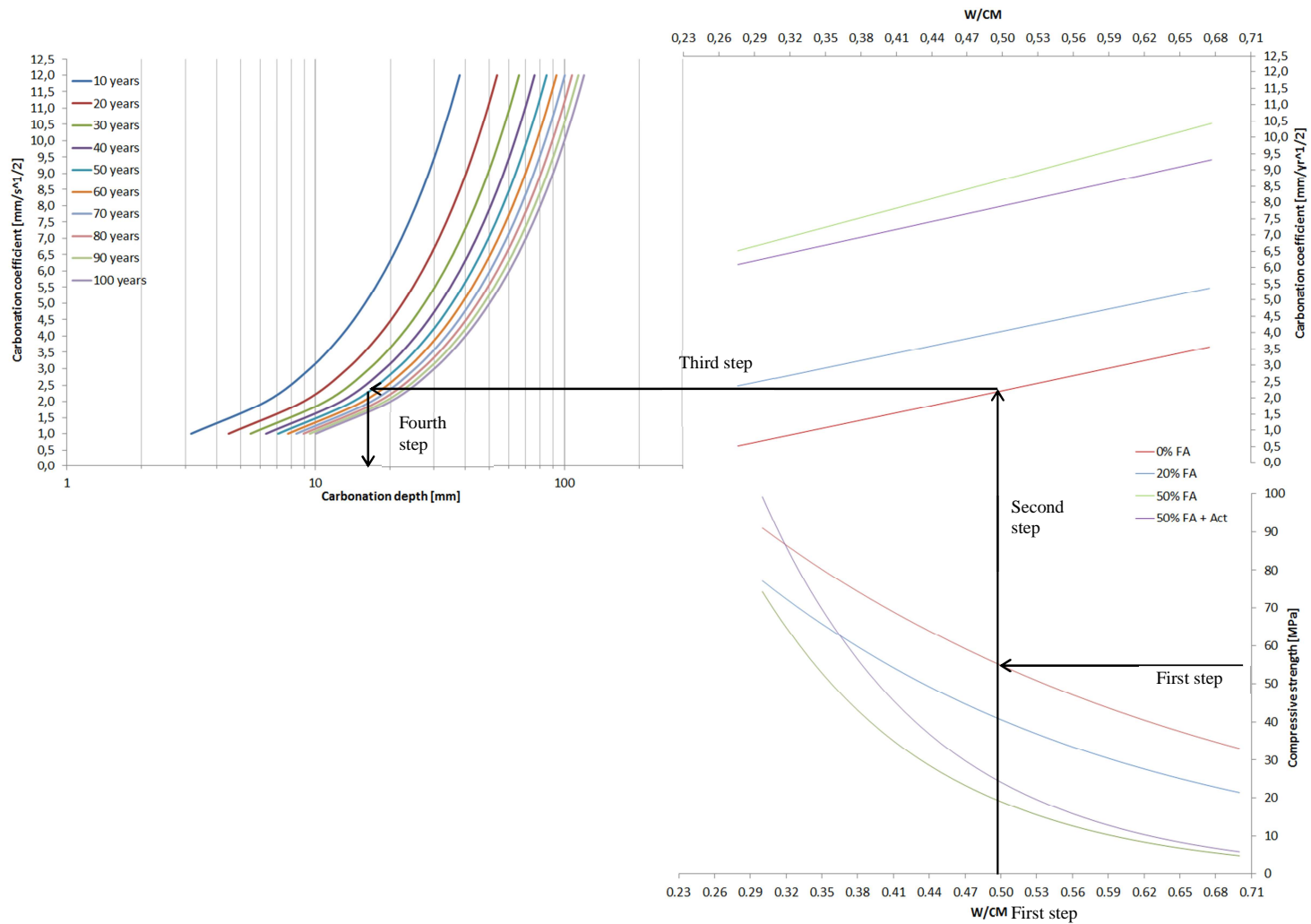
Figure 150 Nomogram for calculation of the carbonation initiation period

7.3 Chloride diffusion model

The model equations are proposed based on the results presented in sections 6.2.4 and 6.3.3, and compared with Life 365 model (Thomas and Bentz, 2008). This model is referenced and described in more detail in the literature review section. As mentioned in the background section, this model does not consider chemical interactions or electrical coupling between ions.

Procedure to calculate the initiation period (each step is explained after section 7.3.1)

- Calculation of the compressive strengths at different water to cementitious material ratios at a reference age of 28 days.
- Calculation of the diffusion coefficients for the different compressive strengths at a reference age of 28 days, $D_{ref(28\,days)}$.
- Calculation of the diffusion decay index, m.
- Calculation of the diffusion coefficient at time t, $D(T)$.
- Calculation of the diffusion coefficient considering temperature changes.
- Calculation of the chloride concentration depending on the temperature and chloride surface concentration.
- Solution of the finite difference using the Crank-Nicholson method for a variable temperature and chloride surface concentration.

The equations for the diffusion coefficient at a reference age, the diffusion decay index and the diffusion coefficient at time t are modified from the Life 365 model, with the exception of the equation for the temperature effect which remains the same as presented in that model. The following is the explanation of how the proposed equations are obtained and the way the finite difference solution is applied.

7.3.1 Diffusion coefficients for different compressive strengths at a reference age (28 days)

Based on correlation equations derived from the data in Figure 136 and as seen in Figure 151, mixes with 50% FA performed better in terms of diffusion coefficient for a given compressive strength. For instance, considering the same compressive strength, the level of diffusion coefficient for mixes with 50% FA is lower compared to control samples with 0% FA and 20% FA.
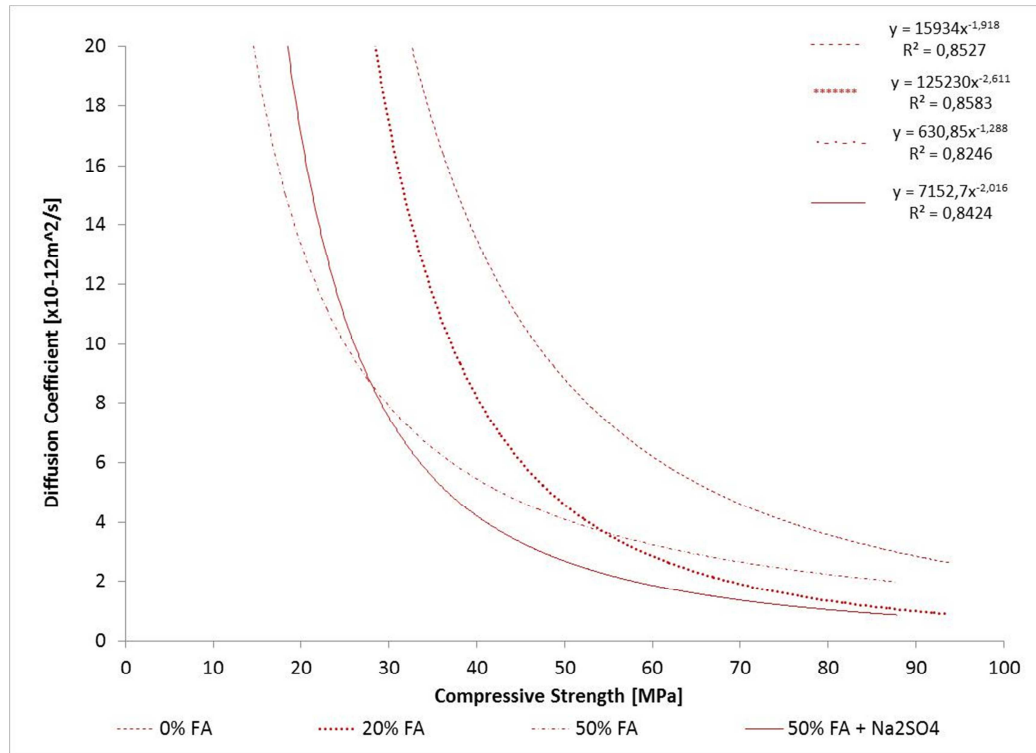
Figure 151 Compressive strength vs diffusion coefficient at a reference age (28 days)

For 0% FA

$$D_{ref} = 15934F^{-1.918}$$ (65)

For 20% FA

$$D_{ref} = 125230F^{-2.611}$$ (66)

For 50% FA

$$D_{ref} = 630.85F^{-1.288}$$ (67)

For 50% FA+Na₂SO₄

$$D_{ref} = 7152.7F^{-2.016}$$ (68)

7.3.2 Chloride diffusion coefficient variation with time for different water to cementitious material ratios

0% FA

For mixes with 0% fly ash, the diffusion coefficient is affected by the W/CM. The reduction of the W/CM positively influences the matrix, reducing the values of the diffusion coefficient. This is shown in Figure 152. The W/CM of 0.426 was not considered for the diffusion decay index due to its unexpected behaviour in Figure

152.
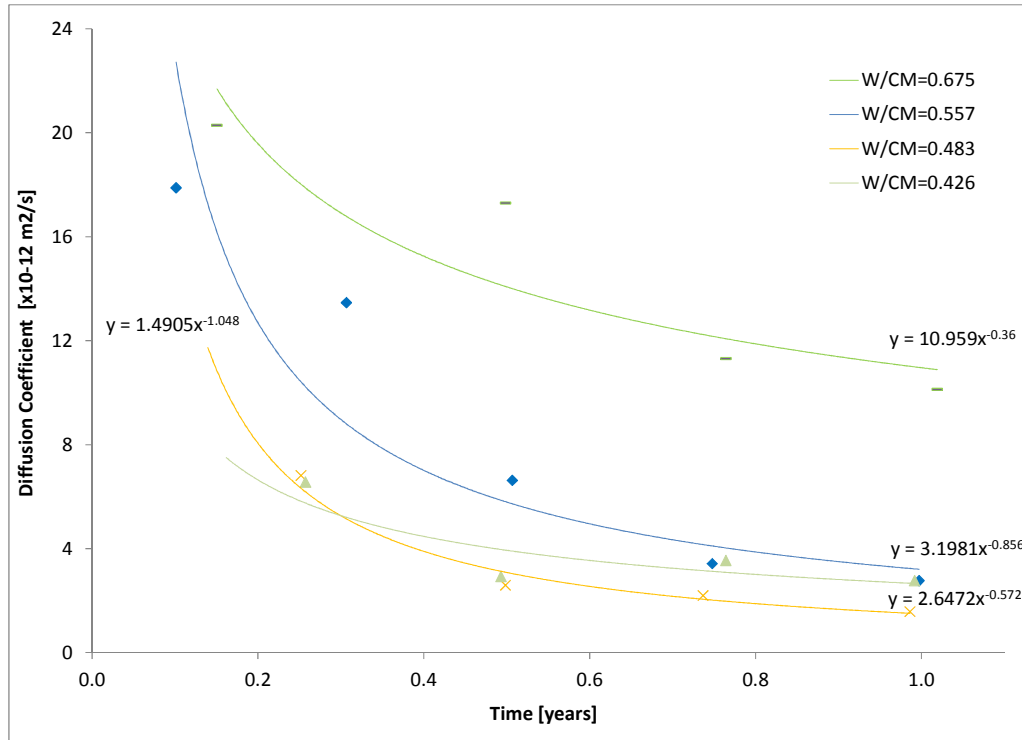
a) Linear scale
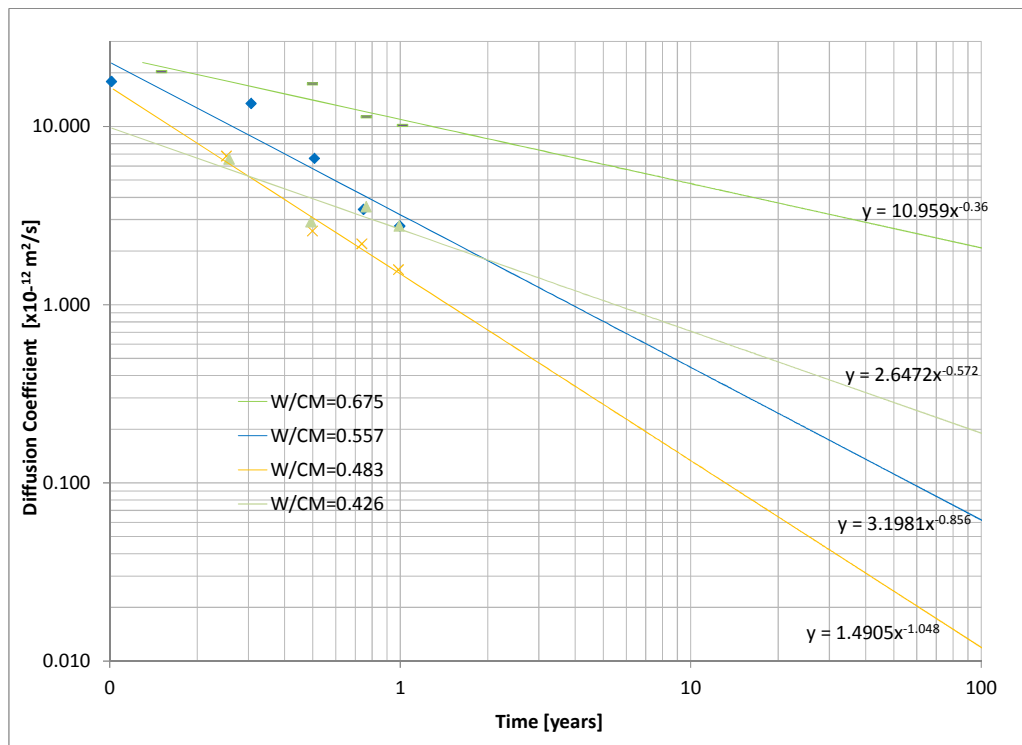
b) Log scale

Figure 152 Time vs Diffusion coefficient for different W/CM and 0% FA

For W/CM=0.675

$$D = D_{ref}\left(\frac{t_{ref}}{t}\right)^{0.36} \tag{69}$$

For W/CM=0.557
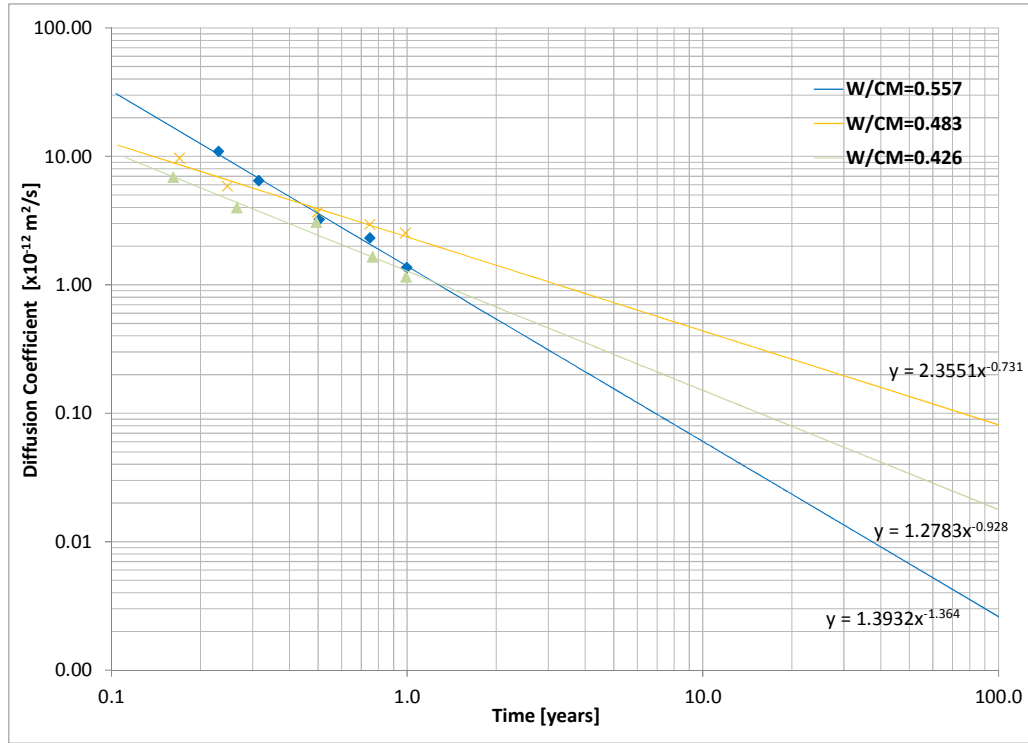
$$D = D_{ref}\left(\frac{t_{ref}}{t}\right)^{0.856} \tag{70}$$

For W/CM=0.483

$$D = D_{ref}\left(\frac{t_{ref}}{t}\right)^{1.048} \tag{71}$$

For W/CM=0.426

$$D = D_{ref}\left(\frac{t_{ref}}{t}\right)^{0.572} \tag{72}$$

20% FA

In general, the way the chloride diffusion coefficient is reduced in time, seems to be similar for different W/CM. Figure 153 presents how there is an evident reduction in diffusion from mixes with a W/CM of 0.675 to 0.426. The behaviour was similar for mixes with 0.557 and 0.483 of W/CM. Figure 153 (b) presents the trend in log scale including extrapolation up to 100 years. The W/CM of 0.483 was not considered for the ageing exponent due to its unexpected behaviour.

a) Linear scale

236
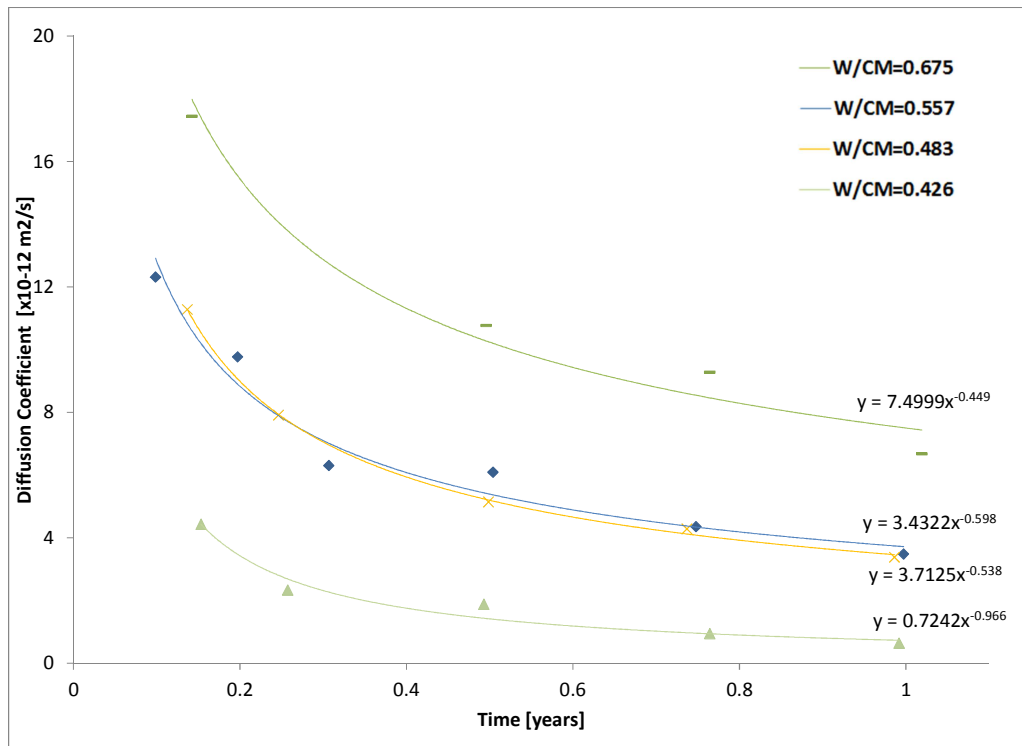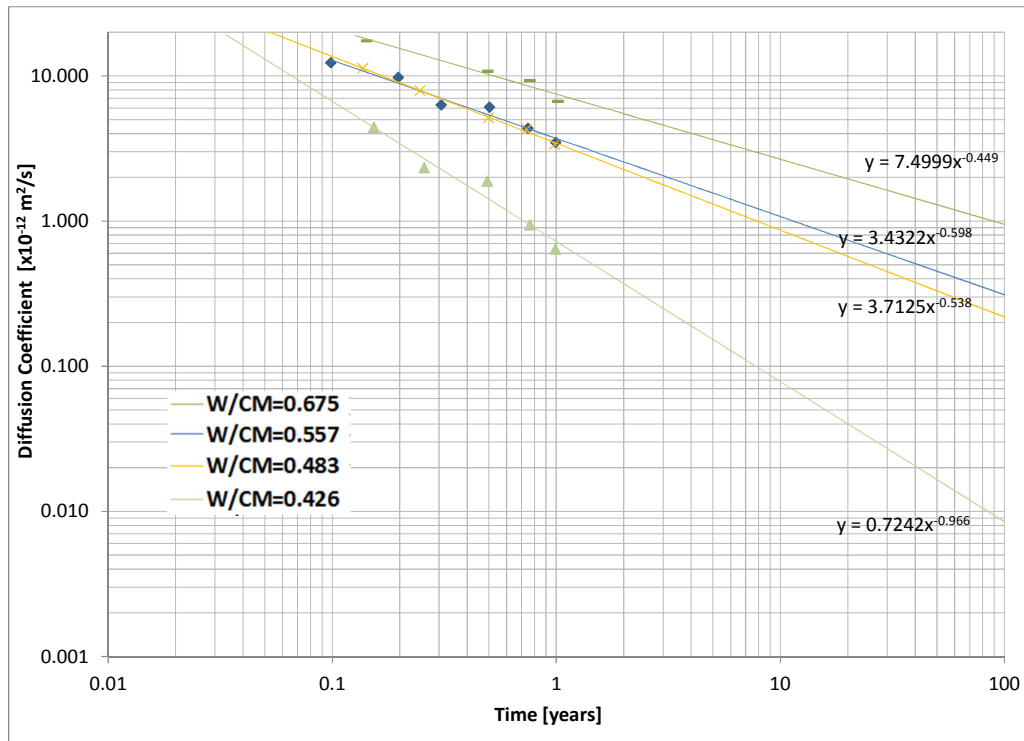
b) Log scale

Figure 153 Time vs Diffusion coefficient for different W/CM and 20% FA

For W/CM=0.675

$$D = D_{ref} \left(\frac{t_{ref}}{t} \right)^{0.449} \tag{73}$$

For W/CM=0.557

$$D = D_{ref} \left(\frac{t_{ref}}{t} \right)^{0.538} \tag{74}$$

For W/CM=0.483

$$D = D_{ref} \left(\frac{t_{ref}}{t} \right)^{0.598} \tag{75}$$

For W/CM=0.426

$$D = D_{ref} \left(\frac{t_{ref}}{t} \right)^{0.966} \tag{76}$$

50% FA

At the first months the diffusion coefficient decreases as the W/CM decreases but after 4 months (0.33 years) concrete with 0.557 has a lower diffusion coefficient in comparison to the W/CM of 0.483 as seen in Figure 154; it also occurred for mixes with Na_2SO_4 in Figure 155. It is important to mention that this variation in the diffusion coefficient for W/CM of 0.557 occurred only in mixes with 50% FA. This trend with a W/CM of 0.557 was not expected and at this moment there is not a

possible explanation for this behaviour. This W/CM was not considered for the diffusion decay index.
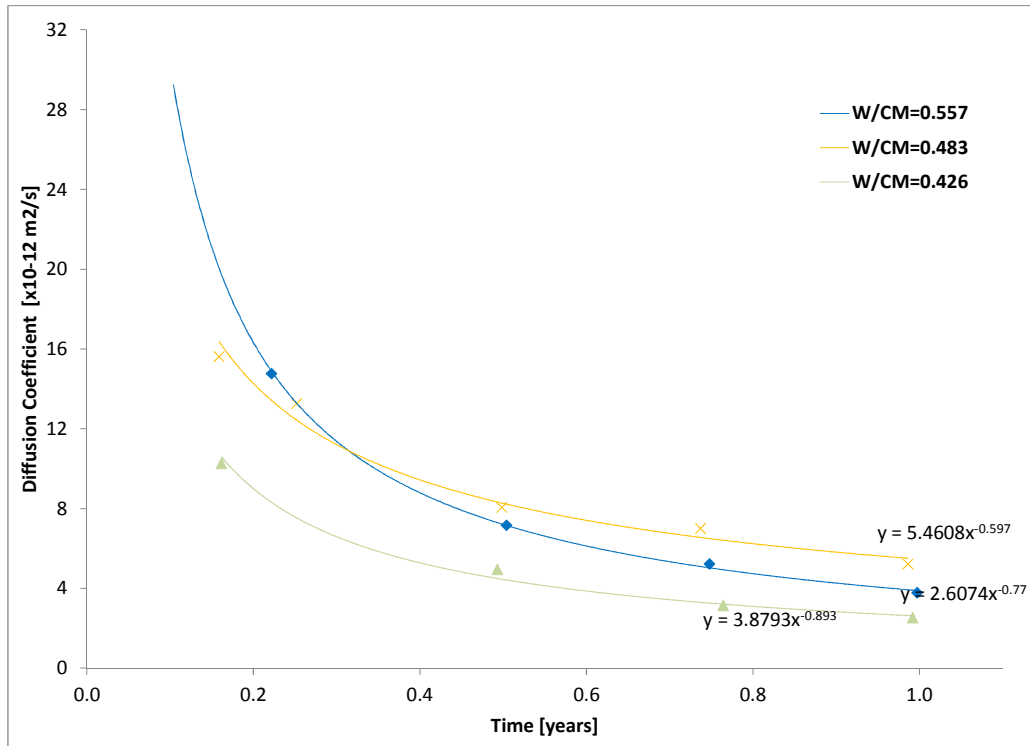
a) Linear scale
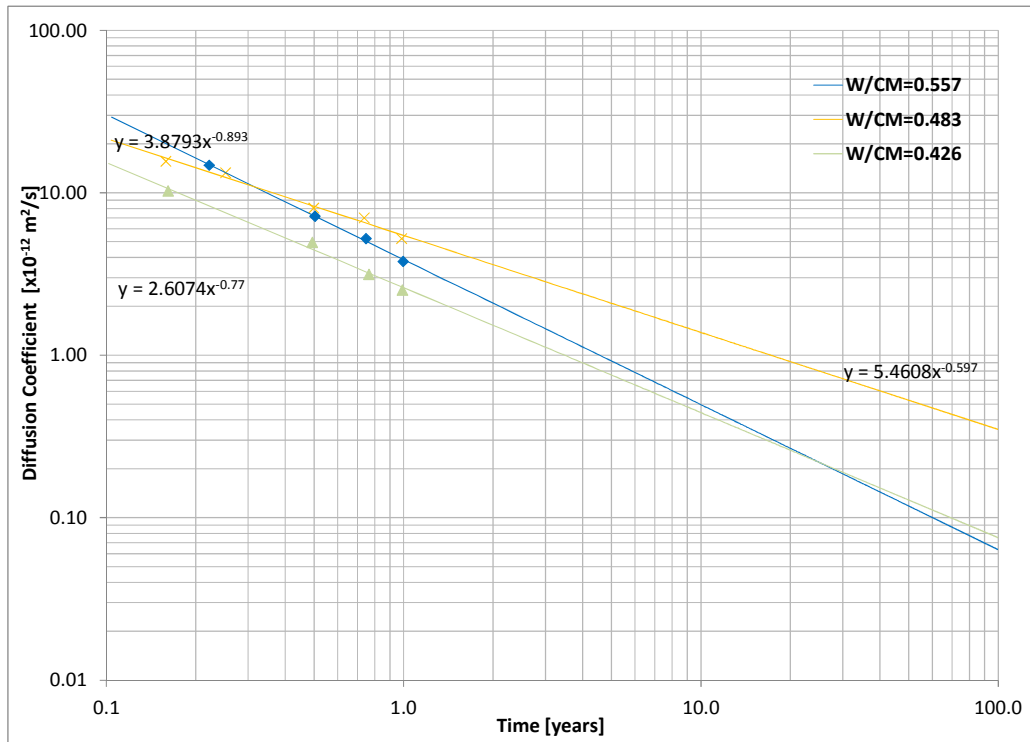
b) Log scale

Figure 154 Time vs Diffusion coefficient for different W/CM and 50% FA

For W/CM=0.557

$$D = D_{ref}\left(\frac{t_{ref}}{t}\right)^{0.893} \tag{77}$$

For W/CM=0.483

$$D = D_{ref}\left(\frac{t_{ref}}{t}\right)^{0.597} \tag{78}$$

For W/CM=0.426

$$D = D_{ref}\left(\frac{t_{ref}}{t}\right)^{0.77} \tag{79}$$
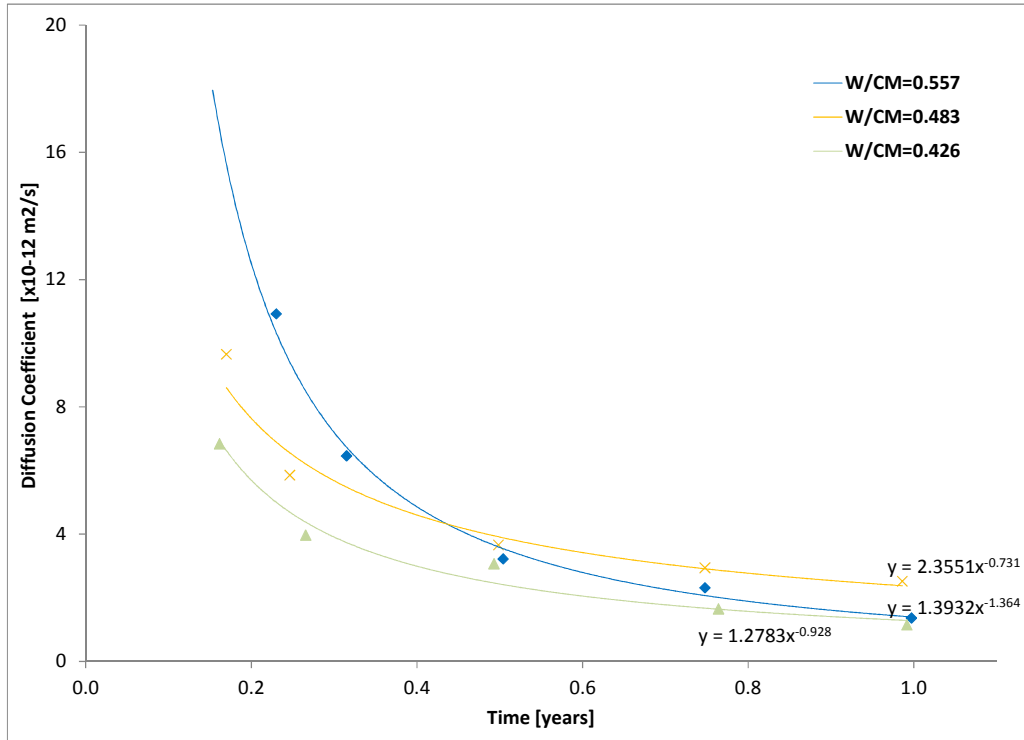
a) Linear scale

b) Log scale

Figure 155 Time vs Diffusion coefficient for different W/CM and 50% FA +

Na$_2$SO$_4$

For W/CM=0.557

$$D = D_{ref} \left(\frac{t_{ref}}{t}\right)^{1.364} \tag{80}$$

For W/CM=0.483

$$D = D_{ref} \left(\frac{t_{ref}}{t}\right)^{0.731} \tag{81}$$

For W/CM=0.426

$$D = D_{ref} \left(\frac{t_{ref}}{t}\right)^{0.928} \tag{82}$$

7.3.3   Diffusion decay index

The diffusion decay index or ageing exponent is used to consider changes with time of the diffusion coefficient due to the continued hydration of the system. The diffusion decay indexes are calculated from figures and equations presented previously in section 7.3.2. As seen in Figure 156, the index is affected by both W/CM, and FA replacement, as well as the presence of Na$_2$SO$_4$. It is important to mention that the following data were not included: W/CM equal to 0.557 for 50% FA mixes, W/CM equal to 0.483 for 20% FA mixes and W/CM equal to 0.426 for 0% FA mixes.

240

There is a difference in the decay index curves of 0.317 between mixes with 0% FA and 50% FA + Na$_2$SO$_4$. The lowest decay levels are present in mixes with 50% FA. The decay indexes for mixes with Na$_2$SO$_4$, are higher than mixes with 50% FA only. As the W/CM is reduced, the decay index increases, and in this case samples with 0% FA have the highest values. According to the Life 365 method (Bentz and Thomas, 2008), as the cement replacement level is increased the diffusion decay index increases, but in this study this pattern is not evident.
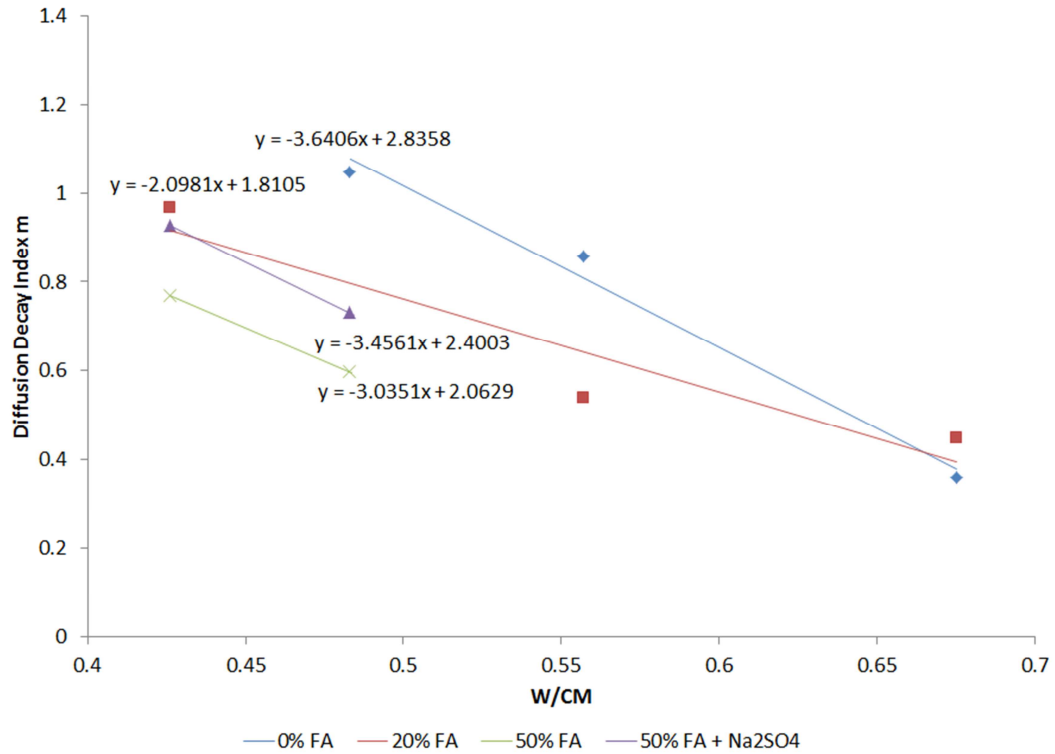
Figure 156 Diffusion decay index for 0% FA, 20% FA, 50% FA, and 50% FA + Na$_2$SO$_4$ at different W/CM

For 0% FA

$$m = -3.6406 \frac{w}{cm} + 2.8358 \tag{83}$$

For 20% FA

$$m = -2.0981 \frac{w}{cm} + 1.8105 \tag{84}$$

For 50% FA

$$m = -3.0351 \frac{w}{cm} + 2.0629 \tag{85}$$

For 50% FA+Na$_2$SO$_4$

$$m = -3.4561 \frac{w}{cm} + 2.4003 \tag{86}$$

241

7.3.4 Chloride concentration for a constant temperature and surface chloride concentration using Crank's solution

The following equation is used to find the diffusion coefficient and it is referenced as Crank's solution (Collepardi, *et al.*, 1972; Crank, 1975; Martys, 1995). It is used when the temperature and the surface concentration are assumed to be constant:

$$C(x,t) = C_0\left(1 - erf\left(\frac{x}{2\sqrt{D_c t}}\right)\right) \tag{87}$$

Where:

$C_{(x,t)}$ = chloride concentration at a defined depth x and time t

C_0 = chloride concentration on the surface

D_c = diffusion coefficient (m^2/s)

erf = error function

The following is an example using the proposed initial equations and Crank's solution with input data defined by the author. It is important to mention that the main objective of the example is to present the calculation procedure. The comparison is included in section 7.3.6 using the programmed algorithm, Life 365 and test results.

$C_0 = 1\%$

Reference age = 28 days

Age of the sample: 1 year

Analysis depth: 3 cm

Temperature: 17.7°C

W/CM: 0.483

Fly ash percentage: 50%

Mix with Na$_2$SO$_4$

Compressive strength calculation at 28 days

$$F = \frac{828.32}{1180.05^{\frac{W}{CM}}}$$

$$F = \frac{828.32}{1180.05^{0.483}}$$

$$F = 27\ MPa$$

Diffusion coefficient calculation at 28 days

$$D_{28} = 7152.7F^{-2.016}$$

$$D_{28} = 7152.7 \cdot 27^{-2.016}$$

$$D_{28} = 9.3 \times 10^{-12} \, m^2/_s$$

Diffusion decay index calculation

$$m = -3.4561 \frac{w}{cm} + 2.4003$$

$$m = -3.4561 \times 0.48 + 2.4003$$

$$m = 0.731$$

Diffusion coefficient at 1 year

$$D = D_{ref} \left(\frac{t_{ref}}{t}\right)^m$$

$$D = 5.9 \times 10^{-12} \left(\frac{28}{365}\right)^{0.731}$$

$$D = 1.4 \times 10^{-12} \, m^2/_s$$

Diffusion coefficient change depending on the temperature

$$D(T) = D_{ref} \exp\left[\frac{U}{R}\left(\frac{1}{T_{ref}} - \frac{1}{T}\right)\right]$$

$$D(17.7°C) = 1.4 \times 10^{-12} \exp\left[\frac{35000}{8.3144621}\left(\frac{1}{293.15} - \frac{1}{290.85}\right)\right]$$

$$D(17.7°C) = 1.3 \times 10^{-12} \, m^2/_s$$

Chloride concentration

$$C(x,t) = C_0\left(1 - erf\left(\frac{x}{2\sqrt{D_c t}}\right)\right)$$

$$C(0.03m, 31536000s) = 1\%\left(1 - erf\left(\frac{0.03}{2\sqrt{1.7 \times 10^{-12} \cdot 31536000}}\right)\right)$$

$$C(0.03m, 31536000) = 0.0009\%$$

The calculated chloride concentration obtained from Crank's solution is low considering that an approximate chloride concentration for corrosion initiation is 0.05% (Thomas and Bentz, 2008), depending on the hydroxide concentration in the pore solution.

7.3.5 Chloride concentration for a variable temperature and surface chloride concentration using the Crank – Nicolson method – Finite difference solution

The finite difference solution used to find the chloride concentration at the surface is the Crank-Nicolson method (Crank and Nicolson, 1947; Wilmott, *et al.*, 1995). The following is the method (Figure 157):

$$\frac{\partial C}{\partial t} = D\frac{\partial^2 C}{\partial x^2}$$

$$\frac{C_j^{n+1} - C_j^n}{\Delta t} = D\left[\theta\frac{C_{j-1}^{n+1} - 2C_j^{n+1} + C_{j+1}^{n+1}}{\Delta x^2} + (1-\theta)\frac{C_{j-1}^n - 2C_j^n + C_{j+1}^n}{\Delta x^2}\right]$$

$$C_j^{n+1} - \frac{\lambda}{2}\theta\left(C_{j-1}^{n+1} - 2C_j^{n+1} + C_{j+1}^{n+1}\right) = C_j^n + \frac{\lambda}{2}(1-\theta)\left(C_{j-1}^n - 2C_j^n + C_{j+1}^n\right)$$

$$a_j C_{j-1}^{n+1} + b_j C_j^{n+1} + c_j C_{j+1}^{n+1} = d_j$$

$$\lambda = 2\frac{D\Delta t}{\Delta x^2}$$

$$a_j = -\theta\frac{\lambda}{2}$$

$$b_j = 1 + \theta\lambda$$

$$c_j = -\theta\frac{\lambda}{2}$$

$$d_j = C_j^n + \frac{\lambda}{2}(1-\theta)(C_{j-1}^n - 2C_j^n + C_{j+1}^n)2)\frac{\lambda}{2}C$$

Where

C = Chloride concentration

n = Time - step

j = Distance - step

Δt = Delta of time

Δx = Delta of distance

$\theta = 0.5$ (Semi-implicit)
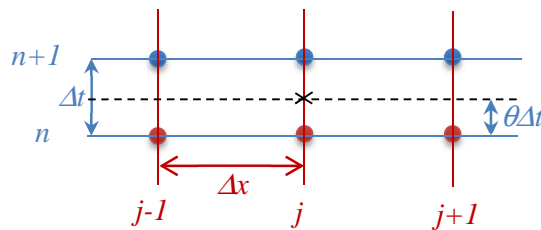
Figure 157 Crank-Nicolson method

As seen in the previous equations, the concentration of chlorides in the element is a function of chloride concentration at the surface, time, and depth. The solution of

the system allows calculation of chloride concentrations at different depths when varying time and chloride concentration at the surface. The number of iterations depends on the total period for the analysis and delta of time; each step or iteration is one delta of time, and based on the time there is a temperature and surface chloride concentration. Depending on these variables, the diffusion is affected as seen in the previous analysis (for constant time, temperature and surface chloride concentration). After the diffusion is calculated, the system is solved, finding the concentration variations depending on depth. In this case, the new chloride concentration is added to the previous value obtained in the last iteration.

The following is an example using the proposed initial equations and using the Crank-Nicolson method to solve the system (Figure 158); in this case, the concrete includes 50% FA without sodium sulfate. This example is presented to show the calculation procedure only. The comparison of results for different W/CM and fly ash levels using the programmed algorithm, Life 365 and test results is presented in section 7.3.6.

Reference age = 28 days

Analysis depth: 3 cm

W/CM: 0.45

Fly ash percentage: 50%

$\Delta t = 30 \ days = 2592000 \ seconds$

$\Delta x = 1 \ cm$

Temperature= Variable

C_0 = Variable

Chloride concentration for corrosion initiation = 0.05%
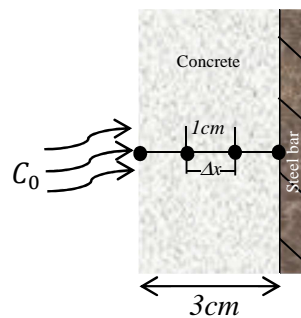
Figure 158 Concrete section

Figure 159 presents the monthly average temperature in a year; chloride concentration per month is presented in Figure 160.
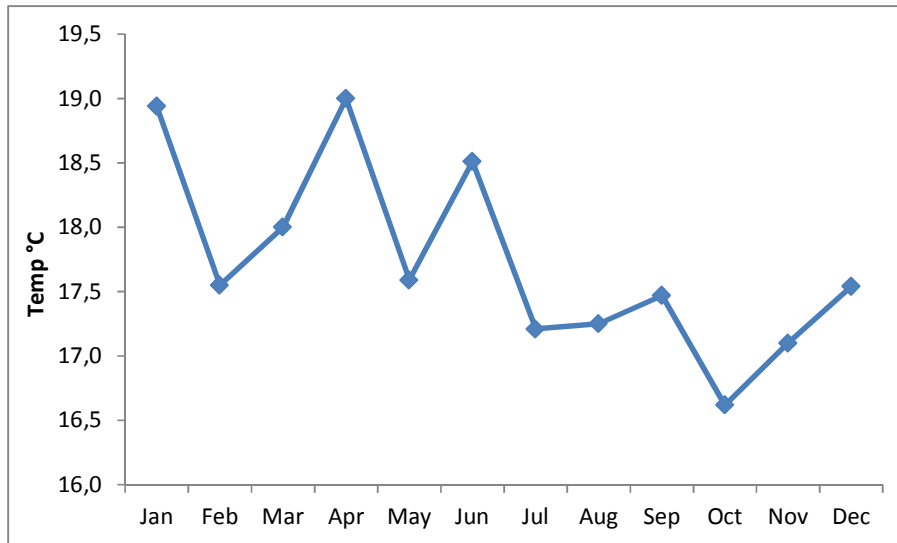
Figure 159 Monthly average temperature
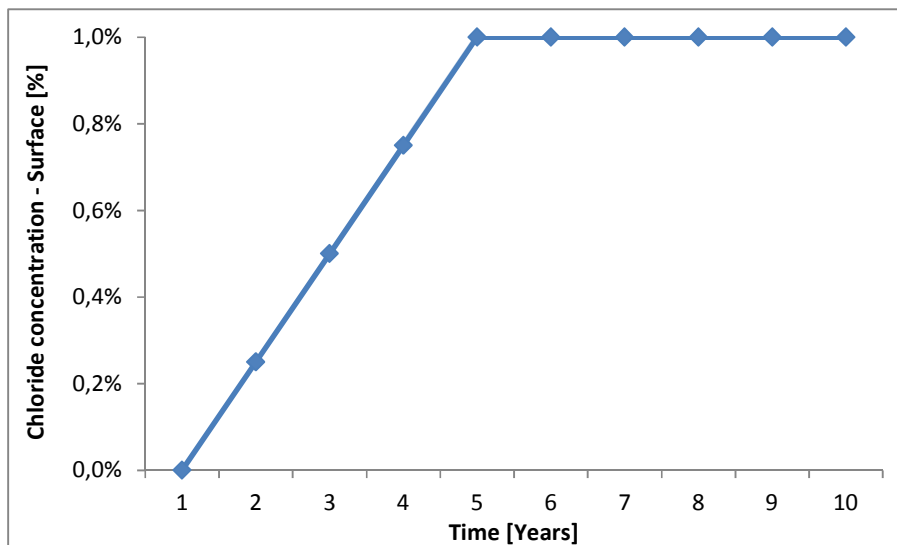
Figure 160 Chloride concentration per year

The following are the results for F, D_{28}, and m, based on the previous analysis:

Compressive strength calculation at 28 days

$$F = 27 \, MPa$$

Diffusion coefficient calculation at 28 days

$$D_{28} = 9.2 \times 10^{-12} \, m^2/s$$

Diffusion decay index calculation

$$m = 0.6971$$

These values are held constant for the rest of the analysis. The following values vary with time and distance; these values are for the first month.

Diffusion coefficient at 1 month

$$D = D_{ref} \left(\frac{t_{ref}}{t}\right)^m$$

$$D = 9.26 \times 10^{-12} \left(\frac{28}{30}\right)^{0.6971}$$

$$D = 8.8 \times 10^{-12} \, m^2/s$$

Diffusion coefficient change depending on the temperature

$$D(T) = D_{ref} exp\left[\frac{U}{R}\left(\frac{1}{T_{ref}} - \frac{1}{T}\right)\right]$$

$$D(18.9°C) = 8.8 \times 10^{-12} exp\left[\frac{35000}{8.3144621}\left(\frac{1}{293} - \frac{1}{292.05}\right)\right]$$

$$D(18.9°C) = 8.4 \times 10^{-12} \, m^2/s$$

Using the previous result, the calculation of the chloride content at different depths is performed:

$$a_j C_{j-1}^{n+1} + b_j C_j^{n+1} + c_j C_{j+1}^{n+1} = d_j$$

$$\lambda = 2\frac{D\Delta t}{\Delta x^2} = 2\frac{8.4 \times 10^{-12} \times 2592000}{0.01^2} = 0.4329$$

$$\theta = 0.5$$

$$a_j = -\theta\frac{\lambda}{2} = -0.5\frac{0.4329}{2} = -0.1082$$

$$b_j = 1 + \theta\lambda = 1 + 0.5 \times 0.4329 = 1.2165$$

$$c_j = -\theta\frac{\lambda}{2} = -0.5\frac{0.4329}{2} = -0.1082$$

$$d_j = C_j^n + \frac{\lambda}{2}(1-\theta)(C_{j-1}^n - 2C_j^n + C_{j+1}^n)$$

$C_{0cm}^{0month} = 0.25\%$ *Chloride concentration at the surface*

$C_{1cm}^{0month} = 0\%$ *Chloride concentration at 1cm*

$C_{2cm}^{0month} = 0\%$ *Chloride concentration at 2cm*

$C_{3cm}^{0month} = 0\%$ *Chloride concentration at 3cm*

$C_{4cm}^{0month} = 0\%$ *Chloride concentration at 4cm*

$$d_{1cm} = C_{1cm}^{0month} + \frac{\lambda}{2}(1-\theta)(C_{0cm}^{0month} - 2C_{1cm}^{0month} + C_{2cm}^{0month}) =$$

$$0 + \frac{0.4329}{2}(1-0.5)(0.25\% - 2\times0 + 0) = 2.7056\times10^{-4}$$

$$d_{2cm} = C_{2cm}^{0month} + \frac{\lambda}{2}(1-\theta)(C_{1cm}^{0month} - 2C_{2cm}^{0month} + C_{3cm}^{0month}) =$$

$$0 + \frac{0.4329}{2}(1-0.5)(0 - 2\times0 + 0) = 0$$

$$d_{3cm} = C_{3cm}^{0month} + \frac{\lambda}{2}(1-\theta)(C_{2cm}^{0month} - 2C_{3cm}^{0month} + C_{4cm}^{0month}) =$$

$$0 + \frac{0.4329}{2}(1-0,5)(0 - 2\times0 + 0) = 0$$

$$\begin{matrix} -0.1082C_{0cm}^{1month} & 1.2165C_{1cm}^{1month} & -0.1082C_{2cm}^{1month} = & 2.7056\times10^{-4} \\ -0.1082C_{1cm}^{1month} & 1.2165C_{2cm}^{1month} & -0.1082C_{3cm}^{1month} = & 0 \\ -0.1082C_{2cm}^{1month} & 1.2165C_{3cm}^{1month} & -0.1082C_{4cm}^{1month} = & 0 \end{matrix}$$

Replacing C_{0cm}^{1month} with 0.25% and C_{4cm}^{1month} with 0%:

$$\begin{matrix} -0.1082\times0.25\% & 1.2165C_{1cm}^{1month} & -0.1082C_{2cm}^{1month} = & 2.7056\times10^{-4} \\ -0.1082C_{1cm}^{1month} & 1.2165C_{2cm}^{1month} & -0.1082C_{3cm}^{1month} = & 0 \\ -0.1082C_{2cm}^{1month} & 1.2165C_{3cm}^{1month} & -0.1082\times0 = & 0 \end{matrix}$$

$$\begin{matrix} 1.2165C_{1cm}^{1month} & -0.1082C_{2cm}^{1month} & 0 = & 5.4106\times10^{-4} \\ -0.1082C_{1cm}^{1month} & 1.2165C_{2cm}^{1month} & -0.1082C_{3cm}^{1month} = & 0 \\ 0 & -0.1082C_{2cm}^{1month} & 1.2165C_{3cm}^{1month} = & 0 \end{matrix}$$

$$C_{1cm}^{1month} = 0.045\%$$

$$C_{2cm}^{1month} = 0.004\%$$

$$C_{3cm}^{1month} = 0.00036\%$$

The following are the results for the first year considering the previous procedure and using Matlab for the iterative process:

$$C_{1cm}^{12months} = 0.11\%$$

$$C_{2cm}^{12months} = 0.04\%$$

$$C_{3cm}^{12months} = 0.01\%$$

It is important to consider that every new analysis includes the chloride concentrations obtained in the previous iteration. The algorithm programmed with Matlab is presented in Appendix 3. This algorithm allows calculation of the end of the initiation period. After five years and eight months the initiation period ends and the propagation period starts (0.05% chloride concentration was reached at 3 cm depth). When the same input data are modelled using Life 365, the initiation period ends after one year and eight months.

$$C_{1cm}^{68months} = 0.44\%$$
$$C_{2cm}^{68months} = 0.16\%$$
$$C_{3cm}^{68months} = 0.05\%$$

7.3.6 Results comparison from programmed algorithm, Life 365 and test results

Life 365 software was used in order to evaluate results from the programmed algorithm. Additionally, Matlab results were compared with real values from chloride concentrations at 1 cm depth for samples left in 3% chloride concentration environment; unfortunately this chloride evaluation was performed after 28 and 90 days only. The following are the tables with the results from Matlab and Life 365. Table 23 does not include the comparison for mixes with sodium sulfate because Life 365 does not consider hybrid cementitious systems with activators. Table 24 presents chloride concentrations including mixes with sodium sulfate and comparing Matlab with real results from section 6.2.5.

Table 23 Results comparison: a) 0% FA, b) 20%, c) 50%

Parameters	0.483/TP/0/		0.557/TP/0/	
	Matlab	Life 365	Matlab	Life 365
Diffusion Coefficient at a reference age - D_{28} [m^2/s]	6.77×10^{-12}	1.26×10^{-11}	9.70×10^{-12}	1.89×10^{-11}
Diffusion decay index m	1.08	0.2	0.81	0.2
End of the initiation period [Months]	1	2.4	1	2.4

a)

Parameters	0.426/TP/20/		0.483/TP/20/		0.557/TP/20/	
	Matlab	Life 365	Matlab	Life 365	Matlab	Life 365
Diffusion Coefficient at a reference age - D_{28} [m^2/s]	4.25×10^{-12}	9.17×10^{-12}	6.85×10^{-12}	1.26×10^{-11}	1.27×10^{-11}	1.89×10^{-11}
Diffusion decay index m	0.92	0.36	0.80	0.36	0.64	0.36
End of the initiation period [Months]	1	2.4	1	2.4	1	2.4

b)

Parameters	0.426/TP/50/		0.483/TP/50/	
	Matlab	Life 365	Matlab	Life 365
Diffusion Coefficient at a reference age - D_{28} [m^2/s]	7.44×10^{-12}	9.17×10^{-12}	1.23×10^{-11}	1.26×10^{-11}
Diffusion decay index m	0.77	0.6	0.60	0.60
End of the initiation period [Months]	1	2.4	1	2.4

c)

It can be seen from the previous tables that Life 365 presented only three D_{28} values for all the evaluated mixes, while with the proposed algorithm, this parameter was different for each mix. Life 365 presented three different D_{28} values because it depends only on W/CM, as mentioned in the literature review. The proposed equations for the D_{28} in the algorithm vary depending on W/CM, fly ash content and compressive strength.

The diffusion decay indexes using Life 365 were different depending on the fly ash percentage; the equation used to calculate this parameter considers fly ash percentage as an input. These values were again different for each mix with Matlab; the diffusion decay index equation depends on fly ash percentage and W/CM. For all the cases, the end of the initiation period is the same for all the mixes. In the case of Life 365 the initiation period ends after 2.4 months while with Matlab it was 1 month.

In terms of chloride concentration, the following table presents the comparison between Matlab calculated values and real results from section 6.2.5. There are some similar results as seen for 0.483/TP/50/A mix. For most of the mixes the chloride concentration is higher using the proposed algorithm. The highest chloride concentration using the algorithm is for the mix 0.557/TP/20; in this case the real value is also high. As mentioned before, chloride concentration analysis includes information up to 3 months only, which does not allow conclusions about the accuracy of the model; thus, it is recommended to perform an additional comparison tracking chloride concentrations in the coming years.

Table 24 Results comparison: a) 0% FA, b) 20%, c) 50%, d) 50% + Na$_2$SO$_4$

Parameters	0.483/TP/0/		0.557/TP/0/	
	Matlab	**Real value**	**Matlab**	**Real value**
Chloride concentration 1 month @ 1 cm	0.030%	0.004%	0.050%	0.000%
Chloride concentration 3 months @ 1 cm	0.080%	0.024%	0.170%	0.008%

a)

Parameters	0.426/TP/20/		0.483/TP/20/		0.557/TP/20/	
	Matlab	**Real value**	**Matlab**	**Real value**	**Matlab**	**Real value**
Chloride concentration 1 month @ 1 cm	0.010%	0.000%	0.030%	0.007%	0.080%	0.001%
Chloride concentration 3 months @ 1 cm	0.040%	0.012%	0.1%	0.052%	0.280%	0.154%

b)

Parameters	0.426/TP/50/		0.483/TP/50/	
	Matlab	**Real value**	**Matlab**	**Real value**
Chloride concentration 1 month @ 1 cm	0.030%	0.000%	0.080%	0.060%
Chloride concentration 3 months @ 1 cm	0.110%	0.162%	0.270%	0.124%

c)

Parameters	0.426/TP/50/A		0.483/TP/50/A	
	Matlab	**Real value**	**Matlab**	**Real value**
Chloride concentration 1 month @ 1 cm	0.010%	0.053%	0.050%	0.048%
Chloride concentration 3 months @ 1 cm	0.040%	0.146%	0.160%	0.164%

d)

7.4 Summary

The following section includes a summary related to the carbonation and chloride models to predict the initiation period.

- The carbonation nomogram is a tool where all the variables are considered to obtain the carbonation depth or the initiation period. This tool was developed for a specific environment conditions presented in Bogotá ($CO_2 \approx 400$ppm, RH $\approx 60\%$). The model also considers concretes with 50% FA and sodium sulfate.

- The carbonation model includes compressive strength, W/CM and fly ash percentage as the main inputs to find the initiation period. It is evident that an increase in fly ash percentage reduces the initiation period significantly. For the case of concretes with 50% fly ash, the lowest W/CM does not help to level 0% FA and 20% FA performance. A carbonation depth of 40 mm is reached in 100 years with a concrete with 0% FA and W/CM of 0.71 or in 40 years with a concrete with 50% FA and sodium sulfate.

- The chloride diffusion model also considers different W/CM, fly ash percentages and a reference compressive strength. The continued hydration is considered by using the diffusion decay index. In this case, the diffusion decay index decreases when the fly ash percentage increases. Considering the same compressive strengths, the diffusion coefficient is lower for concretes with 50% FA and sodium sulfate than concretes with 0% FA and 20% FA.

- The initiation period using the chloride diffusion model can be increased by increasing fly ash percentage and keeping constant the compressive strength compared to 0% FA and 20% FA concretes; to keep the compressive strength constant it is important to reduce the W/CM for 50% FA and sodium sulfate concrete.

- An algorithm was needed to calculate the initiation period due to the required iterative process. This algorithm was programmed using Matlab. The inputs include W/CM, period of analysis, reinforcement depth, section width, x delta, time delta, temperature per month and surface chloride concentration per year. Chloride concentrations for different depths and the end of the initiation period are the outputs of the software.

8 CO_2 Emissions and Cost Comparison of the Activated Hybrid Cementitious Systems

8.1 Introduction

To give a complete assessment of the viability of sodium sulfate activated hybrid cementitious systems for the production of real-life mixed concrete, this chapter concentrates on CO_2 emissions and cost evaluation.

8.2 CO_2 emissions

The calculation of CO_2 emissions includes material production and delivery. The following is the input and output data presented in an Excel sheet. All the calculations for all the mix designs are included in Appendix 4; below are the values presented for the 0.557/TP/50/L/A mix (50% Temopaipa FA, W/CM of 0.557). It is important to mention that the CO_2 factors for cement and fly ash are based on *Cementos Argos* internal database. The CO_2 calculation considers a Bogotá delivery radius of 20 km. Recycled water is used in concrete production according to Colombian standard NTC 3459 *Agua para la elaboración de concreto*.

Mix design quantities

Mix design quantities	kg/m^3
Total cementitious material	316
Cement (10% slag)	158
Fly ash	158
Fine Aggregate	834
Coarse Aggregate	983
Admixtures (Plasticizer + superplasticizer + Sodium sulfate)	7.27
Water	175

CO₂ emission per material

Material	CO₂ [t/kg] / Materials	CO₂ [t/m³]	Source
Cement (10% slag)	7.22×10^{-4}	0.11408	
Fly ash		0.00221	
Fine Aggregate	4×10^{-6}	0.00334	
Coarse aggregate	4×10^{-6}	0.00393	Argos
Admixtures	2.2×10^{-4}	0.00160	
Recycled Water	0	0	

TOTAL CO₂ [t/m³]	0.1251554

Production

Item	Unit/m³	CO₂ [t/unit]	CO₂ [t/m³]	Source
Plant Diesel [l]	1.51	0.0032	0.004872	
Diesel for internal material transport [l]	0.38	0.0032	0.001218	Argos
Energy [kWh]	2.2	0.0005	0.0011594	

TOTAL CO₂ [t/m³]	0.0072494

Distribution and delivery

Item	Unit/m³	CO₂ [t/unit]	CO₂ [t/m³]	Source
Diesel [l]	3.41	0.0032	0.010962	Argos

TOTAL CO₂ [t/m³]	0.010962

Total CO₂ per 1 m³ of concrete (for 20 km radius)

TOTAL CO₂ [t/m³]	0.143
TOTAL CO₂ [kg/m³]	143.37

Figure 161 summarizes the total CO_2 emission for each mix design. As it is seen, the mix with the lowest W/CM and with 50 % of fly ash and sodium sulfate has a lower CO_2 emission compared to control mixes (100% cement and 20% fly ash) with

the highest W/CM. CO_2 emission decreases around 40%. Appendix 4 presents the Excel sheets for all the combinations. The analyses of CO_2 emissions linked to compressive strengths are included in section 8.4.
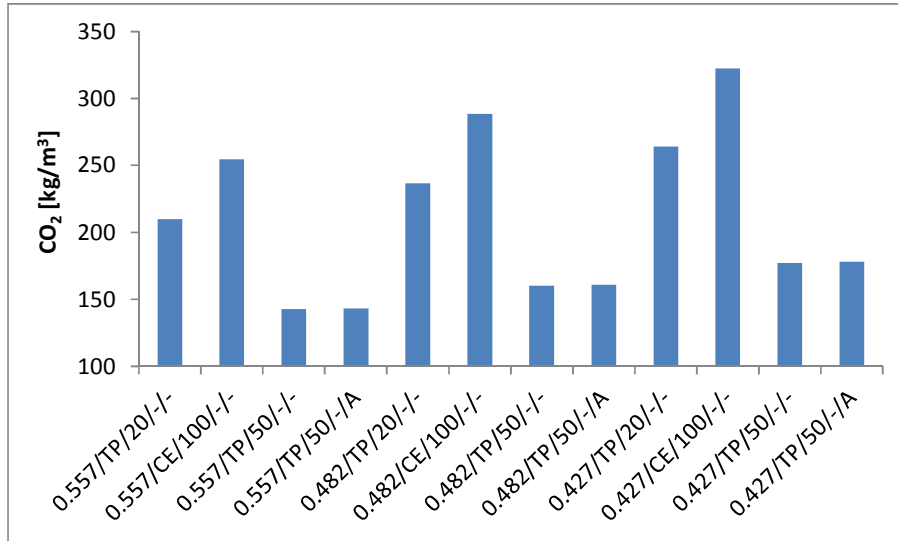
Figure 161 CO_2 emissions

8.3 Costs comparison

Table 25 presents the costs per cubic meter for mixes with W/CM = 0.557. Tables with the rest of the costs comparison are included in Appendix 5. These costs, in current values are initially presented in Colombian pesos and converted to US dollars and British pounds. The source of the costs per material is Argos.

Table 25 Costs evaluation for W/CM=0.557

Materials	Cost/kg	0.557/TP/20/-/-		0.557/CE/100/-/-		0.557/TP/50/-/-		0.557/TP/50/-/A	
		Quantity	Cost	Quantity	Cost	Quantity	Cost	Quantity	Cost
Cement [kg]	**$ 347.06**	253	$ 87,807	316	$ 109,672	158	$ 54,836	158	$ 54,836
Fly ash [kg]	**$ 104.48**	63	$ 6,582		$ 0	158	$ 16,508	158	$ 16,508
Fine aggregate 1 [kg]	**$ 54.71**	683	$ 37,364	696	$ 38,075	667	$ 36,488	667	$ 36,488
Fine aggregate 2 [kg]	**$ 30.50**	171	$ 5,216	174	$ 5,308	167	$ 5,094	167	$ 5,094
Coarse aggregate [kg]	**$ 54.71**	1003	$ 54,877	1013	$ 55,424	983	$ 53,783	983	$ 53,783
Water [kg]	**$ 8.50**	175	$ 1,488	175	$ 1,488	175	$ 1,488	175	$ 1,488
Admixture 1 (Lignosulfonate) [kg]	**$ 1,508.00**	1.42	$ 2,144	1.42	$ 2,144	1.42	$ 2,144	1.42	$ 2,144
Admixture 2 (Polycarboxylates) [kg]	**$ 6,403.00**	1.90	$ 12,140	1.90	$ 12,140	2.69	$ 17,198	2.69	$ 17,198
Activator (Sodium sulfate) [kg]	**$ 1,600.00**							3.16	$ 5,056
Cost [COP]		$	207,618	$	224,250	$	187,539	$	192,595
Cost $ [USD]		$	110	$	118	$	99	$	102
Cost £ [Pounds]		£	65	£	71	£	59	£	61

As it is seen in Figure 162, the increase in the fly ash replacement reduces the cost of the concrete, per cubic meter, by around 15%. Although the fact of including the activator increases the cost, these mixes are still lower in cost than control samples with 20% fly ash and 100% cement. Appendix 5 includes the cost evaluation for all the combinations. The analysis, including costs per MPa is presented in section 8.4
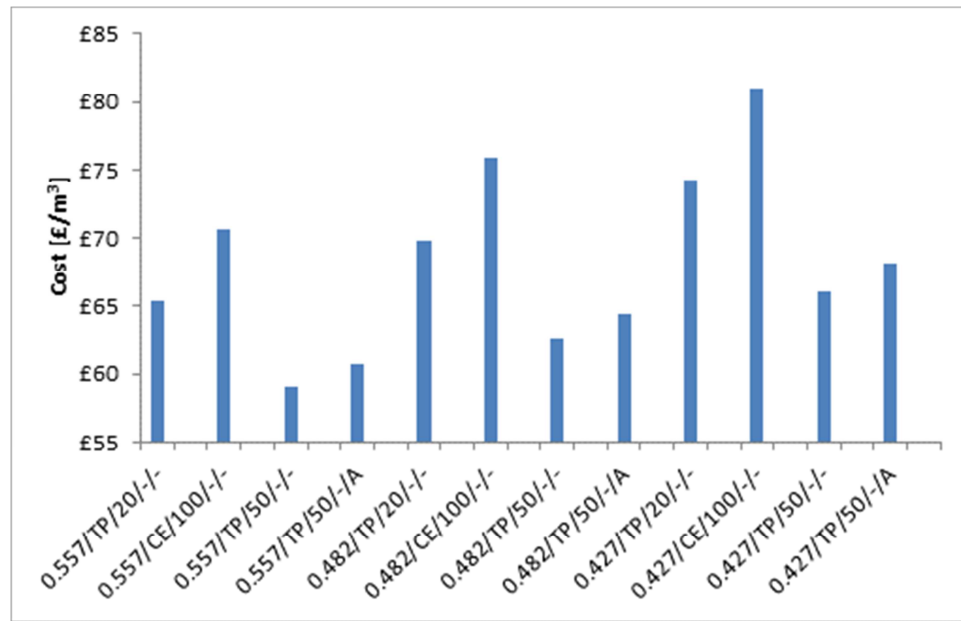
Figure 162 Cost comparison

8.4 CO_2 emissions and costs analysis

In order to make a realistic comparison of CO_2 emissions and costs, the following technical aspects must be considered. As presented in the previous sections of this work, the compressive strength is one of the main parameters to correlate with different performance indicators such as water permeability and diffusion coefficient. It was also mentioned that for the same compressive strength and increasing the level of fly ash replacement, concrete performance is improved in terms of permeability and chloride diffusion coefficient. One additional conclusion from the previous sections was the importance of reducing W/CM in order to improve the compressive strength for samples with fly ash. In this way, based on the previous conclusions and considering Figure 147 (Section 7.2.1), a mix with activator and a W/CM of 0.427 could reach the same compressive strength of a 20% fly ash mix with a W/CM of

0.482 or a 100% cement mix with a W/CM of 0.557. It is important to mention that compressive strengths at 28 days are normally specified for structural design.

After the previous technical considerations, it is important to analyse the CO_2 emissions and costs of the mix with the lowest W/CM and activator compared to the sample with 20% fly ash and W/CM of 0.482, and with 100% PC and W/CM of 0.557. These mixes have the same compressive strengths at 28 days. Table 26 includes these values to compare them. Although the CO_2 and cost levels for the mix with activator are for the lowest W/CM, they are still lower than the control samples with higher W/CM. The CO_2 levels are reduced from 25% to 30% compared to control mixes. In terms of costs, the savings are from £1.68 to £2.54 £/m^3. Among these three mixes, the highest values for costs and CO_2 emissions are for the mix with 100% cement and W/CM of 0.557.

Table 26 CO_2 emissions and costs analysis

Mix Code	CO_2 [kg/m^3]	Cost [£/m^3]
0.427/TP/50/-/A	178,00	68,10
0.482/TP/20/-/-	236,70	69,78
0.557/CE/100/-/-	254,60	70,64

Additionally, the efficiency curves presented in Figure 163 show how the binder, cost and CO_2 emissions behave in terms of compressive strength. It is important to highlight that these plots are based on 28 day compressive strength due to the fact of this being the parameter and age used in most concrete specifications. Although compressive strength at 28 days does not fully display the benefits of fly ash, not only in terms of compressive strength but also durability, this is the reference age for most concrete producers and constructors. The calculation considers the binder (kg), CO_2 (kg) or cost per m^3 per MPa.

Figure 163 (a) presents how, for low compressive strengths, higher amounts of binder per MPa are required as the fly ash percentage increases. Concrete with sodium sulfate reduces the amount of binder per MPa compared to mixes with 50% fly ash. On the other hand, as the compressive strength is increased the gap between 0% FA and 50% FA is reduced.

Figure 163 (b) shows how, for low compressive strengths, concretes with 0% FA are more expensive per MPa than samples with 50% FA. As the compressive strength increases, cost per MPa is similar for the different FA replacement levels. Most of the benefits of using high fly ash replacements and sodium sulfate are seen in Figure 163 (c). This figure presents how for the same compressive strength the lowest CO_2 emission per MPa is produced by mixes with 50% fly ash. Around 2 kg/(m^3·MPa) is the difference between samples with 0% FA and 50% FA. It can be seen that for all the cases, samples with 50% FA were always lower in CO_2 emissions per MPa at different compressive strength levels. For instance, for a compressive strength of 40 MPa, the difference is 1.87 kg/(m^3·MPa) between concretes with 50% fly + Na_2SO_4 and 0% FA. Although these curves considered how fly ash percentage, sodium sulfate, and compressive strength influenced CO_2 emissions, there are some other mix design parameters that may be considered: workability, superplasticisers and aggregates (Purnell and Black, 2012).
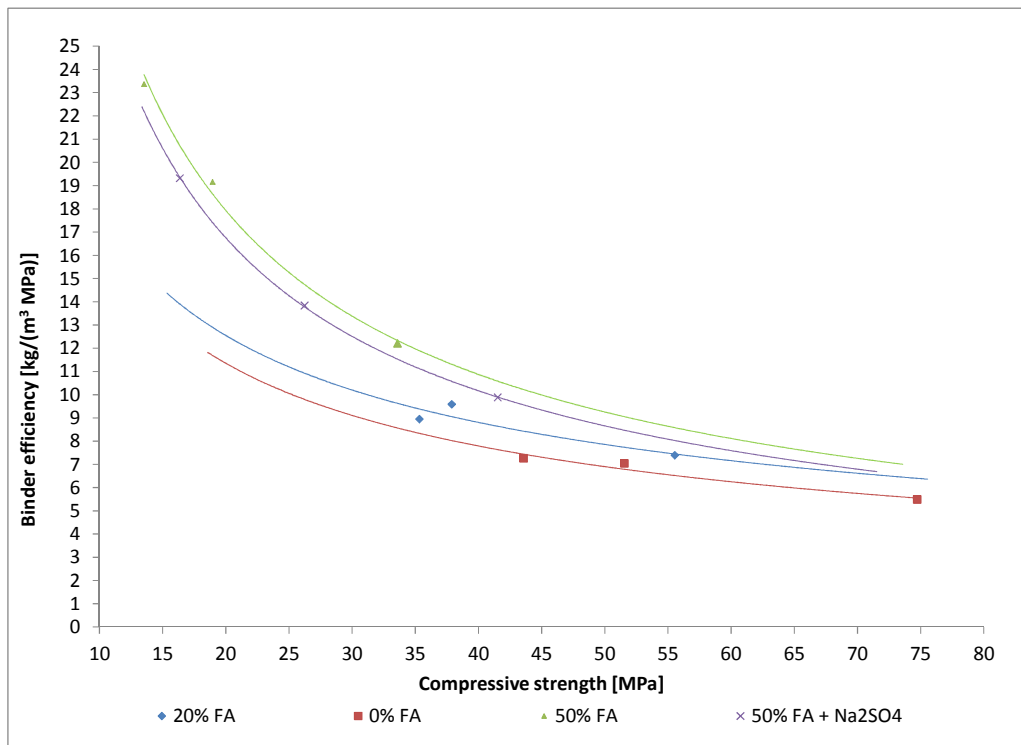
a) Binder
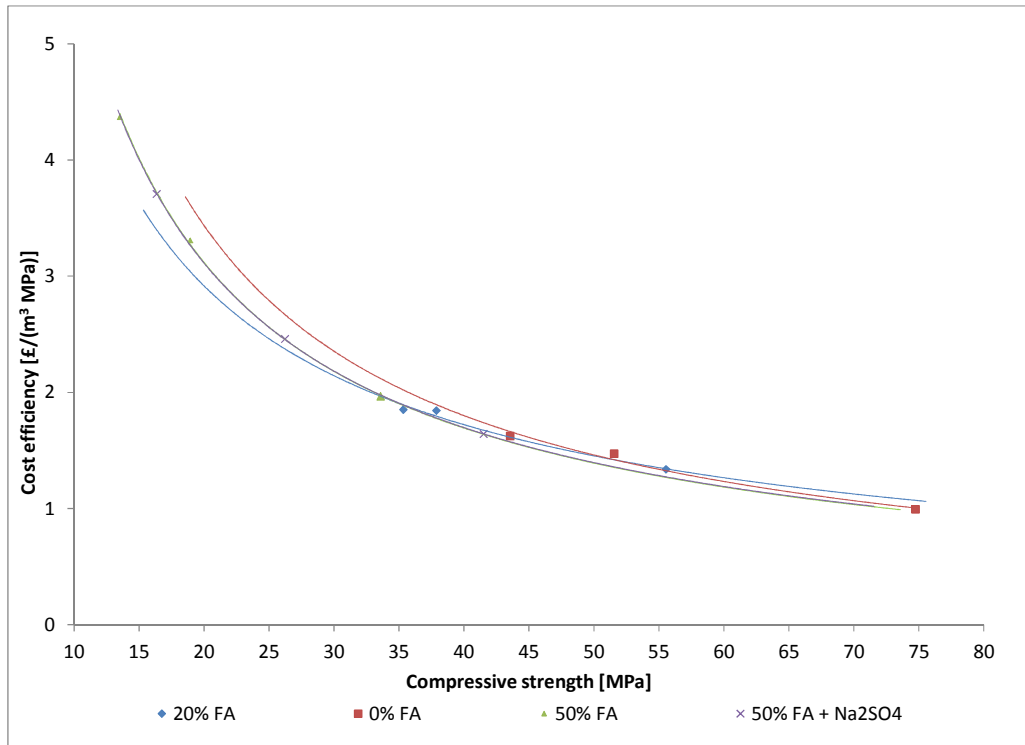
b) Cost
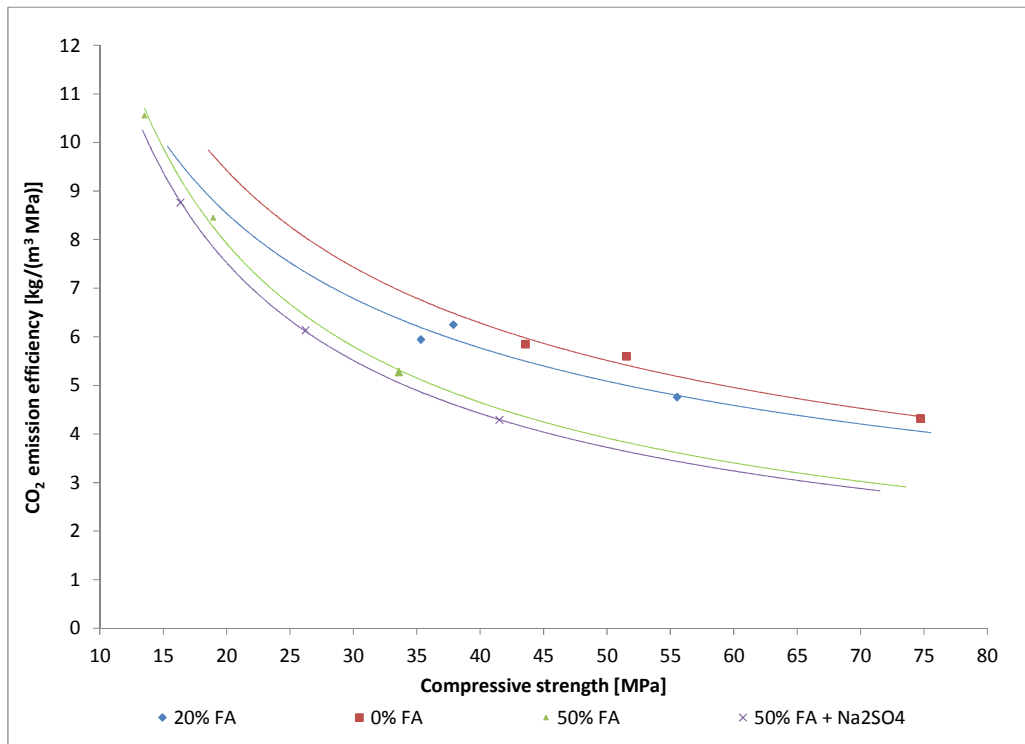
c) CO$_2$

Figure 163 Efficiency curves

8.5 Summary

The following is a summary of the analysis of CO_2 emissions and cost comparisons for a hybrid cementitious material with sodium sulfate:

- One of the main benefits of using this green alternative is the reduction of CO_2 emissions. When this concrete was compared to a 0% FA, it was evident that it is possible to achieve a reduction of 45%.

- When the comparison of CO_2 emissions was performed considering the same compressive strength, it was necessary to reduce the W/CM. Although the total cementitious content for the hybrid cementitious system was increased, CO_2 emissions were still lower by 25% in comparison to the control sample.

- When costs were compared, a reduction of 15% was obtained by using concrete with 50% FA and sodium sulfate. When costs were compared on equal compressive strength basis, the reduction was around 2-4% only.

- According to these results, concrete with 50% fly ash and sodium sulfate can be considered a sustainable alternative, as it can result in reducing the carbon foot-print significantly even when compared on a $kg/(m^3 \cdot MPa)$ basis.

9 Conclusions and Recommendations for Future Research

9.1 Introduction

The complete evaluation of the activated hybrid cementitious system using Colombian fly ash and sodium sulfate covered materials characterization, fresh and hardened concrete properties, and durability performance of laboratory and outdoor cured specimens. Additionally, models were used based on laboratory results to predict the service life (initiation period) of this concrete compared to control samples. Concrete elements (beams) were monitored and analysed simultaneously. The complete study ends with the impact on the environment and costs; CO_2 emissions and cost calculations were included and analysed in terms of compressive strength for the different fly ash percentages.

In this part, conclusions are presented based on the results obtained and analyses carried out in this study. Recommendations for future studies are also included, considering the need to obtain suitable alternatives to reduce CO_2 emissions.

9.2 Materials characterization and paste and mortar evaluation

According to the results, the amorphous content of fly ash was the most influential factor on the compressive strength for mixes with low fly ash content (20%) and without any activator. Fly ash composition was affected by increasing its fineness; the amorphous silica and LOI contents changed for different fineness. As the fineness increased the LOI content decreased; although the amorphous content changed as the fineness was increased, there was not a trend. The amorphous content increase improved the compressive strength; in some cases even when the particle size and the LOI content decreased, the compressive strength decreased, which occurred probably because the amorphous content was low. Depending on the initial amorphous content, fly ash may not need mechanical treatment to improve its reactivity for use in such high volume blends.

263

For mixes with activators, the effect of sodium sulfate in mixes with Termopaipa FA and Fabricato FA was significant at the initial stages of the reaction. The amount of ettringite and the accelerated portlandite consumption were reflected in the compressive strength evolution. On the other hand, sodium sulfate did not have the same effect on Termoguajira FA and Tampa FA; the amounts of ettringite and portlandite consumption were not as significant as those for the first two fly ashes. This was probably due to the higher amount of Fe_2O_3 present in Termoguajira and Tampa fly ashes.

In general, different activators were evaluated and mixes with sodium sulfate presented an acceptable behaviour compared to the control sample. In the case of the commercial fly ash (Tampa FA), it did not perform as expected, probably due to its high Fe_2O_3 content. Initially the low fineness of Termopaipa and Fabricato fly ash and their high LOI content were seen as possible activation problems but it was found that the main influencing factors were the reactive alumina and silica contents and the amount of Fe_2O_3.

The standards for fly ash for use in concrete need to change to enable innovation in construction materials, and hybrid activated systems need to be proposed. For instance, the ASTM C 618 does not include a minimum amorphous content value; the results of this investigation showed the importance of considering it. In the same way for activated systems, fly ash standards must include not only the amorphous content but also a low Fe_2O_3 value.

9.3   Fresh and hardened concrete properties

In the fresh state, the interaction between sodium sulfate, polycarboxylates and lignosulfonates did not have a negative effect. The initial slump was always as expected in the mix design (between 225 +/- 12.5 mm). In terms of slump loss, it was low (less than 12.5 mm). Air content was affected by the dosage of polycarboxylate. In mixes where polycarboxylate was increased, there was an increment in air content between acceptable ranges (1% - 3%). The setting time was also affected with a delay between 1 and 2 hours, influenced by the increase in the effective W/C, and the reaction between the activator sodium sulfate and the aluminium in the fly ash. This delay in terms of setting time for these mixes could be favourable for mass concrete

applications where due to the dimensions and the quantities of required concrete, as the amount of heat released is otherwise too high.

In the hardened state, the compressive strength of concrete was influenced by the curing process in mixes with sodium sulfate. Considering the proper curing, a W/CM of 0.483 for a mix with activator classifies for 24 MPa at 28 days which is equivalent to a W/CM of 0.675 for the control mix with 20% FA. It is important to highlight that samples with 50% FA and sodium sulfate have higher compressive strengths than samples with 50% FA but no sodium sulfate at the same W/CM. From plots of the W/CM vs compressive strength at 28 days for different fly ash replacement and sodium sulfate, concrete mix designs could be developed for different compressive strength specifications and applications.

Compressive strength values were lower using the maturity method compared to values obtained from testing cores and cylinders. It is important to mention that for the first time, maturity evaluation for a concrete with 50% fly ash and sodium sulfate was performed. The highest datum temperature was for concrete with sodium sulfate while the lowest was for 0% FA concrete. This shows the importance of a high curing temperature for concrete with 50% FA and sodium sulfate. According to maturity results, for elements exposed to low temperatures with an early de-moulding process, it is not recommended to use a concrete with 50% fly ash and sodium sulfate. On the other hand, this concrete is recommended for mass concrete such as dams or foundations.

Although most construction projects specify the compressive strength at 28 days, the benefits of using high volumes of fly ash are seen at a later age. In the case of some of the high compressive strength projects, mixes with high volume fly ash and sodium sulfate could be favourable if the target compressive strength is specified at 56 days. In terms of shrinkage, although samples with fly ash presented higher volume reductions probably due to the paste volume increment, there is not a high impact on this parameter compared to control samples; in fact, shrinkage values do not increase significantly after 112 days.

9.4 Durability properties

Mixes with fly ash and sodium sulfate were either comparable or superior to control concretes of the same W/CM in terms of water permeability and chloride diffusion coefficient, when water cured. Outdoor curing adversely affected the performance of the fly ash concretes. The reduction of the W/CM also reduces water permeability and diffusion coefficient. The initial and secondary sorptivity were mostly affected by the curing process; in this case, the W/CM did not play a significant role in reducing the values of this parameter. Carbonation rates were not favourable for mixes with sodium sulfate. Specimen expansions due to alkali silica reaction and sulfate attack were lower for mixes with sodium sulfate.

Most of the durability parameters correlate with the compressive strength; as this property increases, the results of durability evaluation are improved. By combining parameters such as the compressive strength, the curing type, fly ash percentage and activator, the durability prediction value is more accurate.

Water permeability, initial sorptivity, chloride penetration and diffusion coefficient are directly correlated with compressive strength and fly ash percentage for indoor and outdoor curing. In general, concrete behaviour is improved in terms of these parameters when the compressive strength and fly ash percentage increase, and there is an efficient curing process. For instance, for different fly ash percentages, among concretes with the same level of compressive strength and under the same curing, the lower values for water permeability, sorptivity, chloride penetration and diffusion coefficient are observed for samples with the highest fly ash content. It is important to consider that in the case where sodium sulfate is included, concrete performance is improved over that of corresponding concrete without activator.

Concrete elements allowed the evaluation of the durability correlations obtained from the laboratory and outdoors samples. Results obtained from the correlation equations were in agreement with those obtained from the concrete elements. In general, concrete with 50% fly ash and sodium sulfate at 360 days exhibits similar performance to that of the control samples with 20% fly ash in terms of water permeability, initial sorptivity, chloride penetration and diffusion coefficient. Although at early ages, durability performance for concretes with sodium sulfate did

not reach the levels of control samples with 0% and 20% fly ash, with time their performance is improved to the point of levelling the control sample with 20% fly ash at 360 days. For evaluation of concrete elements, the same water to cementitious material ratio was considered but as mentioned before, for concretes with activator the reduction of this parameter allowed improvement in its performance significantly.

The trends observed in the durability parameters mentioned above are not the same for concrete carbonation. In this specific case, the increase in fly ash percentage increases carbonation depth. Although the reduction in the water to cementitious material ratio reduces the carbonation coefficient, fly ash percentage has more impact on this parameter. Although concrete with sodium sulfate has lower carbonation coefficient compared to control concrete with 50% FA, it has high values compared to 0% FA and 20% FA concretes. Carbonation results for concrete elements with sodium sulfate were as negative as expected according to the correlation equations; results from these equations were similar to concrete element results.

Additional concrete elements were cast to test alkali silica reaction using 100% reactive aggregate in the matrix. The element with 0% FA exhibited the highest expansion and the lowest expansion found was for the element with fly ash and sodium sulfate. ASR was reduced due to the higher Al released by the fly ash. The total cement alkalis in concrete were reduced by including high volumes of fly ash.

Concrete beams left in a sulfate solution for 6 months presented expansions. In this case, concretes with 50% fly ash presented the lowest expansions due to the low total C_3A in the matrix. Finally, concrete was left in a chloride solution up to 90 days. Although chloride penetration was high at 90 days for concrete with fly ash and sodium sulfate, the effect of water to cementitious material ratio reduction was evident; obtaining a similar chloride penetration at 90 days comparing 50% fly ash and sodium sulfate concrete with 20% fly ash concrete.

Concretes with high volume fly ash and sodium sulfate, based on the results achieved, comply with specifications for concrete used in structures exposed to sea water; for instance, in the Colombian coastal zone different ports have been built in recent years and one of concrete specification requirements has been a diffusion

coefficient lower than 10×10^{-12} m^2/s. Water tanks and elements exposed to soils are some additional applications for this concrete; expansions for mortars exposed to sulfates lower than the limits mentioned by the ACI 318 are accomplished using the activated hybrid cementitious system. High reactive silica aggregate can be used with this concrete. On the other hand, elements exposed to high CO_2 concentrations or in high polluted cities should not be produced with this concrete due to its high carbonation coefficient values. For elements exposed to sea water or CO_2 emissions, it is important to calculate the initiation period based on the models presented not only in this study but also in the literature.

9.5   Initiation period

The model developed in this study is unique due to the inclusion of equations considering concrete with 50% fly ash and sodium sulfate. The chloride diffusion model considers a water to cementitious material ratio and a reference compressive strength at 28 days. The initial reference diffusion coefficient is calculated with the reference compressive strength using the correlation equations obtained in this study.

For this model, the reference diffusion coefficient is lower for 0% fly ash concrete than for 50% FA + Na_2SO_4 concrete when compared on the same water to cementitious material ratios (W/CM>0.32) basis. Concretes with 50% FA + Na_2SO_4 have lower reference diffusion coefficients compared to samples with 0% and 20% fly ash for the same reference compressive strength. In this model, the diffusion decay index decreases as the fly ash percentage increases, which is consistent with the experimental results obtained here, but reversed compared to much of the literature regarding the effect of fly ash addition on concrete ageing.

Although increasing the fly ash percentage for the same compressive strength increases the initiation period, in order to keep constant the compressive strength it is necessary to reduce the water to cementitious material ratio. For instance, most of the specifications to build concrete piles at ports specify a diffusion coefficient of 10×10^{-12} m^2/s at 28 days, and for this case concrete with 50% fly ash and sodium sulfate, and a compressive strength of 27 MPa allows this requirement to be accomplished. On the other hand, to accomplish this requirement using a concrete with 0% fly ash it is necessary to have a compressive strength higher than 48 MPa. To

268

obtain a compressive strength of 27 MPa with a 50% fly ash and sodium sulfate concrete, a W/CM of 0.48 is needed while for 48 MPa using a 0% fly ash concrete a W/CM of 0.54 is required. It is important to have the performance curves for the different fly ash levels to compare with technical specifications for different construction projects.

A carbonation model presented as a nomogram uses the water to cementitious material ratio and fly ash percentage to obtain the carbonation coefficient. The same as for the chlorides diffusion model, this nomogram is unique due to the inclusion of concrete with 50% fly ash and sodium sulfate. In the case of high fly ash percentage concretes, there is not a W/CM level to give a performance similar to that of 0% or 20% FA concretes.

The effect of the W/CM on each of the fly ash percentage levels is the same, having a similar slope in the plots of W/CM vs carbonation coefficient; this ends in parallel lines, where the distance between 0% FA concrete and 50% fly ash concrete with sodium sulfate is 5.7 mm/yr$^{1/2}$. For instance, according to the nomogram a carbonation depth of 40 mm is reached with a concrete with 0% fly ash and a W/CM of 0.71 in 100 years whilst the same depth of carbonation is achieved in 40 years for a concrete with 50% FA and sodium sulfate. This is based on Bogota´s environment conditions ($CO_2 \approx 400$ppm, RH $\approx 60\%$).

9.6 CO_2 emissions and cost comparison

The positive effect of including high volumes of fly ash in terms of CO_2 emissions and cost is evident from the analysis carried out. The reduction of CO_2 emissions is around 45%, almost half of what a concrete with 0% fly ash produces of the same water to cementitious material ratio. In terms of cost, there is a reduction of 15% comparing 0% FA concrete with 50% FA and sodium sulfate concrete. Although these comparisons are valid, it is important to consider that comparing concrete at the same compressive strength level shows the benefits of including high volumes of fly ash with sodium sulfate in terms of performance; this is possible by reducing the water to cementitious material ratio. In this way, the CO_2 reduction is from 25% to 30% for the same compressive strength when comparing 50% FA and sodium sulfate concrete with 0% and 20% FA concretes. In terms of cost, the reduction is from 2% to 4%.

The binder efficiency evaluation indicates that as the compressive strength is increased, the difference in the binder content between concrete with 0% fly ash and 50% fly ash and sodium sulfate is reduced; at some point, the amount of binder becomes similar to accomplish the same compressive strength. The reduction of CO_2 emissions is also evident in the concrete efficiency evaluation; in this case, when the same compressive strength is considered, the lowest emissions of CO_2 in kg/(m^3. MPa) are produced by concrete with 50% fly ash and sodium sulfate.

9.7 Future research

Following this research, a number of recommendations for future can be made:

- In the characterization of materials section, the influence of the amorphous content on compressive strength evolution was evident. It is necessary to develop more studies on the correlation between the amorphous content, fly ash fineness and compressive strength. Depending on these studies, the viability of including the amorphous content as a characterization parameter in international standards should be considered.

- In the evaluation of sodium sulfate with different fly ashes, fly ashes with higher iron oxide content presented a low reactivity. Therefore, it is important to develop studies on the effect of the iron content on the activation process.

- To reduce the setting time of hybrid cementitious system concretes activated with sodium sulfate. Although setting time increment was not high, it is important to evaluate what exactly is influencing this setting time increment and how to reduce it.

- Based on maturity evaluation, the T_0 value was higher for concrete with sodium sulfate. According to these results, it is important to research on the parameters influencing datum temperature. A reduction in datum temperature could help make this concrete suitable for early demoulding applications in places with a

mild average temperature such as 18°C (Bogotá's average temperature), or under UK conditions.

- To study different alternatives to reduce carbonation coefficient for concretes with high fly ash content, as it was found that there was a significant carbonation in concretes exposed to 400 ppm CO_2 (Bogotá's conditions) with critical reductions in the initiation periods.

- To continue monitoring the concrete elements left outdoors and to start a new study where the obtained correlations are evaluated at 3, 5, 7 and 10 years. For this study, it is important to evaluate element cores and include petrography, especially for elements with reactive aggregate.

References

Aït-Mokhtar A., Belarbi R., Benboudjema F., Burlion N., Capra B., Carcassès M., Colliat J.B., Cussigh F., Deby F., Jacquemot F., de Larrard T., Lataste J.F., Le Bescop P., Pierre M., Poyet S., Rougeau P., Rougelot T., Sellier A., Séménadisse J., Torrenti J. M., Trabelsi A., Turcry P., Yanez-Godoy H., 2013. *Experimental investigation of the variability of concrete durability properties*. Cement and Concrete Research. Vol. 45, pp. 21-36.

Amnadnua K., Tangchirapat W., Jaturapitakkul C., 2013. *Strength, water permeability and heat evolution of high strength concrete made from the mixture of calcium carbide residue and fly ash*. Materials and Design, Vol. 51, pp. 894-901.

Antiohos S., Papageorgiou, A., Papadakis V., Tsimas S., 2007. *Influence of quicklime addition on the mechanical properties and hydration degree of blended cements containing different fly ashes*. Construction and Building Materials, Vol. 22, pp. 1191-1200.

ACI 211.1, 2002. *Standard Practice for Selecting Proportions for Normal, Heavyweight, and Mass Concrete*. ACI Committee 211. Farmington Hills, MI, USA.

ACI 232.2, 2003. *Use of Fly Ash in Concrete*. ACI Committee 232. Farmington Hills, MI, USA.

ACI 318-08, 2008. *Building Code Requirement for Structural Concrete (ACI 318-08) and Commentary*. ACI Committee 318. Farmington Hills, MI, USA.

ACI 361.1, 2000. *Service-Life Prediction*. ACI Committee 365. Farmington Hills, MI, USA.

ASTM C 39/C 39 M – 09, 2009. *Standard Test Method for Compressive Strength of Cylindrical Concrete Specimens*. ASTM International, West Conshohocken, PA, USA.

ASTM C 109/C 109M – 08, 2008. *Standard Test Method for Compressive Strength of Hydraulic Cement Mortars*. ASTM International, West Conshohocken, PA, USA.

ASTM C 143 – 10, 2010. *Standard Test Method for Slump of Hydraulic-Cement Concrete*. ASTM International, West Conshohocken, PA, USA.

ASTM C 150/C 150M – 09, 2009. *Standard Specification for Portland Cement.* ASTM International, West Conshohocken, PA, USA.

ASTM C 157/C 157M – 08, 2008. *Standard Test Method for Length Change of Hardened Hydraulic-Cement Mortar and Concrete.* ASTM International, West Conshohocken, PA, USA.

ASTM C 231/C 231M – 09, 2009. *Standard Test Method for Air Content of Freshly Mixed Concrete by the Pressure Method.* ASTM International, West Conshohocken, PA, USA.

ASTM C 311 – 07, 2007. *Standard Test Method for Sampling and Testing Fly Ash or Natural Pozzolans for Use in Portland-Cement Concrete.* ASTM International, West Conshohocken, PA, USA.

ASTM C 403/C 403 M – 08, 2008. *Standard Test Method for Time of Setting of Concrete Mixtures by Penetration Resistance.* ASTM International, West Conshohocken, PA, USA.

ASTM C 618 – 08, 2008. *Standard Specification for Coal Fly Ash and Raw or Calcined Natural Pozzolan for Use in Concrete.* ASTM International, West Conshohocken, PA, USA.

ASTM C 1012 – 09, 2009. *Standard Test Method for Length Change of Hydraulic-Cement Mortars Exposed to a Sulfate Solution.* ASTM International, West Conshohocken, PA, USA.

ASTM C 1074 – 04, 2004. *Standard Practice for Estimating Concrete Strength by the Maturity Method.* ASTM International, West Conshohocken, PA, USA.

ASTM C 1202 – 10, 2010. *Standard Test Method for Electrical Indication of Concrete's Ability to Resist Chloride Ion Penetration.* ASTM International, West Conshohocken, PA, USA.

ASTM C 1260 – 07, 2007. *Standard Test Method for Potential Alkali Reactivity of Aggregates (Mortar-Bar Method).* ASTM International, West Conshohocken, PA, USA.

ASTM C 1585 – 04, 2004. *Standard Test Method for Measurement of Rate of Absorption of Water by Hydraulic-Cement Concretes*. ASTM International, West Conshohocken, PA, USA.

Atiş C.D., 2002. *Heat evolution of high volume fly ash concrete*. Cement and Concrete Research, Vol. 32, pp. 751-756.

Atiş C.D., 2005. *Strength properties of high volume fly ash roller compacted and workable concrete, and influence of curing condition*. Cement and Concrete Research, Vol. 35, pp. 1112-1121.

Armaghani J.M., Larsen T.J., Romano D.C., 1992. *Aspects of concrete strength and durability*. Transportation Research Record. Vol. 1335, pp. 63-69.

Aydin S., 2013. *A ternary optimization of mineral additives of alkali activated cement mortars*. Construction and Building Materials. Vol. 43, pp. 131-138.

Bakharev T., 2005. *Resistance of geopolymer materials to acid attack*. Cement and Concrete Research, Vol. 35, pp. 658-670.

Bakharev T., 2005. *Durability of geopolymer materials in sodium and magnesium sulfate solutions*. Cement and Concrete Research, Vol. 35, pp. 1233-1246.

Bakharev T., Sanjayan J.G., Cheng Y.B., 2000. *Effect of admixtures on properties of alkali-activated slag concrete*. Cement and Concrete Research, Vol. 30, pp. 1367-1374.

Bakker R.F.M., 1988. *Initiation period*. In: Schiessl P., editor. Corrosion of Steel in Concrete. RILEM/Chapman and Hall, New York, pp. 22 – 55.

Baroghel-Bouny V., Kinomura K., Thiery M., Moscardelli S., 2011. *Easy assessment of durability indicators for service life prediction or quality control of concretes with high volumes of supplementary cementitious materials*. Cement and Concrete Composites. Vol. 33, pp. 832-847.

Basheer L., Kropp J., Cleland D. 2001. *Assessment of the durability of concrete from its permeation properties: a review*. Construction and Building Materials, Vol. 15, pp. 93-103.

Bentz D.P., Clifton J.R., Ferraris C.F., and Garboczi E.J. 1999. *Transport Properties and Durability of Concrete: Literature Review and Research Plan*, NISTIR 6395, U.S. Department of Commerce, Gaithersburg, MD, USA.

Bernal S.A., Mejía de Gutierrez R., Provis J.L., 2012. *Engineering and durability properties of concretes based on alkali-activated granulated blast furnace slag/metakaolin blends.* Construction and Building Materials. Vol. 33, pp. 99-108.

Bernal S.A., Mejía de Gutierrez R., Provis J.L., Rose V., 2010. *Effect of silicate modulus and metakaolin incorporation on the carbonation of alkali silicate-activated slags.* Cement and Concrete Research. Vol. 40, pp. 898-907.

Bernal S., Mejía de Gutierrez R., Delvasto S., Rodriguez E., 2010. *Performance of an alkali-activated slag concrete reinforced with steel fibers.* Construction and Building Materials. Vol. 24, pp. 208-214.

Boddy A., Hooton R.D., Gruber K.A., 2001. *Long-term testing of chloride – penetration resistance of concrete containing high-reactive metakaolin.* Cement and Concrete Research. Vol. 31, pp. 759-765.

Bouzoubaa N., Zhang M.H., Malhotra V.M., 2001. *Mechanical properties and durability of concrete made with high-volume fly ash blended cements using a coarse fly ash.* Cement and Concrete Research. Vol. 31, pp. 1393-1402.

BS EN 197-1:2011 Cement Part 1: *Composition, specifications and conformity criteria for common cements*, London, British Standard Institution.

Building Research Establishment, 1997. *Design of normal concrete mixes.* BRE Press. Second edition. Watford, UK.

Burden D., 2006. *The durability of concrete containing high levels of fly ash.* Thesis (MSc). University of New Brunswick, Canada.

Castellote M., Fernandez L., Andrade C., Alonso C., 2009. *Chemical changes and phase analysis in carbonated OPC paste at different CO_2 concentrations*. Materials and Structures. Vol. 42, pp. 515-525.

CEB, 1997. *New approach to durability design – an example for carbonation induced corrosion.* CEB Bulletin d'information N° 238, Lausanne, Switzerland.

Chareerat T., 2002. *A study on pore volume and physical properties of ordinary Portland cement containing classified fly ash.* M.E. Thesis, Khon Kaen University, Thailand.

Chi M., Huang R., 2013. *Binding mechanism and properties of alkali-activated fly ash/slag mortars*. Construction and Building Materials. Vol. 40, pp. 291-298.

Chindaprasirt P., Homwuttiwong S., Sirivivatnanon V., 2004. *Influence of fly ash fineness on strength, drying shrinkage and sulfate resistance of blended cement mortar*. Cement and Concrete Research, Vol. 34, pp. 1087-1092.

Chindaprasirt, P., Ruangsiriyakul S., Cao H.T., Bucea L., 2001. *Influence of Mae Moh fly ash fineness on characteristics, strength and drying shrinkage development of blended cement mortars*. The Eigth East Asia-Pacific Conference on Structural Engineering and Construction, Singapore. Paper No. 1191.

Claisse P., 2005. *Transport properties of concrete*. Concrete International. January, pp. 43-48.

Collepardi M., Marcialis A., Turriziani R., 1972. *Penetration of chloride ions into cement pastes and concretes* Journal of the American Ceramic Society, Vol. 53, pp. 534-535.

Collins F., Sanjayan, J.G., 1999. *Strength and shrinkage properties of alkali-activated slag concrete containing porous coarse aggregate*. Cement and Concrete Research, Vol. 29, pp. 607-610.

Collins F., Sanjayan, J.G., 1999. *Workability and mechanical properties of alkali activated slag concrete*. Cement and Concrete Research, Vol. 29, pp. 455-458.

Conciatori D., Sadouki H., Brühwiler E. 2008. *Capillary suction and diffusion model for chloride ingress into concrete*. Cement and Concrete Research. Vol. 38, pp. 1401-1408.

Conciatori D., 2005. *Effect of microclimate on the corrosion initiation of steel reinforcement in reinforced concrete structures*. Thesis (PhD). Ecole Polytechnique Fédérale de Lausanne, Switzerland.

Crank J., 1975. *The mathematics of diffusion*. Clarendon Press. Oxford, England.

Crank J., Nicolson P., 1947. *A practical method for numerical evaluation of solutions of partial differential equations of the heat conduction type.* Proceedings of the Cambridge Philosophical Society. Vol. 43, pp. 50-67.

Criado M., Fernández Jiménez A., Palomo A., 2010. *Effect of sodium sulfate on the alkali activation of fly ash.* Cement and Concrete Composites, Vol. 32, pp. 589-594.

Criado M., Palomo A., Fernández-Jimenez A., 2005. *Alkali activation of fly ashes. Part 1: Effect of curing conditions on the carbonation of the reaction products.* Fuel, Vol. 84, pp. 2048-2054.

Daimon M., Akira T., Konido R., 1971. *Through pore size distribution and kinetics of the carbonation reaction of Portland cement mortars.* Journal of the American Ceramic Society. Vol. 54, pp. 423-428.

Davidovits J., 1994. *Properties of geopolymer cements.* Proceedings of the First International Conference on Alkaline Cements and Concretes. Scientific Research Institute on Binders and Materials, Kiev State Technical University. Kiev, Ukraine. pp 131-149.

Davidovits J., 1981. *Synthetic mineral polymer compound of the silicoaluminates family and preparation process.* US Patent 4,472,199.

Davidovits J., 1994. *Global warming impacts on the cement and aggregate industries.* World Resource Review, Vol. 6, pp. 263.

Davis R.E., Carlson R.W., Kelly J.W., and Davis H.E., 1937. *Properties of cements and concretes containing fly ash.* Journal of the American Concrete Institute, Vol 33, pp. 577-612.

De Belie N., Verselder H.J., Blaere B.D., Nieuwenburg D.K., Verschoore R., 1996. *Influence of the cement type on the resistance of concrete to feed acids.* Cement and Concrete Research, Vol. 26, pp. 1717-1725.

Deby F., Carcassès M., Sellier A., 2009. *Simplified models for the engineering of concrete formulations in a marine environment through a probabilistic method.* European Journal of Environmental and Civil Engineering. Vol. 16, pp. 362-374.

Deschner F., Winnefeld F., Lothenbach B., Seutert S., Schwesig P., Dittrich S., Goetz-Neunhoeffer F., Neubaeur J., 2012. *Hydration of Portland cement with high replacement by siliceous fly ash*. Cement and Concrete Research, Vol. 42, pp. 1389-1400.

Detwiler, R., 2002. *Document of Procedures for PCA's ASR Guide Specification*. Portland Cement Association, SN 2407, Skokie, IL, USA.

Dinakar P., Babu K., Santhanam M., 2008. *Durability properties of high volume fly ash self compacting concretes*. Cement and Concrete Composites, Vol. 30, pp. 880-886.

Ditao N., 2003. *Durability and lifeforecast of reinforced concrete*. Beijing: Science Press.

Donatello S., Fernández-Jimenez A., Palomo A., 2013. *Very high volume fly ash cements. Early age hydration study using Na_2SO_4 as an activator.* Journal of the American Ceramic Society, Vol. 96, pp. 900-906.

Donatello S., Maltseva, Fernández-Jimenez A., Palomo A., 2014. *The early age hydration reactions of a hybrid cement containing a very high content of coal bottom ash.* Journal of the American Ceramic Society, Vol. 97, pp. 929-937.

Donatello S., Palomo A., Fernández-Jimenez A., 2013. *Durability of very high volume fly ash cement pastes and mortars in aggressive solutions.* Cement and Concrete Composites, Vol. 38, pp. 12-20.

Duxson P., Fernández-Jiménez J., Provis J.L., Lukey G.C., Palomo A., Van Deventer J.S.J., 2007. *Geopolymer technology: current state of the art*. Journal of Materials Science, Vol. 42, pp. 2917-2933.

Duxson P., Mallicoat S.W., Lukey G.C., Kriven W.M., Van Deventer J.S.J., 2007. *The effect of alkali and Si/Al ratio on the development of mechanical properties of metakaolin-based geopolymers*. Colloids and Surfaces A: Physicochemical and Engineering Aspects. Vol. 292, pp. 8-20.

EHE, 2008. *ANEJO 9° Consideraciones Adicionales sobre Durabilidad*. La Instrucción Española del Hormigón Estructural, Madrid, Spain.

Erdogdu K., Turker P., 1998. *Effects of fly ash particle size on strength of Portland Cement fly ash mortars*. Cement and Concrete Research. Vol. 28, pp. 1217-1222

Freeman E., Gao Y., Hurt R., Suuberg E., 1997. *Interaction of carbon – containing fly ash with commercial air – entraining admixtures for concrete*. Fuel, Vol. 76, pp. 761-765.

Felekoglu B., 2006. *Utilisation of Turkish fly ashes in cost effective HVFA concrete production*. Fuel, Vol. 85, pp. 1944-1949.

Fernández-Jimenez A., Garcia-Lodeiro I., Palomo A., *Durability of alkali-activated fly ash cementitious materials*. Journal of Materials Science, Vol. 42, pp. 3055-3065.

Fernández-Jimenez A., Palomo A., 2003. *Characterization of fly ashes. Potential reactivity as alkaline cements.* Fuel, Vol. 82, pp. 2259-2265.

Fernández-Jimenez A., Palomo A., 2005. *Composition and microstructure of alkali activated fly ash binder: Effect of the activator.* Cement and Concrete Research, Vol. 35, pp. 1984-1992.

García-Lodeiro I., Palomo A., Fernández-Jiménez A., 2007. *Alkali-aggregate reaction in activated fly ash systems*. Cement and Concrete Research, Vol. 37, pp. 175-183.

García-Lodeiro I., Palomo A., Fernández-Jiménez A., Macphee D., 2010. *Effect of calcium additions on N-A-S-H cementitious gels*. Journal of the American Ceramic Society, Vol. 93, pp. 1934-1940.

García-Lodeiro I., Palomo A., Fernández-Jiménez A., Macphee D., 2011. *Compatibility studies between N-A-S-H and C-A-S-H gels. Study in the ternary diagram Na_2O-CaO-Al_2O_3-SiO_2-H_2O*. Cement and Concrete Research, Vol. 41, pp. 923-931.

Garcia T., 2004. *Modelos de predicción de vida útil y metodologías de evaluación de estructuras de hormigón frente a la corrosión de armaduras – análisis crítico.* XVI Curso de Estudios Mayores de la Construcción. Madrid, Spain.

Garboczi E.J., 1990. *Permeability, diffusivity, and micro-structuralparameters. A critical review*. Cement and Concrete Research. Vol. 20, pp. 591-601.

Ge Z., Wang K., 2007. *Properties of ternary cement concrete under various curing conditions*. CBM-CI International Workshop. Karachi, Pakistan.

Glukhovsky, V.D., 1959. *Soil silicates.* Budivelnik Publisher. Kiev, USSR.

Green C., Nanukuttan S., Basheer M., 2012. *Assessing the service life of a structure using performance indicators: a review of service life models and input parameters*. Proceedings of the 3rd International Conference on the Durability of Concrete Structures. Paper number SLM9. Belfast, UK.

Guimaraes A.T.C., Helene P.R.L., 2005. *Diffusion of Chloride Ions in Unsaturated Concrete: Forecast of Service Life in a Wet-Dry Environment*. ACI Special Publication, Vol. 229, pp. 175–194.

Güneyisi E., Gesoglu M. Pürsünlü Ö., Mermedas K., 2013. *Durability aspect of concretes composed of cold bonded and sintered fly ash lightweight aggregates*. Composites: Part B. Vol. 53, pp. 258-266.

Haiyan Z., Duoduo B., Zhengzhong W., 2006. *A model for forecasting carbonization depth of Concrete*. Journal of Wuhan University. Vol. 39, pp. 42-45.

Hall C., 1981. *Water movement in porous building materials - IV. The initial surface absorption and the sorptivity*. Building and Environment, Vol. 16, pp. 201-207.

Hall C., Tse T.K.M., 1986. *Water movement in porous building materials - VII. The sorptivity of mortars*. Building and Environment, Vol. 21, pp. 113-118.

Hannesson G., Kuder K., Shogren R., Lehman D., 2012. *The influence of high volume of fly ash and slag on the compressive strength of self-consolidating concrete*. Construction and Building Materials, Vol. 30, pp. 161-168.

Hansson C.M., Berke N.S., 1989. *Chlorides in concrete*, in: L.R. Roberts, J.P. Skalny (Eds.), Pore Structure and Permeability of Cementitious Materials. Materials Research Society Symposium Proceedings. Vol. 137, pp. 253-270.

He R., Jia H., 2011. *Carbonation depth prediction of concrete made with fly ash*. Electronic Journal of Geotechnical Engineering. Vol. 16, pp. 605-614.

Helene P., Castro-Borges P., 2009. *A novel method to predict concrete carbonation.* Cemento y Concreto – Investigación y Desarrollo. Vol 1, pp. 25-35.

Hermida G., Velandia D., 2012. *Alkaline activators effect over mechanical properties and water penetration in concrete with fly ash.* Concrete with Smart Additives and Supplementary Cementitious Materials Symposium - XXI International Materials Research Congress, Cancun, Mexico.

Herrera A., Juárez C., Valdez P., Bentz D., 2011. *Evaluation of sustainable high-volume fly ash concretes.* Cement and Concrete Composites, Vol. 33, pp. 39-45.

Ho D.W.S, Lewis R.K., 1987. *Carbonation of concrete and its prediction.* Cement and Concrete Research, Vol. 17, pp. 489-504.

Ismail I., Bernal S.A. Provis J.L., San Nicolas R., Brice D.G., Kilcullen A.R., Hamdan S., Van Deventer J.S.J., 2013. *Influence of fly ash on the water and chloride permeability of alkali-activated slag mortars and concretes.* Construction and Building Materials, Vol. 48, pp. 1187-1201.

Ismail I., Bernal S.A., Provis J.L., Hamdan S., van Deventer J.S.J., 2013. *Drying-induced changes in the structure of activated pastes.* Journal of Materials Science, Vol. 48, pp. 3566-3577.

Ismail I., Bernal S.A, Provis J.L., Hamdan S., van Deventer J.S.J., 2013. *Microstructural changes in alkali activated fly ash/slag geopolymers with sulfate exposure.* Materials and Structures, Vol. 46, pp. 361-373.

Khatri R.P., Sirivivatnanon V., 1997. *Methods of deterioration of water permeability of concrete.* ACI Materials Journal. Vol. 94, pp. 1105-1114.

Kosmatka S., Kerkhoff B., Panarese W., 2003. *Design and Control of Concrete Mixtures.* Portland Cement Association. Fourteenth Edition.

Kumar S., Kumar R., 2011. *Mechanical activation of fly ash: Effect on reaction, structure and properties of resulting geopolymer.* Ceramics International, Vol. 37, pp. 533-541.

Kumar R., Kumar S., Mehrotra S.P., 2007. *Towards sustainable solutions for fly ash through mechanical activation*. Resources Conservation & Recycling, Vol. 52, pp. 157-179.

Kühl, H., 1908. *Slag cement and process of making the same.* U.S. Patent 900,939.

Lazniewska-Piekarczyk B., 2014. *The methodology for assessing the impact of new generation superplasticizers on air content in self-compacting concrete*. Construction and Building Materials, Vol. 53, pp. 488-502.

Lange A., Plank J., 2012. *Study on the foaming behavior of allyl ether-based polycarboxylate superplasticizers*. Cement and Concrete Research, Vol. 42, pp. 484-489.

Lee C.Y., Lee H.K., Lee K.M., 2003. *Strength and microstructural of chemically activated fly ash-cement systems.* Cement and Concrete Research, Vol. 33, pp.425-431.

Lee S.H., Sakai E., Diamond M., Bang W.K., 1999. *Characterization of fly ash directly from electrostatic precipitator*. Cement and Concrete Research, Vol. 29, pp. 1791-1797.

Lee, W.K.W. and van Deventer, J.S.J., 2002. *Effects of anions on the formation of aluminosilicate gel in geopolymers*. Industrial and Engineering Chemistry Research, Vol. 41, pp. 4550-4558.

Lee, W.K.W. and van Deventer, J.S.J., 2002. *The effect of ionic contaminants on the early-age properties of alkali-activated fly ash-based cements*. Cement and Concrete Research, Vol. 32, pp. 577-584.

LNEC E-465. *Concrete prescriptive methodology to estimate concrete properties to achieve the design service life under environment conditions XC or XS*. National Laboratory of Civil Engineering. Lisbon, Portugal, 2007.

Long A.E., Henderson G.D., Montgomery F.R., 2001. *Why assess the properties of near-surface concrete?* Construction and Building Materials, Vol. 15, pp.65-79.

Malhotra V.M., 2002. *High-performance, high-volume fly ash concrete,* Concrete International, Vol. 24, pp. 30-34.

Malhotra V.M., Bilodeau A., 1999. *High-volume fly ash system: the concrete solution for sustainable development.* In: Mehta P. K., editor. Concrete technology for sustainable development in the twenty-first century, pp. 43-64.

Malhotra V.M., Mehta P.K., 2002. *High-performance, high-volume fly ash concrete.* Supplementary Cementing Materials for Sustainable Development, Inc., Ottawa, Canada, pp. 101.

Marques P.F., Chastre C., Nunes A., 2013. *Carbonation service life modelling of RC structures for concrete with Portland and blended cements.* Cement and Concrete Composites, Vol. 37, pp. 171-184.

Martys N., 1995. *Survey of concrete transport properties and their measurement.* National Institute of Standards and Technology NIST. U.S. Department of Commerce. Gaithersburg, MD, USA.

Mehta P.K., 1999. *Concrete technology for sustainable development*. Concrete International, Vol. 11, pp. 47- 52.

Mehta P.K., Gerwick B.C., 1982. *Physical causes of concrete deterioration*. Concrete International, Vol. 4, pp. 45-51.

Mehta P.K., Meryman H., 2009. *Tools for Reducing Carbon Emissions Due to Cement Consumption*. Structure Magazine, pp. 11-15.

Mehta P.K., Monteiro P.J.M., 2014. *Concrete, Microstructure, Properties and Materials*. Prentice Hall, Englewood Cliff, NJ, USA.

Mejía R., Delvasto S., Gutierrez C., Talero R., 2003. *Chloride diffusion measured by modified permeability test in normal and blended cements.* Advances in Cement Research. Vol. 15, pp. 113-118.

Mikuni A., Komatsu R., Ikeda K., 2007. *Dissolution properties of some fly ash fillers applying to geopolymeric materials in alkali solution.* Journal of Materials Science, Vol. 42, pp. 2953-2957.

Minard H., 2003. *Etude intégrée des processus d'hydratation, de coagulation, de ridigification et de prise pour un systeme C_3S-C_3A-sulfates-alcalins.* Thesis (PhD). Université de Bourgogne, France.

Mohammadnejad, S., Provis J.L., van Deventer J.S.J., 2013. *Effects of grinding on the preg-robbing potential of quartz in an acidic chloride medium*. Minerals Engineering, Vol. 52, pp. 31-37.

Monteiro I., Branco F.A., de Brito J., Neves R., 2013. *Statistical analysis of the carbonation coefficient in open air concrete structures*. Construction and Building Materials. Vol. 29, pp. 263-269.

Morandeau A., Thiéry M., Dangla P., 2014. *Investigation of the carbonation mechanism of CH and C-S-H in terms of kinetics, microstructure changes and moisture properties*. Cement and Concrete Research. Vol. 56, pp. 153-170.

Moreno E., 2013. *Carbonation coefficients from concrete made with high- absorption limestone aggregate*. Advances in Materials Science and Engineering. Vol. 2014, pp 1-4.

Muethel R.W., 1995. *Investigation of the air content of plastic vs hardened concrete*. Michigan Department of Transportation, Materials and Technology Division. Lansing, MI, USA.

Najafi Kani E., Allahverdi A., Provis J.L., 2012. *Efflorescence control in geopolymer binders based on natural pozzolan*. Cement and Concrete Composites, Vol. 34, pp 25-33.

Nagataki S., Ohga H., Kim E.K., 1986. *Effect of curing conditions on the carbonation of concrete with fly ash and the corrosion reinforcement in long-term tests*. ACI Special Publications. Vol. 91, pp. 521-540.

Nasvi M., Ranjith P., Sanjayan J., 2014. *Effect of different mix compositions on apparent carbon dioxide (CO_2) permeability of geopolymer: Suitability as well cement for CO_2 sequestration wells*. Applied Energy. Vol. 114, pp. 939-948.

Neves R., Branco F., de Brito J., 2013. *Field assessment of the relationship between natural and accelerated concrete carbonation resistance*. Cement and Concrete Composites. Vol. 41, pp. 9-15.

Nixon J.M., Schindler A.K., Barnes R.W., Wade S.A., 2008. *Evaluation of the maturity method to estimate concrete strength in field applications*. Alabama

Department of Transportation, ALDOT Research Project 930-590. Montgomery, AL, USA.

Nurse R.W., 1949. *Steam curing of concrete*. Magazine of Concrete Research, Vol. 1, pp. 79-88.

NT BUILD 492, 1999. *Concrete, Mortar and Cement-Based Repair Materials: Chloride Migration Coefficient from Non-Steady-State Migration Experiments*. Nordtest Method. Espoo, Finland.

NTC 3459, 2001. *Agua para la elaboración de concreto*. Norma Técnica Colombiana, ICONTEC. Bogotá, Colombia.

NTC 4483, 1998. *Método de ensayo para determinar la permeabilidad del concreto al agua*. Norma Técnica Colombiana, ICONTEC. Bogotá, Colombia.

Obla K., Upadhyaya S., Goulias D., Schindler A., Carino N., 2008. *New technology-based approach to advance higher volume fly ash concrete with acceptable performance*. National Ready Mixed Concrete Association, Silver Spring, MD, USA.

Olivia M., Sarker P., Nikraz H., 2008. *Water penetrability of low calcium fly ash geopolymer concrete.* International Conference on Construction and Building Technology, Kuala Lumpur, Malaysia, pp. 517-530.

Olivier J.G.J., Janssens-Maenhout, G., Peters J.A.H.W., 2012. *Trends in global CO_2 emissions; 2012 Report*. PBL Netherlands Environmental Assessment Agency. The Hague/Bilthoven, PBL publication number: 500114022.

Olivier J.G.J., Janssens-Maenhout, G., Muntean M., Peters J.A.H.W., 2014. *Trends in global CO_2 emissions; 2014 Report*. PBL Netherlands Environmental Assessment Agency. The Hague, PBL publication number: 1490.

Owens K., Bai Y., Cleland D., Basheer P., Kwasny J., Sonebil M., Taylor S., Gupta A., 2010. *Activation of High Volume Fly Ash Pastes Using Chemical Activator.* Second International Conference on Sustainable Construction Materials and Technologies, Universita Politecnica delle Marche, Ancona, Italy, pp. 1759-1770.

Özbay E., Karahan O., Lachemi M., Hossain K.M.A., Atiş C. D., 2012. *Investigation of properties of engineered cementitious composites incorporating high volumes of fly ash and metakaolin*. ACI Materials Journal, Vol. 109, pp. 565-571.

Pacheco-Torgal F., Abdollahnejad Z., Camoes A.F., Jamshidi M., Ding Y., 2012. *Durability of alkali-activated binders: A clear advantage over Portland cement or an unproven issue?* Construction and Building Materials, Vol 30, pp. 400-405.

Pade C., Guimaraes M., 2007. *The CO_2 uptake of concrete in a 100 year perspective*. Cement and Concrete Research, Vol. 37, pp. 1348-1356.

Palacios M., Puertas F., 2004. *Stability of superplasticizer and shrinkage- reducing admixtures in high basic media*. Materiales de Construcción, Vol. 54, pp. 65-86.

Palomo A., Grutzeck M.W., Blanco M.T., 1999. *Alkali-activated fly ashes. A cement for the future*. Cement and Concrete Research, Vol. 29, pp. 1323-1329.

Palomo A., Fernández-Jimenez A., Kovalchuk G., Ordoñez L.M., Naranjo M.C., 2007. *OPC - fly ash cementitious systems: study of gel binders produced during alkaline hydration.* Journal of Materials Science, Vol. 42, pp. 2958-2966.

Panagiotopoulou Ch., Kontori E., Perrako Th., Kakali G., 2007. *Dissolution of aluminosilicate minerals and by- products in alkaline media.* Journal of Materials Science, Vol. 42, pp. 2967-2973.

Papadakis V.G., Vayenas C.G., Fardis M.N., 1989. *A reaction engineering approach to the problem of concrete carbonation.* AIChE Journal, Vol. 35, pp. 1639-1650.

Parrott L.J., 1987. *A review of carbonation in reinforced concrete*. BRE, Watford, UK.

Parrot L.J., 1994. *Design for avoiding damage due to carbonation-induced corrosion.* ACI Special Publication. Vol. 145, pp. 283-298.

Paya J., Monzó J., Borrachero M.V., Peris-Mora E., 1995. *Mechanical treatment of fly ashes. Part I: Physico-chemical characterization of ground fly ashes*. Cement and Concrete Research. Vol. 25, pp.1469-1479.

Paya J., Monzó J., Borrachero M.V., Peris-Mora E., Gonzalez-Lopez E., 1996. *Mechanical treatment of fly ashes. Part II: Particle morphologies in ground fly ashes*

(GFA) and workability of GFA-cement mortars. Cement and Concrete Research. Vol. 26, pp. 225-235

Paya J., Monzó J., Borrachero M.V., Peris-Mora E., Gonzalez-Lopez E., 1997. *Mechanical treatment of fly ashes. Part III: Studies on strength development of ground fly ashes (GFA) – cement mortars*. Cement and Concrete Research. Vol. 27, pp.1365-1377.

Paya J., Monzó J., Borrachero M.V., Peris-Mora E., Amahjour F., 2000. *Mechanical treatment of fly ashes. Part IV: Strength development of ground fly ash-cement mortars cured at different temperatures*. Cement and Concrete Research. Vol. 30, pp.543-551.

Pommersheim J., Clifton J., 1985. *Prediction of concrete service-life*. Materials and Structures. Vol. 18, pp. 21-30.

Proske, T., Hainer S., Rezvani M., Graubner C.A., 2013. *Eco-friendly concretes with reduced water and cement contents – Mix design principles and laboratory test*. Cement and Concrete Research. Vol. 51, pp. 38-46.

Poon C., Kou S., Lam L., Lin Z., 2001. *Activation of fly ash/cement using calcium sulfate anhydrite ($CaSO_4$)*. Cement and Concrete Research, Vol. 31, pp. 873-881.

Pourbaix M., 1974. *Applications of electrochemistry in the corrosion science and in practice*. Corrosion Science. Vol. 14, pp. 25-82.

Provis J.L., Myers R.J., White C.E., Rose V., Van Deventer J.S.J., 2012. *X-ray microtomography shows pore structure and tortuosity in alkali-activated binders*. Cement and Concrete Research. Vol. 42, pp. 855-864.

Puertas F., Palomo A., Fernández-Jiménez A., Izquierdo J.D., Granizo M.L., 2003. *Effect of superplasticisers on the behaviour and properties of alkaline cements*. Advances in Cement Research, Vol. 15, pp. 23-28.

Puertas F., Fernández-Jimenez A., Blanco-Varela M.T., 2004. *Pore solution in alkali-activated slag cement pastes. Relation to the composition and structure of calcium silicate hydrate*. Cement and Concrete Research. Vol. 34, pp. 139-148.

Purdon A.O., 1940. *The action of alkalis on blast-furnace slag*. Journal of the Society of Chemical Industry, Vol. 59, pp. 191-202.

Purnell P., Black L., 2012. *Embodied carbon dioxide in concrete: Variation with common mix design parameters*. Cement and Concrete Research. Vol. 42, pp. 874-877.

Qian J., Shi C., Wang Z., 2001. *Activation of blended cements containing fly ash*. Cement and Concrete Research. Vol. 31, pp. 1121-1127.

Rabehi M., Mezghiche B., Guettala S. 2013. *Correlation between initial absorption of the cover concrete, the compressive strength and carbonation depth*. Construction and Building Materials. Vol. 45, pp. 123-129.

Rashad A., 2013. *A comprehensive overview about the influence of different additives on the properties of alkali-activated slag – A guide for civil engineer*. Construction and Building Materials. Vol. 47, pp. 29-55.

Ravikumar D., Peethamparan S., Neithalath N., 2010. *Structure and strength of NaOH activated concretes containing fly ash or GGBFS as the sole binder*. Cement and Concrete Composites. Vol. 32, pp. 399-410.

Ravikumar D., Neithalath N., 2013. *An electrical impedance investigation into the chloride ion transport resistance of alkali silicate powder activated slag concretes*. Cement and Concrete Composites. Vol. 144, pp. 58-68.

Reinhardt H.W., Jooss M., 1998. *Permeability, diffusion and capillary absorption of concrete at elevated temperature in the service range*. Otto-Graf-Journal. Vol. 9, pp. 34-47.

Ribeiro A.B., Machado A. Gonçalves A., Salta M., 2003. *A contribution to the development of performance-related design methods*. RILEM Proceedings, RILEM, Paris. Vol. 29, pp. 223-235.

RILEM Technical Committee 224-AAM, 2014. *Alkali Activated Materials*: *State of the Art Report*. RILEM Reports Volume 13. RILEM/Springer, Dordrecht, Netherlands.

Roy D., 1999. *Alkali-activated cements: Opportunities and challenges*. Cement and Concrete Research. Vol. 29, pp. 249-254.

Roy D., Jiang W., Silsbee M.R., 2000. *Chloride diffusion in ordinary blended, and alkali-activated cement pastes and its relation to other properties*. Cement and Concrete Research. Vol. 30, pp. 1879-1884.

Sustainable Concrete Forum, 2012. *Concrete Industry Sustainability Performance Report.* 6th Report: 2012 performance data. MPA, London, UK.

Saeki T., Ogha H., Nagataki S., 1991. *Mechanism of carbonation and prediction of carbonation process of concrete*. Concrete Library of JSCE. Vol 12, pp. 23-36.

Sahmaran M., Yaman I., Tokyay M., 2009. *Transport and mechanical properties of self consolidating concrete with high volume fly ash.* Cement and Concrete Composites. Vol. 31, pp. 99 – 106.

Saul A.G.A., 1951. *Principles Underlying the Steam Curing of Concrete at Atmospheric Pressure*. Magazine of Concrete Research, Vol. 2, pp 127-140.

Schindler A., Folliard K., 2005. *Heat of hydration models for cementitious materials.* ACI Materials Journal, Vol. 102, pp. 24-33

Schroeder F., Smolczky H.G., 1968. *Carbonation and protection against steel corrosion*. Fifth International Symposium on the Chemistry of Cement. Tokyo. Vol. 4, pp. 188-198.

Sear L.K.A., 2001. *The properties and use of coal fly ash*. Tomas Teldford Ltd. London

Shi C., 2001. *Studies on several factors affecting hydration and properties of lime-pozzolan cements*. Journal of Materials in Civil Engineering. Vol. 13, pp. 441-445.

Shi C., Krivenko P., Roy D., 2006. *Alkali-activated cement and concretes.* Taylor & Francis. London/New York.

Shi C., Fernández Jimenez A., Palomo A., 2011. *New cements for the 21st century: The pursuit of an alternative to Portland cement*. Cement and Concrete Research. Vol. 41, pp. 750-763.

Shi C., Shao Y., 2002. *What is the most efficient way to activate the reactivity of fly ashes?* 2nd Material Specialty Conference of the Canadian Society for Civil Engineering. CSCE. Montréal, Canada. m-29.

Shi X., Xie N., Fortune K., Gong J., 2012. *Durability of steel reinforced concrete in chloride environments: An overview*. Construction and Building Materials. Vol. 30, pp. 125-138.

Shon C.S., Zollinger D.G., Sarkar S.L., 2002. *Alkali-silica reactivity resistance of high-volume fly ash cementitious systems*. Transportation Research Record, pp. 17-21.

Siddique R., 2004. *Performance characteristics of high-volume Class F fly ash concrete.* Cement and Concrete Research. Vol. 34, pp. 487-493.

Sisomphon K., Franke, L., 2007. *Carbonation rates concretes containing high volume of pozzolanic materials.* Cement and Concrete Research. Vol. 37, pp. 1647-1653.

Tang L., 1996. *Chloride transport in concrete: Measurement and prediction*. PhD Thesis. Chalmers University, Gothenburg, Sweden.

Tang L., Nilsson L.O., Basheer P.A.M., 2012. *Resistance of Concrete to Chloride Ingress. Testing and Modelling*, CRC Press, London.

Thiery M., Villain G., Dangla P., Platret G., 2007. *Investigation of the carbonation front shape on cementitious materials: effects of the chemical kinetics*. Cement and Concrete Research. Vol. 37, pp. 1047-1058.

Thomas M.D.A., Bamforth P.B., 1999. *Modelling chloride diffusion in concrete: effect of fly ash and slag*. Cement and Concrete Research. Vol. 29, pp. 487-495.

Thomas M.D.A., Bentz D.C., 2008. *Life-365 Service Life Prediction Model and Computer Program for Predicting the Service Life and Life-Cycle Costs of Reinforced Concrete Exposed to Chlorides*. Manual. Life-365 Consortium, USA.

Tuuti K., 1980. *Service life of structures with regard to corrosion of embedded steel*. ACI Special Publication 65, pp. 223-236.

Tuuti K., 1982. *Corrosion of steel in concrete*. Swedish Cement and Concrete Research Institute. Stockholm, Sweden.

Valenta O., 1970. *The permeability and durability of concrete in aggressive conditions*. Proceedings of the 10th International Congress on Large Dams. Montreal, Canada, pp. 103-117.

Valipour M., Pargar F., Shekarchi M., Khani S., Moradian M., 2013. *In situ study of chloride ingress in concretes containing natural zeolite, metakaolin and silica fume exposed to various exposure conditions in a harsh marine environment*. Construction and Building Materials, Vol. 46, pp. 63-70.

Van den Heede P., Gruyaert E., De Belie N., 2010. *Transport properties of high-volume fly ash concrete: Capillary water sorption under vacuum and gas permeability*. Cement and Concrete Composites. Vol. 32, pp. 749-756.

Van Deventer J.S.J., Provis J.L., 2012. *Technical and commercial progress in the adoption of geopolymer cement*. Minerals Engineering. Vol. 29, pp. 89-104.

Velandia D., Lynsdale C., Ramirez F., Provis J., Hermida G., Gomez A., 2013. *Ultra Optimum Green Concrete Using High Volume Fly Ash Activated Systems*. MRS Proceedings, Vol 1612.

Velandia D., Echeverri W., 2010. *Concreto expuesto a diferentes ataques en Colombia*. Noticreto, Vol. 102, pp. 32-35, 2010.

Walker R., Pavía S., 2011. *Physical properties and reactivity of pozzolans, and their influence on the properties of lime-pozzolan pastes*. Materials and Structures, Vol. 44, pp. 1139-1150.

Wang X.Y., Lee H.S., 2009. *A model for predicting the carbonation depth of concrete containing low-calcium fly ash.* Construction and Building Materials. Vol. 23, pp. 725-733.

Wang B., Wang L., 2004. *Development of studies and applications of activation techniques of fly ash.* International Workshop on Sustainable Development and Concrete Technology, Beijing, Iowa State University. Library of Congress Control Number: 2004101246. pp. 159-169.
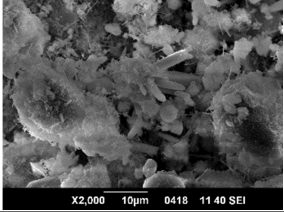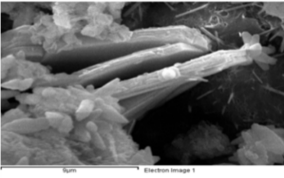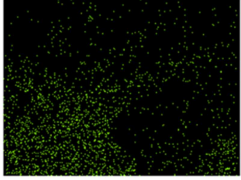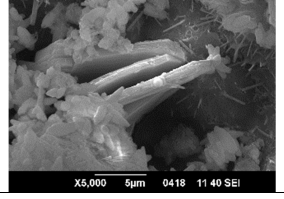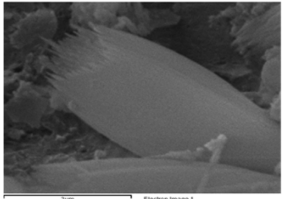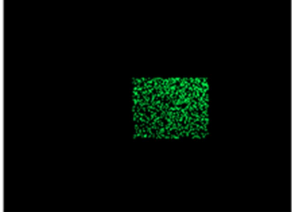
Wei F., Grutzeck M., Roy D., 1985. *The retarding effects of fly ash upon the hydration of cement pastes*. Cement and Concrete Research, Vol. 15, pp. 174-184.
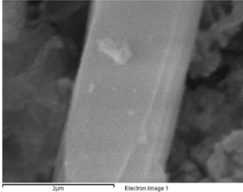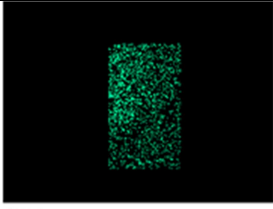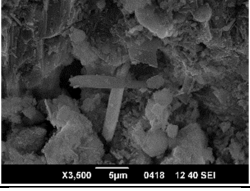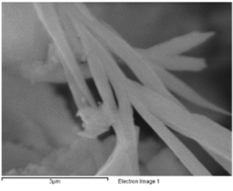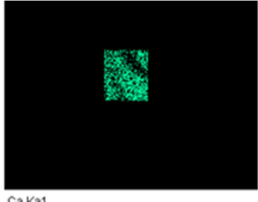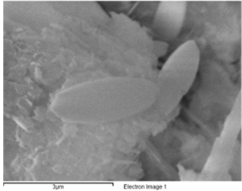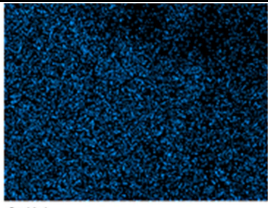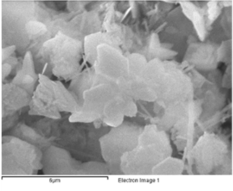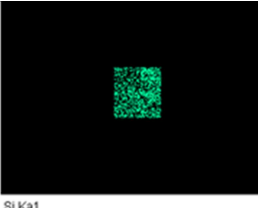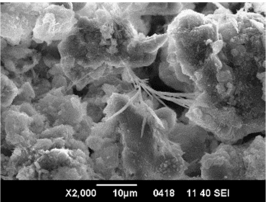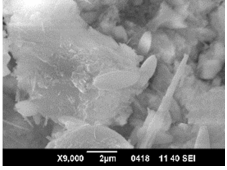
Whiting J., 1895. *Manufacture of Cement*. U.S. Patent 544,706.

Wierig H., 1984. *Long time studies on the carbonation of concrete under normal outdoor exposure*. RILEM Seminar, Hanover, Germany, pp. 239-249.

Wilmott P., Howison S., Dewynne J., 1995. *The mathematics of financial derivatives: a student introduction*. Cambridge University Press, Cambridge, UK.

Wongpa J., Kiattikomol K., Jaturapitakkul C., Chindaprasirt P., 2010. *Compressive strength, modulus of elasticity, and water permeability of inorganic polymer concrete*. Materials and Design, Vol. 31, pp. 4748-4754.

Xiang Y., Guo D., Wu Q., 2012. *Service life prediction of concrete bridges based on concrete carbonation depth near coastal areas*. Proceedings of the 3rd International Conference on the Durability of Concrete Structures, Belfast, UK. Paper number SLM7, pp. 1-6.

Yang K.H., Song J.K., Song K.I., 2013. *Assessment of CO_2 reduction of alkali-activated concrete*. Journal of Cleaner Production, Vol. 39, pp. 265-272.

Younsi, A., Turcry P., Roziere E., Aït-Mokhtar A., Loukili A., 2011. *Performance-based design and carbonation of concrete with high fly ash content*. Cement and Concrete Composites, Vol. 33, pp. 993-1000

Yu Z., Lixue J., 1998. *A practical mathematical model of concrete carbonation depth based on the mechanism*. Industrial Construction. Vol. 28, pp. 16-19.

Zhang H., Ba D., Wang Z., 2006. *A model for forecasting carbonization depth of concrete*. Journal of Wuhan University (Engineering Science). Vol. 39, pp. 42-45.

Zhang J., Lounis Z., 2009. *Nonlinear relationships between parameters of simplified diffusion-based model for service life design of concrete structures exposed to chlorides*. Cement and Concrete Composites. Vol. 31, pp. 591-600.

Zhang Y., Jiang L., 1998. *A practical mathematical model of concrete carbonation depth based on the mechanism*. Industrial Construction. Vol. 28, pp. 16-19.

Zhang Y., Zhang Z., 2014. *Transport properties in unsaturated cement-based materials – A rewiew*. Construction and Building Materials. Vol. 72, pp. 367-379.
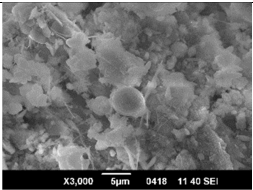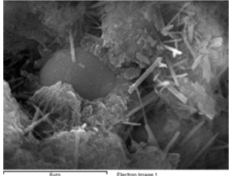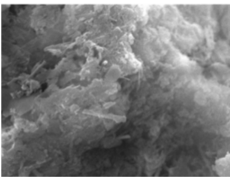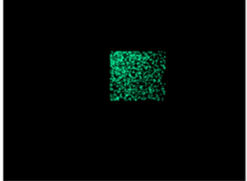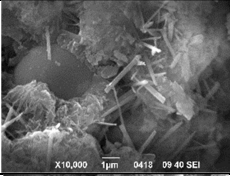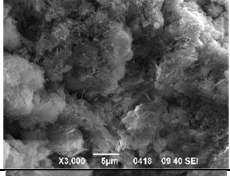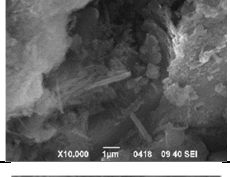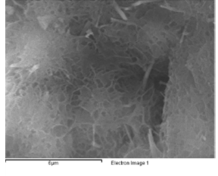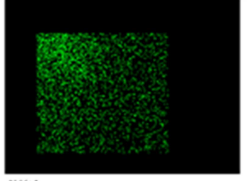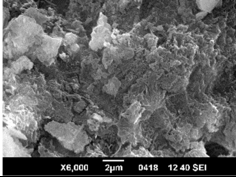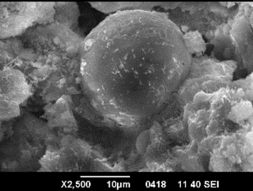
Appendix 1
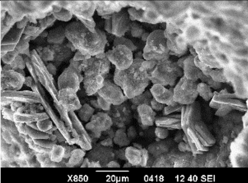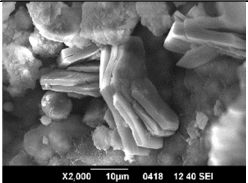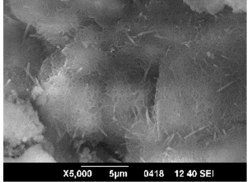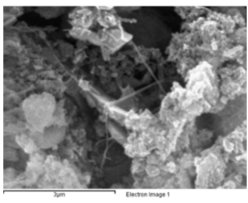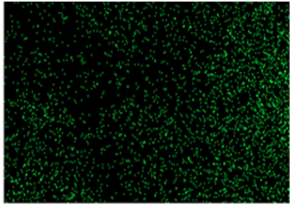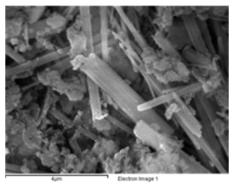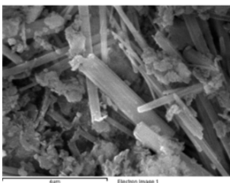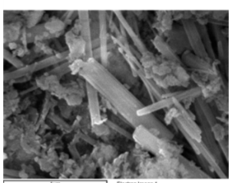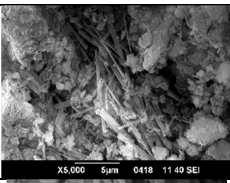
SEM/EDS ANALYSIS
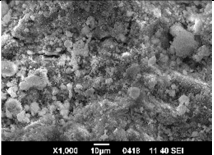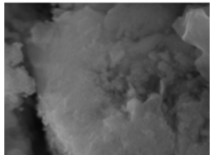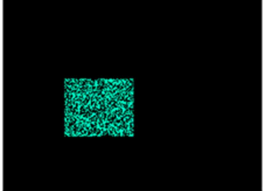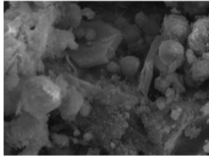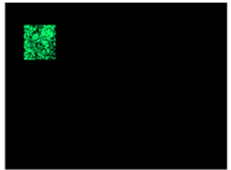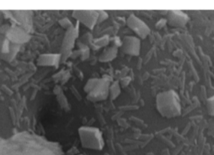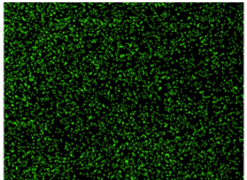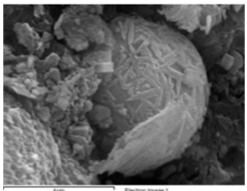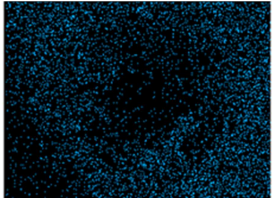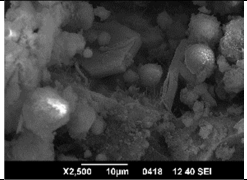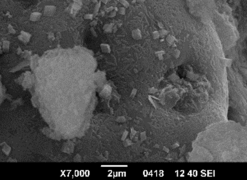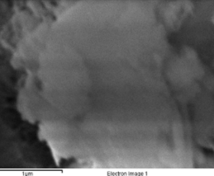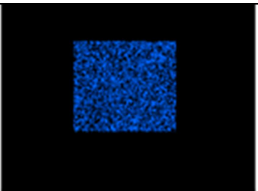
The following table presents the SEM images including the spot analysis. For the spot analysis a region is selected to visualize the distribution of a component. Depending on what is seen in the SEM image, an area is selected to confirm a possible structure formation. In some cases the spot analysis is performed in the complete image instead of a selected square region.
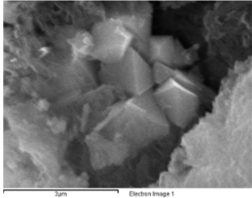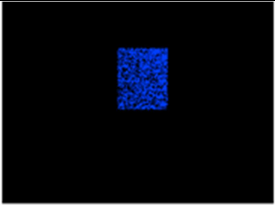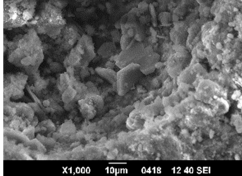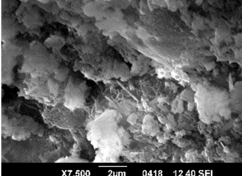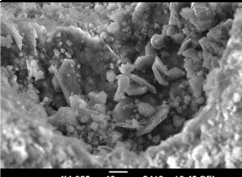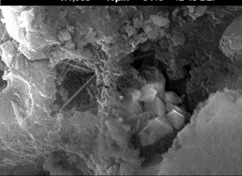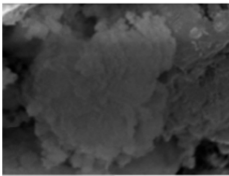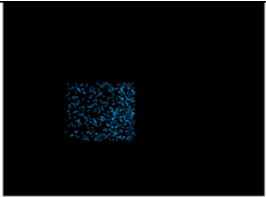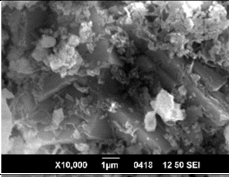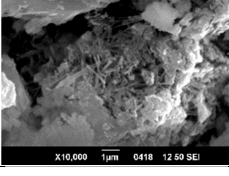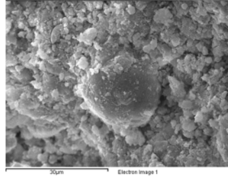
#	Mix ID	Image	Spot analysis
2- S	TP/OS/50/A/1/7		C-S-H ETTRINGITE
13	TP/OS/50/A/1/28		 Ca Ka1
13-S	TP/OS/50/A/1/28		PORTLANDITE C-S-H
13-S	TP/OS/50/A/1/28		PORTLANDITE C-S-H
10-1	FB/OS/50/A/1/7		 Si Ka1
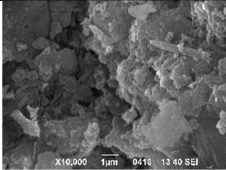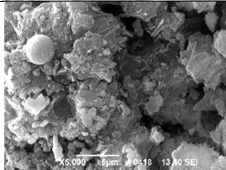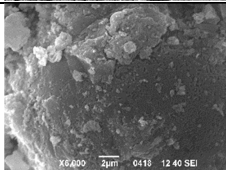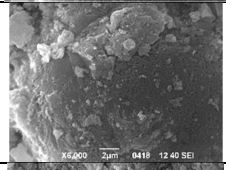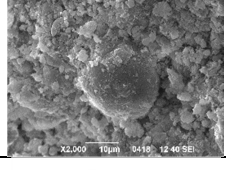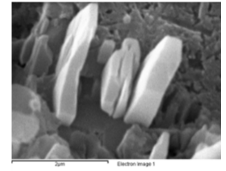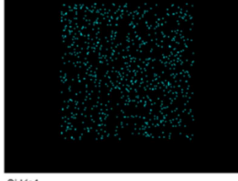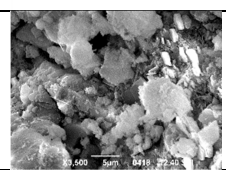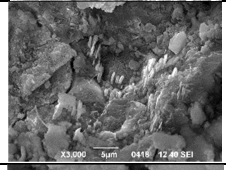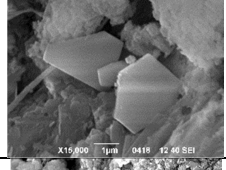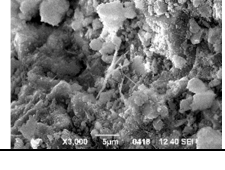
10-2	FB/OS/50/A/1/7		\nSi Ka1
10-S	FB/OS/50/A/1/7		ETTRINGITE
10-S	FB/OS/50/A/1/7		C-S-H\nPORTLANDITE
16-1	FB/OS/50/A/1/28		\nCa Ka1
16-2	FB/OS/50/A/1/28		\nCa Ka1
16-3	FB/OS/50/A/1/28		\nSi Ka1
16-S	FB/OS/50/A/1/28		C-S-H
16-S	FB/OS/50/A/1/28		
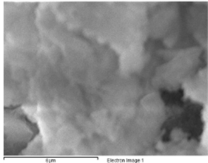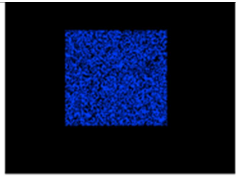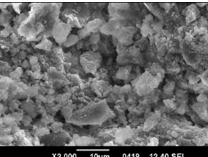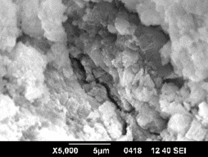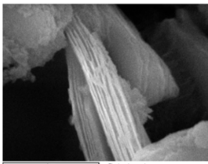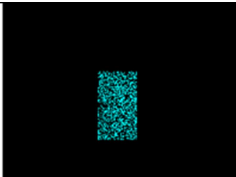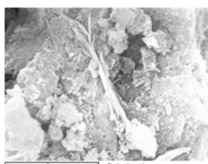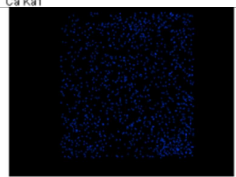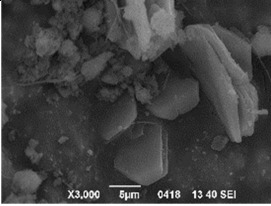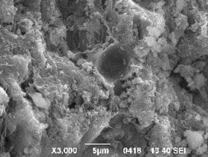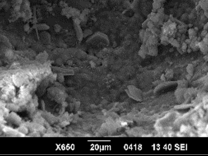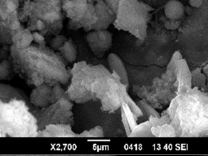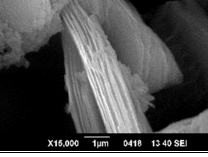
16- S	FB/OS/50/A/1/28			FLY ASH
48-1	TP/OS/50/S/1/7			
48-2	TP/OS/50/S/1/7		 Si Ka1	
48- S	TP/OS/50/S/1/7			FLY ASH SURFACE
48- S	TP/OS/50/S/1/7			ETTRINGITE
48- S	TP/OS/50/S/1/7			
49	TP/OS/50/S/1/28		 Al Ka1	
49-S	TP/OS/50/S/1/28			
49-S	TP/OS/50/S/1/28			ETTRINGITE
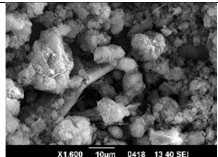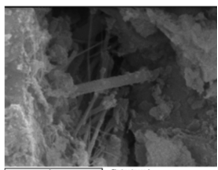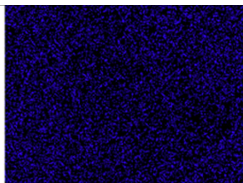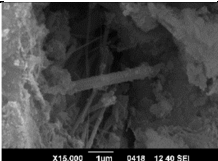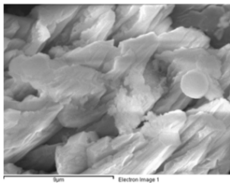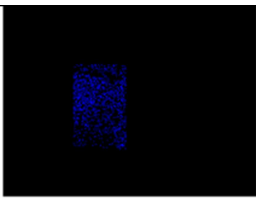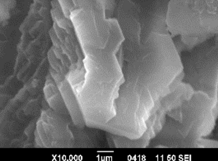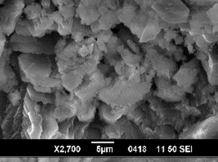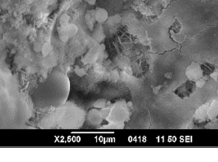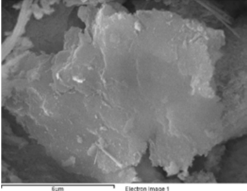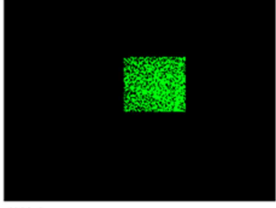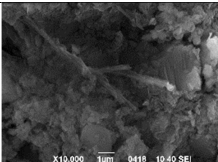
49-S	TP/OS/50/S/1/28		C-S-H
49-S	TP/OS/50/S/1/28		PORTLANDITE
49-S	TP/OS/50/S/1/28		
50	TP/OS/50/S/1/56		
52-1	FB/OS/50/S/1/28		
52-2	FB/OS/50/S/1/28		
52-3	FB/OS/50/S/1/28		
52-S	FB/OS/50/S/1/28		
52-S	FB/OS/50/S/1/28		GYPSUM
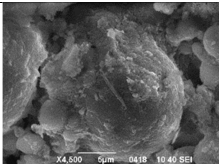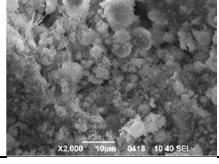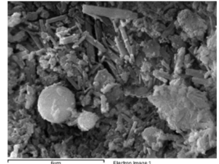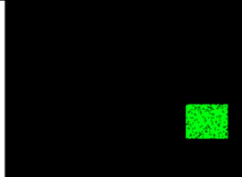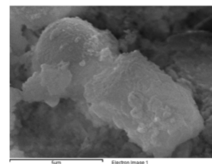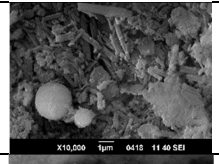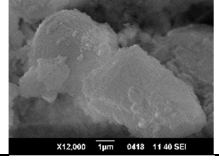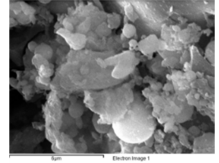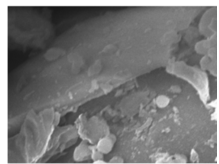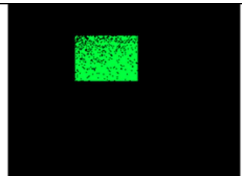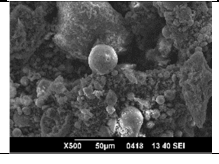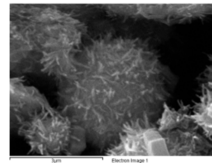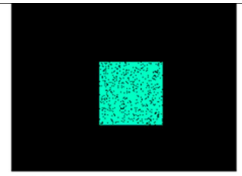
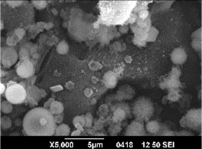|			
52-S	FB/OS/50/S/1/28		
53	FB/OS/50/S/1/56		K Ka1
54-1	TP/75/50/A/1/28		Si Ka1
54-2	TP/75/50/A/1/28		Al Ka1
54-3	TP/75/50/A/1/28		Ca Ka1
54-S	TP/75/50/A/1/28		PORTLANDITE ETTRINGITE C-S-H
54-S	TP/75/50/A/1/28		CUBIC CRYSTALS OVER FLY ASH SURFACE
55-1	FB/75/50/A/1/28		Ca Ka1
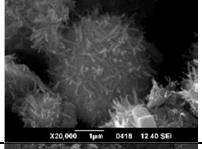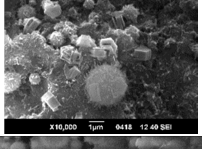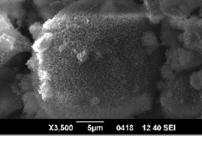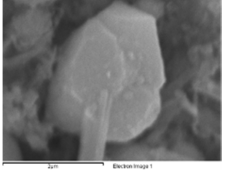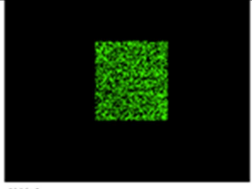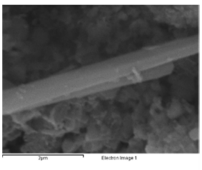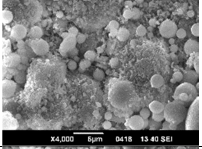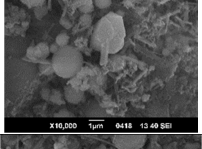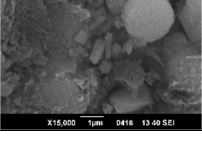
55-2	FB/75/50/A/1/28		Ca Ka1
55-S	FB/75/50/A/1/28		PORTLANDITE
55-S	FB/75/50/A/1/28		
55-S	FB/75/50/A/1/28		
55-S	FB/75/50/A/1/28		
56	TP/75/50/S/1/28		Fe Ka1
56-S	TP/75/50/S/1/28		
56-S	TP/75/50/S/1/28		NEEDLES OF DIFFERENT SIZES
57	FB/75/50/S/1/28		
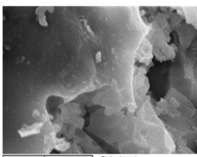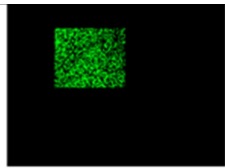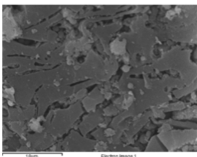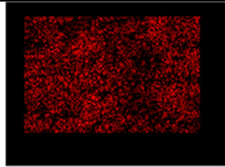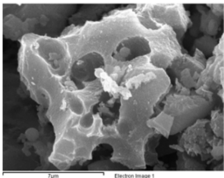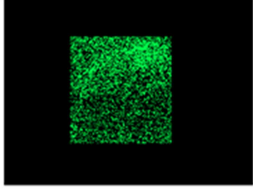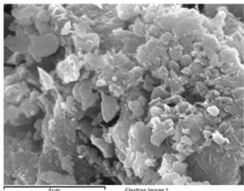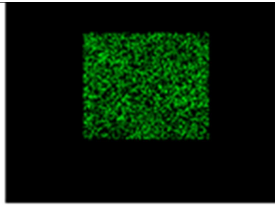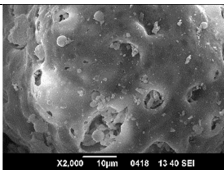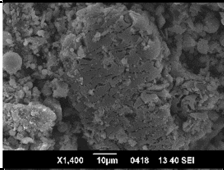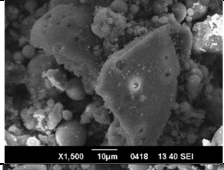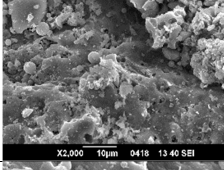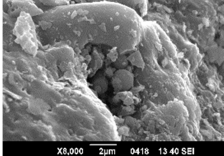
57-S	FB/75/50/S/1/28		
57-S	FB/75/50/S/1/28		
57-S	FB/75/50/S/1/28		FLY ASH SURFACE
57-S	FB/75/50/S/1/28		
57-S	FB/75/50/S/1/28		FLY ASH GRAIN
58	CE/10/0/0/0/7		Si Ka1
58-S	CE/10/0/0/0/7		
58-S	CE/10/0/0/0/7		
58-S	CE/10/0/0/0/7		
58-S	CE/10/0/0/0/7		
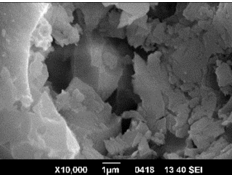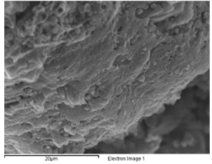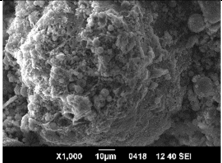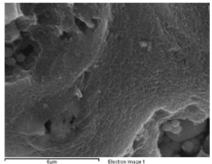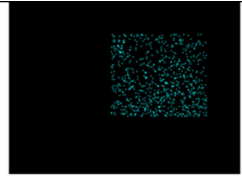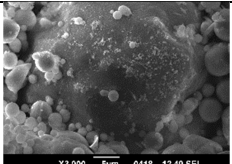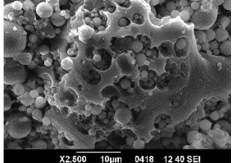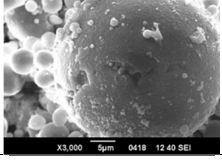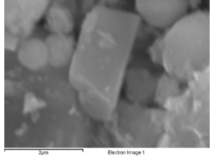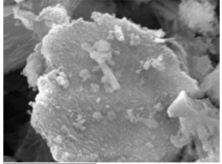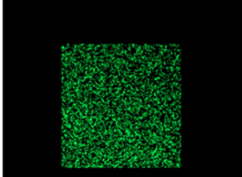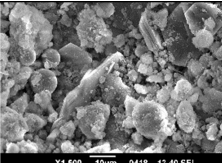
59	**CE/10/0/0/0/28**		Ca Ka1
59-S	**CE/10/0/0/0/28**		
59-S	**CE/10/0/0/0/28**		
60-1	**TP/OS/20/0/0/0/56**		Ca Ka1
60-2	**TP/OS/20/0/0/0/56**		Ca Ka1
60-S	**TP/OS/20/0/0/0/56**		PORTLANDITE C-S-H ETTRINGITE
60-S	**TP/OS/20/0/0/0/56**		
60-S	**TP/OS/20/0/0/0/56**		C-S-H
60-S	**TP/OS/20/0/0/0/56**		C-S-H
60-S	**TP/OS/20/0/0/0/56**		
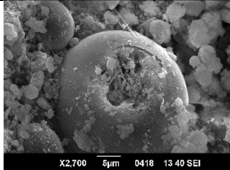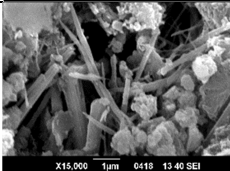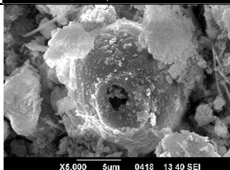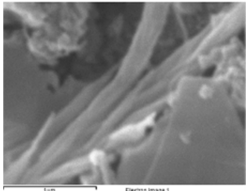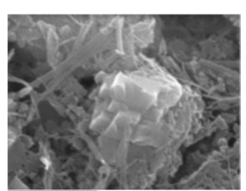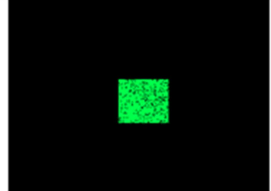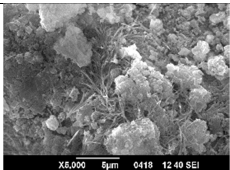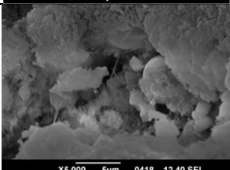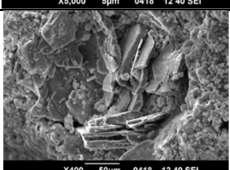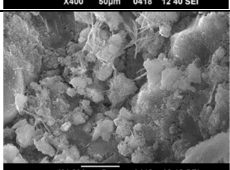
60-S	TP/OS/20/0/0/0/56		C-S-H
61	TA/75/50/A/1/28		Ca Ka1
61-S	TA/75/50/A/1/28		
62	TG/75/50/A/1/28		Ca Ka1
62-S	TG/75/50/A/1/28		CRYSTALS FORMATION
62-S	TG/75/50/A/1/28		C-S-H
62-S	TG/75/50/A/1/28		
27	TG/OS/50/A/1/28		Al Ka1
27-S	TG/OS/50/A/1/28		
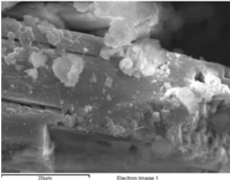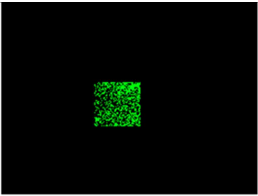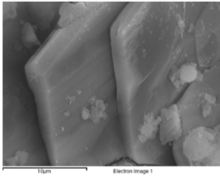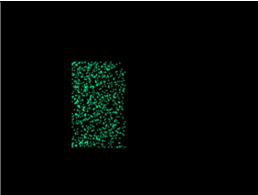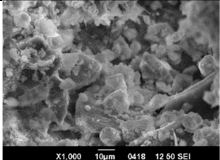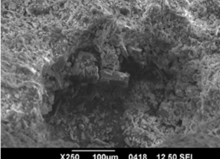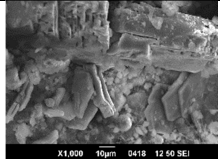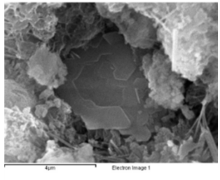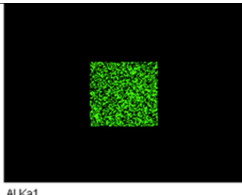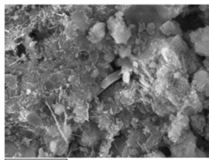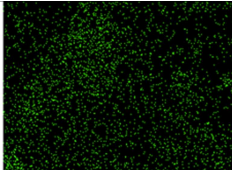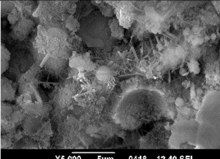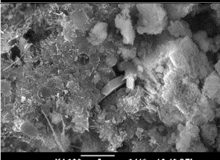
27-S	TG/OS/50/A/1/28			
27-S	TG/OS/50/A/1/28			
63- 1	TA/OS/75/A/1/28			Si Ka1
63- 2	TA/OS/75/A/1/28			Ca Ka1
63-S	TA/OS/75/A/1/28			C-S-H
63-S	TA/OS/75/A/1/28			C-S-H
64-1	TP/OS/100/A/1/28			
64-2	TP/OS/100/A/1/28			Si Ka1
64-S	TP/OS/100/A/1/28			
65	FB/OS/100/A/1/28			Si Ka1
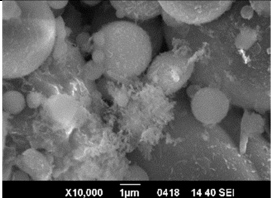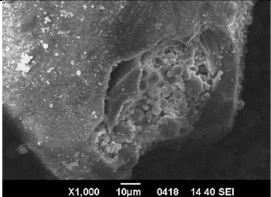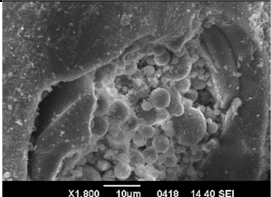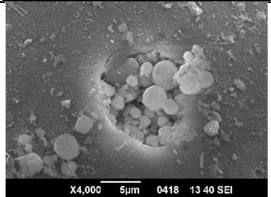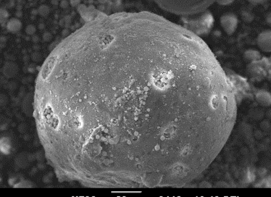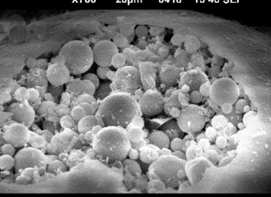
65-S	FB/OS/100/A/1/28			
65-S	FB/OS/100/A/1/28			ETTRINGITE
65-S	FB/OS/100/A/1/28			
65-S	FB/OS/100/A/1/28			
67-1	TA/OS/100/A/1/28			Al Ka1
67-2	TA/OS/100/A/1/28			Ca Ka1
67-S	TA/OS/100/A/1/28			
67-S	TA/OS/100/A/1/28			
67-S	TA/OS/100/A/1/28			
67-S	TA/OS/100/A/1/28			
67-S	TA/OS/100/A/1/28			

68-1	TP/OS/100/S/1/28		Si Ka1
68-2	TP/OS/100/S/1/28		C Ka1_2
68-3	TP/OS/100/S/1/28		Si Ka1
68-4	TP/OS/100/S/1/28		Al Ka1
68-S	TP/OS/100/S/1/28		
68-S	TP/OS/100/S/1/28		
68-S	TP/OS/100/S/1/28		
68-S	TP/OS/100/S/1/28		
68-S	TP/OS/100/S/1/28		

68-S	TP/OS/100/S/1/28			
69	FB/OS/100/S/1/28			 Si Ka1
69-S	FB/OS/100/S/1/28			
70	TG/OS/100/S/1/28			 Si Ka1
70-S	TG/OS/100/S/1/28			FLY ASH GRAINS
70-S	TG/OS/100/S/1/28			
70-S	TG/OS/100/S/1/28			
71	TA/OS/100/S/1/28			 Na Ka1_2
72	TP/75/50/Q/1/28			 Si Ka1
72-S	TP/75/50/Q/1/28			

306

72-S	TP/75/50/Q/1/28			NEEDLES INSIDE FLY ASH PARTICLE
72-S	TP/75/50/Q/1/28			
72-S	TP/75/50/Q/1/28			
73-1	TP/75/50/L/1/28		Ca Ka1	
73-2	TP/75/50/L/1/28		Si Ka1	
73-S	TP/75/50/L/1/28			ETTRINGITE C-S-H PORTLANDITE
73-S	TP/75/50/L/1/28			C-S-H
73-S	TP/75/50/L/1/28			
73-S	TP/75/50/L/1/28			

74-1	FB/75/50/Q/1/28		 Si Ka1
74-2	FB/75/50/Q/1/28		 Si Ka1
74-S	FB/75/50/Q/1/28		
74-S	FB/75/50/Q/1/28		
74-S	FB/75/50/Q/1/28		PORTLANDITE
75-1	FB/75/50/L/1/28		 Al Ka1
75-2	FB/75/50/L/1/28		 Al Ka1
75-S	FB/75/50/L/1/28		
75-S	FB/75/50/L/1/28		

66-S	TG/OS/100/A/1/28		
66-S	TG/OS/100/A/1/28		
66-S	TG/OS/100/A/1/28		
66-S	TG/OS/100/A/1/28		
66-S	TG/OS/100/A/1/28		
66-S	TG/OS/100/A/1/28		

Appendix 2

AMBIENT AND ELEMENT TEMPERATURES
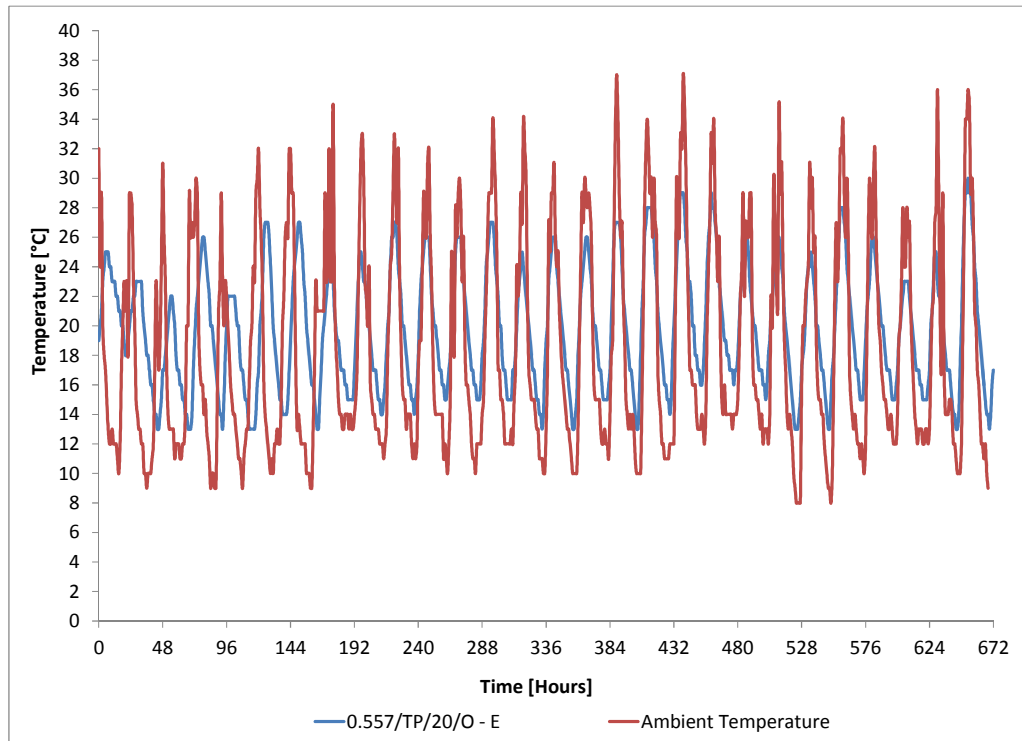
a) 20% FA
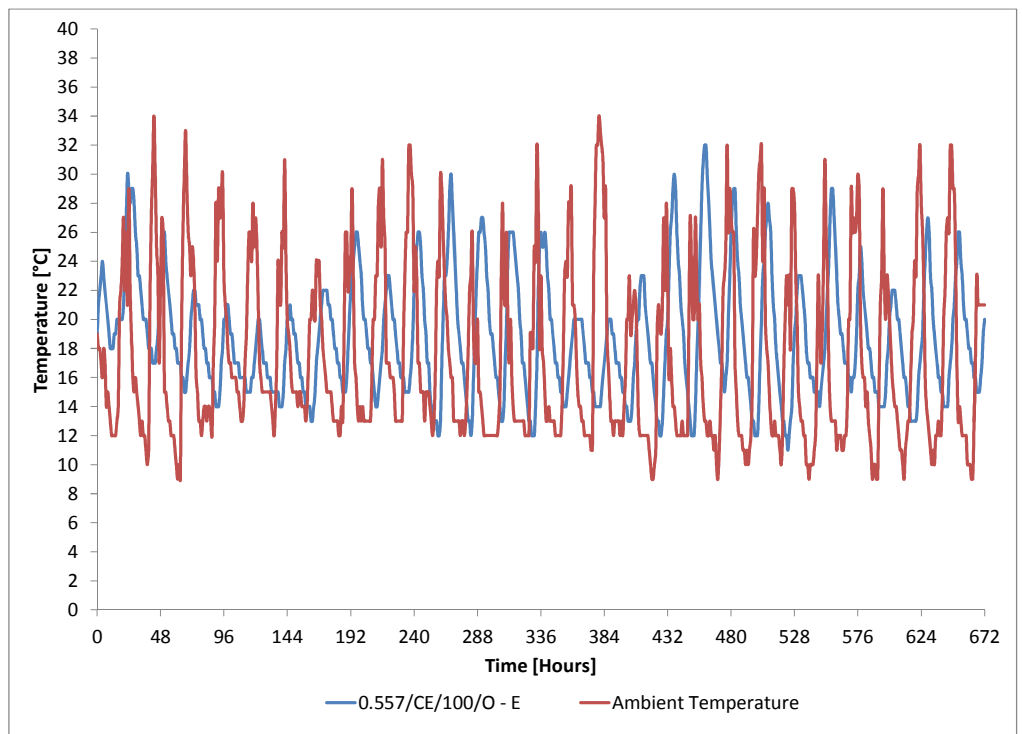
b) 0% FA
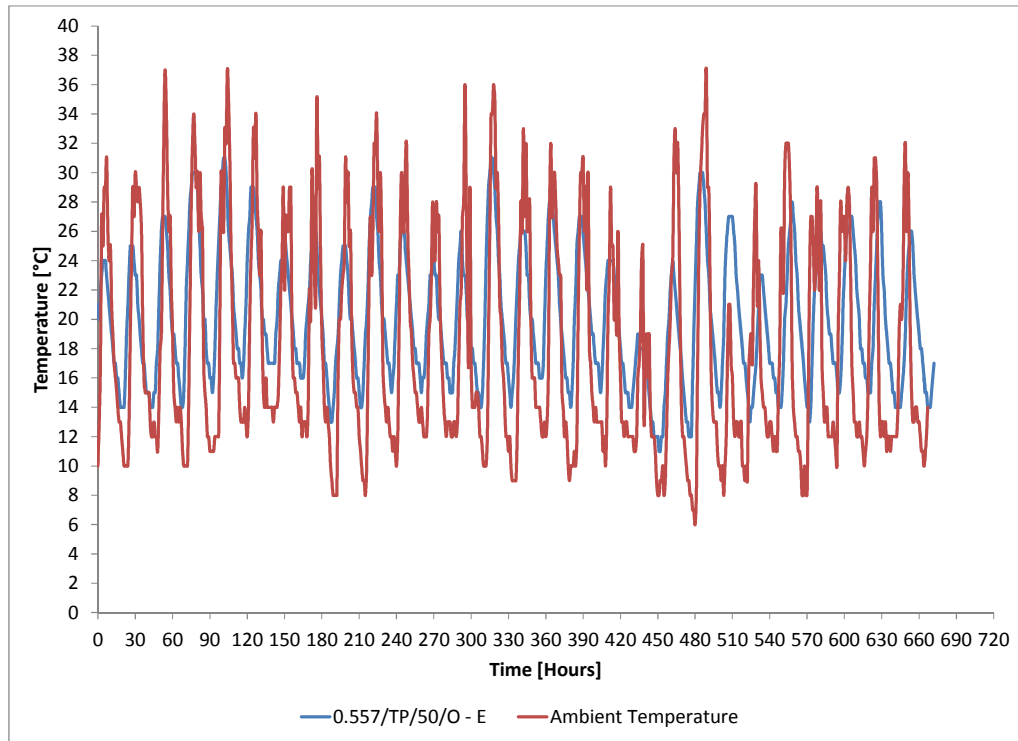
c) 50% FA
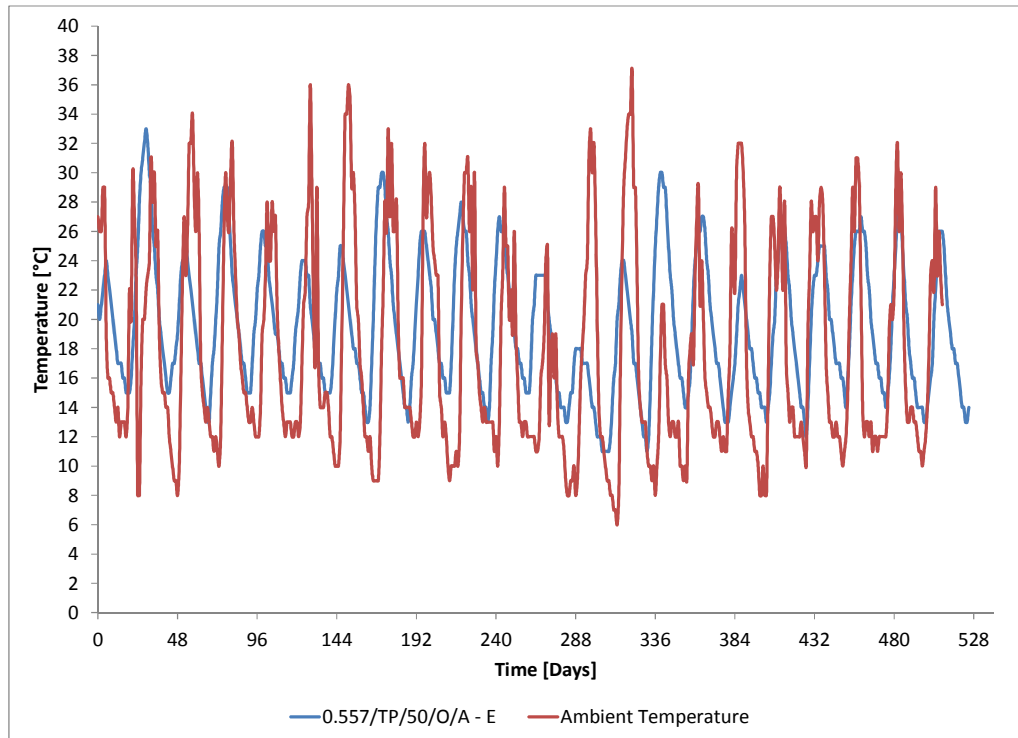
d) 50% FA + Na₂SO₄
Figure 164 Ambient and elements temperature:

CORRELATIONS BETWEEN TEMPERATURE – TIME FACTOR AND COMPRESSIVE STRENGTH FOR DIFFERENT FLY ASH REPLACEMENTS
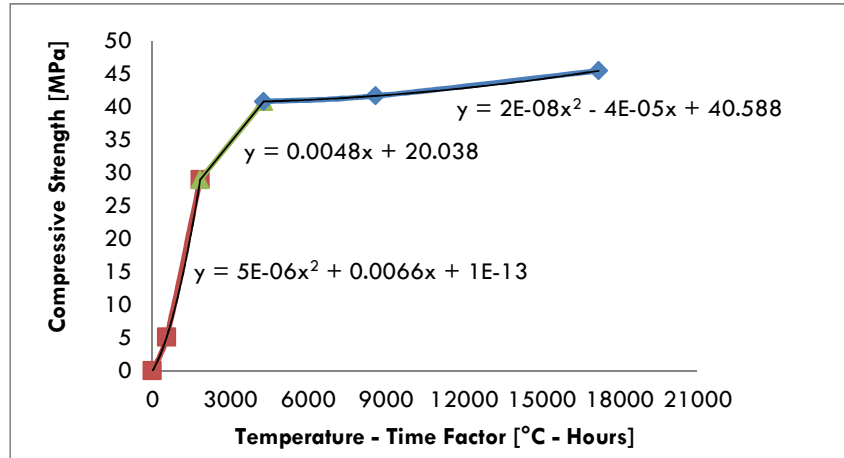
a) 0% FA
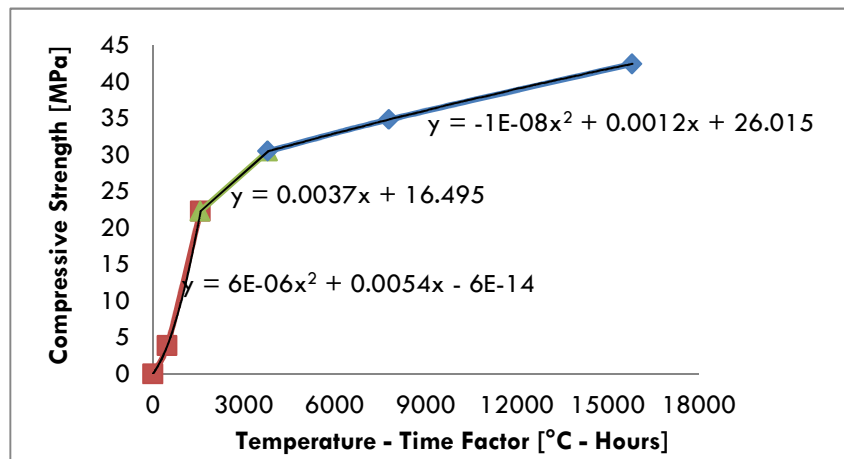
b) 20% FA
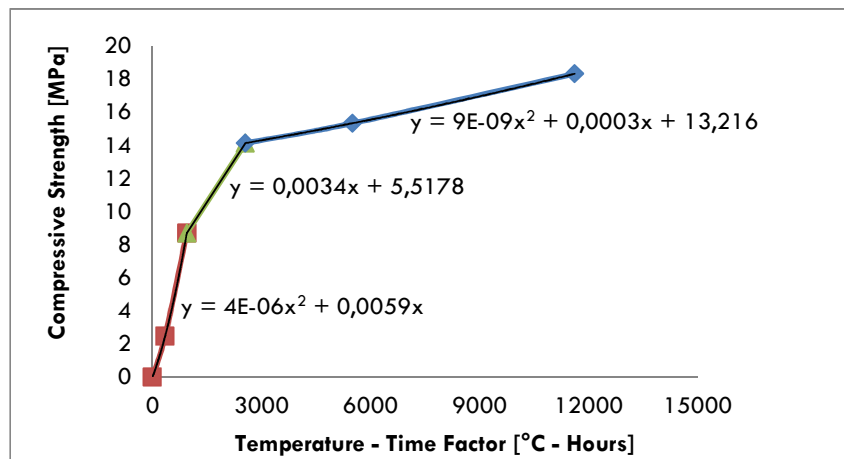
c) 50% FA
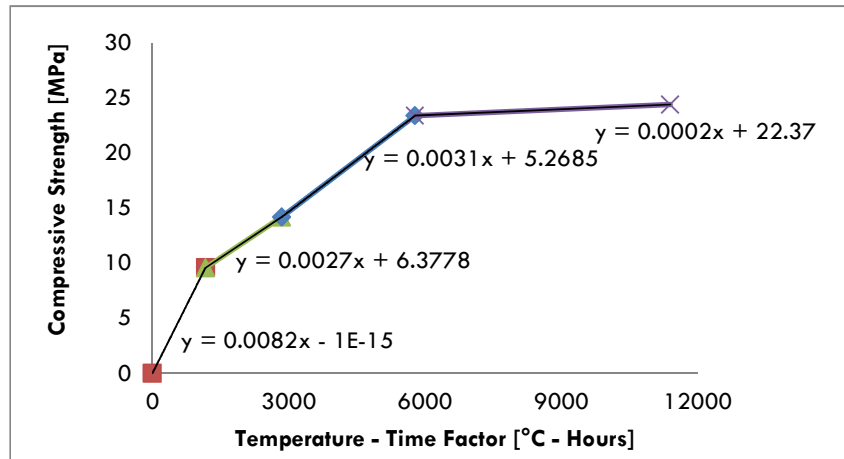
d) 50% FA + Na$_2$SO$_4$

Figure 165 Temperature – Time Factor vs. Compressive strength

COMPRESSIVE STRENGTH COMPARISON USING CYLINDERS, MATURITY AND CORES

Table 27 Compressive strength comparison using cylinders, maturity and cores

a) 0% FA

0% FA	0 d	1 d	3 d	7 d	14 d	28 d
Compressive Strength (MPa) - Cylinders	0	5.09	28.95	40.75	41.61	45.41
Maturity (°C-hours) - Cylinders	0	547	1842	4280	8595	17196
Maturity (°C-horas) - Elements	0	618	1802	3835	7765	15431
Compressive Strength (MPa) - Elements	0	5.99	28.12	38.45	41.48	44.73
Compressive Strength (MPa) - Cores	0	12.33		45.3	49.95	57.7

b) 20% FA

20% FA	0 d	1 d	3 d	7 d	14 d	28 d
Compressive Strength (MPa) - Cylinders	0	3.88	22.3	30.49	34.84	42.46
Maturity (°C-hours) - Cylinders	0	480	1578	3804	7803	15820
Maturity (°C-horas) - Elements	0	529	1519	3472	6929	14016
Compressive Strength (MPa) - Elements	0	4.54	22.04	29.34	33.85	40.87
Compressive Strength (MPa) - Cores	0	4.43	21.4	28.92	37.1	44.7

c) 50% FA

50% FA	0 d	1 d	3 d	7 d	14 d	28 d
Compressive Strength (MPa) - Cylinders	0	2.46	8.7	14.13	15.33	18.32
Maturity (°C-hours) - Cylinders	0	346	944	2556	5503	11618
Maturity (°C-horas) - Elements	0	396	1174	2552	5043	9814
Compressive Strength (MPa) - Elements	0	2.97	12.45	14.20	14.96	17.03
Compressive Strength (MPa) - Cores	0		13.2	16.5	19.5	20.3

d) 50% FA + Na$_2$SO$_4$

50% FA + Na$_2$SO$_4$	0 d	1 d	3 d	7 d	14 d	28 d
Compressive Strength (MPa) - Cylinders	0		9.58	14.19	23.40	24.40
Maturity (°C-hours) - Cylinders	0		1166	2845	5783	11397
Maturity (°C-horas) - Elements	0	276	989	2379	4749	9150
Compressive Strength (MPa) - Elements	0	2.26	8.11	12.80	19.99	24.20
Compressive Strength (MPa) - Cores	0		11	15	26	26.4

Appendix 3

W/CM=0.675 - 0% FA, 20% FA

Mix Designs

Mix Code	0.675/CE/100/	0.675/TP/20/
w/cm	0.675	
f/agr	0.538	
Fly ash [%]	0%	20%
fa/agr	0.475	0.475
Paste Volume [l]	258	266
Cement [kg]	259	207
Fly ash [kg]		52
Fine Aggregate 1 [kg]	734	726
Fine Aggregate 2 [kg]	183	181
Coarse Aggregate [kg]	1014	1003
Water [kg]	175	175
Admixture 1 (Lignosulfonate)	0.45%	0.45%
Admixture 2 (Polycarboxylate)	0.60%	0.60%

Compressive strengths

Mix Code	1 Day [MPa]	3 Days [MPa]	7 Days [MPa]	28 Days [MPa]	56 Days [MPa]	90 Days [MPa]	360 Days [MPa]
0.675/TP/20/L	4	14	19	23	32	32	39
0.675/CE/100/L	8	22	29	38	40	41	46
0.675/TP/20/O	6	15	20	23	29	33	34
0.675/CE/100/O	9	20	29	34	37	41	44

Water permeability

Mix Code	90 Days [mm]	180 Days [mm]	270 Days [mm]	360 Days [mm]
0.675/TP/20/L	60.36	24.27	15.11	14.5
0.675/CE/100/L	51.49	57.76	52.86	41.07
0.675/TP/20/O		81.28	75.7	70.21
0.675/CE/100/O		85.09	76.53	70.41

Initial Sorptivity

Mix Code	28 Days S initial (mm/s$^{1/2}$)	90 Days S initial (mm/s$^{1/2}$)	270 Days S initial (mm/s$^{1/2}$)	360 Days S initial (mm/s$^{1/2}$)
0.675/TP/20/L	0.0049	0.0063	0.0006	0.001
0.675/CE/100/L	0.0036	0.0045	0.001	0.0024
0.675/TP/20/O	0.0134	0.0171	0.0113	0.0091
0.675/CE/100/O	0.0046	0.0053	0.0022	0.0084

Secondary Sorptivity

Mix Code	90 Days	360 Days
	S final (mm/s$^{1/2}$)	S final (mm/s$^{1/2}$)
0.675/TP/20/L	0.0023	0.004
0.675/CE/100/L	0.002	0.0025
0.675/TP/20/O	0.0008	0.0013
0.675/CE/100/O	0.0021	0.0013

Chloride Penetration

Mix Code	28 Days [Coulombs]	90 Days [Coulombs]	180 Days [Coulombs]	270 Days [Coulombs]	360 Days [Coulombs]
0.675/TP/20/L	2488	2906	1166	467	553
0.675/CE/100/L	2191	3301	2225	163	122
0.675/TP/20/O		4450	2077		1326
0.675/CE/100/O		1467	1898	1898	865

Chloride Diffusion Coefficient

Mix Code	180 Days [x10^{-12}m^2/s]	270 Days [x10^{-12}m^2/s]	360 Days [x10^{-12}m^2/s]
0.675/TP/20/L	10.770	9.280	6.67
0.675/CE/100/L	17.290	11.310	10.12
0.675/TP/20/O	11.650	9.630	9.95
0.675/CE/100/O	8.410	7.370	6.64

Carbonation depth

Mix Code	28 Days [mm]	90 Days [mm]	270 Days [mm]	360 Days [mm]
0.675/TP/20/L	1.05	0.3	11	9.99
0.675/CE/100/L	0.6	0	6.1	6.02
0.675/TP/20/O	1.4	3.46	4.48	5.24
0.675/CE/100/O	0.7	1.64	3.32	4.69

Carbonation Coefficient

Mix Code	28 Days [mm/yr$^{1/2}$]	56 Days [mm/yr$^{1/2}$]	90 Days [mm/yr$^{1/2}$]	180 Days [mm/yr$^{1/2}$]	270 Days [mm/yr$^{1/2}$]	360 Days [mm/yr$^{1/2}$]
0.675/TP/20/L	3.79	0.77	0.60	1.79	15.66	10.06
0.675/CE/100/L	2.17	1.28	0.00	1.44	8.69	6.06
0.675/TP/20/O	5.05	6.79	6.97	6.00	6.38	5.28
0.675/CE/100/O	2.53	3.93	3.30	4.60	4.73	4.72

ALGORITHM PROGRAMMED IN MATLAB

INPUT 1

```
% W/CM         Period of analysis      Reinforcement depth
   0.45              10                      .03
% Width           Delta x         Delta Time
.2                .01             2592000
```

INPUT 2

```
%Month  Temperature
1       18.9
2       17.6
3       18
4       19
5       17.6
6       18.5
7       17.2
8       17.3
9       17.5
10      16.6
11      17.1
12      17.5
```

INPUT 3

```
%  Year    Surface chloride concentration
   1         .0025
   2         .005
   3         .0075
   4         .01
   5         .01
   6         .01
   7         .01
   8         .01
   9         .01
   10        .01
   11        .01
   12        .01
   13        .01
   14        .01
   15        .01
   16        .01
   17        .01
   18        .01
   19        .01
   20        .01
```

Gauss

```matlab
function uv=gauss(Kff)
[N,H]=size(Kff);
Aug=Kff;
for c=1:N
    P=Aug(c,c);
    for j=1:H
        Aug(c,j)=Aug(c,j)/P;
    end
        for i=c+1:N
            P=Aug(i,c);
```

```matlab
                    for j=1:H
                        Aug(i,j)=Aug(i,j)-P*Aug(c,j);
                    end
                end

end
for i=N-1:-1:1
    for j=i+1:N
        Aug(i,H)=(Aug(i,H)-Aug(i,j)*Aug(j,H));
    end
end
for i=1:N
    uv(i,1)=(Aug(i,H));
end
uv
```

Main algorithm

```matlab
clear all
load INPUT1 -ASCII
load INPUT2 -ASCII
load INPUT3 -ASCII

amc=INPUT1(1); %water to cementitious material ratio
Ta=INPUT1(2); %Period of analysis
Re=INPUT1(3); %Reinforcement depth
Esp=INPUT1(4); %Width
DeltaX=INPUT1(5); %Delta X
DeltaT=INPUT1(6); %Delta Time
Te=INPUT2;  % Temperature
Cs=INPUT3; %Surface chloride concentration
n=Ta;
L=Esp/DeltaX+1;
in=L-2;
RB=Re/DeltaX
CC=zeros(1,L);
C=zeros(in,1);
DD=zeros(in,1);
k=zeros(in,in);
uv=zeros(in,1);
for s=1:n
    for mm=1:12
    CC(1,L)=0;
    CC(1,1)=Cs(s,2);
    F=576.5/924.06^amc;
    d1=630.85*F^-1.288*1e-12;
    m=-3.0351*amc+2.0629;
    y=s-1;
    Time=mm*30*24*60*60+y*12*30*24*60*60;
    dt=d1*((28*24*60*60)/(Time))^m;
    Tem=273.15+Te(mm,2);
    df=dt*exp(35000/8.3144621*(1/293.15-1/(Tem)));
    Lambda=2*df*DeltaT/DeltaX^2;
    Teta=0.5;
    d=2*(n-1)+2;
    a=-Teta*Lambda/2;
    b=1+Teta*Lambda;
    c=-Teta*Lambda/2;
    TE=Te(mm,2);

        for i=1:in
```

```matlab
        CC(1,i+1)=C(i,1);
        end
        CC(1,1)=Cs(s,2);

        for i=1:in
            if i==1
        DD(1,1)=CC(1,i+1)+Lambda/2*(1-Teta)*(Cs(s,2)-
2*(CC(1,i+1))+CC(1,i+2));
        else if i==in
        DD(in,1)=CC(1,L-1)+Lambda/2*(1-Teta)*(CC(1,L-2)-2*CC(1,L-
1)+Cs(s,2));
        else
        DD(i,1)=CC(1,i+1)+Lambda/2*(1-Teta)*(CC(1,i)-
2*(CC(1,i+1))+CC(1,i+2));
            end
DD;
        end
        end

        for p=1:in

                if p==1
                DD(1,1)=-Cs(s,2)*a+DD(1,1);
                k(p,1)=b;
                k(p,2)=c;
                else if p==in
                DD(in,1)=-c*Cs(s,2)+DD(in,1);
                k(p,p)=b;
                k(p,in-1)=a;
                    else
                       k(p,p-1)=a;
                       k(p,p)=b;
                       k(p,p+1)=c;
                    end
                end

        end

        Kff=[k DD];
        Kff;
        uv=gauss(Kff);
        for i=1:in
        C(i,1)=uv(i,1);
        if uv(RB,1)>=.0005
            'end of the initation period'
        end

        end
     y=s-1
        mm
end

end
for i=1:in
     C(i,1)=uv(i,1);
end
uv;
%BY DIEGO VELANDIA
```

Figure 166 Matlab results

Appendix 4

CO$_2$ EMISSIONS CALCULATION

0.557/CE/100/-/-

Mix design quantities

Mix design quantities	kg/m^3
Total cementitious material	316
Cement (10% slag)	316
Fly ash	0
Fine Aggregate	870
Coarse Aggregate	1013
Admixtures (Plasticizer + superplasticizer)	3
Water	175

CO$_2$ emission per material

Material	CO$_2$ [t/kg] / Materials	CO$_2$ [t/m^3]	Source
Cement (10% slag)	7.22×10^{-4}	0.22816	
Fly ash		0.00000	
Fine Aggregate	4×10^{-6}	0.00348	
Coarse aggregate	4×10^{-6}	0.00405	Argos
Admixtures	2.2×10^{-4}	0.00066	
Recycled Water	0	0	

TOTAL CO$_2$ [t/m^3]	0.236349056

Production

Item	Unit/m^3	CO$_2$ [t/unit]	CO$_2$ [t/m^3]	Source
Plant Diesel [l]	1.51	0.0032	0.004872	
Diesel for internal material transport [l]	0.38	0.0032	0.001218	Argos
Energy [kWh]	2.2	0.0005	0.0011594	

TOTAL CO$_2$ [t/m^3]	0.0072494

Distribution and delivery

Item	Unit/m^3	CO$_2$ [t/unit]	CO$_2$ [t/m^3]	Source
Diesel [l]	3.41	0.0032	0.010962	Argos

TOTAL CO$_2$ [t/m^3]	0.010962

Total CO$_2$ per 1 m^3 of concrete (for 20 km radius)

TOTAL CO$_2$ [t/m^3]	0.255
TOTAL CO$_2$ [kg/m^3]	254.56

0.557/TP/20/-/-

Mix design quantities

Mix design quantities	kg/m^3
Total cementitious material	316
Cement (10% slag)	253
Fly ash	63
Fine Aggregate	854
Coarse Aggregate	1003
Admixtures (Plasticizer + superplasticizer)	3
Water	175

CO$_2$ emission per material

Material	CO$_2$ [t/kg] / Materials	CO$_2$ [t/m^3]	Source
Cement (10% slag)	7.22×10^{-4}	0.18267	
Fly ash		0.00088	
Fine Aggregate	4×10^{-6}	0.00342	
Coarse aggregate	4×10^{-6}	0.00401	Argos
Admixtures	2.2×10^{-4}	0.00066	
Recycled Water	0	0	

TOTAL CO$_2$ [t/m^3]	0.19163904

Production

Item	Unit/m^3	CO$_2$ [t/unit]	CO$_2$ [t/m^3]	Source
Plant Diesel [l]	1.51	0.0032	0.004872	
Diesel for internal material transport [l]	0.38	0.0032	0.001218	Argos
Energy [kWh]	2.2	0.0005	0.0011594	

TOTAL CO$_2$ [t/m^3]	0.0072494

Distribution and delivery

Item	Unit/m^3	CO$_2$ [t/unit]	CO$_2$ [t/m^3]	Source
Diesel [l]	3.41	0.0032	0.010962	Argos

TOTAL CO$_2$ [t/m^3]	0.010962

Total CO$_2$ per 1 m^3 of concrete (for 20 km radius)

TOTAL CO$_2$ [t/m^3]	0.210
TOTAL CO$_2$ [kg/m^3]	209.85

0.557/TP/50/-/-

Mix design quantities

Mix design quantities	kg/m^3
Total cementitious material	316
Cement (10% slag)	158
Fly ash	158
Fine Aggregate	834
Coarse Aggregate	983
Admixtures (Plasticizer + superplasticizer)	4
Water	175

CO₂ emission per material

Material	CO_2 [t/kg] / Materials	CO_2 [t/m³]	Source
Cement (10% slag)	7.22×10^{-4}	0.11408	
Fly ash		0.00221	
Fine Aggregate	4×10^{-6}	0.00334	
Coarse aggregate	4×10^{-6}	0.00393	Argos
Admixtures	2.2×10^{-4}	0.00088	
Recycled Water	0	0	

TOTAL CO_2 [t/m³]	0.124436

Production

Item	Unit/m³	CO_2 [t/unit]	CO_2 [t/m³]	Source
Plant Diesel [l]	1.51	0.0032	0.004872	
Diesel for internal material transport [l]	0.38	0.0032	0.001218	Argos
Energy [kWh]	2.2	0.0005	0.0011594	

TOTAL CO_2 [t/m³]	0.0072494

Distribution and delivery

Item	Unit/m³	CO_2 [t/unit]	CO_2 [t/m³]	Source
Diesel [l]	3.41	0.0032	0.010962	Argos

TOTAL CO_2 [t/m³]	0.010962

Total CO₂ per 1 m³ of concrete (for 20 km radius)

TOTAL CO_2 [t/m³]	0.143
TOTAL CO_2 [kg/m³]	142.65

0.557/TP/50/-/A

Mix design quantities

Mix design quantities	kg/m³
Total cementitious material	316
Cement (10% slag)	158
Fly ash	158
Fine Aggregate	834
Coarse Aggregate	983
Admixtures (Plasticizer + superplasticizer + Sodium sulfate)	7.27
Water	175

CO_2 emission per material

Material	CO_2 [t/kg] / Materials	CO_2 [t/m³]	Source
Cement (10% slag)	7.22×10^{-4}	0.11408	
Fly ash		0.00221	
Fine Aggregate	4×10^{-6}	0.00334	
Coarse aggregate	4×10^{-6}	0.00393	Argos
Admixtures	2.2×10^{-4}	0.00160	
Recycled Water	0	0	

TOTAL CO_2 [t/m³]	0.1251554

Production

Item	Unit/m³	CO_2 [t/unit]	CO_2 [t/m³]	Source
Plant Diesel [l]	1.51	0.0032	0.004872	
Diesel for internal material transport [l]	0.38	0.0032	0.001218	Argos
Energy [kWh]	2.2	0.0005	0.0011594	

TOTAL CO_2 [t/m³]	0.0072494

Distribution and delivery

Item	Unit/m^3	CO$_2$ [t/unit]	CO$_2$ [t/m^3]	Source
Diesel [l]	3.41	0.0032	0.010962	Argos

TOTAL CO$_2$ [t/m^3]	0.010962

Total CO$_2$ per 1 m^3 of concrete (for 20 km radius)

TOTAL CO$_2$ [t/m^3]	0.143
TOTAL CO$_2$ [kg/m^3]	143.37

0.482/CE/100/-/-

Mix design quantities

Mix design quantities	kg/m^3
Total cementitious material	363
Cement (10% slag)	363
Fly ash	0
Fine Aggregate	829
Coarse Aggregate	1017
Admixtures (Plasticizer + superplasticizer)	4
Water	175

CO$_2$ emission per material

Material	CO$_2$ [t/kg] / Materials	CO$_2$ [t/m^3]	Source
Cement (10% slag)	7.22×10^{-4}	0.26209	
Fly ash		0.00000	
Fine Aggregate	4×10^{-6}	0.00332	
Coarse aggregate	4×10^{-6}	0.00407	Argos
Admixtures	2.2×10^{-4}	0.00088	
Recycled Water	0	0	

TOTAL CO$_2$ [t/m^3]	0.270355808

Production

Item	Unit/m³	CO₂ [t/unit]	CO₂ [t/m³]	Source
Plant Diesel [l]	1.51	0.0032	0.004872	
Diesel for internal material transport [l]	0.38	0.0032	0.001218	Argos
Energy [kWh]	2.2	0.0005	0.0011594	

TOTAL CO₂ [t/m³]	0.0072494

Distribution and delivery

Item	Unit/m³	CO₂ [t/unit]	CO₂ [t/m³]	Source
Diesel [l]	3.41	0.0032	0.010962	Argos

TOTAL CO₂ [t/m³]	0.010962

Total CO₂ per 1 m³ of concrete (for 20 km radius)

TOTAL CO₂ [t/m³]	0.289
TOTAL CO₂ [kg/m³]	288.57

0.482/TP/20/-/-

Mix design quantities

Mix design quantities	kg/m³
Total cementitious material	363
Cement (10% slag)	290
Fly ash	73
Fine Aggregate	813
Coarse Aggregate	1002
Admixtures (Plasticizer + superplasticizer)	4
Water	175

CO₂ emission per material

Material	CO_2 [t/kg] / Materials	CO_2 [t/m³]	Source
Cement (10% slag)	7.22×10^{-4}	0.20938	
Fly ash		0.00102	
Fine Aggregate	4×10^{-6}	0.00325	
Coarse aggregate	4×10^{-6}	0.00401	Argos
Admixtures	2.2×10^{-4}	0.00088	
Recycled Water	0	0	

TOTAL CO_2 [t/m³]	0.218545472

Production

Item	Unit/m³	CO_2 [t/unit]	CO_2 [t/m³]	Source
Plant Diesel [l]	1.51	0.0032	0.004872	
Diesel for internal material transport [l]	0.38	0.0032	0.001218	Argos
Energy [kWh]	2.2	0.0005	0.0011594	

TOTAL CO_2 [t/m³]	0.0072494

Distribution and delivery

Item	Unit/m³	CO_2 [t/unit]	CO_2 [t/m³]	Source
Diesel [l]	3.41	0.0032	0.010962	Argos

TOTAL CO_2 [t/m³]	0.010962

Total CO₂ per 1 m³ of concrete (for 20 km radius)

TOTAL CO_2 [t/m³]	0.237
TOTAL CO_2 [kg/m³]	236.76

0.482/TP/50/-/-

Mix design quantities

Mix design quantities	kg/m³
Total cementitious material	363
Cement (10% slag)	182
Fly ash	182
Fine Aggregate	813
Coarse Aggregate	1002
Admixtures (Plasticizer + superplasticizer)	5
Water	175

CO_2 emission per material

Material	CO_2 [t/kg] / Materials	CO_2 [t/m³]	Source
Cement (10% slag)	7.22×10^{-4}	0.13105	Argos
Fly ash		0.00254	
Fine Aggregate	4×10^{-6}	0.00325	
Coarse aggregate	4×10^{-6}	0.00401	
Admixtures	2.2×10^{-4}	0.00110	
Recycled Water	0	0	

TOTAL CO_2 [t/m³]	0.141944

Production

Item	Unit/m³	CO_2 [t/unit]	CO_2 [t/m³]	Source
Plant Diesel [l]	1.51	0.0032	0.004872	Argos
Diesel for internal material transport [l]	0.38	0.0032	0.001218	
Energy [kWh]	2.2	0.0005	0.0011594	

TOTAL CO_2 [t/m³]	0.0072494

Distribution and delivery

Item	Unit/m³	CO_2 [t/unit]	CO_2 [t/m³]	Source
Diesel [l]	3.41	0.0032	0.010962	Argos

TOTAL CO_2 [t/m³]	0.010962

Total CO_2 per 1 m^3 of concrete (for 20 km radius)

TOTAL CO_2 [t/m^3]	0.160
TOTAL CO_2 [kg/m^3]	160.16

0.482/TP/50/-/A

Mix design quantities

Mix design quantities	kg/m^3
Total cementitious material	363
Cement (10% slag)	182
Fly ash	182
Fine Aggregate	813
Coarse Aggregate	1002
Admixtures (Plasticizer + superplasticizer + Sodium sulfate)	8
Water	175

CO_2 emission per material

Material	CO_2 [t/kg] / Materials	CO_2 [t/m^3]	Source
Cement (10% slag)	7.22×10^{-4}	0.13105	
Fly ash		0.00254	
Fine Aggregate	4×10^{-6}	0.00325	
Coarse aggregate	4×10^{-6}	0.00401	Argos
Admixtures	2.2×10^{-4}	0.00176	
Recycled Water	0	0	

TOTAL CO_2 [t/m^3]	0.142604

Production

Item	Unit/m^3	CO_2 [t/unit]	CO_2 [t/m^3]	Source
Plant Diesel [l]	1.51	0.0032	0.004872	
Diesel for internal material transport [l]	0.38	0.0032	0.001218	Argos
Energy [kWh]	2.2	0.0005	0.0011594	

TOTAL CO_2	0.0072494

Distribution and delivery

Item	Unit/m^3	CO$_2$ [t/unit]	CO$_2$ [t/m^3]	Source
Diesel [l]	3.41	0.0032	0.010962	Argos

TOTAL CO$_2$ [t/m^3]	0.010962

Total CO$_2$ per 1 m^{3}of concrete (for 20 km radius)

TOTAL CO$_2$ [t/m^3]	0.161
TOTAL CO$_2$ [kg/m^3]	160.82

0.427/CE/0/-/-

Mix design quantities

Mix design quantities	kg/m^3
Total cementitious material	410
Cement (10% slag)	410
Fly ash	0
Fine Aggregate	789
Coarse Aggregate	1016
Admixtures (Plasticizer + superplasticizer)	4
Water	175

CO$_2$ emission per material

Material	CO$_2$ [t/kg] / Materials	CO$_2$ [t/m^3]	Source
Cement (10% slag)	7.22×10^{-4}	0.29603	
Fly ash		0.00000	
Fine Aggregate	4×10^{-6}	0.00316	
Coarse aggregate	4×10^{-6}	0.00406	Argos
Admixtures	2.2×10^{-4}	0.00088	
Recycled Water	0	0	

TOTAL CO$_2$ [t/m^3]	0.30412656

Production

Item	Unit/m^3	CO$_2$ [t/unit]	CO$_2$ [t/m^3]	Source
Plant Diesel [l]	1.51	0.0032	0.004872	
Diesel for internal material transport [l]	0.38	0.0032	0.001218	Argos
Energy [kWh]	2.2	0.0005	0.0011594	

TOTAL CO$_2$ [t/m^3]	0.0072494

Distribution and delivery

Item	Unit/m^3	CO$_2$ [t/unit]	CO$_2$ [t/m^3]	Source
Diesel [l]	3.41	0.0032	0.010962	Argos

TOTAL CO$_2$ [t/m^3]	0.010962

Total CO$_2$ per 1 m^3 of concrete (for 20 km radius)

TOTAL CO$_2$ [t/m^3]	0.322
TOTAL CO$_2$ [kg/m^3]	322.34

0.427/TP/20/-/-

Mix design quantities

Mix design quantities	kg/m^3
Total cementitious material	410
Cement (10% slag)	328
Fly ash	82
Fine Aggregate	770
Coarse Aggregate	1001
Admixtures (Plasticizer + superplasticizer)	4
Water	175

CO₂ emission per material

Material	CO_2 [t/kg] / Materials	CO_2 [t/m³]	Source
Cement (10% slag)	7.22×10^{-4}	0.23682	
Fly ash		0.00115	
Fine Aggregate	4×10^{-6}	0.00308	
Coarse aggregate	4×10^{-6}	0.00400	Argos
Admixtures	2.2×10^{-4}	0.00088	
Recycled Water	0	0	

TOTAL CO_2 [t/m³]	0.245931936

Production

Item	Unit/m³	CO_2 [t/unit]	CO_2 [t/m³]	Source
Plant Diesel [l]	1.51	0.0032	0.004872	
Diesel for internal material transport [l]	0.38	0.0032	0.001218	Argos
Energy [kWh]	2.2	0.0005	0.0011594	

TOTAL CO_2 [t/m³]	0.0072494

Distribution and delivery

Item	Unit/m³	CO_2 [t/unit]	CO_2 [t/m³]	Source
Diesel [l]	3.41	0.0032	0.010962	Argos

TOTAL CO_2 [t/m³]	0.010962

Total CO₂ per 1 m³ of concrete (for 20 km radius)

TOTAL CO_2 [t/m³]	0.264
TOTAL CO_2 [kg/m³]	264.14

0.427/TP/50/-/-

Mix design quantities

Mix design quantities	kg/m^3
Total cementitious material	410
Cement (10% slag)	205
Fly ash	205
Fine Aggregate	743
Coarse Aggregate	977
Admixtures (Plasticizer + superplasticizer)	5
Water	175

CO_2 emission per material

Material	CO_2 [t/kg] / Materials	CO_2 [t/m^3]	Source
Cement (10% slag)	7.22×10^{-4}	0.14801	
Fly ash		0.00287	
Fine Aggregate	4×10^{-6}	0.00297	
Coarse aggregate	4×10^{-6}	0.00391	Argos
Admixtures	2.2×10^{-4}	0.00110	
Recycled Water	0	0	

TOTAL CO_2 [t/m^3]	0.15886

Production

Item	Unit/m^3	CO_2 [t/unit]	CO_2 [t/m^3]	Source
Plant Diesel [l]	1.51	0.0032	0.004872	
Diesel for internal material transport [l]	0.38	0.0032	0.001218	Argos
Energy [kWh]	2.2	0.0005	0.0011594	

TOTAL CO_2 [t/m^3]	0.0072494

Distribution and delivery

Item	Unit/m^3	CO_2 [t/unit]	CO_2 [t/m^3]	Source
Diesel [l]	3.41	0.0032	0.010962	Argos

TOTAL CO_2 [t/m^3]	0.010962

Total CO$_2$ per 1 m^3 of concrete (for 20 km radius)

TOTAL CO$_2$ [t/m^3]	0.177
TOTAL CO$_2$ [kg/m^3]	177.07

0.427/TP/50/-/A

Mix design quantities

Mix design quantities	kg/m^3
Total cementitious material	410
Cement (10% slag)	205
Fly ash	205
Fine Aggregate	743
Coarse Aggregate	977
Admixtures (Plasticizer + superplasticizer + Sodium sulfate)	9
Water	175

CO$_2$ emission per material

Material	CO$_2$ [t/kg] / Materials	CO$_2$ [t/m^3]	Source
Cement (10% slag)	7.22×10^{-4}	0.14801	
Fly ash		0.00287	
Fine Aggregate	4×10^{-6}	0.00297	
Coarse aggregate	4×10^{-6}	0.00391	Argos
Admixtures	2.2×10^{-4}	0.00198	
Recycled Water	0	0	

TOTAL CO$_2$ [t/m^3]	0.15974

Production

Item	Unit/m^3	CO$_2$ [t/unit]	CO$_2$ [t/m^3]	Source
Plant Diesel [l]	1.51	0.0032	0.004872	
Diesel for internal material transport [l]	0.38	0.0032	0.001218	Argos
Energy [kWh]	2.2	0.0005	0.0011594	

TOTAL CO$_2$ [t/m^3]	0.0072494

Distribution and delivery

Item	Unit/m^3	CO$_2$ [t/unit]	CO$_2$ [t/m^3]	Source
Diesel [l]	3.41	0.0032	0.010962	Argos

TOTAL CO$_2$ [t/m^3]	0.010962

Total CO$_2$ per 1 m^3 of concrete (for 20 km radius)

TOTAL CO$_2$ [t/m^3]	0.178
TOTAL CO$_2$ [kg/m^3]	177.95

Appendix 5

COST EVALUATION

Table 28 W/CM=0.482

Materials	Cost/kg	0.482/TP/20/-/-		0.482/CE/100/-/-		0.482/TP/50/-/-		0.482/TP/50/-/A	
		Quantity	Cost	Quantity	Cost	Quantity	Cost	Quantity	Cost
Cement [kg]	$ 347.06	290	$ 100,648	363	$ 125,984	182	$ 63,165	182	$ 63,165
Fly ash [kg]	$ 104.48	73	$ 7,627		$ 0	182	$ 19,015	182	$ 19,015
Fine aggregate 1 [kg]	$ 54.71	650	$ 35,558	663	$ 36,269	631	$ 34,519	631	$ 34,519
Fine aggregate 2 [kg]	$ 30.50	163	$ 4,972	166	$ 5,064	158	$ 4,820	158	$ 4,820
Coarse aggregate [kg]	$ 54.71	1002	$ 54,822	1017	$ 55,643	981	$ 53,673	981	$ 53,673
Water [kg]	$ 8.50	175	$ 1,488	175	$ 1,488	175	$ 1,488	175	$ 1,488
Admixture 1 (Lignosulfonate) [kg]	$ 1,508.00	1.63	$ 2,463	1.63	$ 2,463	1.64	$ 2,470	1.64	$ 2,470
Admixture 2 (Polycarboxylates) [kg]	$ 6,403.00	2.18	$ 13,946	2.18	$ 13,946	3.09	$ 19,811	3.09	$ 19,811
Activator (Sodium sulfate) [kg]	$ 1,600.00							3.64	$ 5,824
Cost [COP]		$	221,524	$	240,856	$	198,961	$	204,785
Cost $ [USD]		$	117	$	127	$	105	$	108
Cost £ [Pounds]		£	70	£	76	£	63	£	65

336

Table 29 W/CM=0.427

Materials	Cost/kg	0.427/TP/20/-/-		0.427/CE/100/-/-		0.427/TP/50/-/-		0.427/TP/50/-/A	
		Quantity	Cost	Quantity	Cost	Quantity	Cost	Quantity	Cost
Cement [kg]	$ 347.06	328	$ 113,836	410	$ 142,295	205	$ 71,148	205	$ 71,148
Fly ash [kg]	$ 104.48	82	$ 8,567		$ 0	205	$ 21,418	205	$ 21,418
Fine aggregate 1 [kg]	$ 54.71	616	$ 33,698	631	$ 34,519	594	$ 32,495	594	$ 32,495
Fine aggregate 2 [kg]	$ 30.50	154	$ 4,698	158	$ 4,820	149	$ 4,545	149	$ 4,545
Coarse aggregate [kg]	$ 54.71	1001	$ 54,768	1016	$ 55,588	977	$ 53,455	977	$ 53,455
Water [kg]	$ 8.50	175	$ 1,488	175	$ 1,488	175	$ 1,488	175	$ 1,488
Admixture 1 (Lignosulfonate) [kg]	$ 1,508.00	1.85	$ 2,782	1.85	$ 2,782	1.85	$ 2,782	1.85	$ 2,782
Admixture 2 (Polycarboxylates) [kg]	$ 6,403.00	2.46	$ 15,751	2.46	$ 15,751	3.49	$ 22,314	3.49	$ 22,314
Activator (Sodium sulfate) [kg]	$ 1,600.00							4.10	$ 6,560
Cost [COP]		$	235,588	$	257,243	$	209,645	$	216,205
Cost $ [USD]		$	124	$	136	$	111	$	114
Cost £ [Pounds]		£	74	£	81	£	66	£	68